WAVES IN THE MIDDLE ATMOSPHERE

A thesis

presented for the degree

of

Doctor of Philosophy in Physics

in the

University of Canterbury, Christchurch,

New Zealand

by

A.G.Burns

1985

CORRECTIONS

A. G. Burns

WAVES IN THE MIDDLE ATMOSPHERE

Page Numbers	Identification	Correction
15	CNR	After "constant" write "measured by the radar".
15	CNT	After "constant" write "for turbulence".
17	End of writing	Write "Addenda" "$\bar{u}$ Velocity time average". "[u] Zonal velocity average". " u* Velocity deviations from the zonal average". "u_1 Velocity deviations from the time average".
43	End of the first paragraph	Add "Variations in amplitude will also broaden the peak".
55	3rd line from bottom	After "minute" write "average".
57	Line 3	Add ϕ.
57	Second to last line	$-\lvert V_c \rvert$ to V_c^2.
57	Last line	-30 ms^{-1} to -900 m^2s^{-2}.
58	Equation 3.9	"q(t)" becomes "g(t)".
92	Line 19	"althlugh" should be "although".
121	Line 7	"tonvective" should be "convective".
121	Line 16	"winder" should be "winter".
135	In 6.2a (equation)	"ω_B" should be "ω_B^2".
136	In 6.7 (equation)	"$\cos\phi_1$" should be "$\cos^2\phi_1$".
137	In 6.11 (equation)	(x,z) should be (x,t).
138	Line 8	The sentence "This can....." becomes "This can also occur near a critical layer".
140	Line 11	After "than" replace "a¼ of", with "¼, than".
141	Line 12	x should be raised.
141	Equation 6.12	ω^2 should be ω'^2.
143	Line 4	"of" should be "over".
148	Equation 6.21b	Second "B_2" should be "R_2".
149	Line 10	"Hiroto" should be "Hirota".
150	Line 4	"(6.22)" and "(6.28)" should be "(6.24)" and "(6.25)".
150	Line 18	Delete "and ".
150	3rd paragraph	"Equation (6.19)" should read "Equation (6.24)".
154	Line 7	Delete "than".
154	Equation 6.32	Should be $\lvert u_1 \rvert^2 = \frac{\omega_B^2}{\lvert K_z \rvert^2}$
167	Line 31	Add "ω" before "is the frequency".
168	Line 1	Delete "B" on the second "ω_B".

179	Line 23	Change "turbulence" to " Turbopause".
184	Line 9	"to be smaller" should be omitted.
186	Line 19	Delete sentence starting " For instance...".
189	Second paragraph, 1st line	Delete "this" before "orientation".
194	Lines 21 and 23	Change units to m^2s^{-2}.
195	Line 22	After "equation" include "7.5".
212	Line 12	"3.3" becomes "7.10".
217	Line 9	Remove "max".
237	Line 2	Remove "to".
258	Line 8	"c_1" should be "c_x".
264	Line 4	After "stratosphere" add "due to the amplitude and direction of the zonal wind in this region".
266		Delete the paragraph starting "Finally.....
266	Line 29	"K_z^2" should be "$k_{zreal}^{\ 2}$".

ABSTRACT

Studies were made of the dynamics of the atmosphere at heights of between 65 km and 102.5 km at Birdlings Flat over a period of 2½ years. Variance profiles for internal gravity waves were calculated for each month in the 2½ year period. These profiles were similar for each month. The variances remained reasonably steady in most months at heights below 80 km, but increased steadily above 80 km to a maximum at heights between 92.5 km and 97.5 km. Various models were developed to explain this and other features of internal gravity wave behaviour. A simple saturation model explained most of the observed features of internal gravity wave behaviour in this region.

The isotropy of internal gravity waves was also considered. Isotropic behaviour was generally observed below 80 km, but strong anisotropies were observed to occur between 80 km and 95 km. These anisotropies occurred in the same direction in every month at all heights between 80 km and 95 km. Above 95 km the anisotropies were less pronounced. Various explanations for this behaviour have been considered, but no explanation has proved to be entirely adequate. Some consequence of this behaviour have also been discussed.

LIST OF CONTENTS

Continued p.3

Continued p.4

CHAPTER PAGE

Continued p. 5

LIST OF FIGURES

PAGE

PAGE

PAGE

PAGE

PAGE

LIST OF TABLES

PAGE

LIST OF SYMBOLS

a	Constant.
a_i	Coefficients for a quadratic equation.
a_{ij}	MEM filter coefficients.
a,b,c,d	Numbers.
c_x	Horizontal phase velocity.
d.f.	Degrees of freedom.
$f(z,T_o)$	A function.
e_R	Receiver efficiency.
e_T	Transmitter efficiency.
$f(z,T_o)$	A function.
f	Frequency (Chapter 3). Inertial frequency $(2\Omega\sin\phi)$.
g	The acceleration due to gravity.
$g(t)$	Filter function.
h	Half amplitude width of cosine terminator.
$h(t)$	Filter function.
i	Imaginary number ($\sqrt{(-1)}$).
j	Integer.
k	Integer.
k_x	Zonal wavenumber.
k_y	Meridional wavenumber.
k_h	Horizontal wavenumber $\left(k_h^2 = k_x^2 + k_y^2\right)$.
k_{zreal}	Vertical wavenumber.
n	Refractive index.
r	Variable.
t	Period.
t_B	Brunt period.
u	Zonal velocity.
$\dot{u}$	Zonal acceleration.

v	Meridional velocity.
w	Vertical velocity amplitude.
x	Zonal direction. Variable (Chapter 7).
y	Meridional direction.
$x(t)$	Filter function.
z	Height.
A_R	Area of the receiving array.
AIC	Akaike information criterion.
B_o	The earth's magnetic field.
CAT	Criterion autoregressive transfer function.
CNR SEE ERRATA	Refractive index structure constant ~~of the receiver~~. measured by the radar.
CNT SEE ERRATA	Refractive index structure constant ~~of the transmitter~~. for turbulence
F	Fraction of the volume that is filled with turbulence.
$F(\omega)$	Fourier transformed filter function.
FPE	Final prediction error.
$G(\omega)$	Fourier transformed filter function.
H_j^i	Hough function.
$H(\ )$	Four transformed filter function.
I	Magnetic dip angle.
J	Meridional flux of zonal momentum.
K_z	Vertical wavenumber.
L	Horizonal displacement.
M	Filter length. Angular Momentum (Chapter 7).
N	The number of points. Electron density.
NTD	Normalised time discrepancy.
P	Pressure. Cut-off frequency (Chapter 3).
P, P_μ, P_ν	Power function (Chapter 4).
P_R	Receiver power.

P_T	Transmitter power.
Q	Coefficient of Association.
R	Gas constant. Earth's Radius (Chapter 7).
R_i	Richardson number.
R_{iF}	Flux Richardson number.
S^2	Variance.
T	Temperature.
V_a	Apparent velocity.
V'	Apparent velocity corrected for anistropy.
V_T	The "true" velocity.
V_c	The characteristic velocity.
w	Filter weights (Chapter 3). Variable (defined in equation 3.32).
α	Confidence intervals (frequencies).
α'	Constant.
γ	Ratio of specific heats (C_p/C_v).
δ	Dirac delta function.
Δ	Difference. Normalising factor (Chapter 3).
Γ	Dry adiabatic lapse rate ($\equiv g/C_p$).
ζ	The axis in the direction of B_o.
ζ_o	Separation between antennae in the x direction.
η	Separation between antennae in the y direction.
θ	Potential temperature.
κ	Constant (C_p-C_v/C_p).
Λ	Dipole longitude.
λ	Longitude.
λ	Wavelength.
λ_z	Vertical wavelength.
μ	Mean.
ν	Degrees of freedom (Chapter 4). Frequency.
ν_m	Collision frequency between electrons and neutral particles.

ν_N	Nyquist frequency.
ρ, ρ_o	Density.
ρ_i	Correlations.
σ	Standard deviation. Cross section.
σ_1	Pedersen conductivity.
σ_2	Hall conductivity.
τ	Filter length. Shearing stress (Chapter 5).
τ_x, τ_y	Least squares fitted time delays.
τ_{ij}	Time lags for the maximum cross-correlation between aerials.
τ_λ	Drag.
ϕ, ϕ_a	Orientation of motion (Chapter 3).
ϕ_o, ϕ	Geographic latitude.
ϕ_1	Phase angle.
Φ	Dipole latitude.
ω	Angular frequency.
ω'	Intrinsic frequency.
ω_B	Brunt frequency.
Ω	Angular frequency of the earth.

Addenda

$\bar{u}$ cf ERRATA	Velocity time average
$[u]$	Velocity zonal average
u^*	Deviations of velocity from the zonal average
u_1	Deviations of velocity from the time average.

CHAPTER 1

INTRODUCTION

In the last twenty to thirty years there has been a great increase in the amount of information available about the stratosphere, the mesophere and the lower thermosphere. The temperature structure of the upper stratosphere and, with lower resolution, the mesosphere has been studied by satellite derived radiance techniques (e.g. Houghton and Smith (1970)). The lower stratosphere temperatures have been studied for many years using radiosondes. The resolution of the satellite radiometers is poor in the mesosphere due to the size of the half power width of the radiance bands (e.g. see Crane (1979)) so that only the coarsest features are resolved using these techniques. However, satellite techniques do have the advantage of providing global temperature coverage at all levels.

Other techniques must be used to get better resolution in the mesosphere and lower themosphere. Rockets have been regularly used to obtain temperature readings since the early 1960s. Unfortunately, rockets are expensive and hence data from rocket soundings have been sporadic, especially in the southern hemisphere. Mesospheric average temperature profiles are still drawn from rocket data which weights these profiles in favour of northern hemisphere temperatures, which are not necessarily the same as southern hemisphere temperatures (e.g. see Harwood (1975)). This point is important when the effect of background temperatures on wave dynamics is discussed.

Remote sensing is, after an initial investment, cheaper and also more regular. The measurement of winds using meteor trails has a relatively long history for the region near the mesopause and the study of noctilucent clouds has also been undertaken. Partial reflection drifts provides information about motion from 60 to 70 km up to over 100 km. Recently other backscatter techniques such as the LIDAR techniques (Megie and Blamont (1977)) have been used.

Partial reflection drift techniques have been used in this thesis, primarily to study the behaviour of internal gravity waves that have reached sufficient amplitude to become unstable.

In the next chapter an overview of the region that is being studied is given. The mean winds and the mean temperature structure are discussed. The various scales of motion are mentioned with particular emphasis on internal gravity waves.

There is a general discussion of the data in Chapter 3. The techniques used at Birdlings Flat and at Arrival Heights are mentioned and there is an examination of the analysis techniques and errors.

In Chapter 4 spectral analyses are made of the data to determine the power at various frequencies. Thus the periods that are present are found. The relative importance of planetary waves can be compared with that of internal gravity waves by considering the long period variance.

The criteria for stability are considered in Chapter 5. This chapter introduces the concepts that are applied in Chapter 6.

In Chapter 6 the monthly averaged internal gravity wave

variance profiles are considered. These variance profiles are compared with a model of the velocity amplitudes that occur when internal gravity waves break. Changes in the wave amplitude with vertical wavelength are discussed and changes in wave energy with height are considered. Variances for other periods are compared with the variances for periods of less than 3 hours.

Momentum transport is considered in Chapter 7. The relative importance of the various wave components is discussed and the accelerations due to the overall transport of zonal momentum are considered.

Possible variations in the direction of internal gravity wave velocity vectors are studied in Chapter 8. Attempts are made to obtain an explanation for these variations. Some implications of these variations are also studied.

CHAPTER 2

DYNAMICS OF THE ATMOSPHERE

2.1 The mean temperature structure and the prevailing winds.

Quantitative meteorological observations at ground level began with the invention of the thermometer by Galileo in the late 16th century or early 17th century and the invention of the barometer by Torricelli in 1643 (Frisinger (1977)). Pascal arranged for barometric readings to be made at two heights on a mountain. He showed that the atmospheric pressure decreased with increasing height. The temperature was also seen to decrease with increasing altitude.

At the end of the 19th century it was still thought that atmosphereic temperatures, on average, decreased with altitude for all heights. Teisserenc de Bort (e.g.Teisserenc de Bort (1904)) used registering barometers on balloons to demonstrate that, at an altitude of about 10 km, the mean temperature of the atmosphere stopped decreasing and started increasing. Throughout this century more detailed knowledge of the atmosphere has become available and the atmosphere can now be divided into a number of height regions of temperature increase or decrease with small regions in between where the temperature is stable (see figure 2.1).

The behaviour of the atmosphere in the lowest region, the troposphere, is a very large and complicated topic. Apart from this region's function as an energy and momentum source for the waves observed in the mesosphere, the behaviour of the troposphere is not immediately relevant to the theme of this thesis: namely the behaviour of waves in the mesosphere and the lower thermosphere. Therefore, except where it is immediately relevant, the troposphere is not discussed further

Figure 2.1

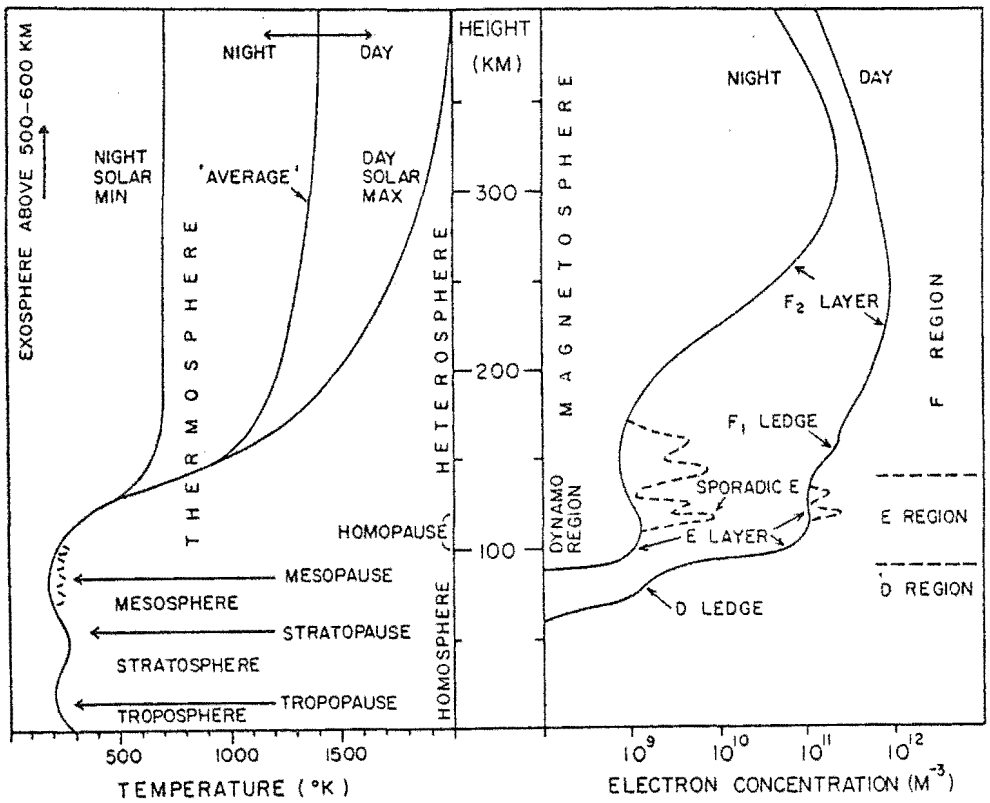

The regions of the atmosphere(after Hines et al(1965)).

and discussion is centred on the regions directly above the troposphere - the middle atmosphere.

The main features of the temperature structure of the middle atmosphere are as follows (see figures 2.2 to 2.3).

The summer stratopause is warmer than the winter stratopause by about 30K. Maximum solstice temperatures are found over the polar regions at a height of about 50 km. In spring and autumn the stratopause is found at similar heights but the maximum is now found to be over the equator rather than at the summer pole.

The minimum temperature at the mesopause is found at the summer pole at an altitude of between 85 km and 90 km with a temperature of about 150K. The maximum value of the mesopause temperature occurs at the winter pole at heights of just over 90 km. The meridional temperature gradient at the mesopause is small in spring and autumn.

The temperature structure and the circulation of the middle atmosphere is mainly driven by the absorption of solar ultraviolet radiation by stratospheric ozone (e.g. Holton and Wehrbein (1980)). This will produce a net heating in the summer hemisphere and a net cooling in the winter hemisphere. The meridional solstice temperature gradient at the mesopause where the winter mesopause is warm and the summer mesopause cold, cannot be maintained by such a mechanism. The warm winter mesopause is caused by subsidence (Kellogg and Schilling (1951)) while the cold summer mesopause occurs when there is a net rising motion at the summer pole at these heights.

So far, no differences have been assumed between hemispheres, the temperature data for figure 2.4 have come from CIRA (COSPAR (1972)). These mesospheric data have been

Figure 2.2

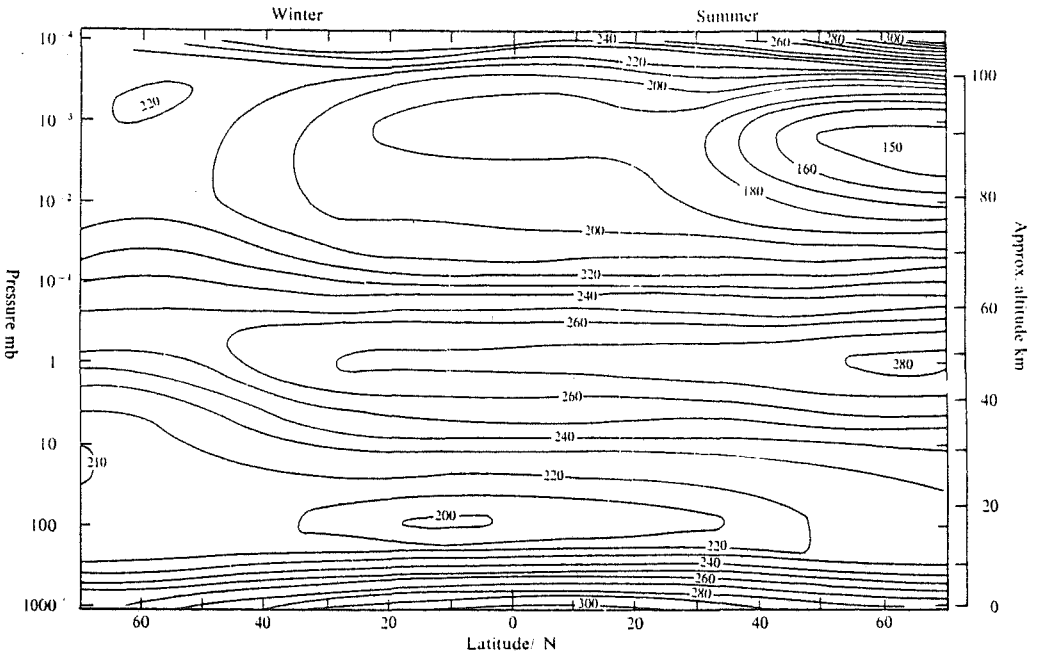

The temperature structure of the atmosphere below 100 km at the solstices(after Houghton(1977)).

Figure 2.3

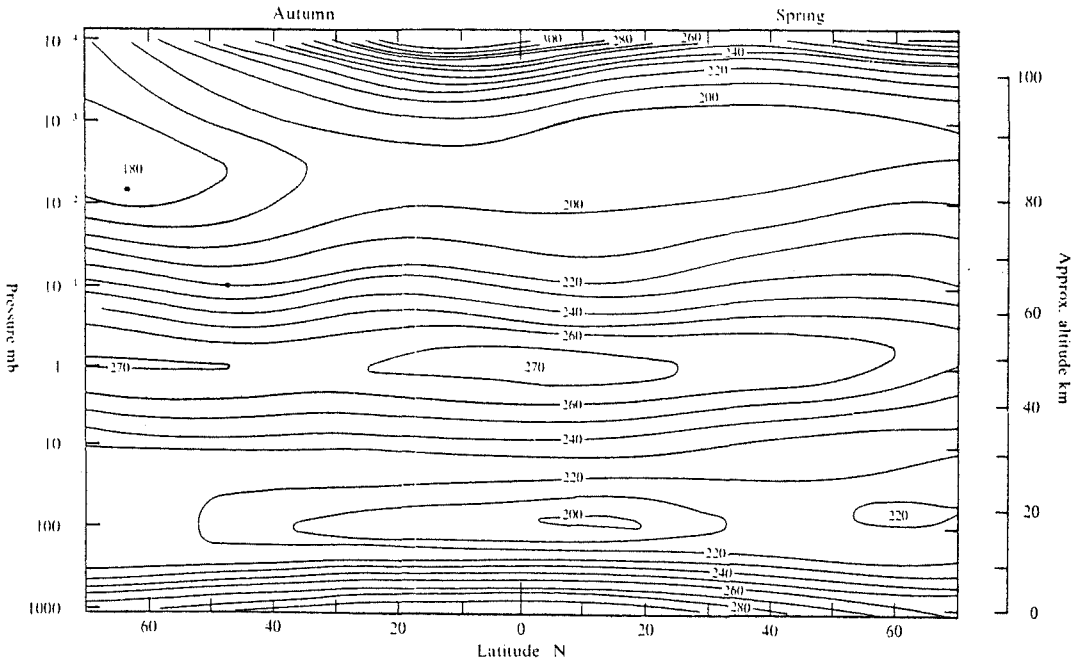

The temperature structure of the atmosphere below 100 km at the equinoxes(after Houghton(1977)).

calculated from rocket derived temperature soundings. These probes have been mainly launched in the northern hemisphere. Whilst this statement is essentially correct for all latitudes, it is especially relevant to the high latitude soundings.

The differences between the northern and southern hemispheres have been well documented for the stratosphere: especially since meteorological satellites have come into use (e.g. see Harwood (1975), Koshelkov (1984)). Unfortunately, fewer temperature data are available for the southern hemisphere mesosphere.

The main differences between the hemispheres in the stratosphere are: the southern hemisphere winters are colder than their northern hemisphere counterparts by about 20K at heights from 15 to 20 km (Labitzke and Barnett (1973)). The southern hemisphere summer stratosphere is warmer than the northern hemisphere summer stratosphere (Barnett (1974), Fritz and Soules (1973) and Labitzke (1980)). These differences probably relate to changes in the earth-sun distance (Fritz and Soules (1970)). Stratospheric warmings (Schoeberl (1978)) occur in both hemispheres but circulation reversals apparently occur only in the northern hemisphere (Labitzke and Barnett (1973)).

There are few southern hemisphere mesospheric rocket data available. Consequently, the CIRA (COSPAR (1972)) profiles (see figure 2.4) really reflect the temperature structure of the northern hemisphere mesosphere. Rocket data from Molodezhnaya (latitude $67^{o}40'$S, longitude $45^{o}51'$E) (Sehra (1975), Sehra and Harihorn (1981)) can be compared with the high latitude CIRA (COSPAR (1972)) data taken at Point Barrow (71N).

From these data, which are rather limited in both hemispheres in terms of the number of soundings made,

Figure 2.4

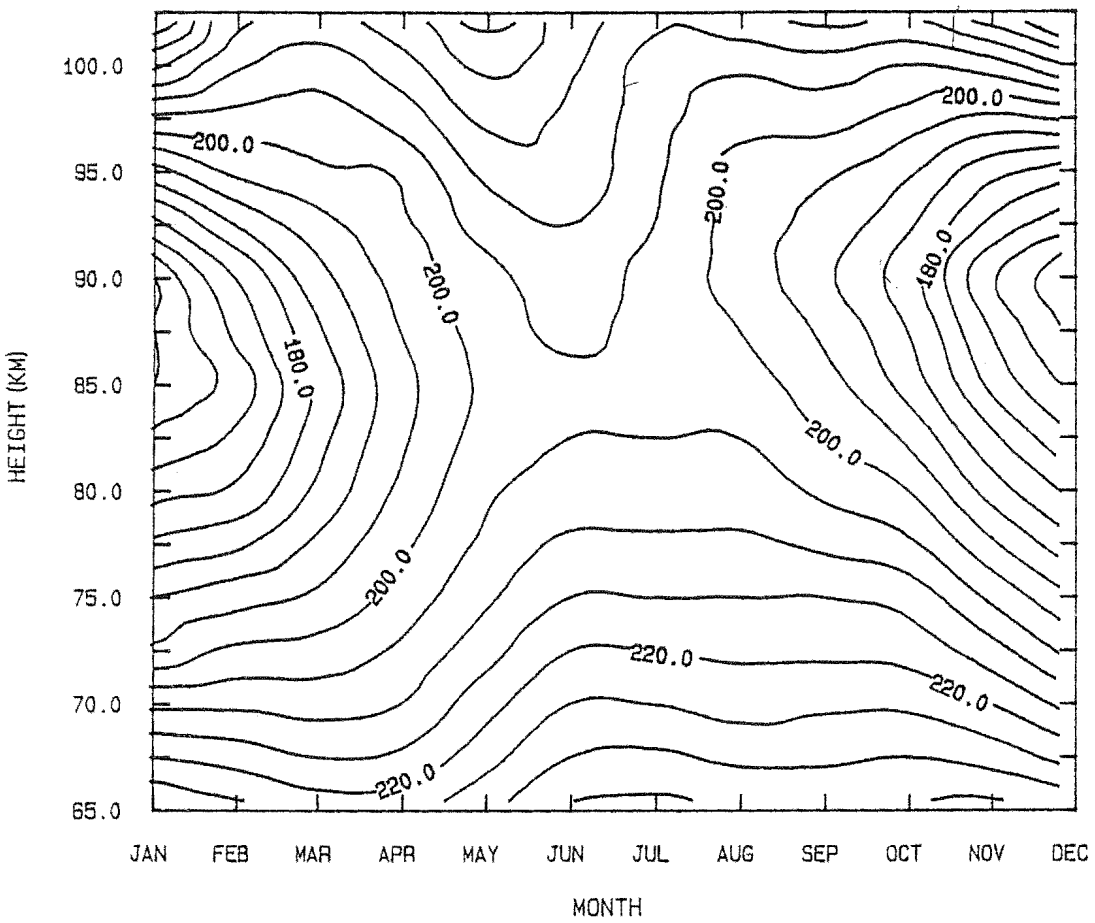

Temperatures for latitude 45N adapted for the southern hemisphere seasons. CIRA(1972)data is used.

Figure 2.5

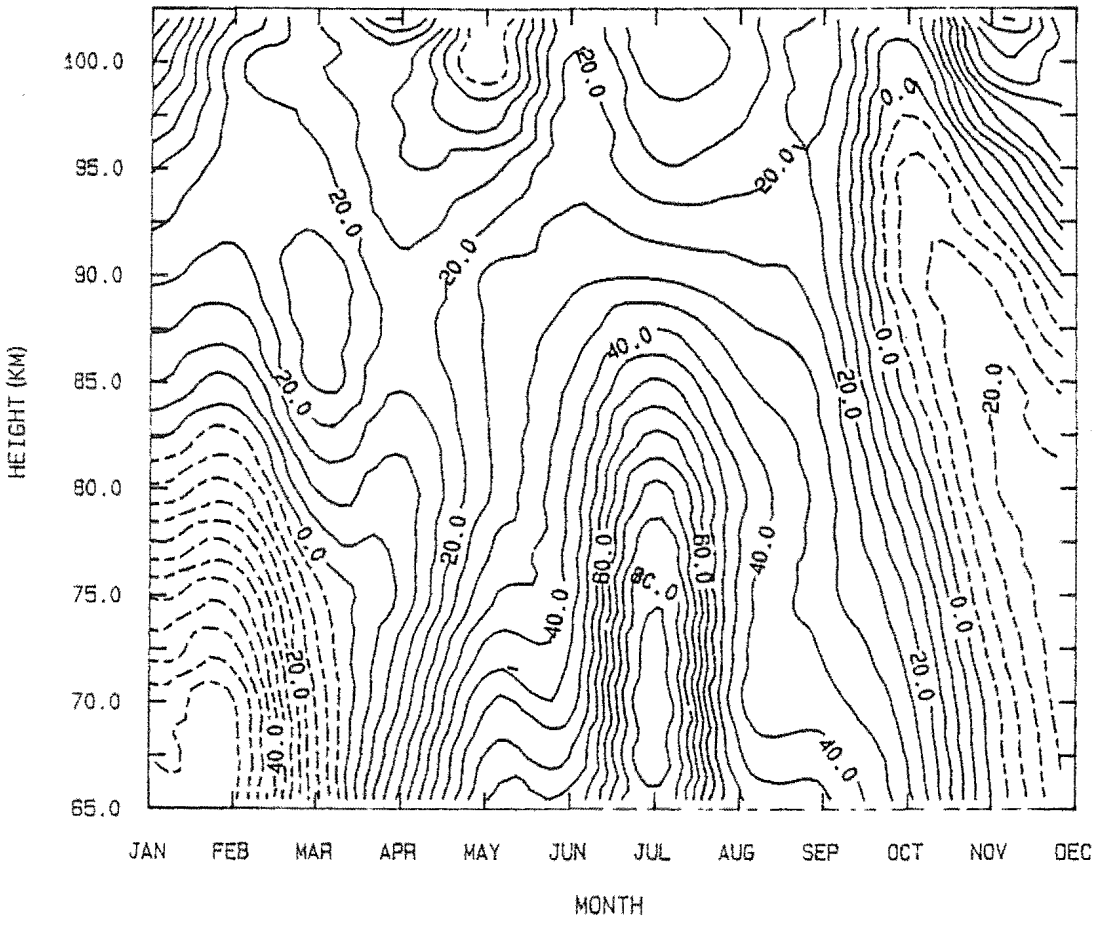

Monthly averaged zonal winds for a latitude of 45N altered for the southern hemisphere seasons. Eastward winds are positive,westward winds are negative.

it appears that the 70S mesosphere is colder in winter than the northern hemisphere mesosphere. Unlike the stratosphere, the whole southern hemisphere mesosphere may be colder than the northern hemisphere mesosphere in winter as well.

The CIRA (COSPAR (1972)) data that are used to determine the mean velocities in figure 2.5 are based on soundings made in the southern hemisphere at heights below 60 km, but are based on northern hemisphere soundings at heights greater than 60 km. These data can be supplemented both by later northern hemisphere data (e.g. Nastrom, Balsley and Carter (1982), Hess and Geller (1978)) and by southern hemisphere data (e.g. Vincent and Ball (1981), Elford (1976) and Birdlings Flat data (figures 2.6 to 2.9 for the Birdlings Flat data).

The main features of zonal wind circulation in the middle atmosphere are: a strong eastward jet exists in the winter above the stratopause at mid-latitudes; a weaker and somewhat less well defined westward jet is found at similar heights and latitudes in the summer. The situation is more confused in the tropics due to a strong long period component in the zonal wind.

The two years of Birdlings Flat zonal wind data (figures 2.6 and 2.7 for 1981 and 1982) show similar behaviour in both years, although the eastward mesospheric jet is much lower in the winter of 1981, when it occurs at a height of less than 65 km, than it is in 1982, when the jet is centred at 70 km. However, a lower jet may be present in 1982 as the amplitude of the zonal wind appears to be increasing with decreasing altitude in July and August. In both years the minima, where the amplitude of the zonal wind is about zero, occur in spring and autumn at heights near 100 km. The autumnal minimum is the more clearly defined of the two minima.

Figure 2.6

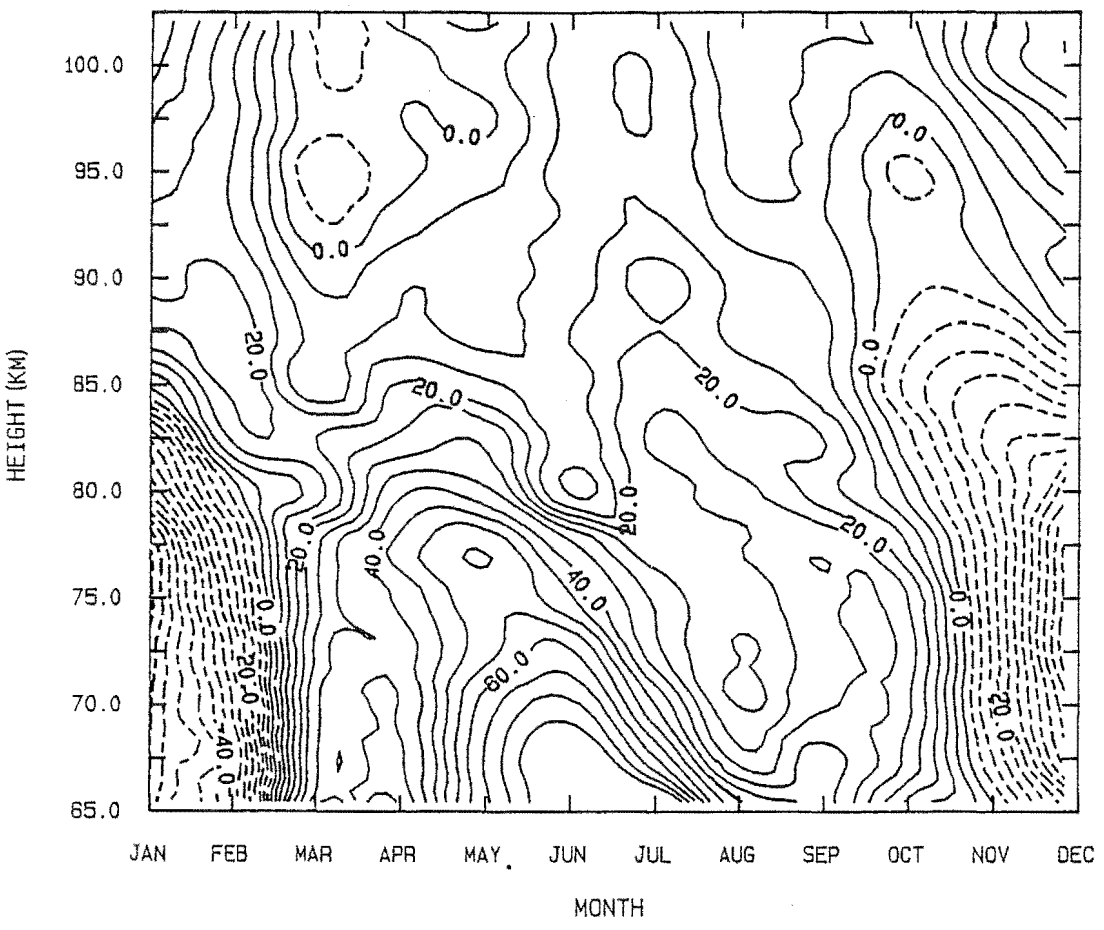

Monthly averaged zonal winds over Birdlings Flat in 1981.
Eastward winds are positive, westward winds are negative.

Figure 2.7

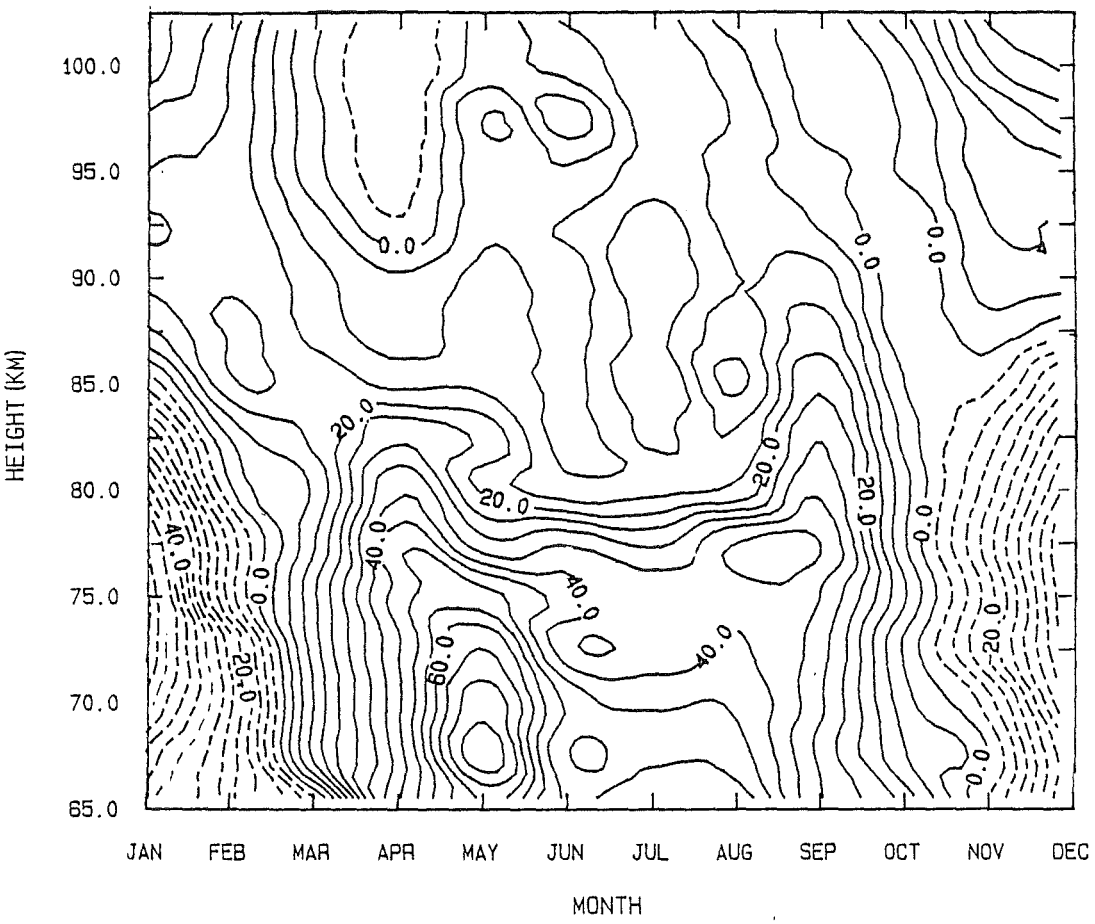

Monthly averaged zonal winds over Birdlings Flat in 1982.
Eastward winds are positive,westward winds are negative.

This minimum occurs in March and April in both years. The spring minimum is height dependent, occurring in September at 100 km and later at lower heights. Corresponding eastward wind maxima occur at 100 km in the months of December and January and June and July.

The westward jet is strongest in December and January, occurring at heights up to 80 km in these months in both years, with a possible amplitude maximum of 50-70 m/s being found at about 75 km. The circulation reversal from westward to eastward zonal winds occurs in the February-March period in both years. The reverse transition from eastward to westward winds occurs at the higher heights, and may be associated with the weak winds found at the mesopause and in the lower thermosphere in spring. At 85 km this change from eastward to westward winds occurs in the September-October period in both years, while at 70 km this change is found in the October-November period.

These Birdlings Flat data are generally in agreement with the northern hemisphere data of the CIRA (COSPAR (1972)) model. Figure 2.5 has been adapted from this CIRA data for the equivalent southern hemisphere months. In this model atmosphere the winter eastward jet has an amplitude of more than 85 m/s at altitudes from 65 km to 75 km in January (July in the northern hemisphere). This jet apparently occurs at greater altitudes in the northern hemisphere. The transition from eastward to westward zonal wind conditions occurs at about the same time in both hemispheres. In the CIRA (COSPAR (1972)) model this transformation takes place in November (May) in the 65 km to 75 km height range and in October (April) for heights near 90 km. However, the transition from westward to eastward winds occurs "later"

in the northern hemisphere: taking place in the months of "March or April" (September or October) rather than the February-March (August-September) wind change seen in the southern hemisphere mesosphere. Furthermore, the westward jet is both lower and slightly weaker in the northern hemisphere: having an amplitude of less than 50 m/s at altitudes of less than 70 km in "January" (July) compared with amplitudes of nearly 60 m/s at 75 km in January in the southern hemisphere. Wind transitions also occur at different times at 100 km in the northern hemisphere. Westward winds appear in March in the southern hemisphere at 100 km whereas the westward winds are found in "May" (November) in the northern hemisphere. The strong eastward jet that occurs in the summer at these heights is found in "November" (May) in the northern hemisphere and in the December to January period in the southern hemisphere.

The behaviour of meridional winds is not as well documented as the behaviour of zonal winds. The amplitudes of meridional winds are smaller than the amplitudes of zonal winds at 70 km. However, above 90 km the amplitudes of meridional winds and zonal winds are similar. The behaviour of the meridional winds is similar in both years (1981 and 1982) at Birdlings Flat. A southward jet, with an amplitude of 20 m/s, is found in autumn and early winter at heights lower than 80 km. Southward winds exist at these heights throughout the rest of winter and spring. A transition from southward to northward winds occurs in November, but this transition does not occur at the same time in different years. The transition from northward to southward winds occurs in early February. At 100 km summer winds are southward with northward winds occurring through most of the winter, autumn and spring. The strongest winds occur in autumn at 100 km.

Figure 2.6

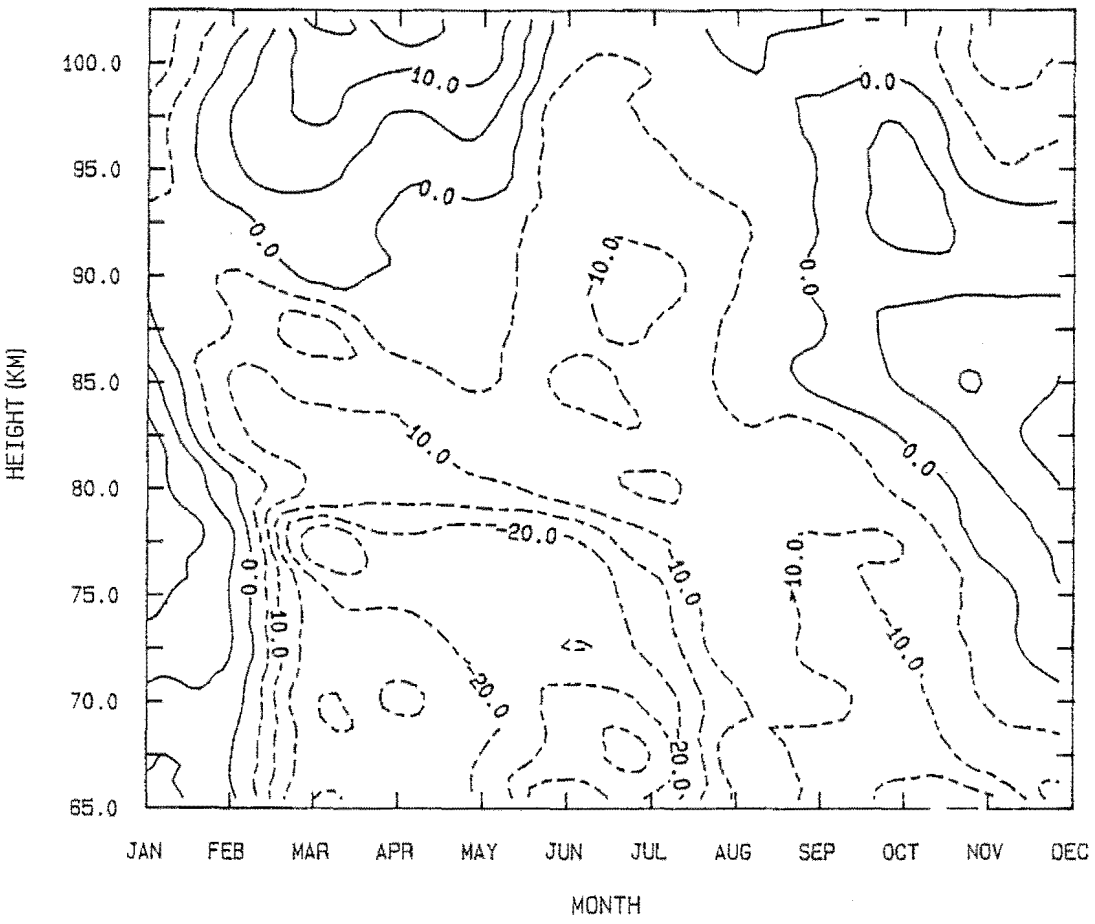

Monthly averaged meridional winds over Birdling s Flat in 1981. Northward winds are positive,southward winds are negative.

Figure 2.9

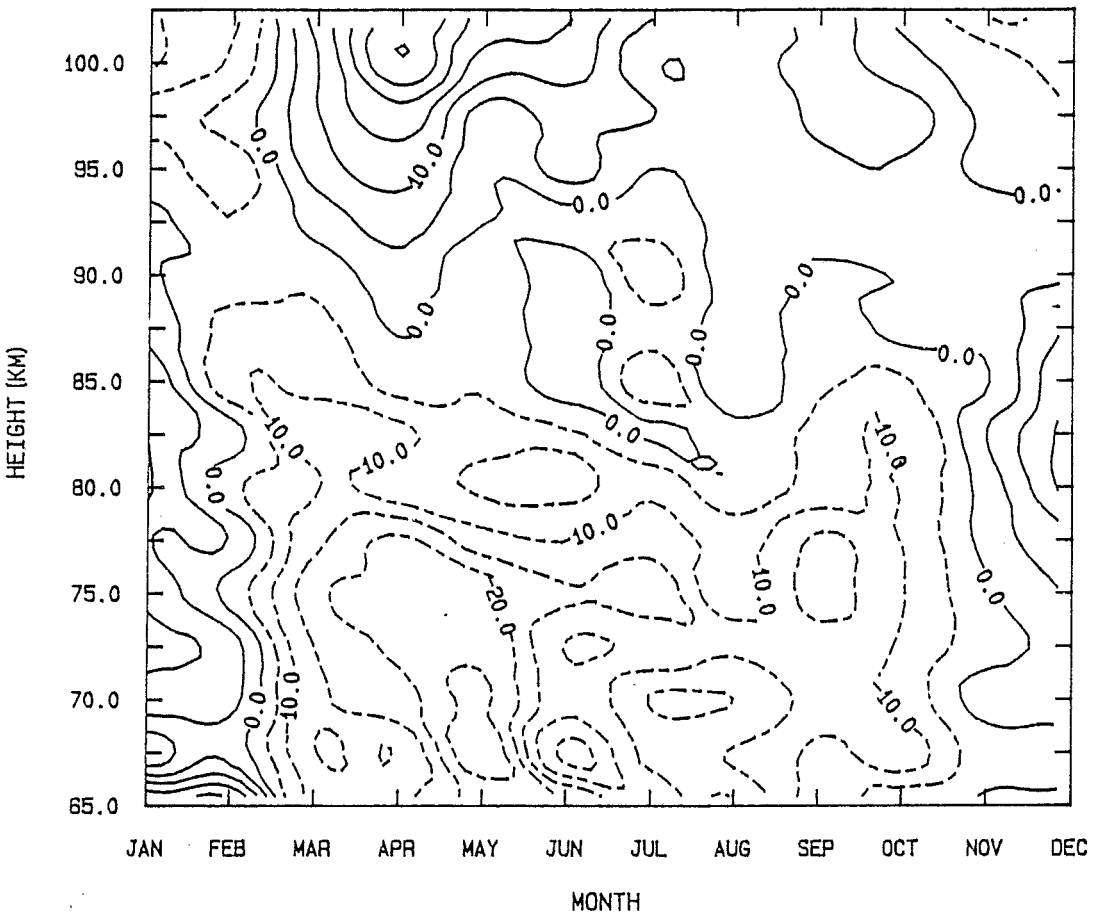

Monthly averaged meridional winds over Birdlings Flat in 1982. Northward winds are positive,southward winds are negative.

2.2 Other Motions in the Mesosphere.

Annual variations in the wind pattern were discussed in the last section. If one ignores long term climate changes, for which insufficient data has been gathered in the stratosphere and mesosphere, the longest time scale that needs to be considered is the one corresponding to the solar cycle. Although there is a connection between the solar cycle and particle activity, the effect of changes in solar output on the neutral atmosphere is harder to determine. Venne et al. (1983) looked for a connection between the solar cycle and the neutral atmosphere by comparing the 10.7 cm solar flux with 300 mbar winds. They concluded that the relationship was not statistically significant. However, studies at higher levels have produced positive results; always bearing in mind that Any time series involving stratospheric and mesospheric data has involved the use of very few solar cycles. Groves (1968) found that some variation of temperature with solar cycle was possible but not certain. Groves used data obtained over Fort Churchill in the early 1960's. Lindblad (1967 , 1968) found that atmospheric densities derived from meteor observations changed by a factor of 1.5 over a solar cycle. Sprenger and Schminder (1969) found changes in the wind system with the same period as the solar cycle. More recently Dartt et al. (1983) have found changes in the maximum wind strength in the 80 to 100 km region. They found that there are stronger winter eastward winds and weaker summer eastward winds during the solar maximum than those that exist in the transition years. The increasing length of the time series data available should furnish more information about the effects of the solar cycle on the dynamics of the mesosphere and lower thermosphere.

The quasi-biennial oscillation is a significant feature in the tropical stratosphere and it can also be seen at latitudes of 60N to 70N (Kats (1968 pp.68 to 70)). Coy (1979a) found that the period of the quasi-biennial oscillation varies from 2 to 2.5 years, while Quiroz (1981) found a value of the period of between 21 and 34 months. Eastward winds last for 12 months and westward winds for 15 months, on average, at 30 km. Similarly, Coy (1979a) found that the leading edge of the eastward shear zone is usually sharper than the leading edge of the westward shear zone. The quasi-biennial oscillation is strong in the equatorial stratosphere but is much weaker both above and below this region (Coy (1979a), Quiroz (1981)). Outside the tropics the quasi-biennial oscillation is weaker. However, Kats (1968, pp. 68 to 70) found an amplitude in the polar (70N,S) stratosphere (50 mb) of about 1K compared with the equatorial amplitude of about 2K at 50 mb. Amplitudes were very small in the middle latitudes. There is a downward phase propoagation of this oscillation with varying descent rates suggesting that there is a dynamical forcing by tropical waves (Quiroz (1981)). This is consistent with the theoretical calculations of Lindzen and Holton (1968), who model the quasi-biennial oscillation using upward propagating Kelvin and Rossby-gravity waves as the generating mechanism. This oscillation is of little relevance when the dynamics of the middle and high latitude mesosphere, mesopause and lower thermosphere are considered.

The semi-annual oscillation is strong near the equatorial tropical tropopause (Newell et al. (1972)) and in the equatorial upper stratosphere and mesosphere (Kats (1968)). Wallace (1973) and Kats (1968) both give detailed descriptions of the behaviour of the semi-annual wave in the equatorial regions; Crane (1979) has found a pronounced semi-annual oscillation throughout the global temperature field at upper mesosphere heights. There is an amplitude peak in the high latitudes. In the lower mesosphere and stratosphere there

are phase variations with latitude. McGregor and Chapman (1978) found amplitudes of 4K at the equatorial stratopause and up to 10K near the polar stratopause.

Up to this point discussion has been concerned with long period oscillations that affect the values of the mean monthly winds which are used throughout this thesis as the prevailing winds. These prevailing winds are primarily due to the annual changes discussed in the previous section.

In the rest of this section four types of motion will be discussed: planetary waves; tides; internal gravity waves; turbulence. Although it is convenient to divide atmospheric motions into separate components like this, interactions between types of motion do occur. For example, planetary scale wave motions affect the total background wind field which in turn causes critical layers for internal gravity waves.

Waves that have zonal wavelengths that are large fractions of the earth's circumference are commonly called planetary scale waves or Rossby-Haurwitz waves (after Rossby (1939) who developed the theory of planetary scale wave propagation on a beta-plane model of the earth and Haurwitz (1940) who developed planetary wave theory for a spherical earth).

There are various types of planetary scale waves. One type of planetary wave is the stationary wave which is associated with surface features, such as the distribution of oceans and continents, the temperature of the sea surface, topographic features and varying amounts of cloudiness (Houghton (1978)). Travelling planetary waves that have periods of longer than about 30-40 days can also be regarded as stationary planetary waves when studying monthly wind information.

Theoretical studies have been made of the conditions under which these waves will be vertically propagating. These studies indicate that the forced planetary scale waves are most likely to be vertically propagating in the wind system that typically occurs in the winter stratosphere (Charney and Drazin (1961), Dickinson (1968), Matsuno (1978) and Simmons (1974)). Furthermore, planetary waves with small zonal wavenumbers penetrate through the winter stratosphere far more easily than those with higher zonal wavenumbers. Therefore, longer zonal wavelength planetary waves are expected to dominate the spectrum of planetary waves in the middle atmosphere. Note that vertical propagation of waves implies either upward or downward transport of energy, depending on the direction of horizontal propagation and the phase tilt.

Satellite derived radiance measurements have greatly increased knowledge of the behaviour of planetary scale waves in the middle atmosphere. Hirota (1976) has compared stationary waves in both hemispheres. Van Loon and Jenne (1972) found that most of the variance of stationary waves was due to the first three zonal wavenumbers in the troposphere. Harwood (1975), Barnett (1977), Hirota and Barnett (1977), and Hartmann (1976) have all studied latitude and height variations of planetary scale waves. The amplitude of stationary planetary waves reaches a maximum near the stratopause (Barnett (1977), Hirota and Barnett (1977), Green (1972) and Hartmann (1976)). Above this height wave amplitudes decrease rapidly. The amplitude of forced travelling planetary waves behaves similarly. The meridional maximum of the amplitude of stationary waves occurs in the region of 60N to 70N (Labitzke (1980)). Stationary waves dominate planetary wave activity in the northern hemisphere, but travelling waves are more important in the southern

hemisphere (Chapman and Peckham (1980)).

Travelling planetary waves have a longer history of theoretical study than stationary waves. Laplace derived a tidal equation for oscillations in a thin layer of fluid surrounding a rotating sphere. Hough (1898) developed two sets of solutions for this equation. The first set corresponds to tides. The second set, called "oscillations of the second class", are a set of travelling planetary waves, usually labelled as being free modes.

Travelling planetary waves are particularly important in the southern hemisphere (e.g. Harwood (1975), Chapman and Peckham (1980)), where eastward travelling zonal wavenumber 2 modes dominate the winter planetary wave variance in the middle atmosphere (e.g. Harwood (1975), Burns (1980)). Harwood (1975) found a zonal wavenumber 2, eastward travelling planetary wave which, when it was travelling at a regular speed, had a phase shift of about 15½ degrees of longitude per day. Burns (1980) found a zonal wavenumber 2, eastward travelling planetary wave with a period of 5 days, which was also present in ionospheric data. Both waves were vertically propagating in the stratosphere. Some theoretical models do predict forced planetary waves. Simmons (1974) found eastward travelling waves forced by a stationary, transient, non-resonant feature. Northern hemisphere planetary wave activity is dominated by stationary waves. However, some vertically propagating travelling modes are seen in winter, Venne and Stanford (1979) have observed an eastward travelling, zonal wavenumber 1 mode with a period of 4 days in the winter polar stratosphere of both hemispheres. A westward travelling, zonal wavenumber 1 mode with a period of between 7 and 11 days has been seen in the northern hemisphere winter stratosphere (Venne

and Stanford (1979), Burns (1980)). Venne and Stanford (1979) and Chapman and Peckham (1980) show that power exists over a range of different wave periods. Chapman and Peckham (1980) find periods of 24, 12, 8, 6 and 4½ days for zonal wave number 1 in northern hemisphere winter data at heights corresponding to a pressure of 100 mb. Venne and Stanford (1979) find periods of 40, 16, 10 and around 4 days in the winter of both hemispheres for zonal wavenumber 1 at heights of between 30 km and 45 km (channel B23 on the nimbus-5 selective chopper radiometer). A westward travelling planetary wave which has a period of about 10 days and is upward propagating has been seen in summer in the stratosphere by Hirota (1976) and in the stratosphere and ionosphere by Burns (1980). The global extent of the 10-day wave suggests that, instead of being locally forced, this wave may be associated with a free mode, perhaps the H_3^1 mode (Burns (1980), Salby (1984)), which has a period of about 10 days in realistic zonal winds (see Dickinson and Williamson (1972)). The term H_m^n refers to the Hough function of a wave, where n is the horizontal wave number and m is the meridional wave-number. Schoeberl and Geller (1976) calculated that the H_3^1 mode could be vertically propagating in summer. If this happens the amplitude would increase in the regions where the wave is vertically propagating, which is consistent with observations of the 10-day wave at 30 km and 50 km. Although there are different periods for propagating waves in the middle atmosphere, all show a phase tilt with height that is consistent with the upward transportation of energy. Propagating planetary waves will transport energy from ground level to the stratopause.

As has already been mentioned, free oscillations are solutions to Laplace's tidal equation. In the real atmosphere

they are modified by wind and temperature variation, often making their identification with free oscillations difficult. One example of this is the 10-day wave discussed in the previous paragraph. However, some modes are easier to associate with free oscillations. A zonal wavenumber 1 mode with a period of about 5 days has been identified as the H_2^1 free mode (Rodgers (1976), Fraser (1977), Madden (1978a), (1978b),(1979), Burns (1980)). The vertical and meridional structures of this mode are identical with those expected for the H_2^1 mode that was modelled by Geisler and Dickinson (1976). Geisler and Dickinson found that realistic wind shears did not seriously affect the frequency or the horizontal structure of the H_2^1 mode. The summer zonal wind structure caused a large amplitude response in the mesosphere, possibly because the mode became locally propagating near the westward jet. Conversely, winter eastward winds tended to damp this mode in the stratosphere and mesosphere. Rodgers (1976) confirmed the predictions made by Geisler and Dickinson (1976) about the amplitude and phase of this mode near 50 km.

Another free mode that has been mentioned is a zonal wavenumber 1 wave, which has a period of about 16 days. Madden (1978a), (1978b), (1979) tentatively identified this mode with the H_4^1 free oscillation. The characteristics are similar: the horizontal structure compares well with that of the H_4^1 mode and the amplitude is greatest near 60N.

A travelling planetary wave with a period near 2 days was noted by Muller (1972) and by Kal'chanko and Bulgakov (1973). The period of this wave is near 51 hours in the northern hemisphere summer (Kingsley et al.(1978), Muller and Nelson (1978) using meteor winds). Coy (1979b) found a 2-day wave in tropical radiosonde data measured near the stratopause. Rodgers and Prata (1981) used satellite derived

radiances from the Nimubs satellites to give a description of the horizontal and vertical structures of this mode. Salby (1981) compared these results with the expected behaviour of the H_3^3 mode in realistic zonal wind shears and found a good agreement between theory and experiment. Craig et al. (1980) studied the structure of the 2-day wave using partial reflection drifts measurements at Birdlings Flat, Adelaide and Townsville. They concluded that the 2-day wave was a zonal wavenumber 3 mode with a period of about 48 hours in the southern hemisphere. Smith (1981) associated the features of this wave with the behaviour of the H_3^3 mode in realistic winds.

Apart from free modes, planetary wave activity decreases markedly in amplitude near the stratopause. Consequently, the effect of planetary waves in the mesosphere is much less important than the effect of atmospheric tides and internal gravity waves.

Atmospheric tides have been intensively studied over a relatively long period of time. As a result of this, the amount of literature on tides is very large. So a very general discussion is made, emphasizing, in particular, tidal activity over Birdlings Flat.

Tides are forced by either solar heating or by gravity. The amplitudes of the lunar gravitational tides are considerably less than those of the tides that result from solar heating. As lunar tides are much less important in terms of their effect on the earth's atmosphere, they will not be considered further in a discussion that aims primarily to investigate motions other than tidal motions. Solar tides have amplitudes of the order of between 10 and 20 ms^{-1} near the mesopause at Birdlings Flat (Smith (1981)). The amplitude of the semi-diurnal tide is generally greater than the amplitude of the diurnal tide because there is a Hough

function corresponding to a semi-diurnal tide that matches the solar heating distribution, whereas no diurnal tide Hough function matches the solar heating distribution very well. Also, the dominant diurnal mode at high latitudes is the (1, -2) trapped mode (Forbes (1983)). As this mode is evanescent, little amplitude growth occurs with height. Hence, the diurnal tide will tend to be suppressed compared with the semi-diurnal tide (e.g. Lindzen (1979) or Chapman and Lindzen (1970)). Satellite derived ozone and water vapour data have allowed more realistic tidal models to be developed in the last few years (e.g. Waterscheid and DeVore (1981), Groves (1983), Forbes and Garret (1980), Hong and Lindzen (1976) and Lindzen and Hong (1974). There is very good agreement between theory and observation for the semi-diurnal tide (Lindzen (1979) and Forbes (1983)). The diurnal tide is less amenable to accurate modelling as it has, for example, a wide frequency peak appearing in its power spectrum (Smith (1981)), that is, the phase of the diurnal tide is variable. Variations in amplitude will also broaden the peak. SEE ERRATA

Internal gravity waves are of smaller scale than the tides but they do have some features in common. These buoyancy waves are forced motions of the atmosphere, typically with horizontal scales from 10s to 100s of kilometres. In the mesosphere vertical scales are restricted by viscous damping to values of greater than 100 m at heights around 80 km, and to values greater than 1 km at heights around 100 km (Hines (1974)). The upper limit of vertical wavelength occurs when the wave is external, that is, there is no vertical phase shift with height. These external gravity waves have been seen by Hersé et al. (1980), who saw vertically evanescent waves with a horizontal wavelength of between 200 and 300 km and a period of about 15 minutes in

Jicamarca radar data. A simple mathematical model (Hines (1974) : see Appendix 1) gives an exponential increase of wave amplitude with height.

If a suitable damping mechanism is not in effect, then these waves will grow to an amplitude where the wave is no longer linear, and instabilities due to breaking will occur. Breaking is defined as the condition where the waves reach sufficiently large amplitudes to be unstable and to thus generate turbulence. Hodges (1969) suggested that the growth of internal gravity waves is sufficiently large in the mesosphere to be restricted by this mechanism. Turbulence will then limit the wave to at least a constant amplitude above the point of breaking. Hodges (1967) found that the observed velocity shear due to internal gravity waves was not sufficiently strong for the Richardson number (a measure of stability defined in Chapter 5) to decrease below ¼. The value of the Richardson number of ¼ is a commonly given boundary for the onset of turbulence (e.g. Miles (1961), Howard (1961)). Hodges (1967) calculated how the Richardson number behaves when wave amplitudes are large and found that the condition for the onset of turbulence was convective instability: the condition in which the temperature of the atmosphere decreases more rapidly with height than the adiabatic lapes rate giving a Richardson number of less than zero. Lindzen (1981) developed this concept further and showed how internal gravity wave breaking could produce drag on the mean flow.

Ball (1981) calculated variance profiles which showed that internal gravity wave amplitude was restricted to amplitudes below 20-30 m/s at heights below 80 or 85 km. Furthermore, these profiles showed no apparent amplitude restrictions above 85 km up to the highest heights measured. At the very least, this suggests that far less energy and

momentum loss takes place at heights above 85 km than takes place at heights below 85 km. Several ideas about this amplitude increase need to be tested. The first idea is that this amplitude increase represents a growth in wave amplitude of a wave unaffected by any amplitude restrictions other than molecular viscosity. The second problem is to see if there are any major seasonal changes in the variance plots, or to see if the variance plots change markedly from year to year. Any theory of internal gravity wave breaking is going to have to account for the seasonal and height changes, or lack of them, in the spectrum of the variance.

The question of the horizontal isotropy of internal gravity waves amplitudes has been investigated by Vincent and Stubbs (1977), Ball (1981), Vincent and Ball (1977) and Vincent and Ball (1981). A slight anisotropy was noticed in certain months at the latitude of Adelaide, however this did not consistently occur throughout the year (Ball (1981)). In a later chapter (Chapter 8), zonal-meridional wind vectors are plotted to gain an insight into any isotropic/anisotropic effects (preferred direction). Explanations for the observed behaviour of the preferred direction of internal gravity wave propagation are attempted in that chapter.

At this point it is worthwhile to discuss the effects of the breaking of internal gravity waves on the general circulation in the mesosphere and lower thermosphere. In Section 2.1 the problem of reconciling the observed temperature structure near the mesopause with the radiative energy input to the atmosphere was mentioned. The temperature structure that exists in this region must be maintained by heating due to subsidence in winter and by cooling due to a net rising motion in winter (Kellogg and Schilling (1951)). Wave energy transport also results in net heating or cooling (Plumb (1982)).

If the continuity equation is applied to those vertical velocities (equation 7.12, see Ebel (1974)) it can be seen that net vertical motion implies the existence of net meridional motion. The Coriolis acceleration acting on this meridional motion must be balanced by a wave induced drag (Houghton (1978), Holton (1982), (1983), Plumb (1982), Fritts (1984) etc.).

Plumb (1982) invoked wave eddy transport processes to balance the Coriolis acceleration. In summer the transport processes must be able to produce eastward torques to balance the Coriolis torque, while in winter westward torques must be produced, Plumb (1982) also stated that transport by planetary waves could not be the primary mechanism involved in balancing the Coriolis acceleration near the mesopause as the level of planetary wave activity is low in summer. Note that in the stratosphere the Coriolis torques are low in summer and the accelerations due to meridional transport of zonal momentum have the correct signs to produce drag opposing Coriolis accelerations (see Newell et al. (1972)).

The mechanism by which internal gravity waves produce the drag has yet to be discussed. Elford (1979) found that tides transported zonal momentum meridionally in summer but not in winter. In summer the sign of the resulting drag was such that the resulting accelerations opposed the Coriolis accelerations, but that the magnitudes of the accelerations produced were far too small to counter the Coriolis acceleration. The results in Chapters 7 and 8 do show that internal gravity waves are capable of transporting zonal momentum meridionally and thus cause accelerations. However,the signs of the accelerations caused by this transport are the same throughout the year. Furthermore, even in summer when the drag due to the meridional transport of zonal momentum opposes the Coriolis force, the acceleration due to eddy transport are of much smaller magnitude

than the Coriolis accelerations.

A much more suitable mechanism by which internal gravity waves can counter the Coriolis accleration is the vertical transport of zonal momentum. Below the height of breaking the vertical flux of zonal momentum is constant (Eliassen and Palm (1960). As internal gravity waves approach critical layers, this flux goes to zero (Fritts (1984)).

Lindzen (1981) made calculations of the acceleration that would result from changes in the vertical flux of zonal momentum at heights above the height at which the internal gravity wave breaks. The magnitudes of the resulting accelerations (135 m s^{-1} day^{-1} in summer and -102 m s^{-1} day^{-1} in winter) were large enough to balance the torque due to the Coriolis force. Vincent and Reid (1983) measured values for this flux for heights between 80 km and 90 km in May at Adelaide. They found values ranging from 10 to 20 m s^{-1} day^{-1}. Smith and Lyjak (1985) found residual acccelerations when terms other than internal gravity waves had been removed. This residual corresponded to drag due to internal gravity waves. They found that the residual acceleration required was around 25 m s^{-1} day^{-1} at 65 km in the middle latitudes. Numerical models have been used by Schoeberl et al. (1983)) and Apruzese et al. (1982) to estimate required accelrations due to internal gravity wave drag. Schoeberl et al. (1983) found values of the maximum acceleration required varying from 27 m s^{-1} day^{-1} to 178 m s^{-1} day^{-1}, depending on the mean velocity profiles used. Apruzese et al. (1983) required maximum zonal accelerations of 40 m s^{-1} day^{-1} at 80 km in the middle latitudues.

Models incorporating accelerations of about these values (e.g. Holton (1982), Dunkerton (1982)) produce reasonably realistic zonal wave saturation into a model of the general circulation of the middle atmosphere. Thus the gross features

of the mesospheric circulation can be explained when drag is incorporated into circulation models (Plumb (1982)).

Finally, some scales of motions have not been discussed. Acoustic waves are longitudinal waves with frequencies greater than the acoustic cut off frequency. Acoustic waves are not discussed further. Turbulence is the group of irregular motions that occur in the atmosphere and in other "fluids". Turbulence is seen to exist up to the turbopause which occurs at heights from 100 km to 110 km. However, the rocket data reported by Barat (1968) suggests that the turbulent motion is interspersed with non-turbulent motion below the turbopause. The possibility that this behaviour represents regions of internal gravity wave breaking is tantalizing, but insufficient information is available to draw any definite conclusions.

CHAPTER 3

THE DATA AND THE ANALYSIS OF THE DATA

3.1 Introductory remarks

The thrust of this thesis is primarily analytical in as much as no experiment was developed to obtain data. Therefore, experimental details become relevant only if they pertain to the analysis of the data. A full description of the drifts experiment can be found in Smith (1981).

The data can conveniently be divided into two types. Firstly, those that are measured "locally", that is at the University of Canterbury's two field stations that make drifts measurements. These are situated at Birdlings Flat (latitude 43.8°S, longitude 172.7°E) and at Arrival Heights (latitude 77.8°S, longitude 166.7°E). Secondly, there are the general atmospheric data, more specifically the CIRA (COSPAR (1972)) data. The data used from CIRA were mainly in the form of monthly mean temperatures and densities.

One major problem lies in equating data that come from different places: for example, various workers have indicated that there are major differences in stratospheric temperatures between the two hemispheres (e.g. Harwood (1975)). Another example is the difference between the scatter diagrams of u and v given for Scott Base and for Birdlings Flat in chapter 8.

3.2 Temperature data

The CIRA (COSPAR (1972)) temperature data are averaged around the first day of each month. This is one difference from the drifts data, which have, for convenience, been averaged to the centre of the month.

These CIRA (COSPAR (1972)) data use rocket derived temperature soundings. The techniques used include the use of falling spheres, grenade measurements and pressure gauge measurements. The error in the measurements of temperatures from grenade soundings is given as having a maximum value of less than 6K at 80 km. The error at 60 km is less than 2K. However, the error in the calculation of mean temperatures is going to depend upon the number of soundings and the amount of "noise". This "noise" consists of periodic and non-periodic motions with time scales less than the averaging period.

The problem of relating data from different places has already been mentioned in the previous chapter. The CIRA (COSPAR (1972)) data have been measured at a variety of different stations. However, no southern hemisphere data have been used in the temperature model from stations further south than Woomera (latitude $30^{\circ}57'S$, longitude $136^{\circ}31'E$). Thus the data from a latitude of 30° to the pole are comprised entirely of northern hemisphere measurements. Clearly, any differences that occur between the hemispheres may have major effects on models that are based on these data. Sehra and Hariharn (1981) have used rocket soundings along lines of approximately constant longitude, and have compared northern hemisphere data with southern hemisphere data. They have also compared readings at longitudes of between 40E and 80E with measurements made at longitudes of between 40W and 95W. There were insufficient stations operating at heights greater than 65 km between December and February to draw conclusions about the temperature structure of the southern hemisphere summer mesosphere. However, the use of ship launched rockets between June and August allowed fairly detailed temperature fields to be drawn in these months. The northern hemisphere winter temperature profile measured over the years from 1969

to 1971 (figure 3.1) is in good agreement with the profiles given by Houghton (1977) (figures 2.2 and 2.3) for the northern hemisphere winter. Houghton used CIRA (COSPAR (1972)) data and other data. Agreement between Houghton's (1977) temperature field and the temperature plots given by Sehra and Hariharn (1981) is also good in the northern hemisphere summer (figure 3.2) although there are more differences in summer than winter. Thus, the northern hemisphere temperature fields used by Sehra and Hariharn (1981) are reasonably reliable and by extension the southern hemisphere temperature fields are also probably reliable. However, this statement cannot be made without reservations. Two of the northern stations, Volgograd and Heiss Island, have been used in compiling the CIRA (COSPAR (1972)) temperature tables. The data used by Sehra and Hariharn (1981) do come from different years from CIRA (COSPAR (1972)) data. Hence the data are not entirely independent, but the large number of stations used by CIRA (COSPAR (1972)) and the different years used should imply that the data used by Sehra and Hariharn (1981) need not be typical of all northern hemisphere temperature data. Thus, as the northern hemisphere temperature data used by Sehra and Hariharn (1981) does seem to behave in a typical fashion, it is reasonable to assume that the southern hemisphere rocket data are fairly typical of the mean temperature field that is found in the southern hemisphere. The differences between the temperature structures of the two hemispheres have been discussed in the previous chapter, so that no useful purpose would be served by reiterating that discussion here except to say that significant differences do occur between the two hemispheres and that CIRA (Cospar (1972)) data reflect northern hemisphere conditions.

Sehra and Hariharn (1981) show that differences in temperature field may occur with longitude. However, as the data that Sehra and Hariharn use in the region between 40W and

Figure 3.1

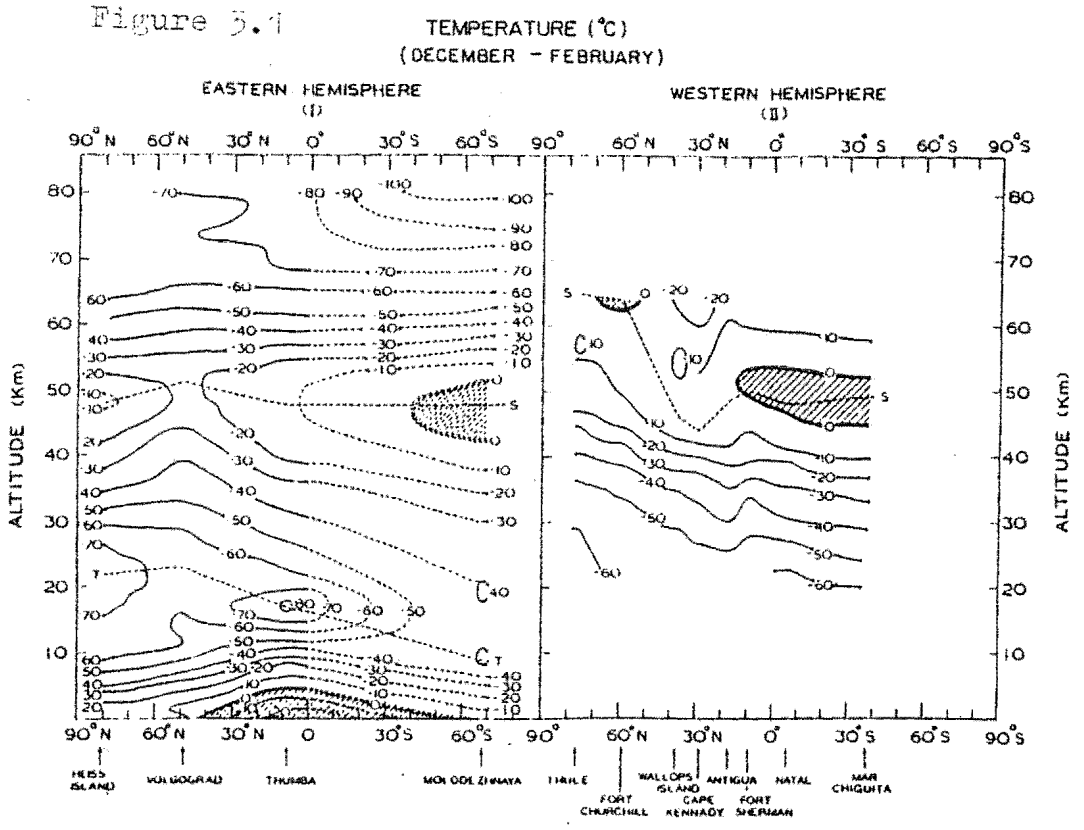

Temperature profiles for the December to February period(after Sehra and Hariharn(1981)).

Figure 3.2

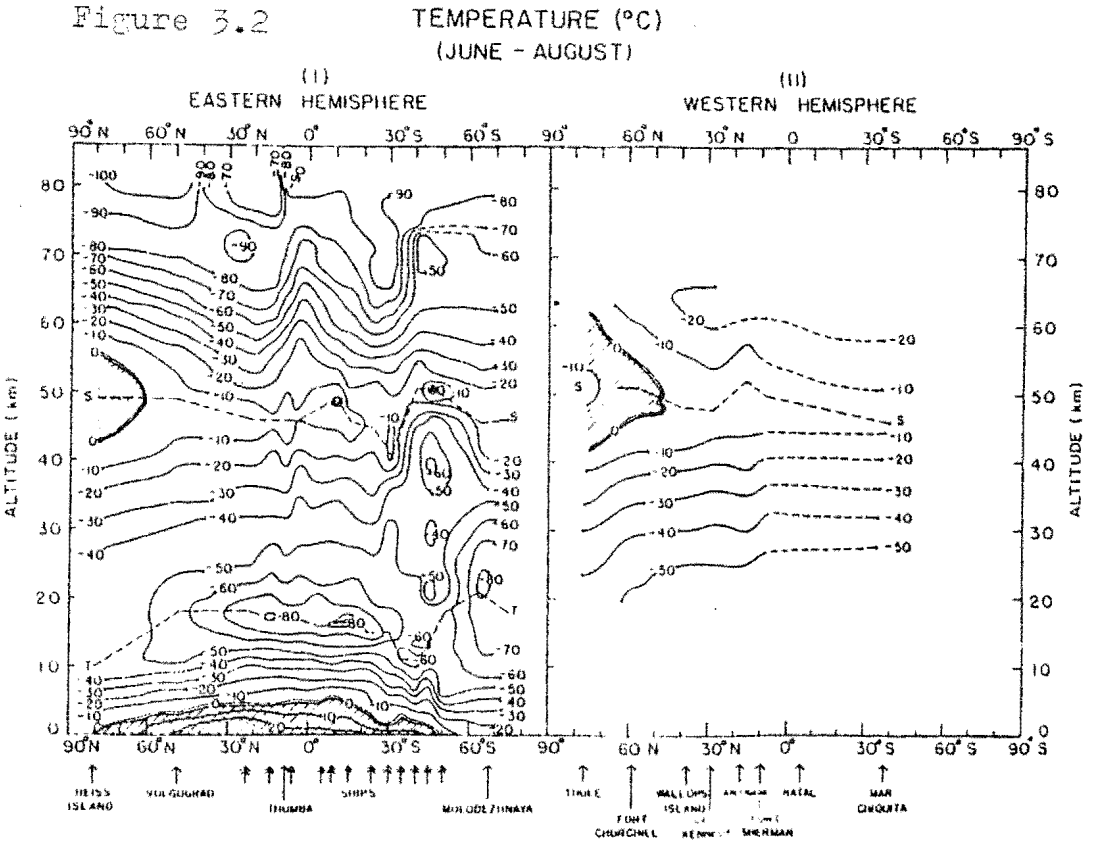

Temperature profiles for the June to August period (after Sehra and Hari rn(1981)).

95W do not extend to heights above 65 km to 70 km, most of these differences could possibly be explained as being due to stationary planetary waves, which would not be expected to penetrate much higher (e.g. Charney and Drazin (1961), Simmons (1974)).

Thus, the CIRA (COSPAR (1972)) temperature data used is expected to reflect northern hemisphere conditions rather than southern hemisphere conditions. Effects of these differences are mentioned in chapter 6.

3.3 CIRA wind and density data

There is no extensive use of CIRA (COSPAR (1972)) wind data in this thesis. Where possible locally determined mean zonal winds are used.

Zonal assymmetries are very noticeable in these wind data. The assymmetries are sufficiently large for CIRA (COSPAR (1972)) to publish separate data for different longitudes at heights between 25 km and 60 km. This effect is especially noticeable in winter. This last point suggests that the difference may be due to stationary planetary waves. If this is the case then the observed decrease in amplitude of these waves above about 65 km (Houghton (1978)) will lead to a far greater degree of zonal symmetry at heights above 65 km. Sehra and Hariharn (1981) also find such differences below 70 km : the maximum height of their wind data.

Clearly, if differences in winds occur around a line of latitude near the stratopause, then differences can also be expected between the hemispheres. This is indeed the case. The possibility that differences occur in the zonal winds at heights of between 65 km and 102.5 km at the latitude of Birdlings Flat has been discussed in the previous chapter. Some differences occur, but there are enough similarities to

permit the use of northern hemisphere wind data to model southern hemisphere winds between 65 km and 102.5 km provided that care is taken.

Density data are used in determining energies and momenta in chapters 7 and 8. There are no comparisons between the densities in the southern hemisphere and the densities in the northern hemisphere available. But, given the differences between the temperature fields in the two hemispheres, different density fields should also be expected.

Consideration has not been given to longer term climatic effects. The lack of long term data at these heights makes such discussion pointless.

3.4 Partial reflection drifts data

The partial reflection drifts data used in this thesis are measured at Birdlings Flat and Arrival Heights.

A full description of the drifts experiment is inappropriate as the work done in this thesis has involved the analysis of the data not the preparation of the experiment. However, the geometry of the receiving aerials may be important when considering the effects discussed in chapter 8. Similarly, the rejection criteria for the data is important, as is any justification for regarding the observed drifts of charge particles as being good indicators of the neutral winds in the D-region.

This last point has been checked by various workers by comparing partial reflection drift measurements with other wind measurements. The relative cheapness of the partial reflection drifts experiment, once the station has been established, compared with rocket based wind measurements means that, if the drifts do reflect the motion of the neutral atmosphere, the drifts experiment is a useful way of studying

the motion of the neutral atmosphere in the mesosphere and the lower thermosphere. Therefore, several workers have compared partial reflection drifts with other wind measurements in the D-region. Stubbs (1973) and Stubbs and Vincent (1973) have compared drift velocities from meteors with partial reflection drifts at Adelaide. They found good agreement between the two methods. Felgate et al. (1975) and Wright et al. (1976) have also compared meteor drifts with partial reflection drifts. Wright et al. (1976) found a high correlation between the two, and Felgate et al. (1975) found that the two were comparable. Vincent et al. (1977) compared partial reflection drifts with winds derived from falling spheres dropped by rockets that were launched at Woomera. These measurements overlapped in both space and in time. The agreement between the two techniques was good.

These measurements indicate that partial reflection drifts are a suitable method for determining the motion of the neutral atmosphere in the D-region.

The geometry of the Birdlings Flat partial reflection drifts experiment is given by Smith (1981) Fraser (1968). The receiving aerials are comprised of 3 dipole arrays forming a right angled isosceles triangle with two sides measuring 250 m (twice the wavelength of the signal). The arrays are aligned about 8 degrees off the north-south and east-west axes. The signal operates at a frequency of 2.4 Mhz and has a 30μs pulse width corresponding to a height difference of 4.5 km. The data are sampled at 2.5 km intervals. The full correlation analysis (Briggs et al. (1950), Phillips and Spencer (1955)) and other considerations about the analysis of the raw data are given by Smith (1981). The data from 8 heights are scanned over a period of 64 seconds with 20 to 25 minute average interval between scans (Smith (1981)). SEE ERRATA

The Arrival Heights experiment is set up in the form

of a right angled triangle. The data are sampled at 2 km height intervals from a height of 67 km up to a height of 97 km. A 2.9 Mhz signal is used and the pulse width is 30μs (Fraser (1984)).

Several criteria have been used to remove data that may be suspect. The time that the autocorrelation takes to fall to 0.5 is tested : a minimum value of 0.3 seconds is used so that phenomena associated with interference are removed (Smith (1981)).

The normalised time discrepency should be less than 0.2. Where the normalised time discrepency (NTD) is defined as

$$NTD = \frac{|\Sigma \tau_{ij}|}{\Sigma |\tau_{ij}|} \qquad (3.1)$$

The τ_{ij} are the time lags for maximum cross-correlation between aerials (Smith (1981)). In the numerator of equation 3.1 the time lags τ_{ij} are taken in cyclic order.

Assuming that the separation between antennae is defined as ζ_o in the x direction and η_o in the y direction, the apparent velocity V_a is defined by

$$\frac{1}{V_a^2} = \frac{\tau_x^2}{\zeta_o^2} + \frac{\tau_y^2}{\eta_o^2} \qquad (3.2)$$

where τ_x and τ_y are least squares fitted time delays (Smith (1981)).

The true velocity is defined as (Smith (1981))

$$V_{Tx} = \frac{(V_c')^2}{V_x'} \qquad (3.3a)$$

$$V_{Ty} = \frac{(V_c')^2}{V_y'} \qquad (3.3b)$$

V' is the apparent velocity corrected for anistropy.

$$V_a = V' \cos(\phi - \phi_a) \qquad (3.4)$$

The term ϕ_a is defined as

$$\phi_a = \tan^{-1}\left(\frac{\tau_y}{\tau_x}\right) \tag{3.5}$$

and ϕ is defined as

$$\phi = \tan^{-1}\left(\frac{V_{Ty}}{V_{Tx}}\right) \tag{3.6}$$

V_{Tx} and V_{Ty} are the x and y components of the true velocity. SEE ERRATA V'_c is defined as

$$V'^2_c \equiv \frac{\zeta_o^2}{\tau_{kx}^2} \tag{3.7}$$

for two antennae aligned in the x direction with a separation $(\zeta_o, 0)$. V'_c is the velocity that is needed if the fall off in the autocorrelation function is to be described solely in terms of the drift of a steady pattern. τ_{kx} is the time lag required for the autocorrelation to fall off to the same level as the space correlation between the two antennae. V_{ax} is the x component of the apparent velocity. Large velocities are eliminated, as faster velocities are associated with interference (Smith (1981)). The limits were set such that the true velocity must be less than 300 m/s and the apparent velocity must be less than 200 m/s

Given that

$$V_c^2 = V'^2_c - V_T^2 \tag{3.8}$$

where V_c^2 is called the characteristic velocity, it appears that V_c^2 cannot be less than zero. In other words, the square of the fading velocity, caused solely by the drift of a steady pattern, cannot be smaller than the square of the true velocity. However, in practice Fraser and Vincent (1970) have suggested that statistical fluctuations in V'_c and V_T may cause negative value of V_c^2. Thus the selection criterion used is V_c^2 SEE ERRATA must be greater than $-100\,m^2s^{-2}$. SEE ERRATA

Differences between the apparent velocity and the "true" velocity are taken into account by setting upper limits for $|\phi_a - \phi|$ of $\pi/2$ and for V_a/V of 3.

If the axial ratio is too large (say greater than 2) then the ellipse is elongated. This elongation may be caused by stray effects such as meteor trails (e.g. see Manson and Meek (1977)), thus these data where the axial ratio is too large,are rejected.

3.5 The short period (< 3 hour) filter

The analysis techniques used in this thesis are, on the whole, relatively simple. Such complexity as exists can be found in the maximum entropy method of spectral analysis, which is discussed in chapter 4, and to a lesser extent in the unsuccessful attempts to extract information about variations of wave amplitude with vertical wavelength (chapter 7).

Three hourly means were calculated for each month's data. These three hourly means were then subtracted from the raw data. Thus long period components were removed from the data. For comparison other filters with lengths of 2 hours, 4 hours and 6 hours were also tried.

The filter characteristics can be determined by taking the Fourier transformation of the convolution of the data with the filter. We define a filter

$$h(t) = \delta(t) - g(t) \qquad (3.9)$$

SEE ERRATA

where g(t) is defined as

$$g(t) = \begin{cases} \frac{1}{\tau} , & |t| \leq \tau/2 \\ 0 , & |t| > \tau/2 \end{cases} \qquad (3.10)$$

where the filter length is called τ.

Therefore, the Fourier transformation is

$$F(\omega) = \int h(t)*x(t)\exp(i\omega t)dt \ . \qquad (3.11)$$

Using convolutions and defining the Fourier transformations of h(t), x(t) and g(t) as $H(\omega)$, $X(\omega)$, and $G(\omega)$ the Fourier transformation is now

$$F(\omega) = X(\omega)(1 - G(\omega)) \qquad (3.12)$$

$G(\omega)$ is just

$$G(\omega) = \frac{\sin\left(\frac{\omega\tau}{2}\right)}{\left(\frac{\omega\tau}{2}\right)} \qquad (3.13)$$

The frequency response of the term $(1 - G(\omega))$ is given in figure 3.3. Thus figure 3.3 has defined the frequency response of the filtered data.

Given this filter response, the leakage of the filter can be considered. For convenience it is arbitrarily assumed that leakage is negligible when the filter power is down by an order of magnitude from the maximum filter power. This occurs for this filter when the frequency is about $1/(4\tau)$, that is, at a period of approximately four times the filter length. For a 3-hour filter this corresponds to a period of 12 hours, suggesting that contributions from the semi-diurnal tide are not of major importance, certainly not more than 2 m/s. Leakage at the frequency corresponding to the ter-diurnal tide occurs with the filter power at about $\frac{1}{5}$ of full power. Given the much lower amplitude of this wave compared with the diurnal tide, this contribution can have only a minor effect on the variance.

Similar checks can be made on the leakage that occurs when 2,4 and 6-hour filters are applied to the data. Obviously more leakage from the various tides is expected when the 4 and 6-hour filters are applied and less is expected

Figure 3.3

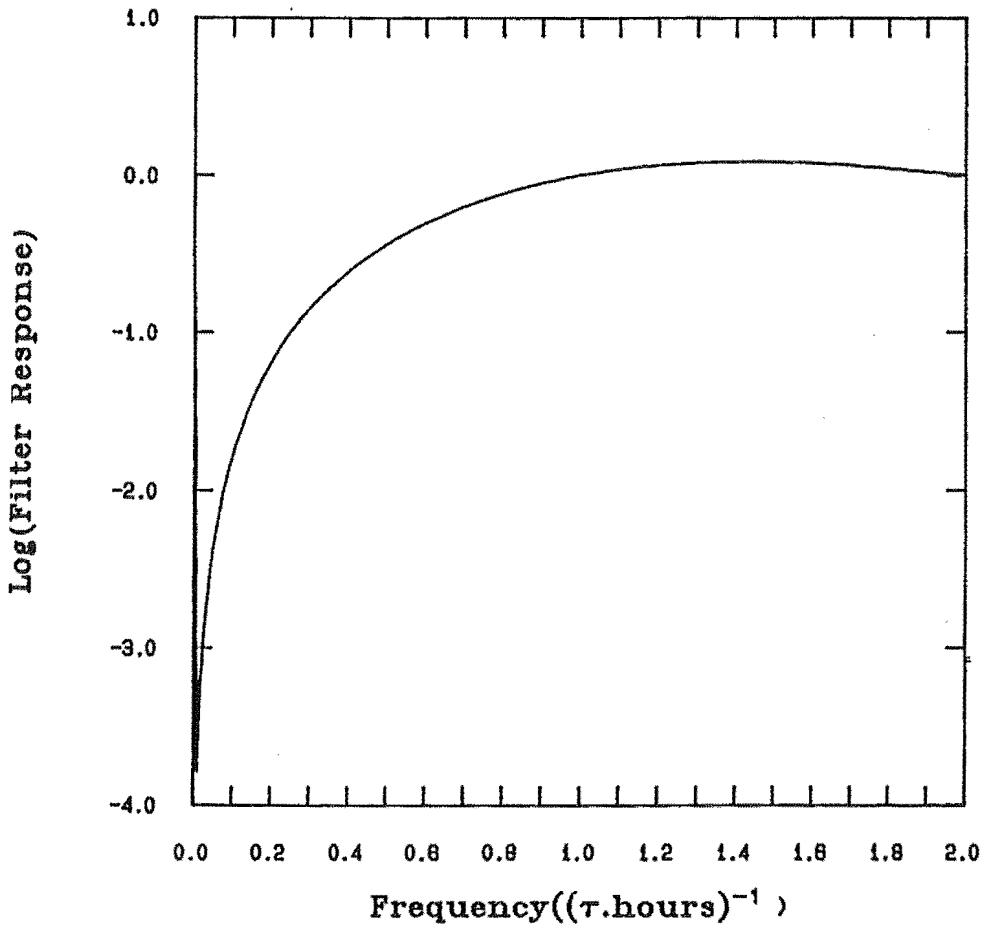

The filter obtained when τ hourly averages are subtracted from the raw data.

when the 2-hour filter is applied. Variance plots made for data using the 4 and 6-hour filters are not very different in shape from those made for data using a 3-hour filter (see chapter 7). Only small changes in amplitude occur.

All analysis of data "at internal gravity wave frequencies" was done for these filtered data.

3.6 Reasons for choosing a 3 hour filter

The choice of the range of this filter (<3 hours) was made as a compromise between finding the shortest period possible and using a sufficiently large number of data to calculate reasonably stable means. Typical days of data are given in tables 3.1 and 3.4. These days were picked by selecting one day of the month and calculating the number of data that occurred during each hour. The day used in December was the 22nd rather than the 11th because no data was available on December 11th 1981. Readings were taken at heights below 80 km in the daytime only. However, very few echoes occur outside these hours. A 2 hour filter might have been sufficient, but it was felt that the greater number of points was important in a situation where means are being subtracted from the points used to construct the mean. The reasons for this are as follows: When the τ hour mean is subtracted from the raw data, an uncertainty due to the calculation of the mean $SZ_{\alpha/2}/\sqrt{N}$ is introduced (see equation (3.31). Some of the standard deviation may be due to uncertainties that occur in the drifts experiment.

Possible uncertainties in the winds are discussed by Fraser (1968). These uncertainties cannot be separated from the uncertainties due to atmospheric motion. While a large enough set of τ hour samples reduce the effect of this uncertainty it is still desirable to reduce the value of this uncertainty in each τ hour sample,especially in cases where only a small number

For tables 3.1 to 3.4 see

APPENDIX I

of samples are considered such as the variance in specific directions that is discussed in Chapter 8. If an arbitrary cut-off value for the desirable sample size of 4 is assigned, the effects of using 2 and 3 hour averages can be considered. A filter length of much longer than 3 hours leads to added complications due to leakage from tides. April 11th 1981 is considered. Periods when the number of points were zero or one are not used because removal of means leaves no signal in these cases. For 45% of the 2 hour averaging periods used on this day, 4 or more points were found. In 64% of the 3 hour averaging periods 4 or more points occurred. Thus the reliability of individual τ hour periods increases markedly when the period is raised from 2 to 3 hours. As the total number of points remaining is the same in each case, the error is thus reduced. When 5 to 8 hour and 8 to 24 hour periods were considered, 2 hour averages were used to obtain a more convenient Nyquist frequency ($f_N = \frac{1}{2\Delta t}$). As the uncertainties in the 2 hour averages appear as high frequency noise, the band pass filter acts to reduce these uncertainties.

3.7 Simple subtractive band pass filters

Other filters were used to obtain other period ranges. The analysis of data in the tidal range requries a filter that will isolate motions with periods of between 8 and 24 hours. The first filter that was used to isolate this period range was a simple one involving the subtraction of daily means from 8 hour means. There are two major problems with this filter.

The first problem is one that is going to occur in any filter used to isolate this period range at Birdlings Flat. The problem is that very little data is obtained below 85 km at night. Consequently, the period range

between 8 and 24 hours was studied only at heights of 85 km and above.

The second problem relates specifically to the filter that is being used. This is the frequency response that is obtained when 24 hour averages are subtracted from 8 hour averages. The response of the filter can be calculated using two square filters.

Where

$$g_1(t) = \begin{cases} \frac{1}{\tau_1} , & |t| \leqslant \tau_1/2 \\ 0 , & |t| > \tau_1/2 \end{cases} \qquad (3.14)$$

Similarly

$$g_2(t) = \begin{cases} \frac{1}{\tau_2} , & |t| \quad \tau_2/2 \\ 0 , & |t| > \tau_2/2 \end{cases} \qquad (3.15)$$

So that $g_1(t)*x(t)$ and $g_2(t)*x(t)$ defines the application of these square filters to the raw data. Subtracting one square filter from the other gives the filtered data $h(t)*x(t)$. Thus

$$g_1(t)*x(t) - g_2(t)*x(t) = h(t)*x(t)$$

where $\tau_1 < \tau_2$ and $*$ implies a convolution.

Therefore the Fourier transform of this filter is

$$(G_1(f) - G_2(f))X(f) = H(f)X(f) .$$

The G_i are defined by

$$G_i(f) = \frac{\sin\left(\frac{2\pi f\tau_i}{2}\right)}{\left(\frac{2\pi f\tau_i}{2}\right)} \qquad (3.16)$$

Thus $H(f)$ is defined as

$$H(f) = \frac{\sin\left(\frac{2\pi f\tau_1}{2}\right)}{\left(\frac{2\pi f\tau_1}{2}\right)} - \frac{\sin\left(\frac{2\pi f\tau_2}{2}\right)}{\left(\frac{2\pi f\tau_2}{2}\right)} \qquad (3.17)$$

The filter response function is given for τ_1 = 8 hours and τ_2 = 24 hours in figures 3.4 and 3.5. Several points are apparent from these figures. Firstly, no signal gets through this filter from motions with a period of 8 hours and only 43% of the amplitude is passed for motions with a period of 12 hours. Just over 80% of the amplitude is passed for motions with a period of 24 hours and considerable leakage occurs from lower frequencies. For example, between 20% and 30% of the amplitude of the 2 day wave would be passed. There is also some leakage from high frequency motions.

A 5 to 8 hour filter of this sort has similar problems (see figures 3.6 and 3.7).

3.8 Least squares band pass filtering

Obviously a filter like those described above cannot be said to isolate the period range given, so another type of filter needs to be considered. A least squares filter of the type described by Behannon and Ness (1966) was used as a band pass filter to pass the frequency ranges required.

The weights of a low pass filter are given by Behannon and Ness (1966) as

$$L_k = \left[\frac{\cos\pi kh}{1-4k^2h^2}\right] \left[\frac{\sin\pi k(P+h)}{\pi k}\right] \quad , k \neq 0 \qquad (3.18a)$$

$$L_o = P+h \qquad (3.18b)$$

Where P is the cut-off frequency given in terms of the Nyquist frequency ($f_N = 1/(2\Delta t)$) so that $P = f_{cut\text{-}off}/f_N$, h is the half amplitude width of the cosine terminator of the square filter and h is also expressed in terms of the Nyquist frequency, $h = f_{half\ amplitude}/f_N$.

There is a pole in L_k ($L_k \to \infty$) when $k.h = \frac{1}{2}$. L'Hopital's theorem is used to evaluate $\frac{\cos\pi kh}{1-4k^2h^2}$ in this case

Figure 3.4

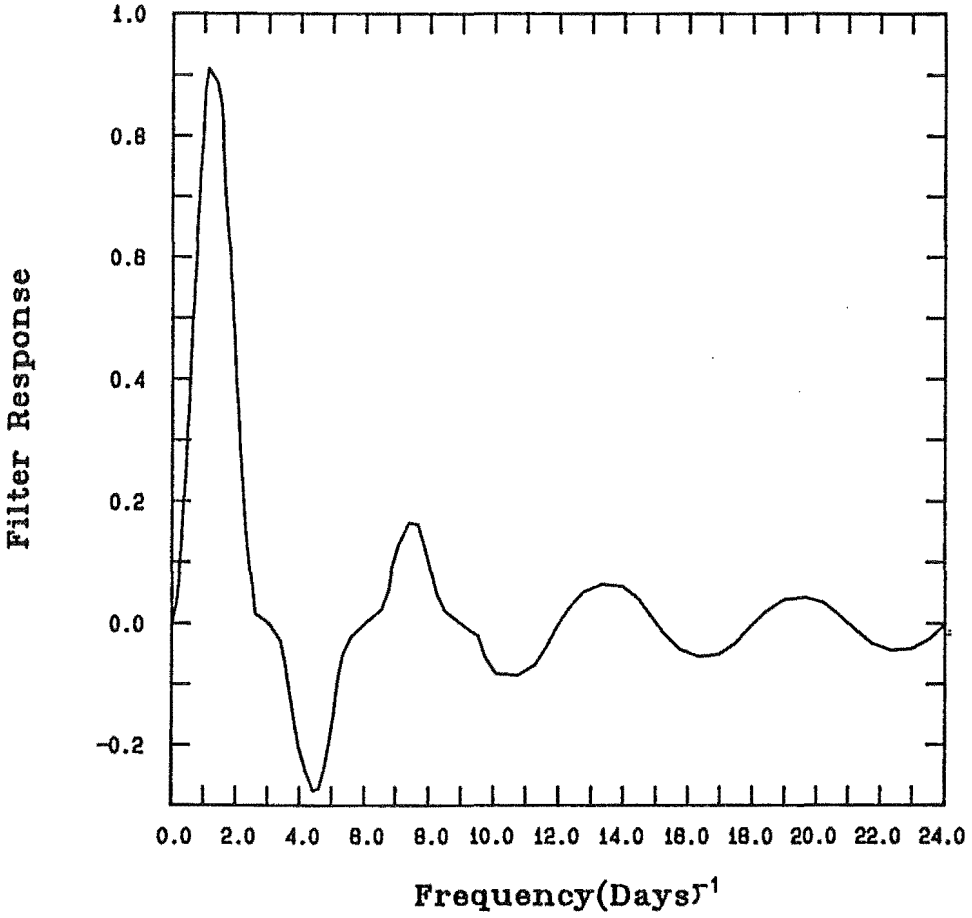

The filter obtained when 24 hourly averages are subtracted from 8 hourly averages.

Figure 3.5

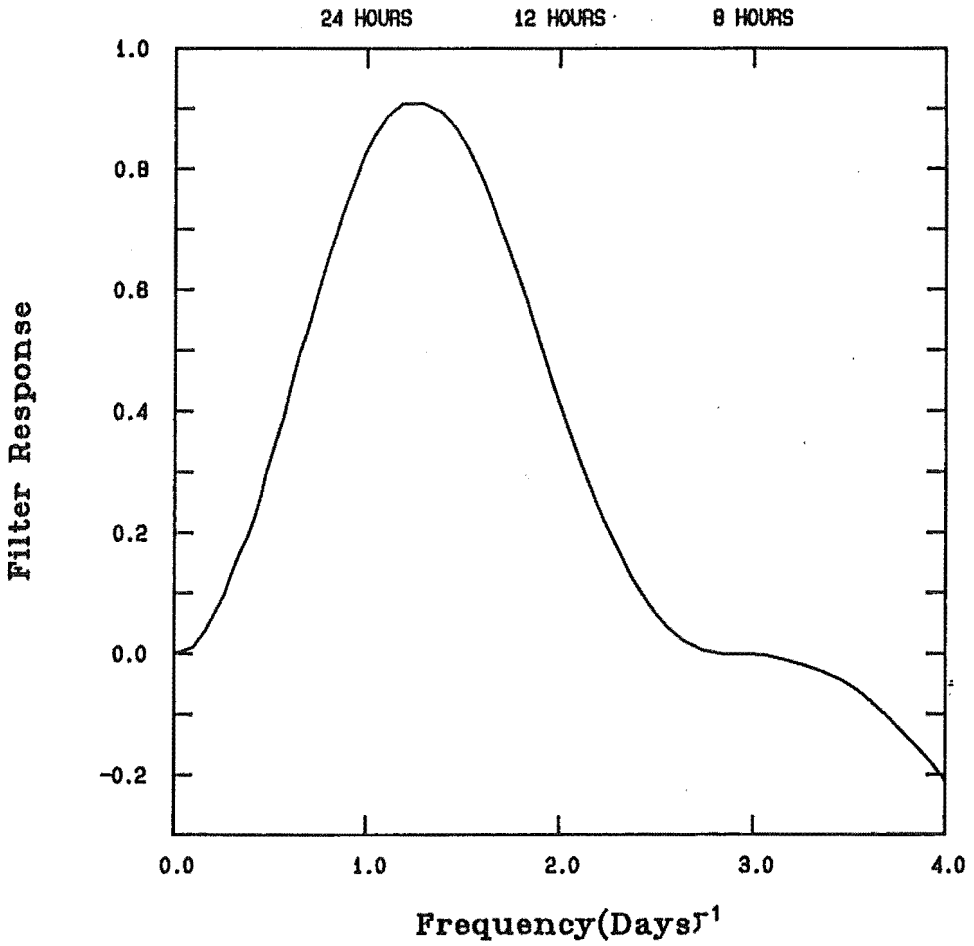

The filter obtained when 24 hourly averages are subtracted from 8 hourly averages. Only frequencies of up to 4 cycles per day are included for clarity.

Figure 3.6

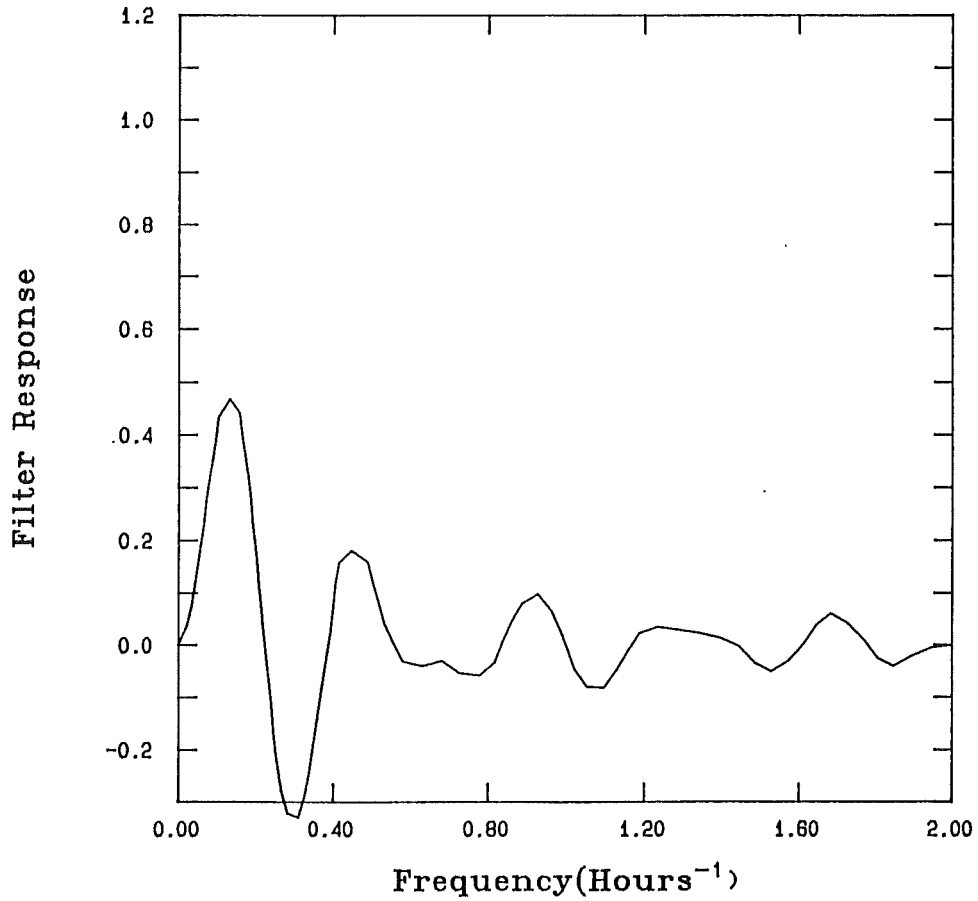

The frequency response of the filter that is obtained when 8 hour averages are subtracted from 5 hour averages.

Figure 3.7

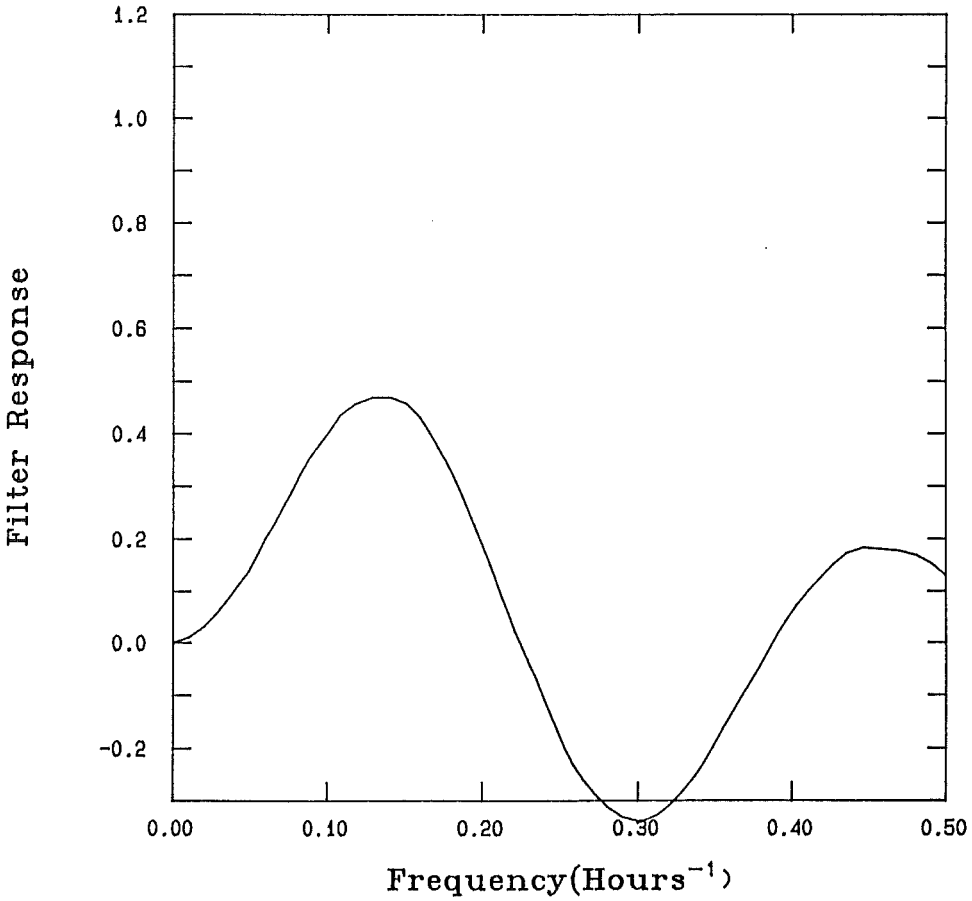

The frequency response of the filter that is obtained when 8 hour averages are subtracted from 5 hour averages. Only periods of more than 2 hours are included for clarity.

(Behannon and Ness (1966)). The value of $\frac{\cos kh}{1-4k^2h^2}$ is then π/k.

These filter weights must be normalised. Behannon and Ness (1966) suggest that this can be done using

$$W_k = L_k + \frac{\Delta}{2N+1} \tag{3.19}$$

where N is the number of filter weights and Δ is defined by

$$\Delta = 1 - (L_o + 2\sum_{k=1}^{N} L_k) \tag{3.20}$$

A low pass filter can be converted into a band pass filter by multiplying the filter in the frequency domain by an exponential (shift theorem) so that

$$W_k^{\text{Band pass}} = 2\cos(\pi kq/f_N) W_k^{\text{Low pass}} \tag{3.21}$$

The filter is now centred at a frequency q.

The frequency response of the Behannon and Ness (1966) filter can be calculated from

$$W(p) = W_o + 2\sum_{k=1}^{N} W_k \cos(\pi kp) \tag{3.22}$$

where p is defined as $p = f/f_N$.

The filter responses for the Behannon and Ness (1966) filters acting on 2 hour averages are given in figure 3.8 for the 5 to 8 hour filter and figure 3.9 for the 8 to 24 hour filter.

In both cases the side bands are small despite the small number of filter weights used (N = 10). The worst effect is the leakage of almost 15% from mean motions for the 8 to 24 hour filter which is a little larger than desirable. However, at the heights at which this 8 to 24 hour data is discussed, this represents an error of at most about 3 m s^{-1} and usually considerably less. Leakage is less than 30% for periods greater than 45 hours or less than 7 hours with leakage decreasing rapidly beyond these boundaries. However, leakage is still 20% at 48 hours ; a possible source

Figure 3.8

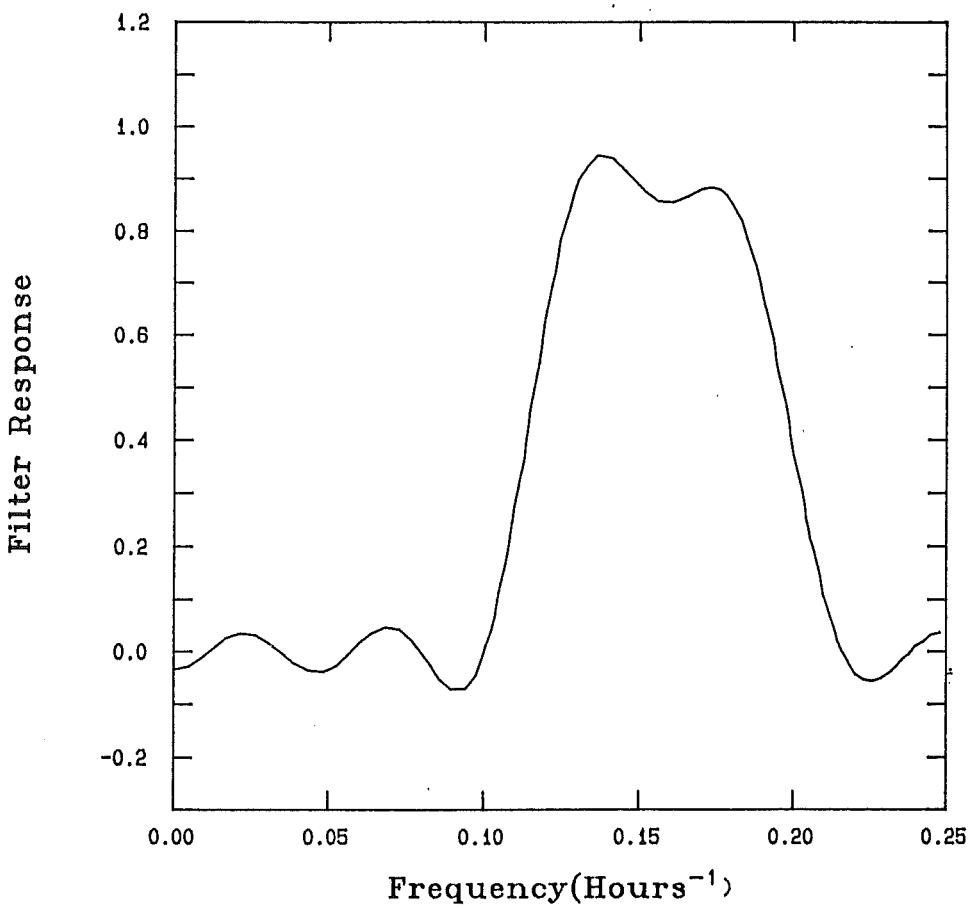

The frequency response of the filter that is obtained obtained when a Behannon and Ness bandpass filter is applied to 2 hourly averaged drifts data. The Behannon and Ness filter passes motions with periods of between 5 and 8 hours.

Figure 3.9

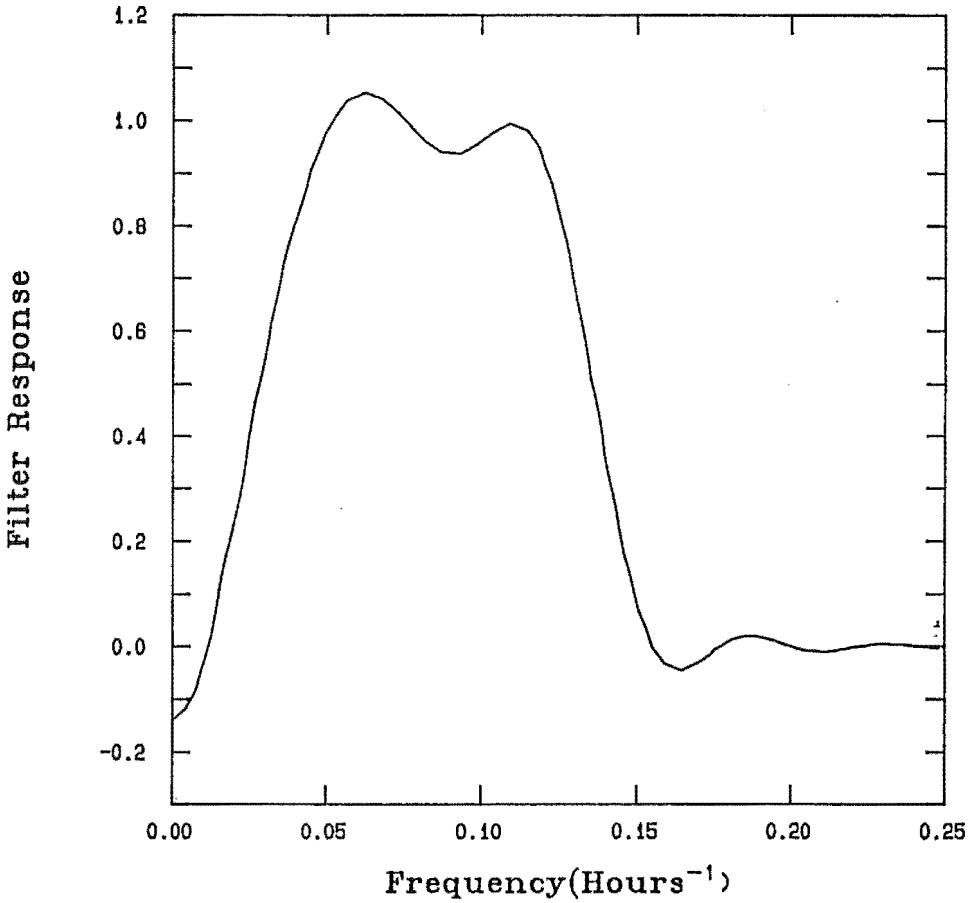

The frequency response of the filter that is obtained obtained when a Behannon and Ness bandpass filter is applied to 2 hourly averaged drifts data. The Behannon and Ness filter passes motions with periods of between 8 and 24 hours.

of error when the 2 day wave is present (see Chapter 2). In the 8 to 24 hour band itself over 90% of the signal is passed at all frequencies.

Truncation is more of a problem for the 5 to 8 hour filter with only 40% of the signal being passed at a period of 5 hours. This percentage increases to 80% at a 5½ hour period. About 80% of the signal is passed at 8 hours, and greater percentages of the signals are passed at periods between 5½ and 8 hours. Approximately 30% of the signal is passed at about 8.7 hours and about 4.9 hours. Only a very small percentage of the signal (< 10%) is passed for periods greater than 9 hours and less than 4.6 hours, so leakage is not a problem for this filter.

Thus both of these filters pass a useful percentage of the signal in the band that they are quoted as passing.

3.9 The long period filter

The filter response for the filter labelled "periods greater than 1 day" still needs to be considered. Monthly mean winds were subtracted from the individual wind data over this month for this filter. The resulting data were then averaged over daily intervals. This filter is not equivalent to the filter used earlier to subtract 24 hour averages from 8 hour averages (and 8 hour averages from 4 hour averages). The filter labelled periods greater than 1 day are as follows:

Firstly, the filter $(\delta(t)-g_2(t))$ acts on the data $x(t)$, where $\delta(t)$ is the impulse function and $g_2(t)$ is defined as

$$g_2(t) = \begin{cases} 1/\tau_2 , & |t| \quad \tau_2/2 \\ 0 , & |t| > \tau_2/2 \end{cases}$$

and τ_2 varies from 28 days to 31 days.

Thus the first filter is

$$(\delta(t) - g_2(t)) * x(t) \tag{3.24}$$

where * is the convolution of the first two terms with the third.

The daily averages of the resulting data are calculated to obtain a filter function $h(t)*x(t)$

$$h(t)*x(t) = (g_1(t)*g_1(t)*g_2(t))*x(t) \tag{3.25}$$

where $g_1(t)$ is defined by

$$g_1(t) = \begin{cases} \frac{1}{\tau_1} & , \ |t| \leq \tau_1/2 \\ 0 & , \ |t| > \tau_1/2 \end{cases} \tag{3.26}$$

and the period τ_1 = 1 day.

The Fourier transform of this process is

$$H(f)X(f) = (G_1(f) - G_1(f)G_2(f))X(f) \tag{3.27}$$

where the $G_i(f)$ are defined as

$$G_i(f) = \frac{\sin(2\pi f\tau_i/2)}{(2\pi f\tau_i/2)} \ . \tag{3.28}$$

Thus $H(f)$ is defined as

$$H(f) = \frac{\sin(2\pi f\tau_1/2)}{(2\pi f\tau_1/2)} - \frac{\sin(2\pi f\tau_1/2)}{(2\pi f\tau_1/2)} \cdot \frac{\sin(2\pi f\tau_2/2)}{(2\pi f\tau_2/2)} \tag{3.29}$$

The response function for this filter, with τ_1 = 1 day and τ_2 = 30 days, is given in figures 3.10 and 3.11. Two points are worth noting here.

Firstly, this filter suffers from similar problems to the other filters that involved the subtraction of averages, however for several reasons these problems are not so important in this case. Large side bands occur. The strongest of these bands are centred on frequencies of about 1.3 days^{-1} and about 2.3 days^{-1}. However, at the tidal

Figure 3.10

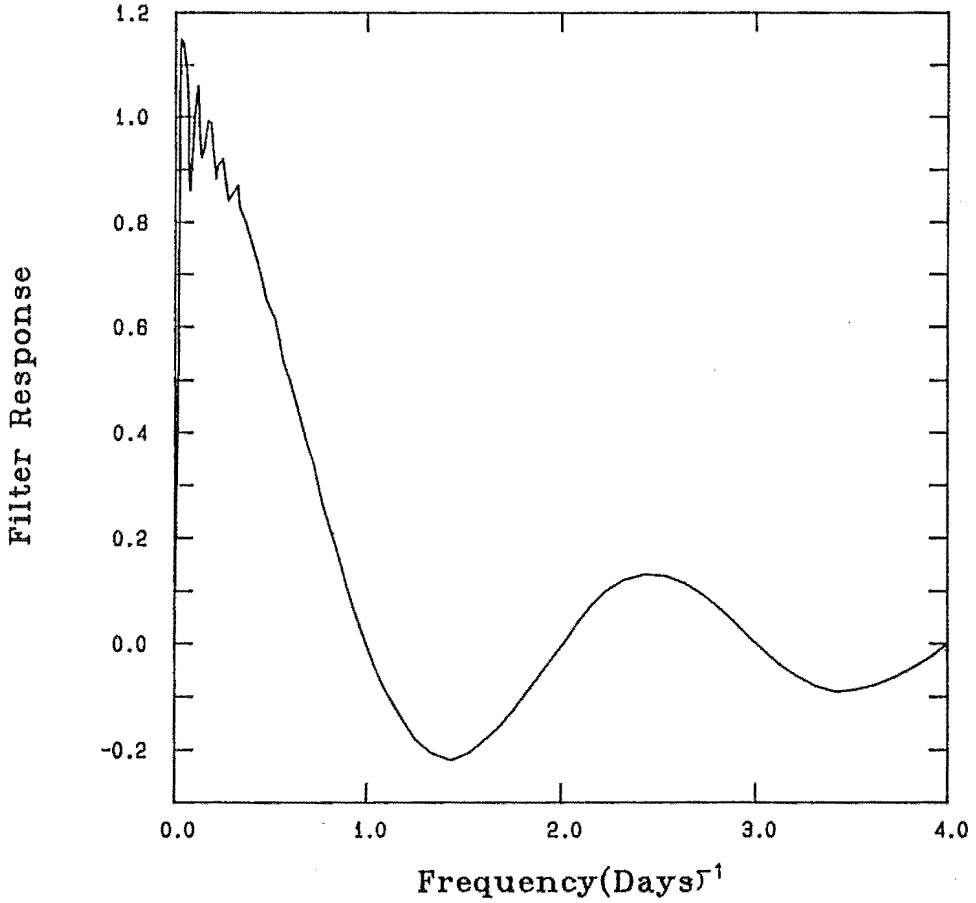

The filter obtained when 30 day averages are subtracted from 24 hour averages. Only frequencies of up to 4 cycles per day are included for clarity.

Figure 3.11

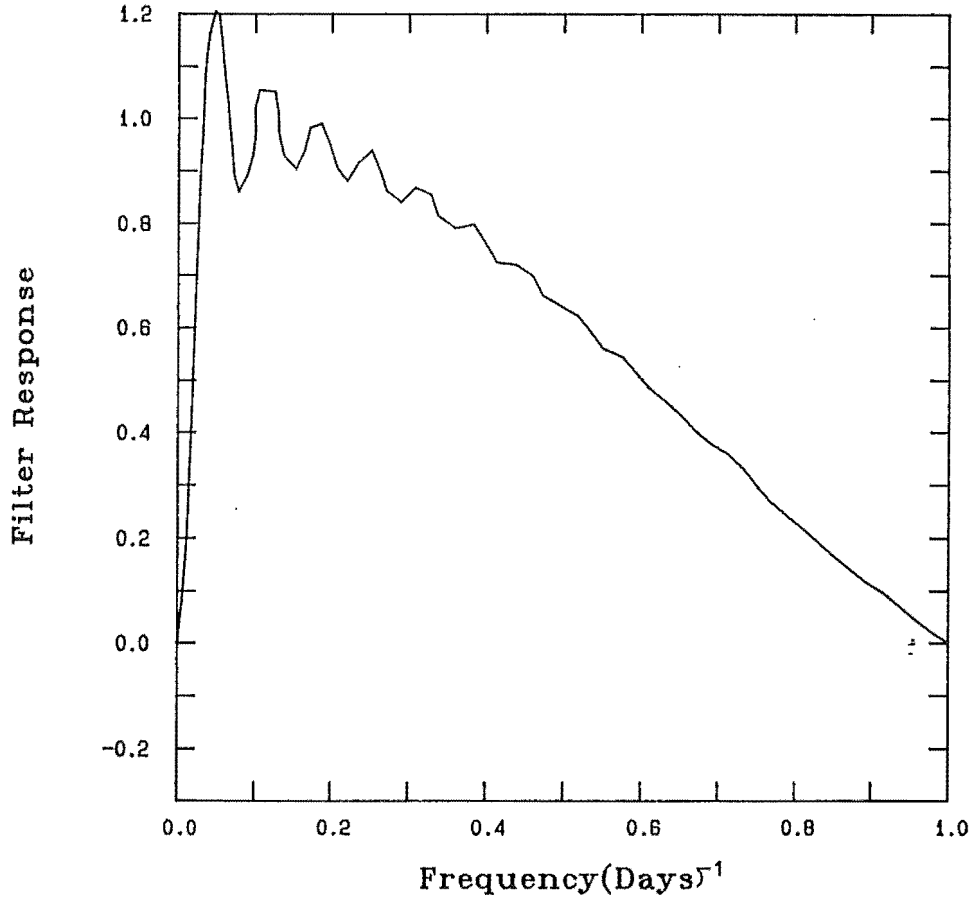

The filter obtained when 30 day averages are subtracted from 24 hour averages. Only frequencies of up to 1 cycle per day are included for clarity.

frequencies of 1 day^{-1}, 2 $days^{-1}$ and 3 $days^{-1}$ the response of this filter is zero, so that leakage from known tidal modes is not important. Another problem is that a steady decline is found in the percentage of the signal passed from 80% at 0.4 $days^{-1}$ to 0% at 1 day^{-1}. However, the aim of this filter is to isolate planetary scale motions and the only documented planetary scale wave that occurs in this frequency range is the "2 day wave" (see Chapter 2 for references). This is the major fault of this filter: only 60% of the signal is passed at a period of exactly 2 days.

Secondly, over 80% of the signal is passed for all frequencies between 0.03 $days^{-1}$ and 0.4 $days^{-1}$. Thus, apart from the "2 day wave", all but the longest period travelling planetary waves will be adequately represented by this analysis.

3.10 Independence of the data

Applying a filter affects the independence of the data. The uncertainties in equation 3.31 and 3.32 include the number of independent points. Blackman and Tukey (1958) give the number of degrees of freedom that occur when a filter is applied as

$$d.f. = N\Delta f_{filter}\, 2\Delta t \qquad (3.30)$$

Where N is the number of points, Δf_{filter} is the width of an equivalent "ideal" filter that is square in the frequency domain and t is the sampling interval. When no filter is applied, equation 3.30 becomes $N\frac{2\Delta t}{2\Delta t} = N$ as required. Similarly if the bandwidth of the filter is zero then no information is available about the spectrum.

3.11 Uncertainties in parameters

The uncertainties given for mean winds are calculated from the confidence intervals given by Jenkins and Watts

(1968), as

$$\pm \sigma Z_{\alpha/2} / \sqrt{N} \tag{3.31}$$

where σ is the standard deviation, $Z_{\alpha/2}$ is the two-tailed $1-\alpha$ confidence interval for a normal distribution and N is the number of independent points in the sample.

The uncertainties in the correlations can be found by using the variables for the sample (Bendat and Piersol (1971, p.128))

$$W_{\mu} = \tfrac{1}{2} \ell n \frac{1+r_{xy}}{1-r_{xy}} \tag{3.32}$$

which has a standard deviation

$$\sigma = 1/\sqrt{(N-3)} \tag{3.33}$$

where r_{xy} is the sample correlation coefficient and N is the number of independent data points. The confidence interval for μ_w the mean of w is

$$w_{\mu} + Z_{\alpha/2} / \sqrt{N-3} < \mu_w < w_{\mu} - Z_{\alpha/2} / \sqrt{N-3} \tag{3.34}$$

The upper and lower estimates of μ_w can be calculated if the sample correlation is known. These values of μ_w can then be used to calculate the upper and lower estimates of the correlation ρ_{xy}

$$\rho_{xyupper} = \frac{\exp(2\mu_{w+})-1}{\exp(2\ _{w+})+1} \tag{3.35}$$

and

$$\rho_{xylower} \quad \frac{\exp(2\mu_{w-})-1}{\exp(2\mu_{w-})+1} \tag{3.36}$$

3.12 Pulse retardation and biases introduced by data selection

A point that needs discussion is the effect of pulse retardation on the heights quoted for the data in this thesis.

Figure 3.12

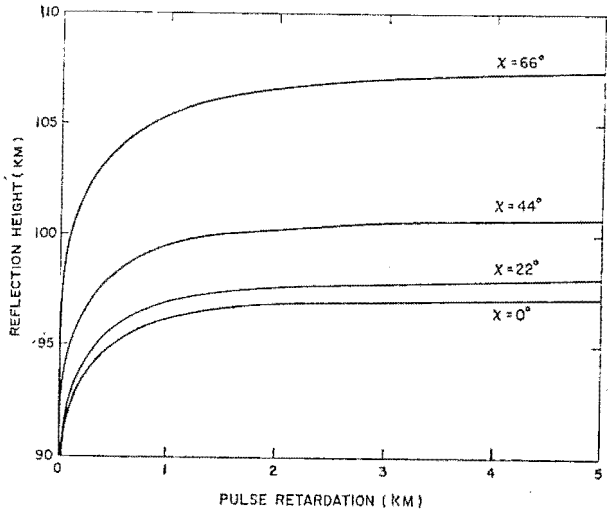

Pulse retardation of a 2.4 Mhz pulse vertically incident on an α-Chapman layer which has a critical frequency of 3.54 MHz. The scale height is 8 km and the height of maximum electron density for an overhead sun is 108 km. The gyrofrequency is 1.6 MHz and the geomagnetic field is inclined at 22^{o} to the vertical (Fraser and Kockanski (1970)).

Fraser and Kochanski (1970) have considered the effects of pulse retardation on the heights of the drifts experiment at frequencies of 2.4 Mhz at Birdlings Flat. In winter there is no problem as the maximum retardation at noon is less than ½ a kilometre (see figure 3.12). At the equinoxes the solar zenith angle is about 44^{o} so that a systematic error is introduced at 100 and 102.5 km around noon, when the actual height is less than 100 km. In summer this effect is important over a larger part of the day and includes measurements down to 97.5 km. Using values from throughout the day reduces the importance of pulse retardation, but the values given in summer for heights 102.5 km and 100 km in particular should be regarded as those that occur at a lower height.

Another problem occurs in taking the monthly means at heights below 80 to 85 km. There are no reflections at night at these heights so that the mean winds are biased by the diurnal tide. The averages are over a period of approximately 10 hours so the semi-diurnal tide has little effect. The diurnal tide has amplitudes of between 10 and 15 m s^{-1} at these heights (e.g. see Forbes (1984)) so a bias of up to about 8 m s^{-1} can be included in the mean winds for the worst possible phase.

3.13 Other considerations

Lastly, the restrictions that occur due to the nature of the data need to be considered. The height resolution restricts the minimum vertical wavelength that is observed. The large increase in variance at heights greater than about 80 km creates problems as the data are not stationary with height. Detrending is difficult because it must be based on the assumption that the behaviour of all data reflects

the behaviour of individual waves. Given the exp(z/2H) amplitude increase with height when the wave is smaller than breaking amplitude and the probable destruction of the wave at some height greater than the breaking point, there can be no justification for such an assumption.

The various restrictions that have been applied to the data have removed some signal as well as decreasing the noise level. The remaining information is discussed in the following chapters.

CHAPTER 4

SPECTRAL ANALYSIS

4.1 Spectral analysis techniques: General

Since Blackman and Tukey (1958) reported their technique of cross-spectral analysis, based on Fourier transforming the correlation function, several techniques for determining unknown periodicities in time series have been developed.

The periodogram technique became popular when the power of digital computers made it practicable (Jones (1965)).

The appliction of the fast Fourier transform (Cooley and Tukey (1965)) to spectral analysis increased the speed of computations, thus making large analysis problems more tractable.

The major problem with both the Blackman and Tukey (1958) spectral analysis technique and the periodogram method is that assumptions are implicitly made about the extension of the time series beyond the existing data. The assumption made by the Blackman and Tukey (1958) technique is that the data are everywhere zero outside the known data. The periodogram method assumes thar the data are periodic, with a period equal to the length of the time series (Childers (1978)). Burg (1967), (1968) approached the problem of spectral analysis in a new way. Burg's method involved calculating a spectrum, but assuming the minimum knowledge about the behaviour of the data outside the known time series. This technique is known as the maximum entropy method (MEM). MEM techniques are particularly suitable for the analysis of short time series and of truncated sinusoids (Ulrych (1972)). These MEM techniques are used in this

thesis because of the ability of MEM techniques to calculate the spectrum of short time series and despite some disadvantages that will be discussed later. Generalizations of Burg's (1967), (1968) techniques to include multi-channel spectral estimation have been developed by Morf et al. (1978), Jones (1976), Strand (1977a), (1977b), and others.

Another technique, the maximum likelihood method (MLM), is a high resolution method that uses a fixed wavenumber window whose shape is a function of the wavenumber at which the spectral estimate is obtained (Capon (1969)). The maximum likelihood method, unlike the maximum entropy method, is not based on the autocorrelation function. That is, the inverse transformation of the maximum likelihood spectrum will not produce, in general, the correlation coefficients (Childers (1978)). MEM and MLM spectra are related The MLM spectrum is equal to the average of the reciprocals of the MEM spectrum obtained from one point up to the MEM filter length (Burg (1972)).

Finally, a method called the minimum cross entropy method has been described recently by Shore and Johnson (1980) and by Shore (1981). This method takes into account prior information about the spectrum (Shore (1981)) and is a generalization of the maximum entropy method (Pestiaux and Berger (1983), Shore (1981)). The minimum cross entropy and the maximum entropy spectra are equivalent when the prior estimate for the latter is white noise (Pestiaux and Berger (1983)). The minimum cross entropy technique should be used when the spectrum of the real data is created by a process that is not compatible with the spectral type of the maximum entropy spectrum. That is, the maximum entropy method is an autoregressive process so (Ulrych and Bishop (1975)), if the data was created by a moving average process,

the analysis technique would not be compatible with the technique used to generate the data. Hence, errors can result when an autoregressive technique is used to analyse a spectrum generated by a non-autoregressive process (Gutowski et al. (1978)).

Akaike (1976) has also proposed an autoregressive moving average model for estimating the spectrum.

The maximum entropy method has been used throughout this thesis. One reason for this is that some of the data series used had very few points. In both the Blackman and Tukey (1958) and the periodogram methods of analysis there is always a trade off between bias and resolution. Resolution is defined as the ability to separate peaks at different frequencies, whilst bias is the deviation of the spectral function from the true spectrum. This trade off becomes critical when the number of data points is small. There will be little reliability in a Blackman and Tukey (1958) spectrum that has sufficient resolution to be useful if there is less than about 100 data points (e.g. see Burns (1980)). The problems are similar for periodogram analysis (Lacoss (1971)). The resolution of the maximum entropy method is slightly better than the resolution of the maximum likelihood method. The minimum cross entropy technique is a new method and is not as well documented as the older method.

The rest of this chapter consists of a brief overview of single channel maximum entropy methods and the application of these techniques to the monthly time series to give an idea of the modes that are present in the mesosphere and lower thermosphere above Christchurch.

4.2 The maximum entropy method: An overview

The maximum entropy method can be used to calculate a spectrum for which the minimum knowledge of the data has been assumed.

Following Ulrych and Bishop (1975) the information known about a system is defined as

$$I = \log \frac{1}{p(u)} \tag{4.1}$$

where p(u) is the probability of the occurrence of any event. Equation (4.1) can be integrated over all values of the independent variable u, to obtain a value H, the average information per unit of the time interval. H is called the entropy of a system.

$$H = -\int_{-\infty}^{\infty} p(u) \log(p(u)) du \tag{4.2}$$

Therefore, the entropy is a measure of the lack of knowledge about the structure of the system.

Equation (4.2) is defined in terms of the probability function p(u). In order to gain information about the spectrum in the frequency domain, the entropy must be redefined in terms of the power at a frequency ν. But there is no unique mapping from p(u) to P(ν), where P is the power spectral function (Ables (1974)).

If P(ν) is treated as the power gain function of a linear filter acting on white noise, then the entropy of the input signal to the filter and the entropy of the output signal from the filter can be defined in terms of their amplitude probability functions. The difference between the input and output entropies is then defined as (Ables (1974))

$$\Delta H = \int_{-\infty}^{\infty} \log P(\nu) d\nu \quad . \tag{4.3}$$

The entropy of the output signal must be maximised so that the lack of assumed knowledge about the system is maximised, no matter what the entropy of the input signal is. This implies that the change in the entropy of the system must be maximised by using an appropriate $P(\nu)$. However, there are constraints on this condition. The Fourier transform of the spectrum must be equal to the covariance terms. That is

$$\int_{-\infty}^{\infty} P(\nu) e^{-i2r\nu n\Delta t}\, d\nu = \rho_n \quad . \tag{4.4}$$

A solution for the power spectrum can be found by using the calculus of variations (Smylie et al. (1973), Edward and Fitelson (1973)) which leads to the following power spectral function (Anderson (1974)).

$$P_\nu = \frac{P_M \Delta t}{\left| 1 - \sum_{j=1}^{M} a_{Mj} \exp(-i2r\nu j\Delta t) \right|^2} \tag{4.5}$$

The frequency ν is limited to the interval $-\nu_N \leqslant \nu \leqslant \nu_N$. The Nyquist frequency ν_N is defined as $\nu_N = \frac{1}{2\Delta t}$, where Δt is the interval between points. P_M is a constant and the a_{Mj} are filter coefficients. These are defined by the following equation (Anderson (1974): for a derivation see Smylie et al. (1973)).

$$\begin{bmatrix} \rho_o & \rho_1 & \cdots & \rho_M \\ \rho_1 & & & \cdot \\ \cdot & & & \cdot \\ \cdot & & & \cdot \\ \cdot & & & \\ \cdot & & & \\ \cdot & & & \\ & & & \rho_1 \\ \rho_M & \cdots & & \rho_1 \; \rho_o \end{bmatrix} \begin{bmatrix} 1 \\ -a_{M1} \\ \\ \\ \\ \\ \\ \\ -a_{MM} \end{bmatrix} \quad \begin{bmatrix} P_M \\ O \\ \cdot \\ \cdot \\ \cdot \\ \cdot \\ \cdot \\ \\ \\ O \end{bmatrix} \tag{4.6}$$

The ρ_i are covariance terms. The covariance matrix is a Toeplitz matrix (see Claerbout (1976)). A recursive solution for the coefficients a_{mj} and for P_M can be found using the techniques developed by Levinson (1947) and Durbin (1960). Anderson (1974) has detailed the application of these techniques to maximum entropy spectral analysis.

4.3 The reliability of MEM spectra and problems with the calculation of these spectra

One problem that occurs in the method outlined in the previous section is that the order, M, used in equations (4.5) and (4.6) has not been defined. If too few filter coefficients are used then the sum of the squares will be too large and the mean square error of prediction will be too large (Tong (1976)). Hence, the resolution will be poor. If the order of the filter coefficients is too large the residual sum of the squares will be smaller, but the autoregressive filter coefficients will be unreliable and the mean square error of prediction will be too large (Tong (1976)). In other words, spurious peaks may be found if too many filter coefficients have been used. Therefore, it is important to find the correct length of the prediction filter using an objective criterion.

Several objective techniques have been proposed. Akaike introduced a technique called the final prediction error method (see Akaike (1974), Ioannidis (1975), Gersch and Sharpe (1973), Landers and Lacoss (1977), Ulrych and Bishop (1975) and Haldoupis (1981)). The modified form of this criterion is that the final prediction error (FPE) is given by (Landers and Lacoss (1977), Ioannidis (1975)).

$$FPE = \frac{N+(M+1)}{N-(M+1)} P_M \qquad (4.7)$$

The optimum filter length is found by taking the value of M for which the FPE is a minimum. Ulrych and Bishop (1975) suggest that looking for the first minimum is more appropriate for autoregressive and autoregressive moving average processes, but that this technique will severely underestimate the filter length needed for nearly periodic data.

Ulrych and Bishop (1975) have also modified equation (4.7) for the case when the mean has not been removed from the data prior to the estimation of the autoregressive parameters so that

$$FPE_M = \left(\frac{N+M}{N-M}\right) P_M \quad . \tag{4.8}$$

Two other criteria have been applied to the calculation of the order of the filter coefficients. Akaike (1974) proposed a system called the Akaike information criterion (AIC) which is based on the maximum likelihood function. Landers and Lacoss (1977) define this criterion as

$$AIC(M) = \ell n(P_M) + 2\,{}^{M}/_{N} \quad . \tag{4.9}$$

Secondly, Parzen (1974) developed a means of determining the filter length called the "criterion autoregressive transfer function" which he abbreviated to CAT. Parzen's (1974) original formula involved knowing the estimation of the mean square prediction error for an infinite order autoregressive function. This was shown to be not necessary and CAT can be determined by (Landers and Lacoss (1977) and Parzen (1980)).

$$CAT(M) = \frac{1}{N} \sum_{j=1}^{M} \frac{1}{\hat{P}_j} - \frac{1}{\hat{P}_M} \tag{4.10}$$

where

$$\hat{P}_j = {}^{N}/_{(N-j)} P_j \quad . \tag{4.11}$$

Landers and Lacoss studied these three criteria by applying them to the time series of a complex harmonic with white noise added. They concluded that the three criteria gave an acceptable length for the autoregressive filter when the noise level was low. However, when the amplitude of the white noise was large compared with the amplitude of the signal, the criteria tended to underestimate the length of the prediction filter. That is, longer prediction filters than those estimated by the three criteria are needed when the noise level is high.

The accuracy of an autoregressive model is dependent on the type of data that is used (e.g. see Gutowski et al. (1978)). The three criteria (4.7), (4.9) and (4.10) have been used as an objective method of estimating the optimum filter length.

Toman (1965) showed that frequency shifts occur in truncated sinusoids that are analysed using the periodogram method of spectral analysis. Toman found that, when the truncation length was less than 0.58 times the length of the sinusoid, the peak in the spectrum corresponding to this sinusoid was shifted to a frequency of zero.

Chen and Stegan (1974) discussed the application of MEM to truncated sinusoids. Ulrych (1972) found no frequency shift in the MEM spectrum when the corresponding peak, that was analysed by the periodogram method was shifted to zero. More precisely, Ulrych found no frequency shift using the MEM method when the data were comprised of information from about 0.57 time one cycle of the sinusoid. However, Chen and Stegen (1972) found that, in similar situations using MEM, the spectral peak did shift a little. The amount that the peak shifted was dependent on the initial phase; the number of data points sampled, thus in their

investigation, the length of the sinuosid studied; the noise level that was present.

The maximum entropy method is a useful spectral analysis technique that assumes less information about the data and has better resolution than the conventional analysis techniques, such as periodogram analysis and Blackman and Tukey (1958) spectral analysis. Furthermore, MEM is a more accurate technique for analysing short data series and data comprised of truncated sinusoids than either of the older analysis methods. However, a major drawback exists in the difficulty of estimating the correct length for the auto-regressive filter. It is difficult to produce an objective optimum filter length estimation that is both accurate and can be applied to all types of data.

4.4 Some applications of the analysis techniques

In the previous section it was emphasized that one of the major problems that occurs when MEM analysis is used is in finding the optimum length for the prediction filter. Three criteria have been developed for finding the optimum length of the prediction filter: the final prediction error (FPE); the Akaike information criterion (AIC); the criterion autoregressive transfer function (CAT).

The values of these three criteria are plotted against the number of filter coefficients (figure 4.1). The data are a time series of 3 hour wind averages at a height of 90 km measured in July 1981. The criteria have been scaled to fit into the interval 0 to 10, hence no label has been placed on the vertical scale. The method of scaling is that each criterion has been multiplied by a constant and then another constant has been subtracted from this total to bring the criterion into the 0 to 10 range. Therefore, no information

Figure 4.1

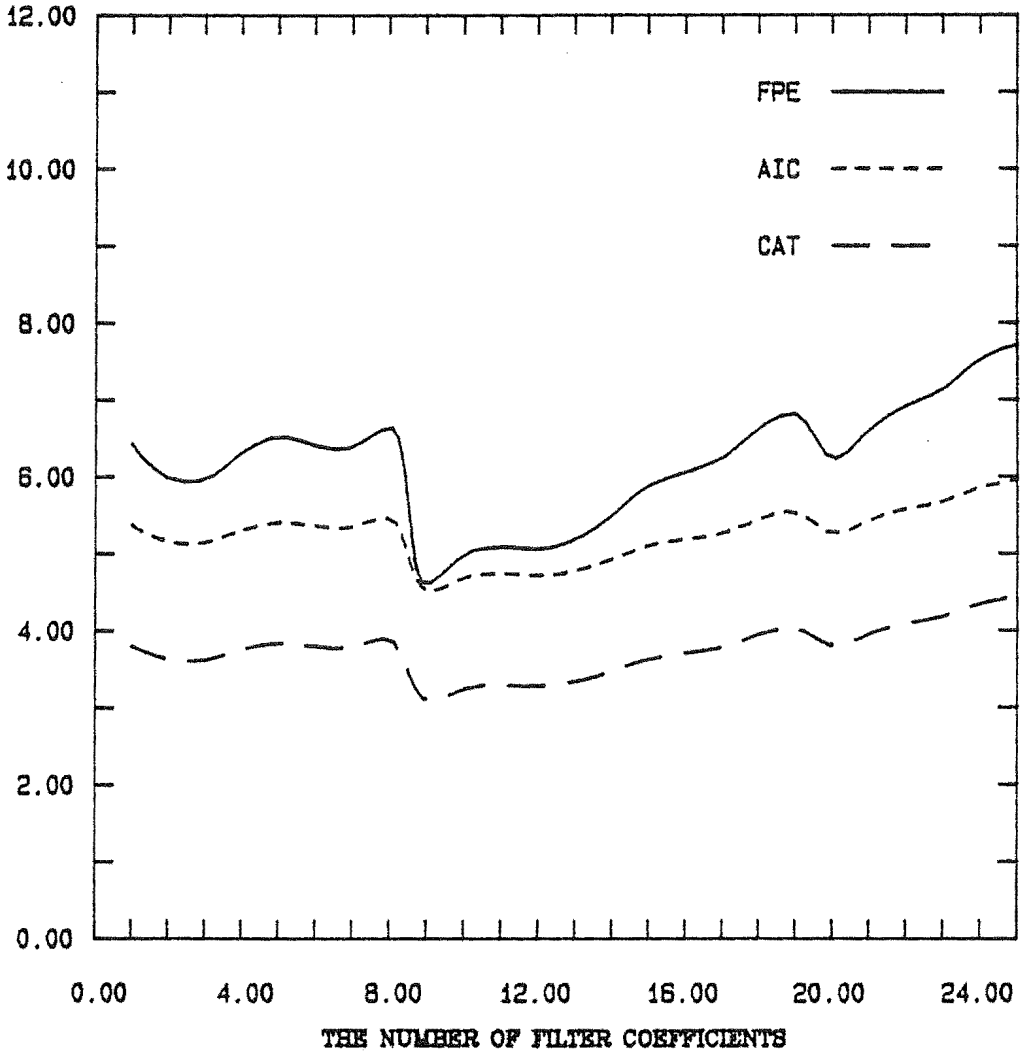

Three criteria for measuring the length of the prediction filter in MEM spectral analysis. The data used are drifts measured at 90KM in July 1981.

about the minima is lost and the number of filter coefficients at which the minima occur have not changed. However, the minima are more apparent on the plot. Thus the position of the absolute minimum on the graph should occur at the optimum filter length, provided that the criterion used is reliable.

In figure 4.1 the 3 criteria all have their absolute minima at same filter length. Furthermore, the first minimum also occurs at the same filter length for each of the 3 criteria. So, for this time series, the 3 criteria all give the same length for the optimum filter. Therefore the 3 criteria are consistent for this time series and thus give an objective means of determining the optimum length of the prediction filter.

The FPE criterion has been used to determine the prediction filter length for the spectra discussed in the rest of this chapter. However, an attempt was made to standardise the filter length for a given time series length. Thus, although most of the analyses have used the optimum filter length, occasionally the filter length is too short and resolution has suffered. SEE ERRATA

The spectral plots are of two types. The first kind involves analysing data consisting of 3 hour wind averages. This method shows the semi-diurnal tide, the diurnal tide, the two day wave and some long period internal gravity wave activity. However, the frequency of the peaks in this last case is not expected to be consistent with height, nor are the same peaks expected to be seen in different months. The second type of plot involves the spectral analysis of daily averaged wind data. These analyses are designed to show which planetary wave modes are present in the atmosphere at heights of about 90 km.

The power spectrum of the 3 hourly averages of zonal winds in July 1981 are shown in figure 4.2. The spectrum has two sets of peaks that occur at the same frequency at more than one height: one set corresponds to the diurnal tide and the other set corresponds to the semi-diurnal tide. Frequency peaks corresponding to the semi-diurnal tide occur at periods of slightly less than 12 hours for all three heights (85 km, 90 km, 100 km). However, spectral peaks occur at a period of about 24 hours only at heights of 85 km and 90 km. A spectral peak with a period of about 20 hours is found in the anslysis of 100 km data. This peak may also correspond to the diurnal tide. Those peaks corresponding to the diurnal tide are of greater magnitude than the peaks corresponding to the semi-diurnal tide. Some spectral peaks also occur at frequencies of between 0.10 and 0.17 cycles per hour. The power appears to be roughly constant with frequency for frequencies between 0.10 and 0.17 cycles per hour. However, the spectral peaks occurring in this frequency range make it difficult to detect trends.

The frequency shifts away from the tidal periods reflect uncertainties in determining both the frequency of the peak and any phase variations in the tides themselves.

Peaks also occur in the spectral analysis of zonal drifts that have been averaged over a day in July 1981 (figure 4.3). One set of peaks corresponds to a mode with a period of about 4 days. This peak occurs at all three heights (85 km, 90 km and 100 km) and may be caused by the 4-day zonal wavenumber 1 wave described by Venne and Stanford (1979). Venne and Stanford used satellite derived radiances occurring in the stratosphere. They found the 4 day wave to be strong in the middle and high latitudes. The other set of spectral peaks occurs at frequencies of between 0.05 and 0.12 cycles per day. No identification of this set of peaks

Figure 4.2

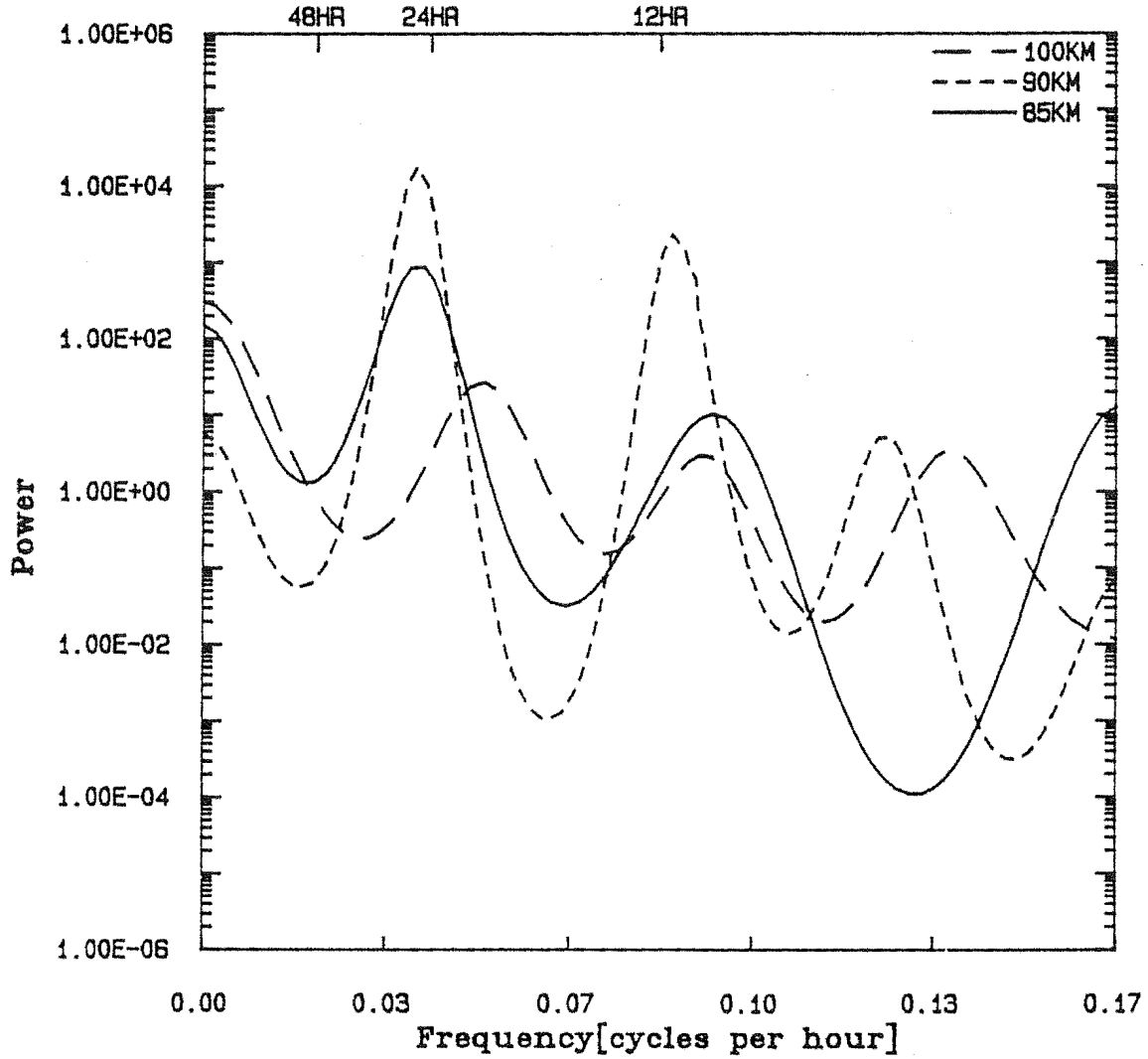

Power spectra of zonal drifts for various heights in July 1981 at Birdling s Flat. Only the relative power at each height is important.

Figure 4.3

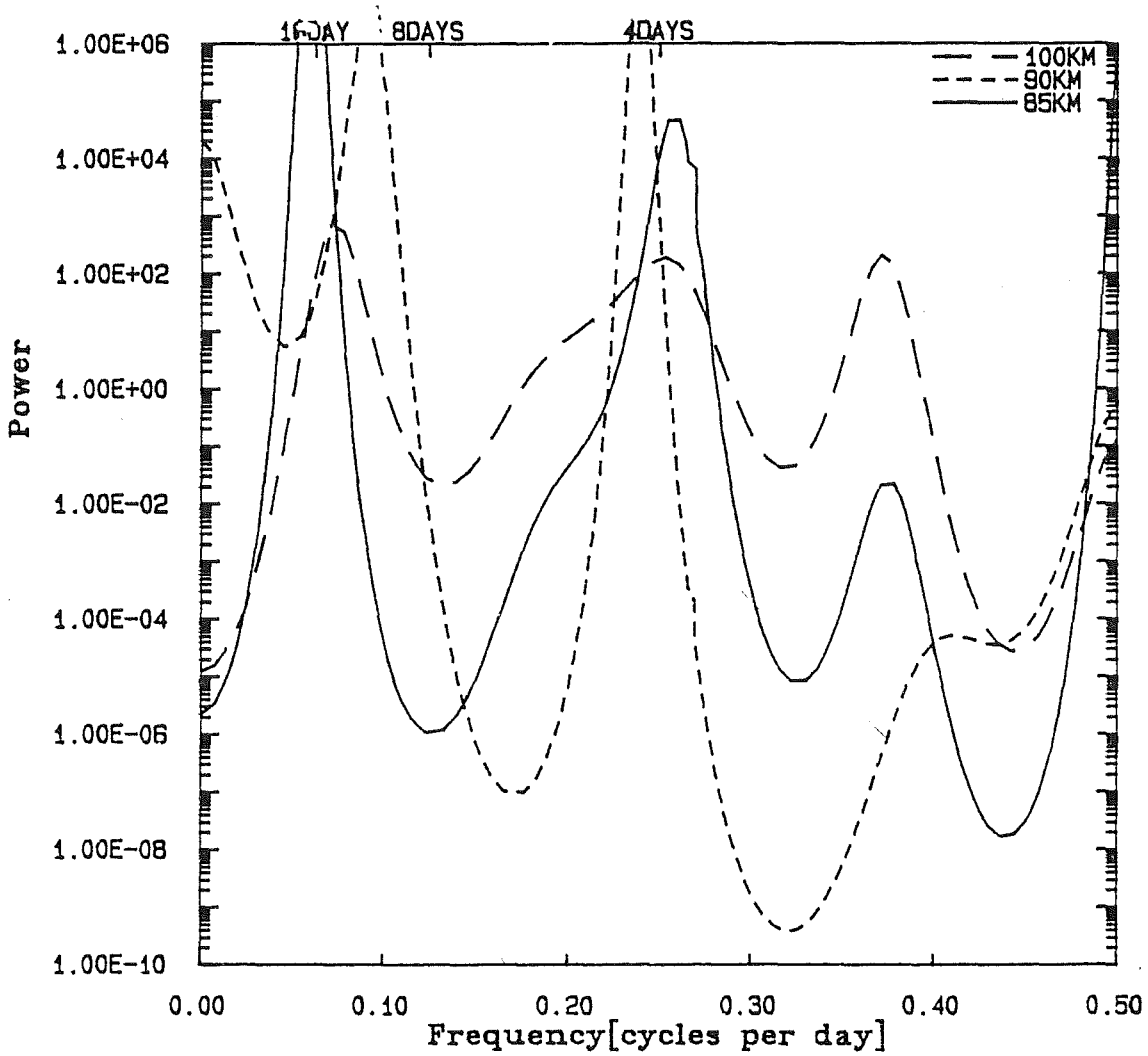

spectra of zonal drifts for various heights in July 1981 at
ıgs Flat. Only the relative power at each height is important.

with known atmospheric waves is possible with the information available in this spectrum. Spectral peaks occur in both the 85 km and the 100 km data at frequencies of between 0.35 and 0.40 cycles per day. These peaks also correspond to known planetary wave activity in the atmosphere.

Broad spectral peaks with a period of about 2 days are found in the analysis of 3 hourly averaged wind data measured in January 1981 (figure 4.4). The spectral peaks that occur in the anslysis of data from 85 km and 90 km are centred at a period of 48 hours. A peak occurs with a period of 33 hours in the analysis of winds at 100 km. The 48 hour peak at 85 km has a high frequency ledge which suggests that some of the power is due to higher frequency activity. Both this broadening and the peak that apparently occurs at a period of 33 hours at 100 km may in fact be due to a peak that has been frequency shifted by phase or other considerations from the frequency of the diurnal tide. Peaks occur at frequencies near the frequency expected for the semi-diurnal tide at all 3 heights. The frequency of these peaks varies a little over the heigh range studied. Spectral peaks exist in the 0.10 to 0.17 cycles per hour frequency range. Two peaks occur at different heights at a period of just over 8 hours. The power does not appear to vary with increasing frequency for frequencies of between 0.10 and 0.17 cycles per hour.

A mode with a period of between 5 and 6 days was found at all 3 heights when the time series of daily averaged winds measured in January 1981 was analysed (figure 4.5). The "5-day" spectral peak occurs at a lower frequency (longer period) at 90 km than at 85 km and 100 km. This spectral peak is probably caused by the H_2^1 free mode (see chapter 2). Another set of peaks occurs at a period of about 3 days. This set cannot be identified with any planetary wave mode known at other heights. The power of the spectra at all 3 heights

Figure 4.4

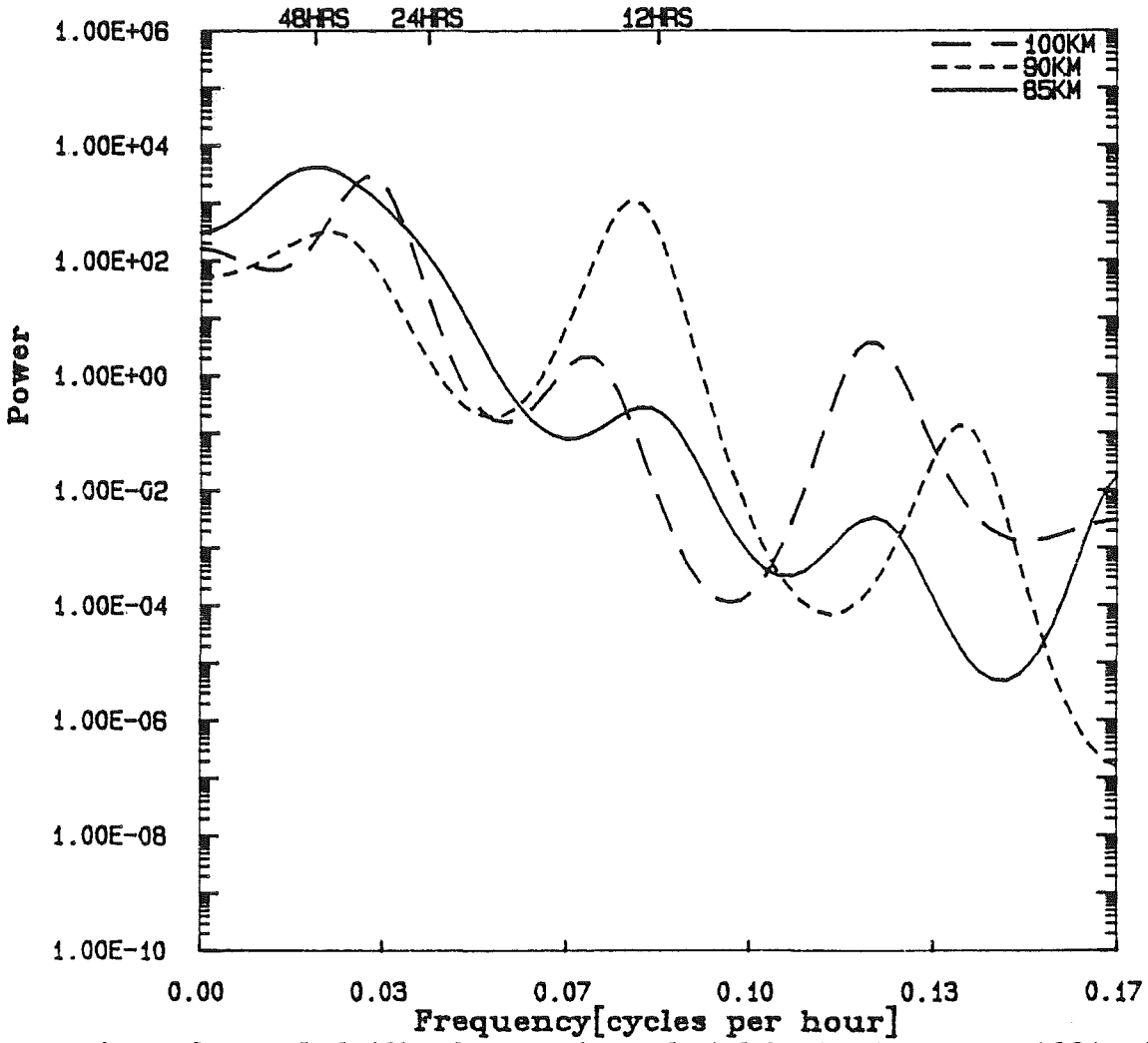

ır spectra of zonal drifts for various heights in January 1981 at lings Flat. Only the relative power at each height is important.

Figure 4.5

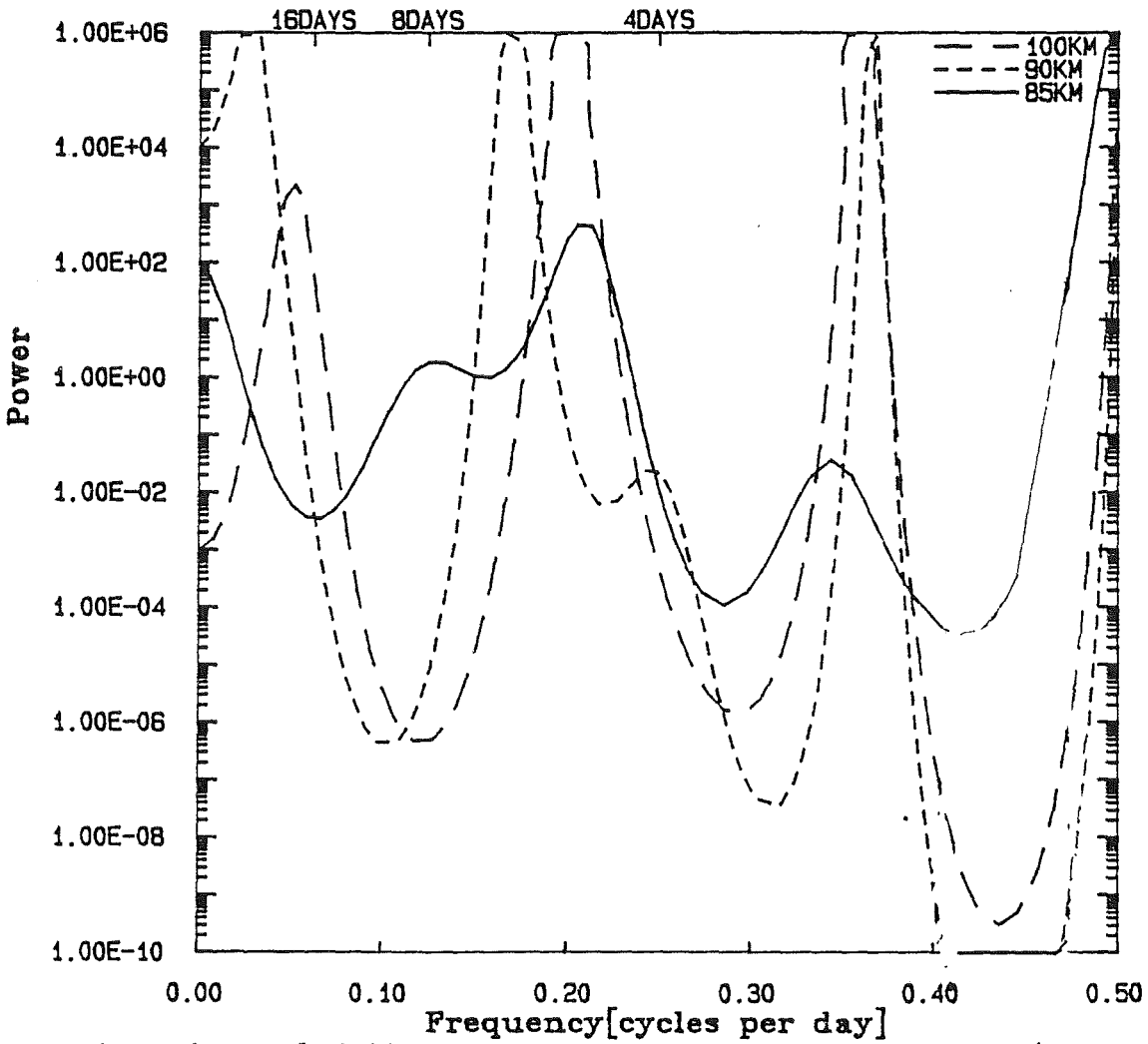

wer spectra of zonal drifts for various heights in January 1981 at dlings Flat. Only the relative power at each height is important.

increases as the frequency approaches 0.5 cycles per day. This may be caused by the strong 2-day wave that occurs in January.

In April 1981 (figure 4.6) a peak in the spectrum corresponding to the semi-diurnal tide appears at all 3 heights in the analysis of the 3 hourly averaged winds. The frequency of these spectral peaks changes with height. The peak at 100 km has a lower frequency (longer period) than the spectral peaks at lower heights. A spectral peak corresponding to the diurnal tide occurs only at 90 km. However, a spectral peak exists in the 85 km data, at a period of 2 days, that has a ledge extending to a frequency that corresponds to the diurnal tide. Spectral peaks that have frequencies corresponding to periods of about 2 days occur in the spectra at heights of 85 km and 100 km, but not at 90 km. Although there is no noticeable trend in the power spectrum between frequencies of 0.10 and 0.17 cycles per hour, the overall trend across the whole frequency range (0.0 to 0.17 cycles per hour) is that the power decreases with increasing frequency.

A number of spectral peaks appear in the analysis of the average daily winds in April 1981 (figure 4.7). Some of the spectral peaks that occur at 100 km have been shifted in frequency from the frequency of the peaks that are found at 85 km and 90 km. A "5-day wave" is certainly found at 85 km and 90 km. This is possibly the H_2^1 free mode. However, problems occur in trying to associate known waves with power spectral peaks when no other knowledge is available apart from the frequency (Burns (1980)). Spectral peaks occur at all 3 heights with periods of between 10 and 16 days. Other peaks occur at periods of between 3 and 3½ days and of about 2½ days.

Figure 4.6

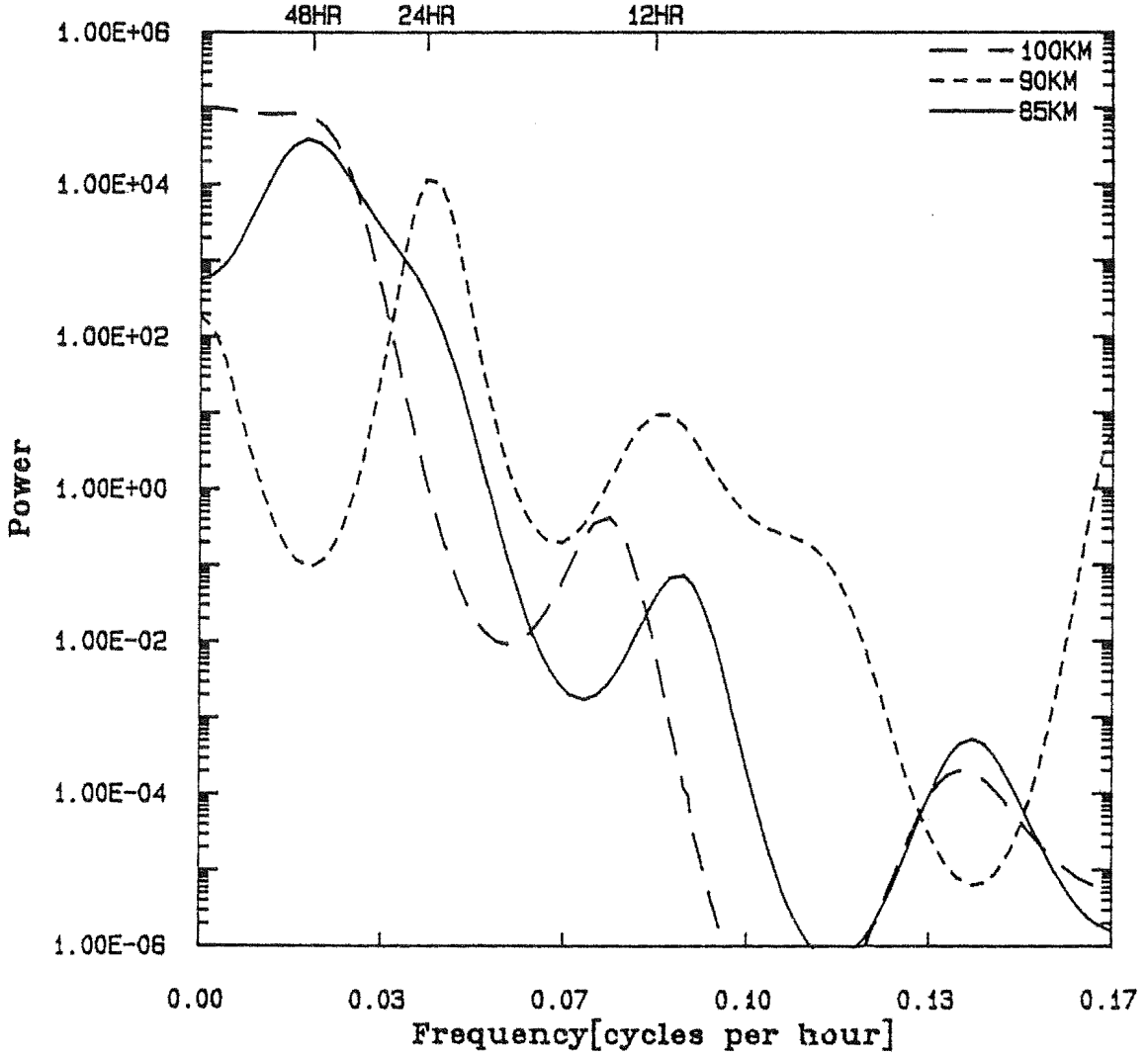

: spectra of zonal drifts for various heights in April 1981 at
ings Flat. Only the relative power at each height is important.

Figure 4.7

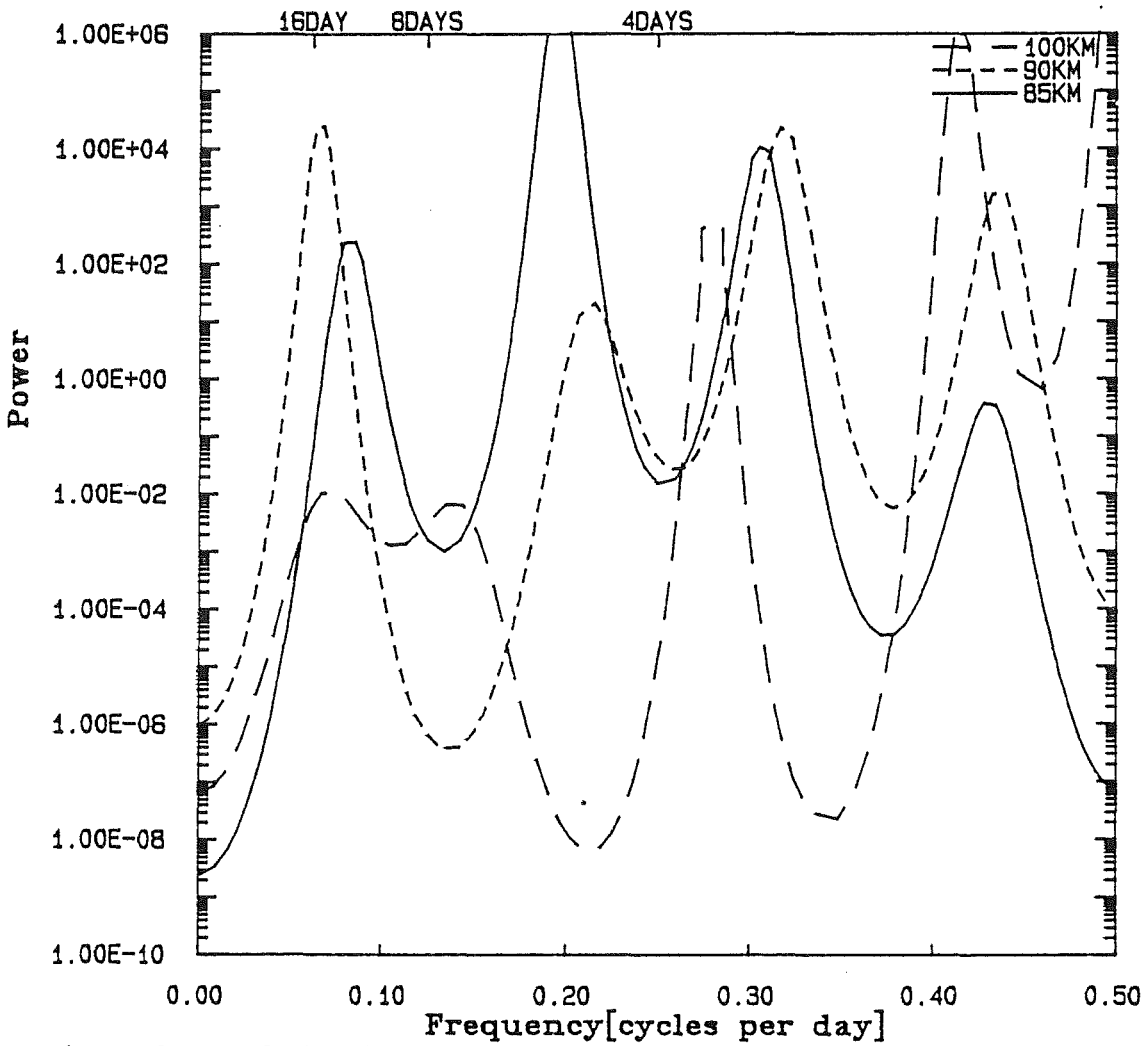

spectra of zonal drifts for various heights in April 1981 at
ıgs Flat. Only the relative power at each height is important.

The last monthly analysis to be discussed is the analysis of October 1981 wind data.

The 3 hourly averaged analysis produces spectral peaks at all 3 heights at a frequency corresponding to the diurnal tide (see figure 4.8). Evidence of the semi-diurnal tide appears only at heights of 90 km and 100 km. There are no peaks corresponding to the 2-day wave in October. Several peaks occur at frequencies of between 0.10 and 0.17 cycles per hour. The power appears to decrease with increasing frequency in this frequency range, but it is difficult to quantify this decrease.

Figure 4.9 gives the power spectra of daily averaged winds in October 1981. The spectral peaks at 90 km appear to have been shifted in frequency relative to the spectral peaks at 85 km and 100 km. There are peaks at all 3 heights that represent motion with a period of between 10 and 16 days. Spectral peaks with periods of between 5 and 7 days appear at all 3 heights. As in the April data spectral, peaks occur at periods of between 3 and 3½ days and of about 2½ days.

These analyses of winds in the mesosphere and lower thermosphere can be compared with analyses of stratospheric radiance data measured by the Nimbus IV selective chopper radiometer (see Houghton and Smith (1970) and Abel et al. (1970)). A MEM cross-spectral analysis was done on these data using the program developed by Strand (1977)). The cross-spectral resolution found in this analysis is not as good as the power spectral resolution that is found using the single channel MEM analysis. The radiance data analysed are zonal wavenumber 1 data at the latitude of Campbell Island in 1971 (latitude 52.6S, longitude 169.2E). The heights used are those for channel A and channel C (see figure 4.10). Coherency is used to show the frequencies at which peaks occur. The

Figure 4.3

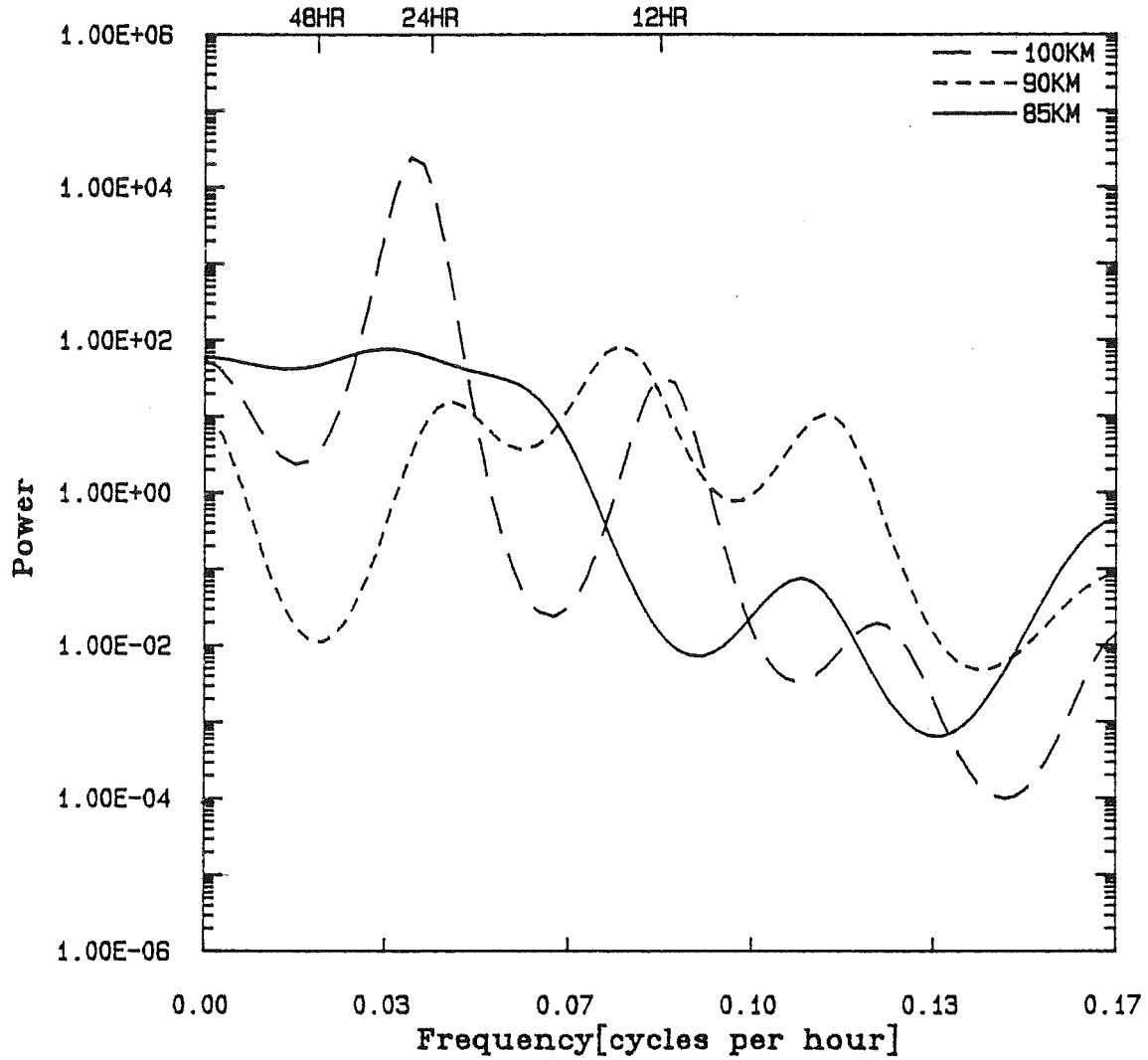

Power spectra of zonal drifts for various heights in October 1981 at Birdling's Flat. Only the relative power at each height is important.

Figure 4.9

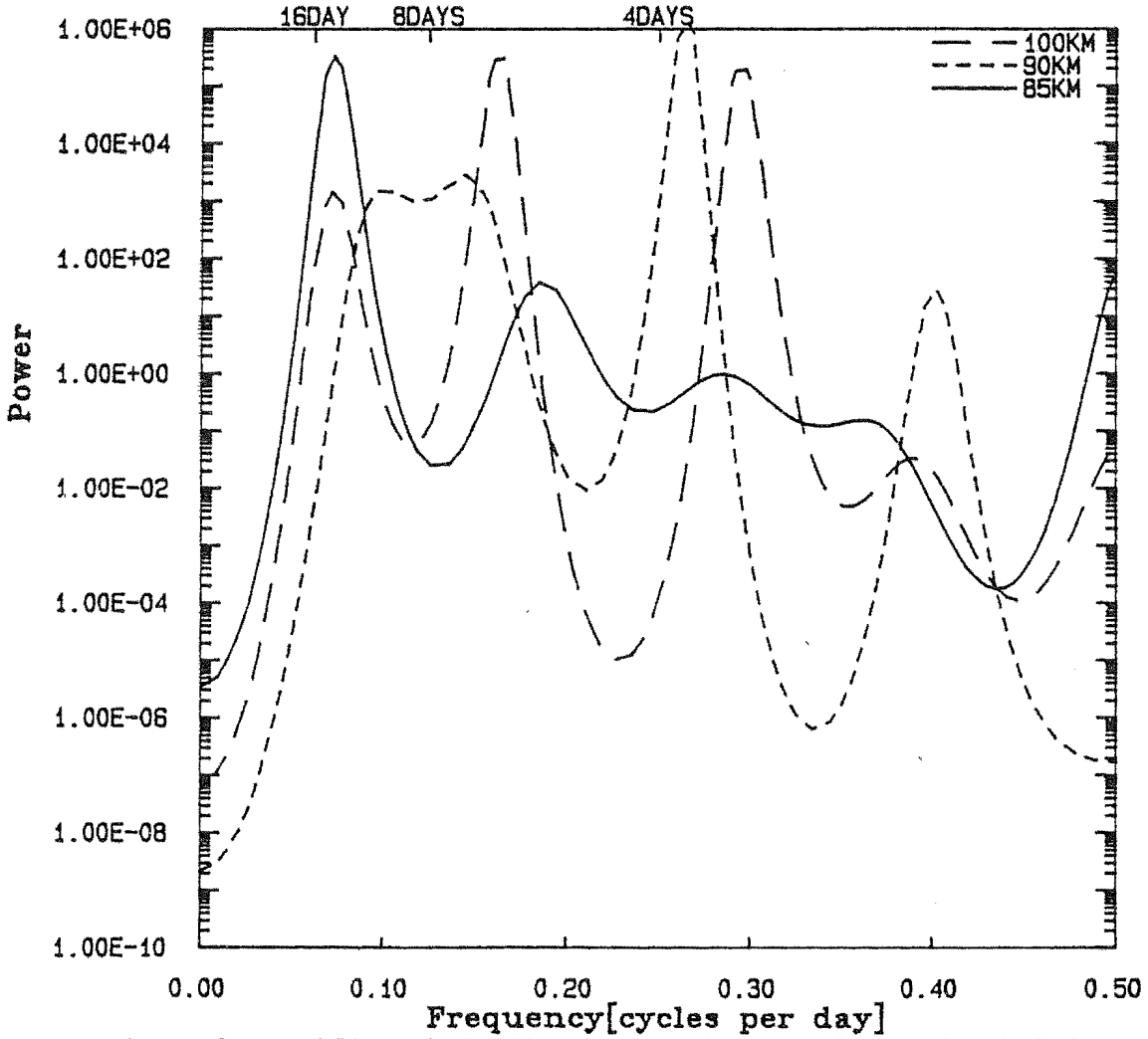

ɔwer spectra of meridional drifts for various heights in October 1981 at rdlings Flat. Only the relative power at each height is important.

Figure 4.10

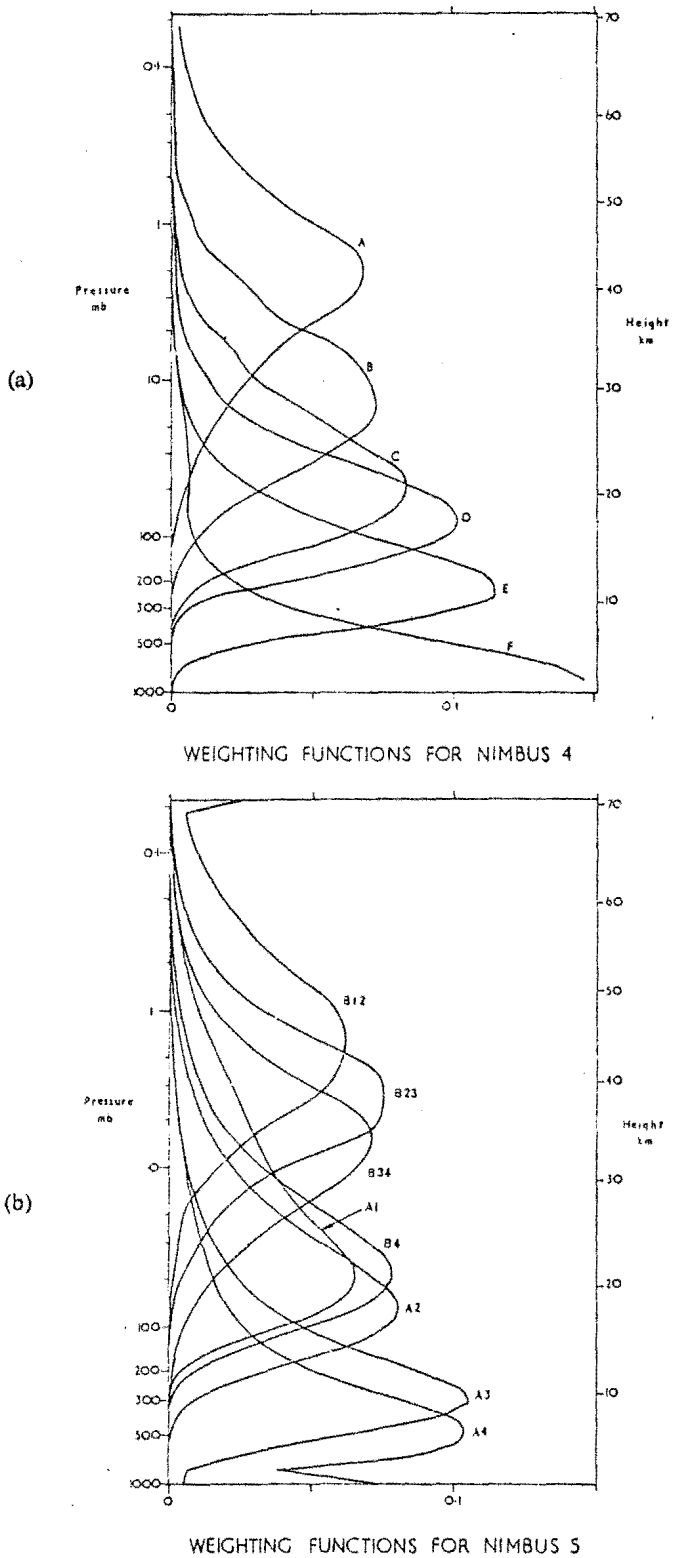

The weighting functions of the Nimbus 4 (a) and the Nimbus 5 (b) selective chopper radiometers(after Barnett et al (1975)).

results obtained for winter (June, July and August) are presented in figure 4.11. Those for summer (January, February and March) are presented in figure 4.12.

In winter a peak appears in the spectral analysis of wind data. This peak has a frequency of between 0.08 and 0.10 cycles per day (figure 4.3). A peak occurs in the same frequency range in the anslysis of stratospheric radiance data. There is also a broad peak in the spectral analysis of straospheric radiances that is caused by the 4-day zonal wavenumber 1 wave described by Venne and Stanford (1979). A spectral peak with this period also occurs in the analysis of wind data obtained at Birdlings Flat.

A "5-day" wave and a spectral peak with a frequency of between 0.35 and 0.47 cycles per day appear in the straospheric radiance data in summer (figure 4.12). Two peaks with similar frequencies are found in the anslysis of January 1981 wind data (figure 4.5).

In the 3 hourly averaged plots all planetary wave peaks, apart from those that correspond to the 2-day wave, overlap so that the longer period planetary wave power (for periods greater than say 20 days) cannot be easily distinguished from the power that occurs for the familiar short period motions (such as the 5-day wave). The daily averaged plots do show such a separation and so are more useful in estimating the power of long period planetary waves. At all heights in April and in October there is little power at the long period wave frequencies compared with the power at other planetary wave frequencies (figures 4.7 and 4.9). In July there is comparatively little power in long period waves at 85 km and 100 km (figure 4.3). This is not the case in January when the power at frequencies of between 0.0 and 0.05 cycles per day is comparable with the power at other frequencies.

Figure 4.11

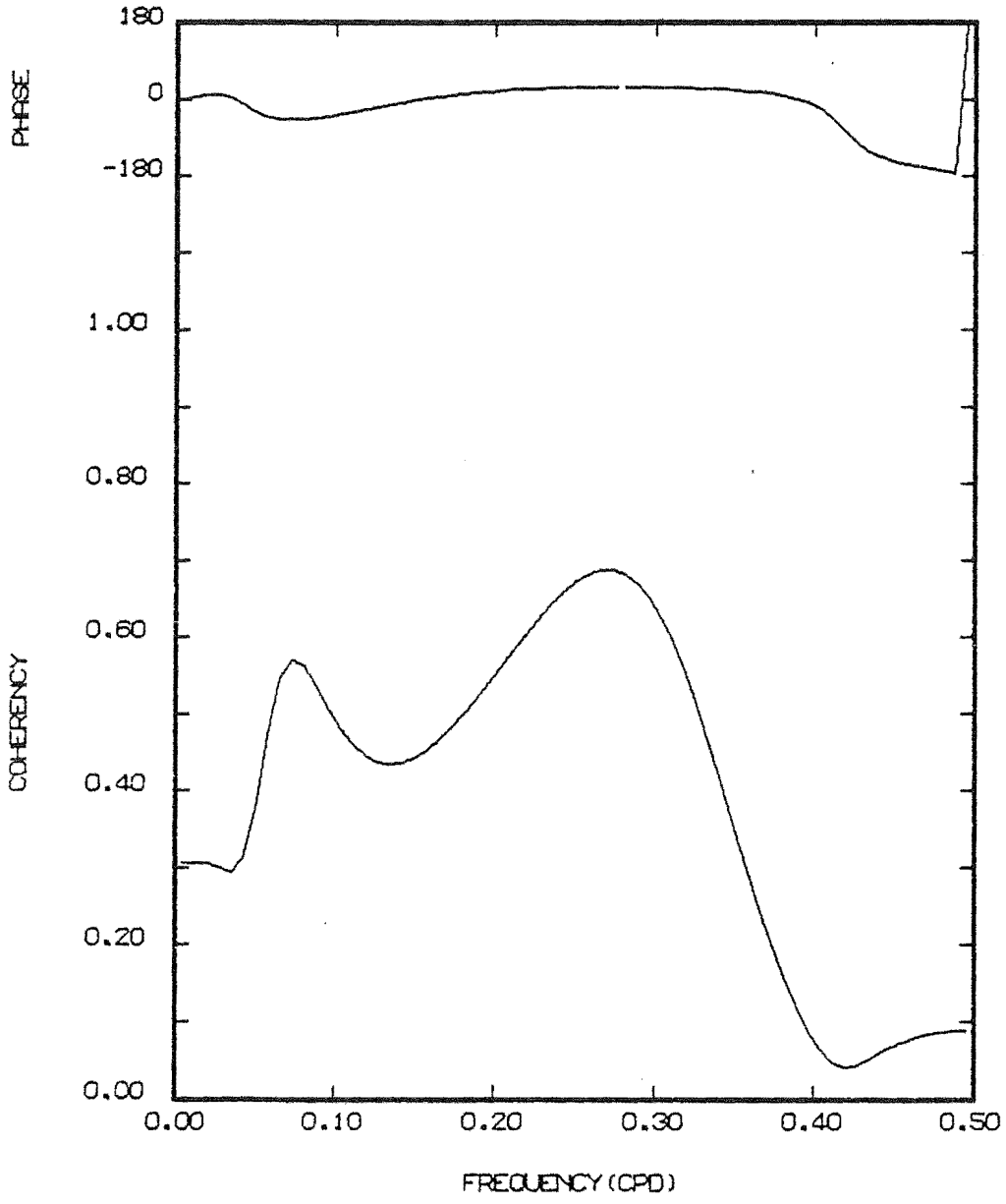

COHERENCY BETWEEN RADIANCE,ZONAL WAVENUMBER 1,CHANNEL A AND RADIANCE,ZONAL WAVENUMBER 1,CHANNEL B AT CAMPBELL ISLAND IN WINTER.

Figure 4.12

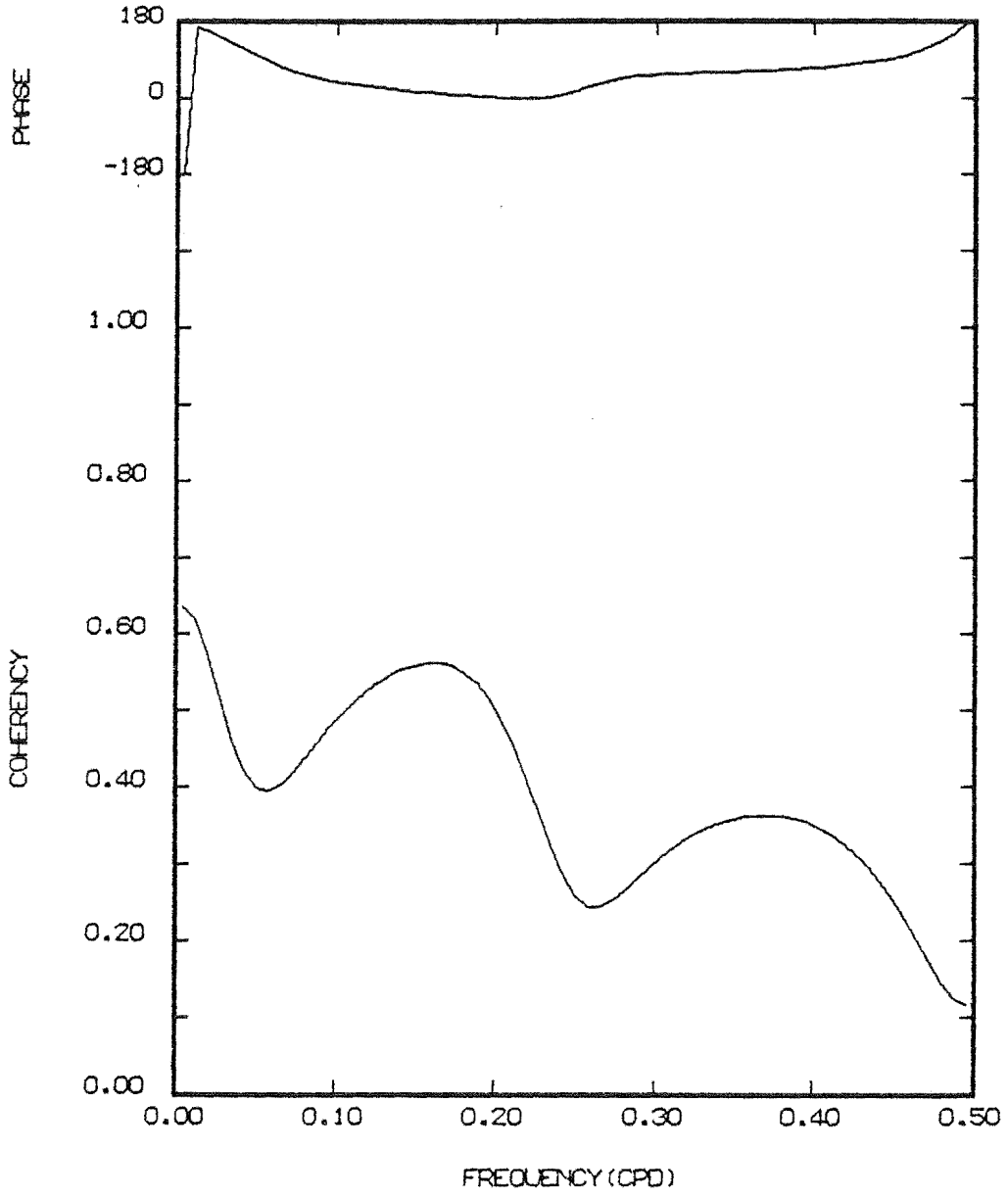

COHERENCY BETWEEN RADIANCE,ZONAL WAVENUMBER 1,CHANNEL A AND RADIANCE,ZONAL WAVENUMBER 1,CHANNEL B AT CAMPBELL ISLAND IN SUMMER.

Figures 4.13 to 4.16 show the total variance of the daily wind averages for several months in 1981.

In July (figure 4.13) the variance of motions with a period greather than one day decreases from 1300 m^2s^{-2} at 67.5 km to about 200 m^2s^{-2} at 90 km. Thus, the contribution of planetary sclae waves to the total wind field above about 75 km is going to be small compared to the contribution by internal gravity waves in winter (see chapter 6). However, planetary waves may still cause changes to the local background wind and temperature fields that will affect the behaviour of internal gravity waves.

Figure 4.14 shows the changes of variance with height in January. There is a peak value of planetary wave variance at heights of about 80 km. If this variance increase is common in the summer mesosphere, then it may be caused by modes that may become locally vertically propagating in the summer wind conditions. For example, Geisler and Dickinson (1976) predicted that the 5-day zonal wavenumber 1 free mode (the H_2^1 mode) would be locally vertically propagating in the mesosphere in normal summer wind conditions. Such vertical propagation causes amplitude increases with increasing height. Similarly other free modes such as the H_3^1 mode (see Salby (1984)) may become locally vertically propagating at some heights. The amplitude of the H_3^1 mode will also be enhanced in regions were it is vertically propagating.

The variance of motions with periods greater than 1 day is not large in either April or October (figures 4.15 and 4.16). Overall, the contribution of these long period motions is much less than the contribution of internal gravity waves above about 75 km.

Figure 4.13

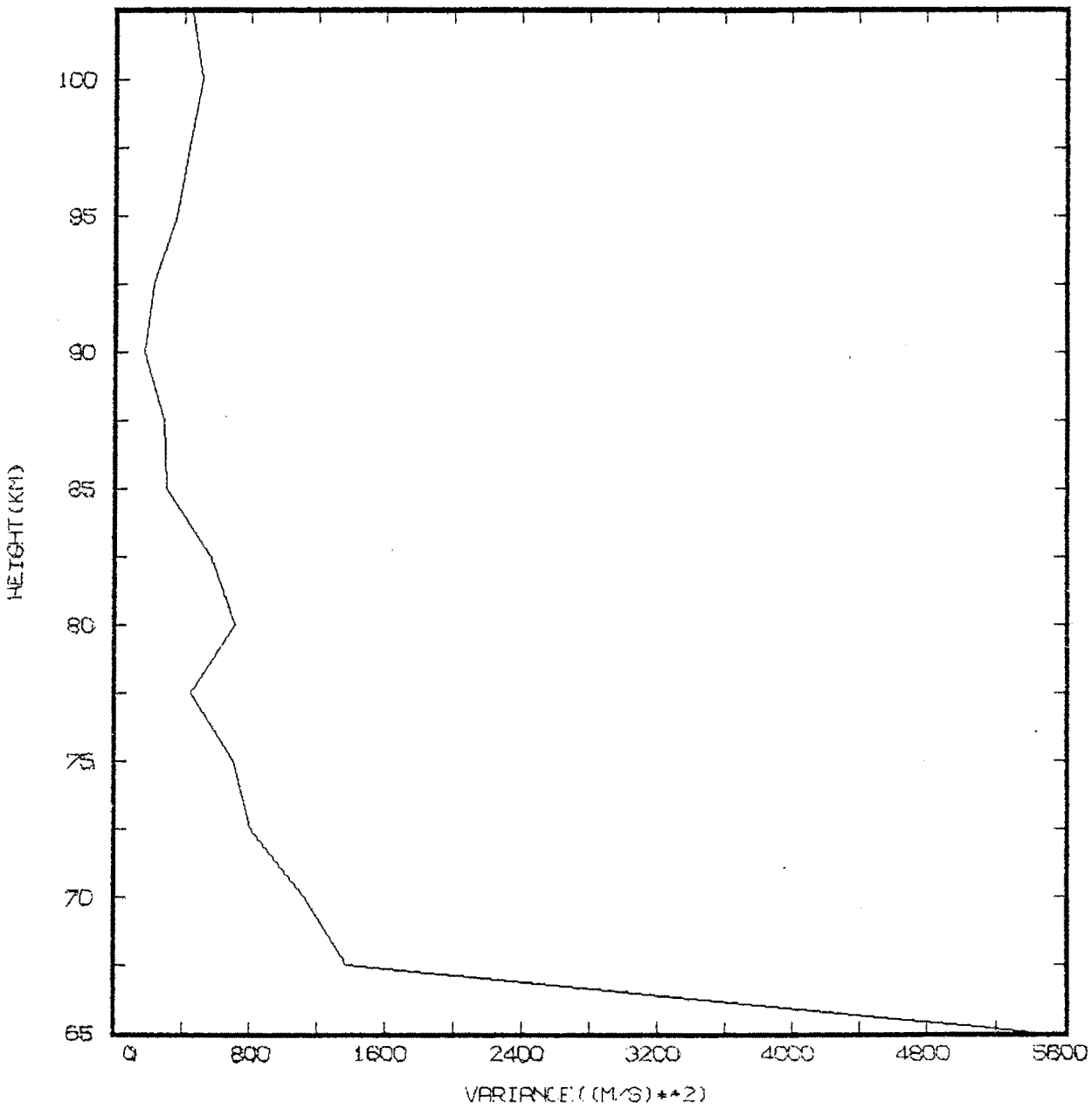

THE VARIANCE OF DRIFT VELOCITIES AT
FREQUENCIES GREATER THAN 1
DAY IN JULY 1981.

Figure 4.14

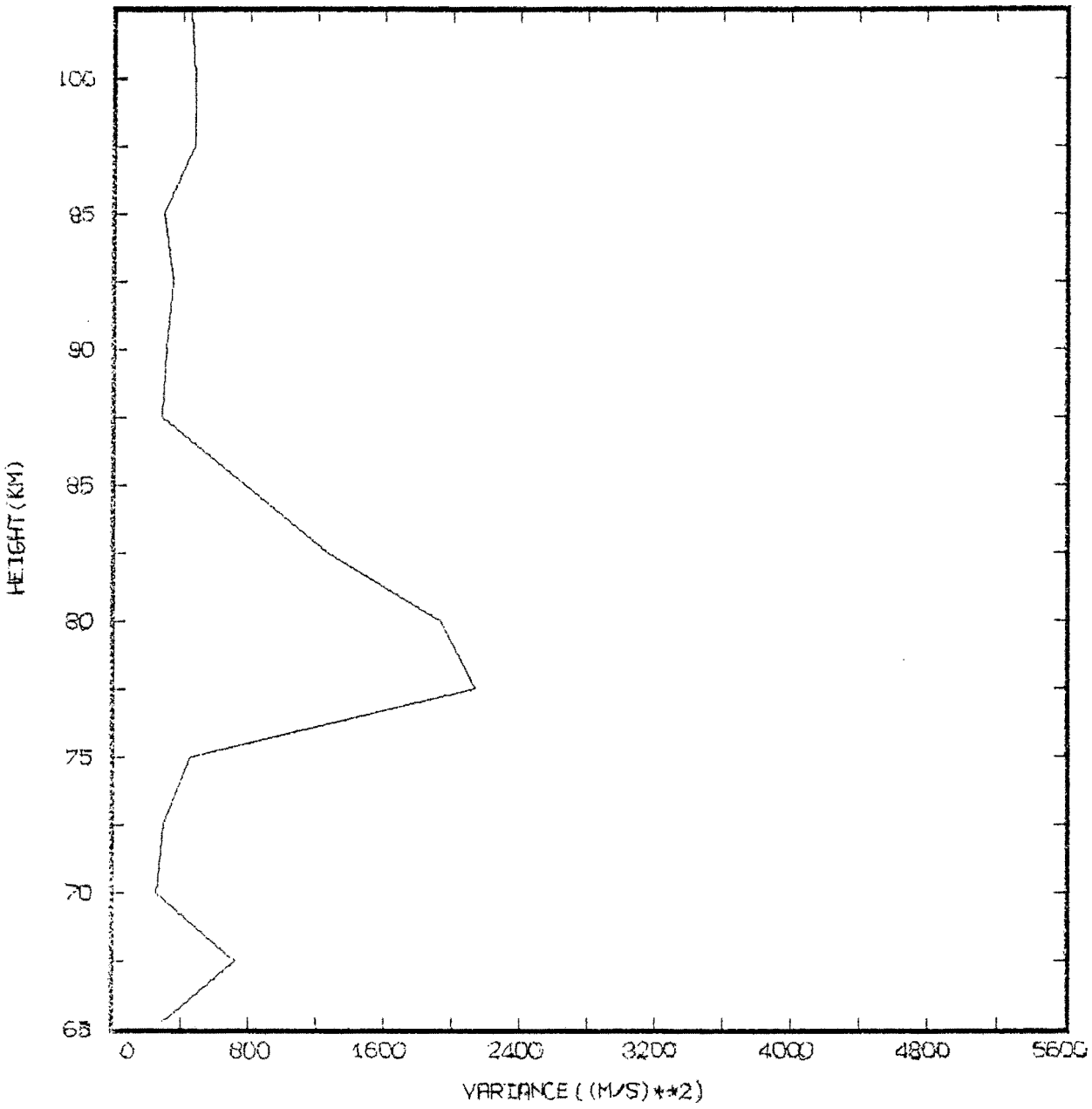

THE VARIANCE OF DRIFT VELOCITIES AT
FREQUENCIES GREATER THAN 1
DAY IN JANUARY 1981.

Figure 4.15

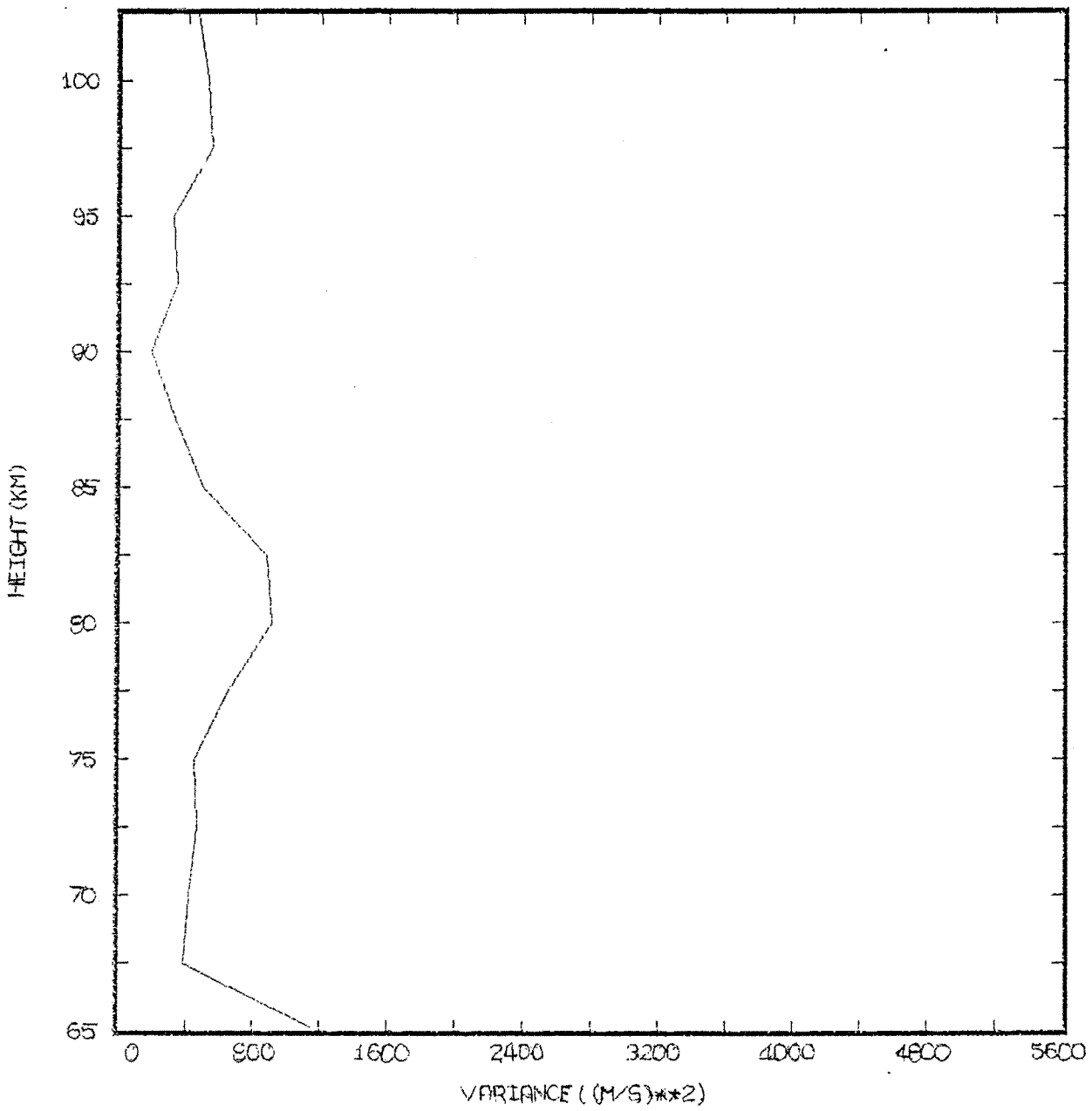

THE VARIANCE OF DRIFT VELOCITIES AT
FREQUENCIES GREATER THAN 1
DAY IN APRIL 1981

Figure 4.16

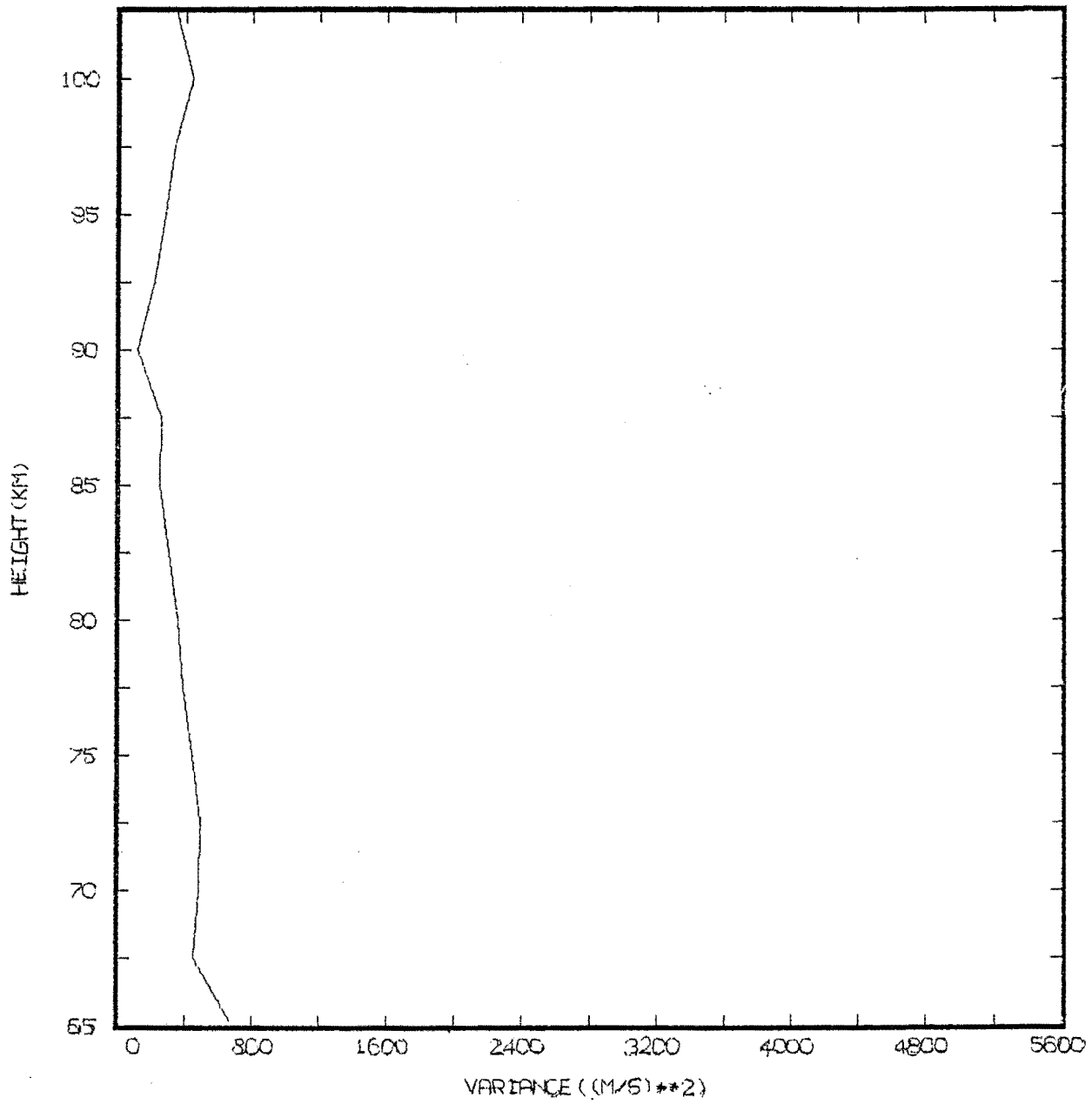

THE VARIANCE OF DRIFT VELOCITIES AT
FREQUENCIES GREATER THAN 1
DAY IN OCTOBER 1981.

CHAPTER 5

AMPLITUDE RESTRICTIONS AND INSTABILITY

5.1 Introductory remarks

The problem of whether the internal gravity wave spectrum is saturated or not arose from the variance plots calculated by Ball (1981). Internal gravity wave amplitudes were restricted to a certain maximum value at heights lower than 80 km or 85 km. This suggested that a mechanism was needed that could keep the wave amplitude below a set value. Above 80 km to 85 km the variance increases rapidly with increasing height, and any mechanism that accounts for the limitation of wave amplitude below 80 km to 85 km would also have to permit the increase in wave amplitudes at greater heights. This can only happen if the mechanism can change or be cut off at 80 km. In the rest of this chapter the reasons for such changes in the variance plots are considered, particularly with reference to atmospheric stability.

5.2 Atmospheric stability and the Richardson number

Internal gravity waves increase in amplitude exponentially with height in the absence of damping. If damping is not important then the waves will grow to a sufficiently large amplitude for the linear assumptions used in Appendix I to be not applicable. Two types of non-linearity are: energy transfer between modes (e.g. see Spizzichino (1969)); wave breaking causing turbulence (e.g. see Hodges (1969), Lindzen (1981)).

A useful criterion for determining the stability of a fluid where shear zones are present is the Richardson number (Ri) defined as

$$Ri = \frac{g}{T} \frac{\left(\Gamma + \frac{dT}{dz}\right)}{\left(\frac{du}{dz}\right)^2} \qquad (5.1)$$

where g is the acceleration due to gravity, T is the temperature of the fluid at the point where the stability is being measured, u is the velocity of the fluid at that point and Γ is the dry adiabatic lapse rate. Only the dry abiabatic lapse rate is considered because of low humidity in the mesosphere.

A large positive Richardson number implies that the fluid is stable. For a small positive Richardson number the fluid may be unstable. When the Richardson number is less than zero the fluid is unstable. The fluid becomes convectively unstable when the Richardson number decreases to zero. The atmosphere can be treated as a fluid where the Richardson criterion does apply. Generally the atmosphere is stable for mean motions throughout the mesosphere and lower thermosphere, but local fluctuations from the mean state can lead to low Richardson numbers and hence instability.

It is worthwhile to examine the effects on a fluid of differing values of the Richardson number. The most obvious boundary that needs to be considered is that which occurs where the Richardson number goes from positive to negative values. That is, when the Richardson number is zero. As the denominator of equation 5.1 will always be positive and defined, the numerator must go to zero if the Richardson number is zero. But this is just the condition for convective instability, namely, the temperature gradient is decreasing faster than the adiabatic lapse rate. Any parcel of fluid that is accelerating upwards will continue to accelerate while those conditions occur and hence the atmosphere will be unstable.

Although this is the most obvious boundary when studying the instability of internal gravity waves, several other boundaries need to be considered. Miles (1961) and Howard (1961) considered small perturbations of a shear flow in an inviscid, incompressible fluid. They showed that a Richardson number greater than ¼ was a sufficient condition to ensure that the flow was stable.

However, a lack of stability might not be a strong enough criterion to determine whether a wave does become unstable. Howard (1961) and Miles (1961) showed that stability is assured if the Richardson number is greater than ¼ everywhere in the fluid. But instability does not necessarily occur if the Richardson number is less than ¼ (Howard and Maslowe (1973)). Obviously, in the case where the Richardson number is less than zero, instability does occur, but there may be some other value of the Richardson number at which turbulence will occur.

Townsend (1958) considered stability from the viewpoint of when turbulent motion could possibly cease to exist if it was already present. In other words, the minimum possible value that the Richardson number could have when turbulence might not be present. Therefore, Townsend (1958) has set a lower limit of the value for which the wave will produce turbulence. Townsend (1958) studied the conditions for which a fluid would be turbulent or laminar. The boundary between the two regimes was found to occur when the flux Richardson number was ½. (The flux Richardson number (Ri_F) is defined as (Houghton (1977))

$$Ri_F = \frac{-g}{T} \frac{Q}{C_p \tau \frac{du}{dz}} \qquad (5.2)$$

where Q is the vertical flux of heat and τ is the shearing stress. The other symbols are defined elsewhere.) This

corresponds to the ordinary Richardson number, defined in equation 5.1, having a value of 0.08. Therefore, if the Richardson number is less than 0.08, turbulence occurs. Townsend (1958) also reported several experiments that supported the validity of his theoretical arguments, finding the onset of turbulence to occur when the Richardson number was 0.1.

Woods (1969) looked at the conditions where a flow that was already turbulent would become laminar. He found that, if the Richardson number was greater than unity, then the reverse transition from turbulent to laminar condition always occurs. This condition seems unlikely to affect the onset of internal gravity wave breaking.

The terms convective instability and velocity shear instability need to be defined.

Velocity shear instability arises because the vertical shear of horizontal velocities is sufficiently large to cause turbulence at some critical Richardson number. This type of critical Richardson number is that experimentally found by Townsend (1958).

Another form of instability is convective instability. Convenctive instability occurs when the temperature gradient decreases more rapidly than the dry adiabatic lapse rate (Γ). A particle that is accelerated upwards continues accelerating upwards. Convective overturning then occurs and stability is renewed. The critical point for such instability is a Richardson number of zero and hence a local Brunt frequency of zero.

Hodges (1967, 1969) considered the growth of wave amplitude with height and the ultimate limiting of the wave amplitude due to the onset of turbulence. Hodges (1967) calculated that, for short period internal gravity waves, the

magnitudes of velocity shears would have to be much larger than those actually observed in the mesosphere to produce turbulence due to the Richardson number falling below ¼. In other words shear instability is unlikely to be the cause of the breaking of short period internal gravity waves. Hodges (1967) then went on to calculate the conditions in which breaking would occur and found that this coincides with the parts of the wave for which the velocity shear is zero. Thus internal gravity wave breaking is due to convective instabilities. This problem has been discussed for a wider range of frequencies by Fritts and Rastogi (1985). They concluded that, when the frequency was much larger than the inertial frequency ($f \equiv 2\Omega\sin\phi$), convective instability dominates internal gravity wave breaking. Lindzen (1968) concluded that wave breaking also restricted the amplitude of atmospheric tides.

At this point it is worthwhile to define the terms wave breaking and saturation. Breaking is the condition that occurs when the amplitude of the wave is large enough for turbulence to be generated in part of the wave. Saturation refers to the limitation of wave amplitude due to instabilities (breaking) or wave-wave interaction (Fritts (1984)).

The problems of the critical value for the onset of turbulence and the mechanism for the breaking of internal gravity waves have been studied in a number of laboratory experiments since Orlanski and Bryan (1969) found that much more energy was required to produce velocity shear instability in internal gravity waves than was required to produce convective instability.

A number of laboratory experiments considered related problems. McEwan (1971, 1973) and Orlanski (1972) concluded that convective instabilities caused the breaking in internal

gravity waves. Delisi and Orlanski (1975) found that local overturning occurred for large wave amplitudes and that there was a crtical amplitude at which this effect began to occur.

More recently Thorpe (1978) made calculations of the conditions required for wave breaking in laboratory experiments that included a mean velocity shear in the flow. Thorpe found that the effect of this shear was to reduce the amplitude needed for the onset of convective instability. McEwan (1983) found that the Richardson number was critcally low only in the immediate region where convective instability occurred. In other words, the regions where velocity shear instability and convective instability occur virtually coincide. Koop's (1981) laboratory experiments produced convective instability in both critical layer and non-critical layer flows. Koop found that virtually no internal gravity wave momentum flux penetrates the critical region. Koop and McGee (1984 - as reported in Fritts (1984)) observed velocity shear instabilities in two dimensional internal gravity wave fields, but found that convective instabilities were more easily generated.

This laboratory work, which indicates that convective instability is the dominant method of internal gravity wave breaking, has been supplemented by theoretical models of the behaviour of the Richardson number when the amplitude of internal gravity waves is large.

Since Hodges' (1967) theory studies that pertain directly to the conditions for instability due to internal gravity waves have been added to the earlier work of the general conditions for the onset of turbulence (e.g. Miles (1961), Howard (1961) and Townsend (1958)), Fritts and Geller (1976) produced numerical models of the behaviour of internal gravity waves approaching critical layers. They

found that the region where the Richardson number was below ¼ was a little larger than the region where the Richardson number was below zero, but that convective instability dominated most of the critical region. Fritts (1982) found that the region where convective instability could occur was almost identical to the region where velocity shear instability could occur. Thus convective instability is expected to dominate shear instability, a result that is consistent with the laboratory experiments discussed earlier.

A recent theoretical study (Fritts (1985)) has considered the importance of wave-wave interactions in limiting the amplitude of internal gravity waves. Fritts found that convective instability was more important than wave-wave interactions in limiting the amplitudes, but that wave-wave interactions acted to decrease the amplitude of which convective instabilities could occur.

Observational studies have found that internal wave breaking due to velocity shear instabilities can occur in the stratosphere. Sato and Woodman (1982) studied the correlations between echo strength and wind shears due to long period internal gravity waves. The results indicated that maximum echo strength (and hence maximum turbulence - see Chapter 6) occurred when the velocity shear was a maximum. Barat (1982) used anenometers suspended from balloons to measure stratospheric wind shear. Barat also found that turbulence was associated with the maximum wind shear due to internal gravity waves. Barat (1983), using a similar experiment, concluded that strong wind shears due to long period inertio-gravity waves were associated with turbulence in the stratosphere. Balsley et al (1983) explained the summer echoes that were received from the mesosphere above Poker Flats as being due to turbulence generated by velocity shear instabilities in

long period inertio-gravity waves.

At first sight these results seem to contradict both the extensive data from laboratory experiments and the theoretical calculations which find that convective instability causes the breaking of internal gravity waves. However, Fritts and Rastogi (1985) pointed out that, while short period internal gravity waves break due to convective instability, internal gravity waves with periods near the inertial frequency ($f \equiv 2\Omega\sin\phi$) are more likely to break due to high wind shears. Their results are discussed more fully in Chapter 6.

There is some evidence of convective instability for short period internal gravity waves in the mesosphere. Lindzen (1981) pointed out that the amplitude of the temperature fluctuations in the rocket data given by Theon et al. (1967) for heights above about 50 km in winter and 70 km in summer were large enough to produce convective instabilities above Wallops Island (38N). The winter profiles at Fort Churchill also include waves with sufficiently large amplitudes to produce convective instabilities. Philbrick et al. (1983) have published rocket derived winter mesospheric temperature profiles which include wave amplitudes that are large enough to produce convective instabilities.

Thus for motions with periods of less than 3 hours the most likely form of instability is expected to be convective instability. In the next chapter consideration is given to the type of profiles that are expected to occur when internal gravity wave amplitudes are limited by convective instability.

5.3 Variance plots and amplitude restrictions

From the discussion in section 5.2 it can be seen that internal gravity wave amplitudes are restricted to values by the onset of turbulence when the Richardson number falls below some limiting value. Therefore, it is reasonable to assume that the amplitude of internal gravity waves will be restricted to some maximum value. Lindzen (1981) observed that neutral or unstable lapse rates could be found above 50 km in winter and above 70 km in summer. Variance profiles above these heights should show some effects of wave breaking above these heights, which include virtually all of the heights studied in the partial reflection drifts experiment. In practice, internal gravity wave variance profiles do have restricted amplitudes below heights of from 80 km to 85 km, but there is a marked increase in amplitude above this height (e.g. see Ball (1981)). If breaking is in fact the main mechanism that controls the amplitudes of internal gravity waves at these heights, then the model used must explain the increase in variance with height above 80 km as well as the constant variance with height below this altitude. Similarly, any other mechanism that is used to explain the observed variance profile must be able to explain the changes of variance with height, as well as any seasonal changes that might exist in the variance profiles.

The first diagrams that are required are a series of variance-height profiles over a year. To avoid being overwhelmed by a large number of diagrams, these variance height profiles have been included in 3-dimensional plots of variance, height and month (figures 5.1 and 5.2). Some information is lost, or at least obscured, when this technique is used and where necessary individual and seasonal profiles are included. Generally, the two years graphed in figures 5.1

Figure 5.1

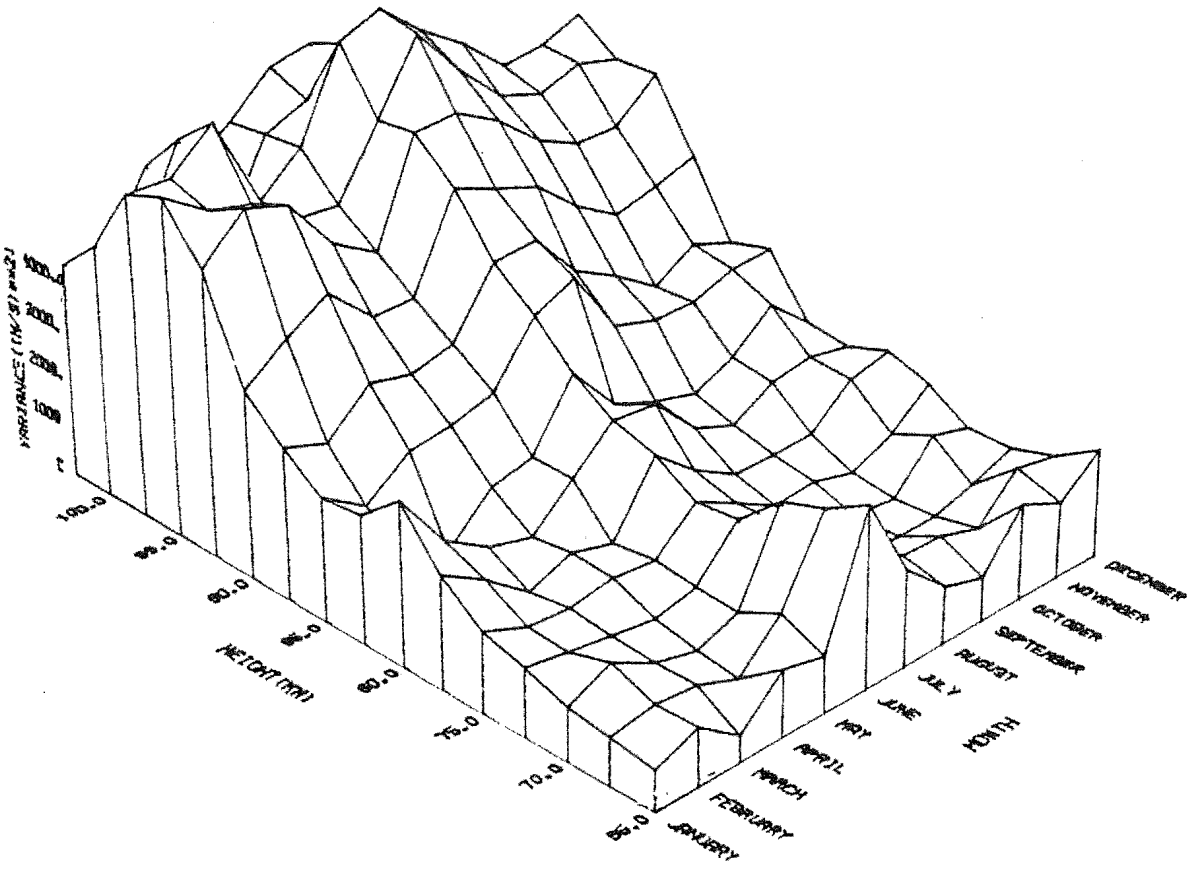

The variance due to short period motions over Birdling's Flat in 1981. A 3 hour filter is used to isolate these motions.

Figure 5.2

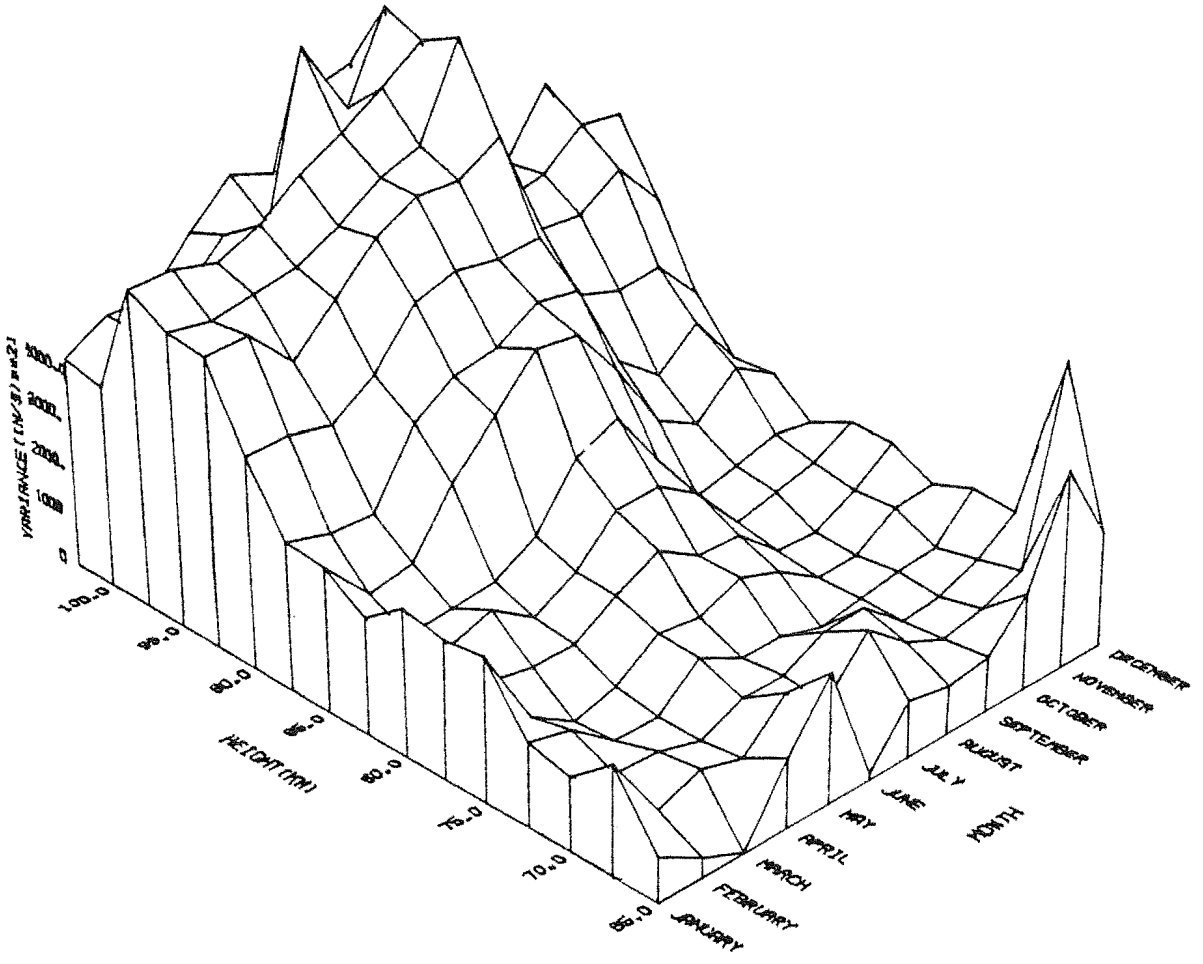

The variance due to short period motions over Birdling's Flat in 1982. A 3 hour filter is used to isolate these motions.

and 5.2 are similar: amplitudes begin to increase markedly near 77.5 km in winter and at about 85 km in summer. Variances are at a maximum in winter at nearly every height. There is a secondary maximum in summer. The values of variance are the least reliable at 65 km and 67.5 km, where these values have been calculated with the use of very little data. At about 90 km up to about 1000 data points have been measured in a month after filtering has taken place. Notice that in all months the variance decreases above about 95 km. The data at these heights consist of a large number of points. Therefore, this feature needs to be explained when the profiles are being discussed.

At this stage it is by no means apparent that the behaviour of the various profiles needs to be explained in terms of wave breaking or that it should be explained in this way.

The first question that needs to be answered is whether or not the mechanism that retricts the variance ceases to operate above 77.5 km in winter and above 85 km in summer. If this is the case then the amplitude should increase approximately as the exp(Z/2H) function determined from Hines' (1960) equations and the variance should increase as exp(Z/H).

Table 5.1 shows that the value of H is about 6 km in the region above 80 km to 85 km. Therefore, if the amplitude is increasing without restriction, the variance profiles should increase as exp(Z/H), where H = 6 km. Figures 5.3 to 5.8 are plots of the logarithm of variance against height that have been divided into seasons. Two lines are drawn on each graph showing the slope of the expression exp(Z/H). One line corresponds to H = 6 km, the other corresponds to H = 12 km. In each "season" the slope has a different value, but in no season is the slope of the variance profile as large as the

TABLE 5.1 THE SCALE HEIGHT OF THE ATMOSPHERE AS A FUNCTION OF HEIGHT AND MONTH

Height (km)	January	February	March	April	May	June	July	August	September	October	November	December
65	6.8	6.7	6.6	6.6	6.7	6.9	7.0	6.9	6.9	6.9	7.0	6.9
67.5	6.5	6.4	6.3	6.4	6.6	6.8	6.8	6.7	6.7	6.8	6.7	6.6
70	6.2	6.2	6.1	6.2	6.4	6.6	6.6	6.6	6.6	6.6	6.5	6.3
72.5	5.8	5.9	5.9	6.1	6.3	6.5	6.5	6.5	6.5	6.4	6.2	6.0
75	5.6	5.7	5.8	5.9	6.2	6.3	6.3	6.3	6.3	6.3	6.0	5.7
77.5	5.4	5.4	5.6	5.9	6.1	6.2	6.2	6.2	6.2	6.1	5.7	5.5
80	5.1	5.2	5.5	5.8	6.0	6.1	6.1	6.1	6.0	5.9	5.5	5.2
82.5	4.9	5.0	5.4	5.7	5.9	6.0	6.0	6.0	5.9	5.7	5.3	5.0
85	4.7	4.9	5.3	5.7	5.9	6.0	6.0	6.0	5.8	5.5	5.1	4.8
87.5	4.7	5.0	5.4	5.7	5.9	6.1	6.0	5.9	5.7	5.4	5.0	4.7
90	4.7	5.2	5.5	5.8	6.0	6.1	6.0	5.8	5.6	5.4	4.9	4.5
92.5	5.1	5.4	5.7	5.9	6.1	6.2	6.0	5.8	5.7	5.5	5.1	4.9
95	5.5	5.8	5.9	5.9	6.2	6.3	6.1	5.8	5.8	5.6	5.4	5.2
97.5	6.0	6.0	6.0	6.1	6.4	6.3	6.1	5.9	5.9	5.8	5.7	5.8
100	6.5	6.2	6.1	6.3	6.5	6.4	6.1	6.1	6.1	6.0	6.1	6.4
102.5	6.9	6.4	6.3	6.5	6.7	6.4	6.2	6.3	6.4	6.4	6.6	6.9

Figure 5.3

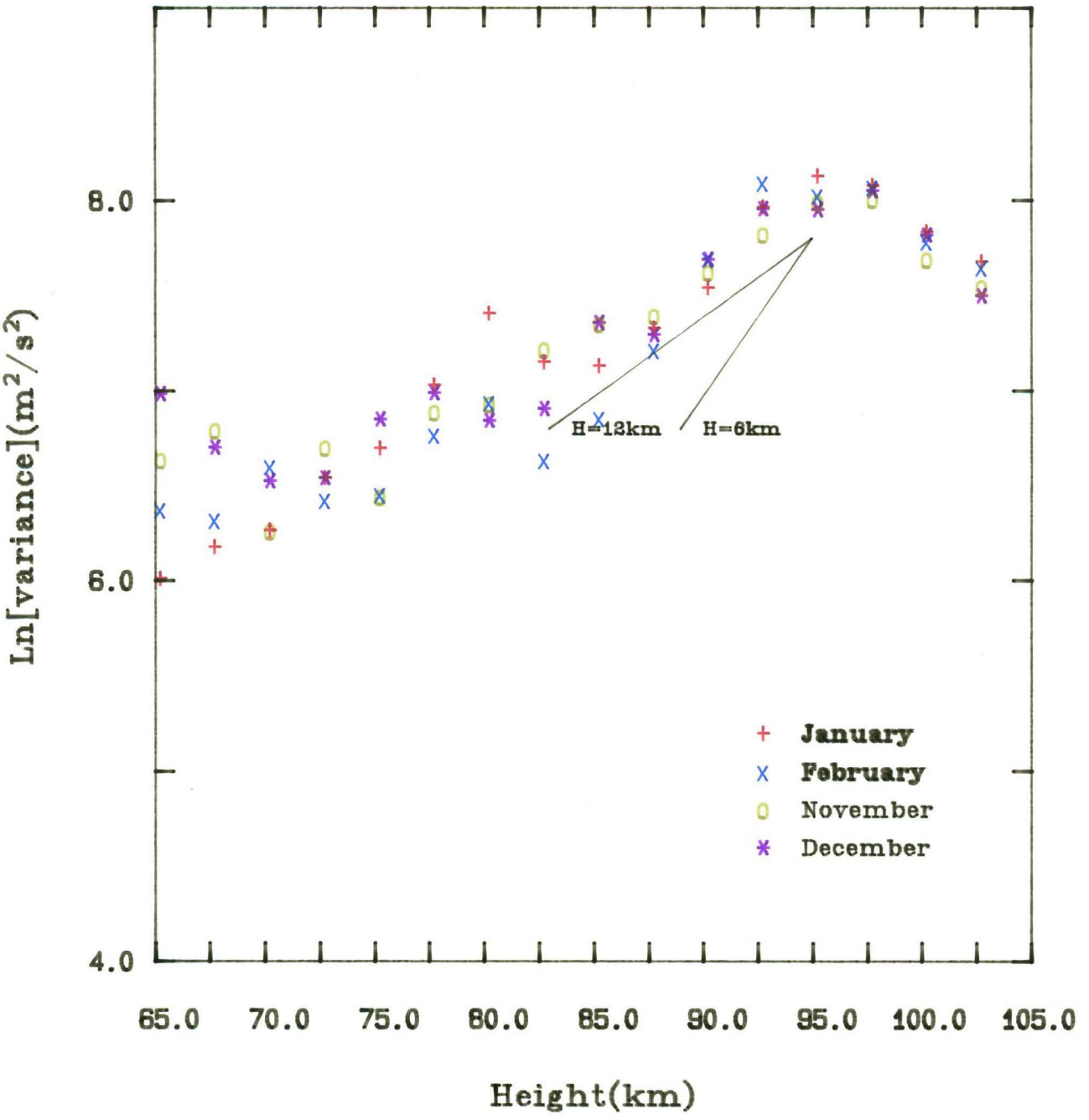

The natural logarithm of the variance for frequencies of less than 3 hours at Birdlings Flat in the summer months of 1981.

Figure 5.4

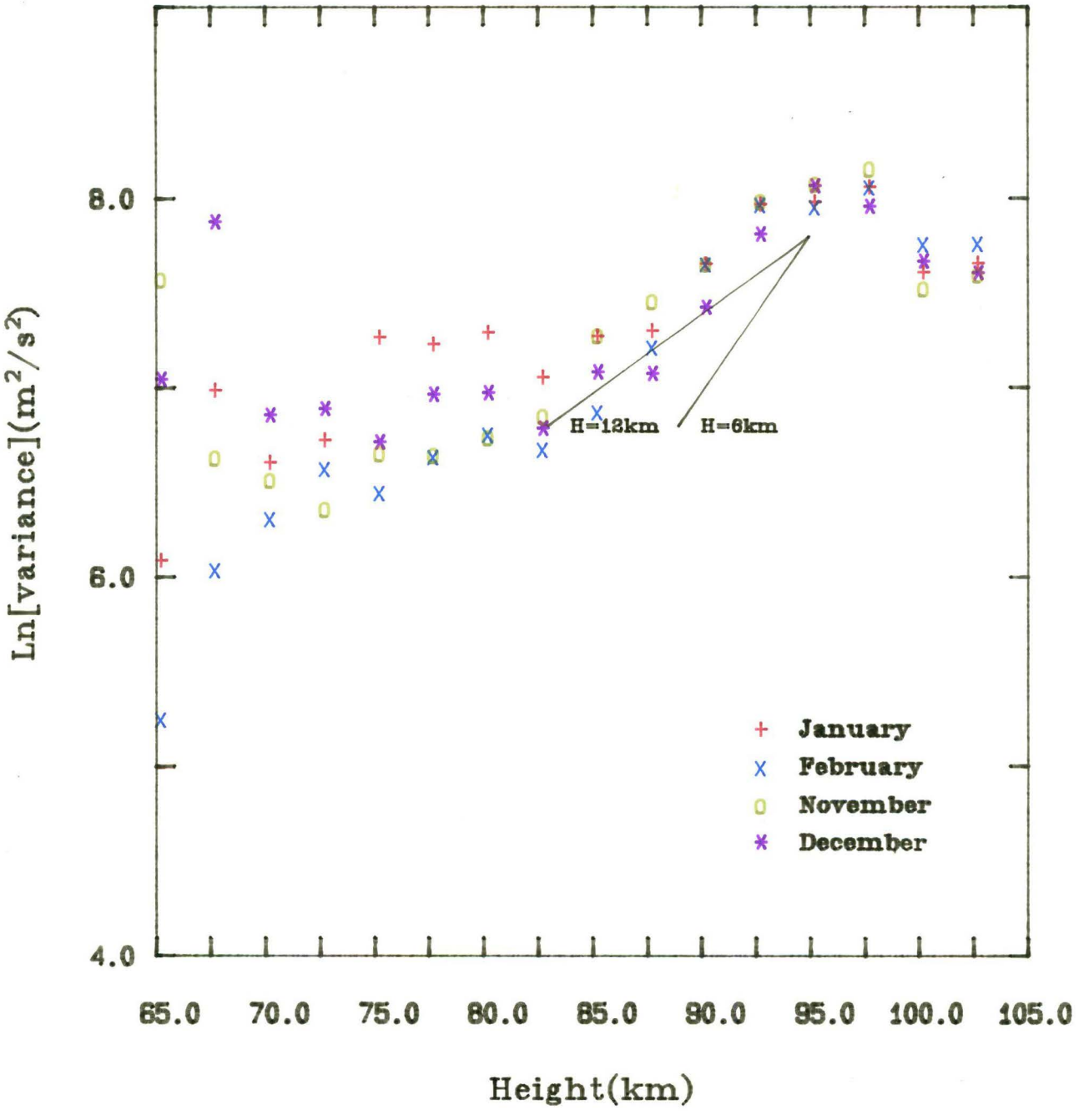

The natural logarithm of the variance for frequencies of less than 3 hours at Birdlings Flat in the summer months of 1982.

Figure 5.5

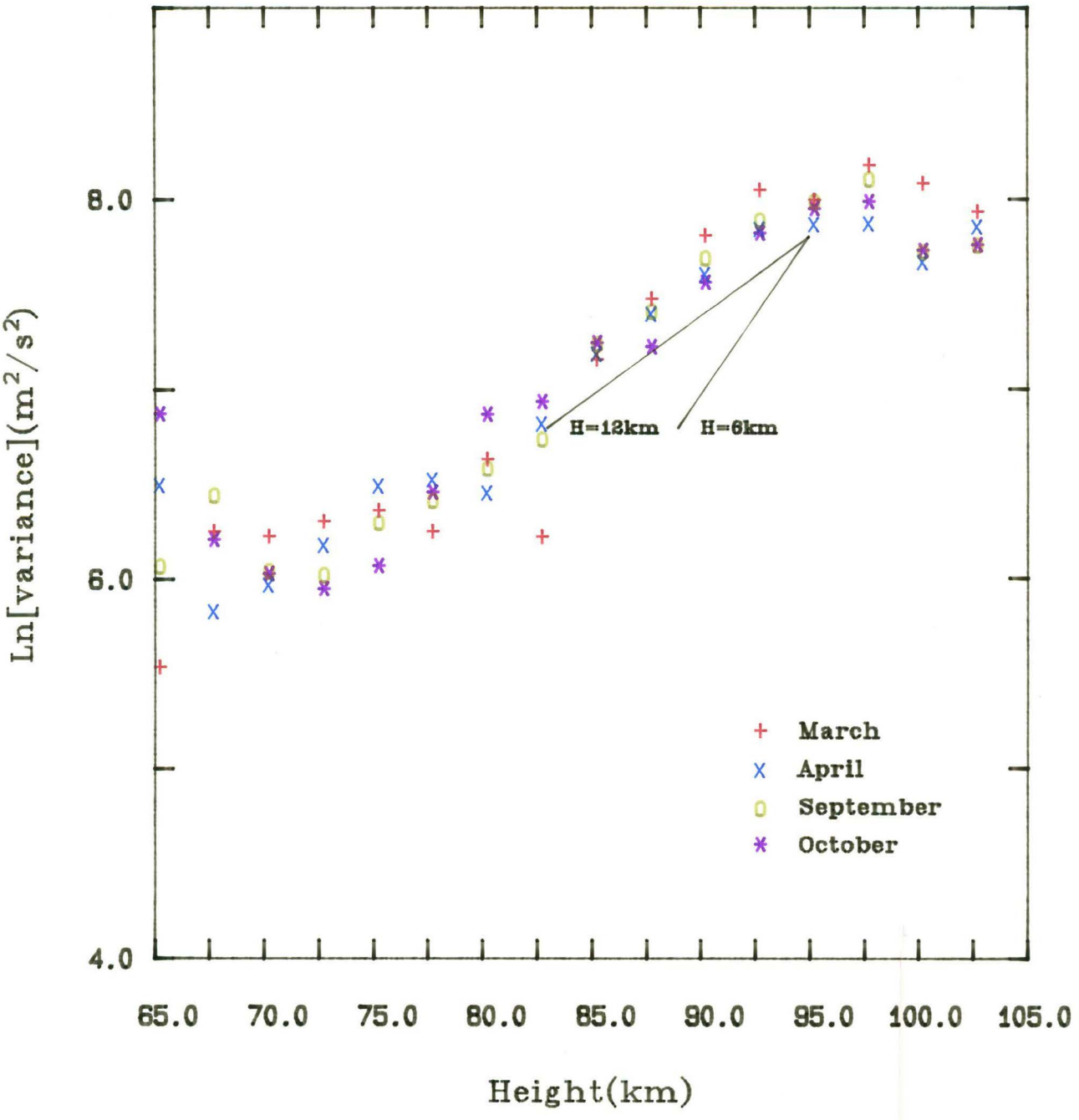

The natural logarithm of the variance for frequencies of less than 3 hours at Birdlings Flat in the equinoctial months of 1981.

Figure 5.6

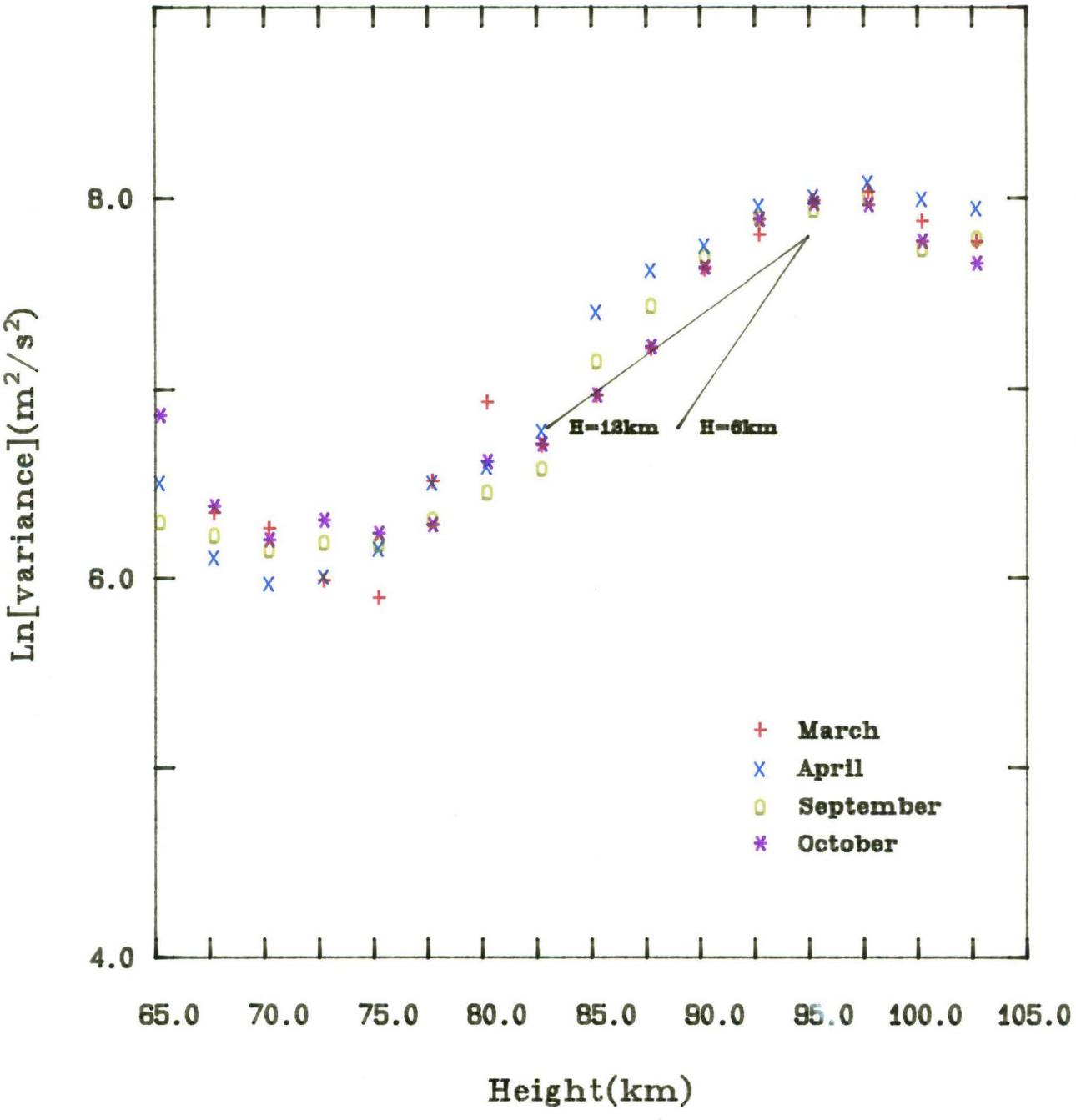

The natural logarithm of the variance for frequencies of less than 3 hours at Birdlings Flat in the equinoctial months of 1982.

Figure 5.7

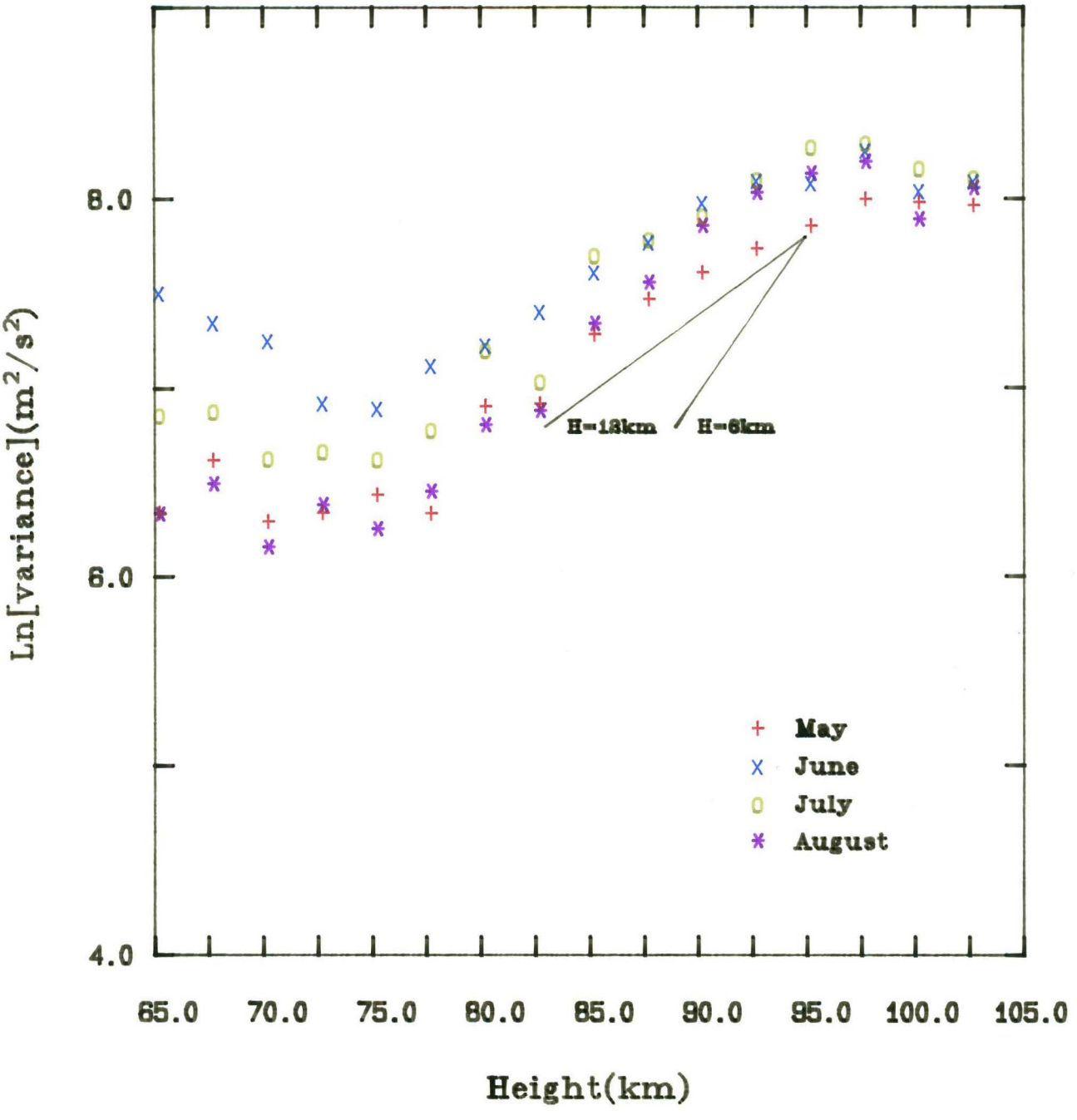

The natural logarithm of the variance for frequencies of less than 3 hours at Birdlings Flat in the winter months of 1981.

Figure 5.8

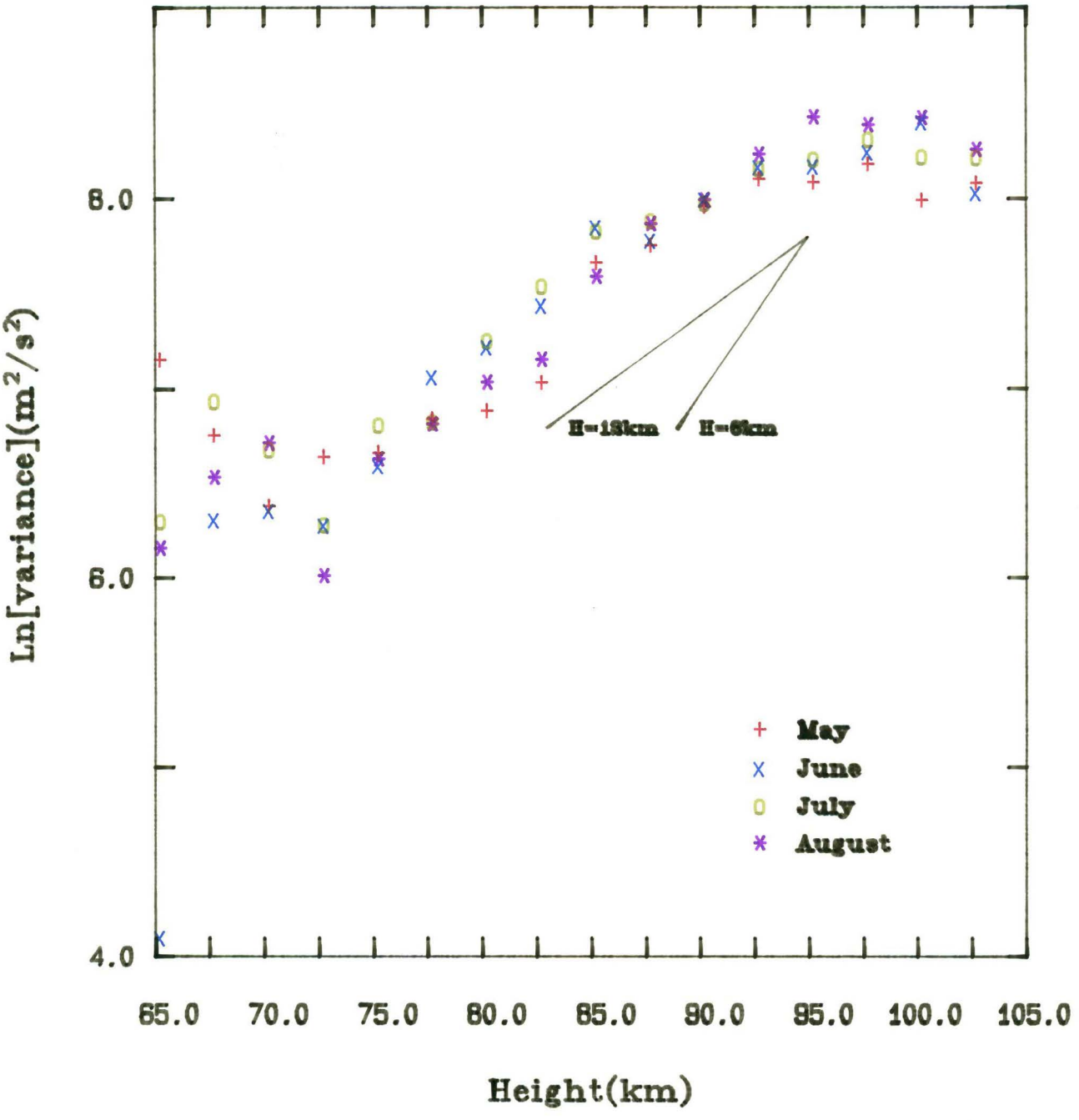

The natural logarithm of the variance for frequencies of less than 3 hours at Birdlings Flat in the winter months of 1982.

exp(Z/2H) function. The profiles in the 85 km to 92.5 km height range would correspond to scale heights from 1.5 to 2 times larger than the scale heights actually found in this region. Therefore, the increase in the variance cannot be ascribed merely to the removal of the mechanism that limits amplitudes to values below 20 to 30 m/s.

One other point that can be obtained from these graphs is the consistency of values of variance in any one season at any particular height greater than about 80 km. Again, the assumption that appears to be best is that there is a strong controlling mechanism acting at these heights which does not change in a "season" and for any particular "season" does not change over the 2 years that were studied.

In this region where the amplitude and hence the power is increasing rapidly, comparatively little energy should be lost from the wave into the surrounding dynamical system. This point is discussed further later in the thesis.

In this chapter the background to instability has been outlined. In the next chapter these ideas will be applied in the form of a model of the variance profiles which will then be compared with the experimental variance profiles.

CHAPTER 6

A SIMPLE MODEL OF VELOCITIES OBTAINED FROM WAVE BREAKING CONSIDERATIONS

6.1 Introduction

The problem that was outlined in the last chapter involved explaining the variance profiles that were obtained for data with periods of less than 3 hours. The most promising explanation involved invoking wave breaking amplitude restrictions limiting the velocities at each height. To be successful, this wave breaking model must explain not only the almost constant variance below 80 km, but also the increase in variance up to about 95 km and the changes in variance above this height. It has already been established that the rate of increase is not sufficiently great for the increase to be due to the increase in amplitude that occurs when the density decreases and the energy remains constant.

In this chapter the idea that the variance profiles can be explained by a simple wave breaking model using the Richardson number criterion is tested. The problem of whether convective instability or shear instability is the dominant form of wave restriction is discussed.

The presence of zonal winds modifies the characteristics of internal gravity waves by giving rise to an intrinsic frequency of the wave relative to the mean flow ($\omega - u_o.k$). That is a Doppler shift occurs. This point is discussed qualitatively but the nature of the data prevents the calculation of either the average phase velocity or the average horizontal wavelength so quantitative solutions involving intrinsic frequencies are difficult to estimate.

The Behannon and Ness (1966) filters that are described

in Chapter 3 allow 5 to 8 hour and 8 to 24 hour period ranges to be isolated. The result from the 8 to 24 hour filter is dominated by the tides. The variances in this period range can be compared with the known experimental and theoretical changes of amplitude with height for the individual tides, (e.g. see Chapman and Lindzen (1970), Lindzen (1979) and Forbes (1984)). The amplitudes of these variances are also compared with the amplitudes of motions with periods of less than 3 hours and with the amplitudes of other period ranges.

Attempts are made to calculate changes of saturation amplitude with vertical wavelength. The variance profiles for motions with periods of less than 3 hours are used to determine changes in wave energy with height.

6.2 Wave Breaking Conditions and the Richardson Number

The Richardson number criterion has been involved by Hodges (1967) in discussing limits on internal gravity wave growth with height.

The Richardson number Ri is defined by

$$R_i = \omega_B^2 / |\partial u/\partial z|^2 \qquad (6.1)$$

where $\frac{\partial u}{\partial z}$ is the vertical shear of horizontal winds and ω_B is the Brunt frequency defined as

SEE ERRATA

$$\omega_B^2 = \frac{g}{T}\left(\Gamma + \frac{dT}{dz}\right) \qquad (6.2a)$$

$$= -g\left(\frac{1}{\rho}\frac{\partial \rho}{\partial z} + \frac{g}{\gamma R T}\right) \qquad (6.2b)$$

where R is the gas constant per kg mole per unit molecular mass

$\Gamma = g/c_p$ is the dry adiabatic lapse rate

γ is the ratio of specific heats $(\frac{c_p}{c_v})$

ρ is density,

T is temperature

and g is the accleration due to gravity.

For an isothermal atmosphere the equilibrium value of the Brunt frequency is

$$\omega_{Bo}^2 = \frac{(\gamma-1)g}{\gamma H} \tag{6.3}$$

where γ is the ratio of specific heats,

g is the acceleration due to gravity

and H is the scale height, defined as (Houghton (1978))

$$H = RT/g \tag{6.4}$$

It is assumed that ρ, v and T can be expressed as perturbations

$$\rho = \rho_o + \rho_1 + \ldots \tag{6.5a}$$

$$v = v_o + v_1 + \ldots \tag{6.6b}$$

and $$T = T_o + T_1 + \ldots \tag{6.5c}$$

but that terms of order greater than 1 are negligible. Furthermore, it is assumed that u_1 represents a two dimensional wave of the form

$$u_1 = u_{1\,0}\exp(i(\omega' t - k_x x - K_z z) \tag{6.6}$$

where $u_{1\,0}$ is the amplitude of the wave

ω' is the intrinsic frequency such that $\omega' = \omega - k_x u_o$

k_x is the horizontal wavenumber

and K_z is the vertical wavenumber.

Using the relationship between the density and the velocity amplitudes of internal gravity waves that was given by Hines (1974, Chapter 7), Hodges (1967) found the Richardson number at a particular point in space to be

SEE ERRATA

$$R_i \approx \frac{1-A_1\sin\phi_1}{A_1^2\cos^2\phi_1} \tag{6.7}$$

where A_1 is defined as

$$A_1 = u_o \left\{\frac{\gamma}{4(\gamma-1)RT_o}\left(1 + \left(\frac{2k_{z\,real}kT_o}{g}\right)^2\right)\right\} \tag{6.8}$$

and the phase ϕ_1 as

$$\phi_1 = \omega t - \tan^{-1} \frac{2k_{zreal} RT_o}{g} \qquad (6.9)$$

Thus at any particular point the local Richardson number can be treated as varying only with time as a wave passes. Thus as ϕ_1 changes, values of A_1 of greater than 1 can cause the Richardson number to decrease to levels at which the atmosphere can become locally convectively unstable.

Maxima and minima of the Richardson number can be found by differentiating equation 6.7 with respect to ϕ_1.

The resulting formula

$$\frac{\partial R_i}{\partial \phi_1} = 0 = -A_1{}^3 \cos^3\phi_1 + (1-A_1 \sin\phi_1) A_1{}^2 2\cos\phi_1 \sin\phi_1 \qquad (6.10)$$

has solutions that are odd multiples of $\pi/2$.

Thus the unstable regions can be expected to be centred on values of ϕ_1, when ϕ_1 is equal to odd multiples of $\pi/2$. In this simple model values of ϕ_1 that are odd multiples of $\pi/2$ correspond to the times when the velocity shear

$$\left|\frac{\partial u_1}{\partial z}\right|_{(x,z)} = \omega_{Bo}{}^2 A_1 |\cos\phi_1| \qquad (6.11)$$

is equal to zero and thus velocity shear instability is not the cause of wave breaking for short period internal gravity waves. SEE ERRATA

6.3 Richardson Number Instabilities and Wave Amplitude Increases with Height

Decreases of energy with height require a mechanism to cause this dissipation (e.g. instabilities, molecular viscosity). The latter mechanism damps waves with vertical wavelengths of <0.1 km at 80 km and <1 km at 100 km (Hines (1974, p.254)). See also Fukao et al. (1985) who study waves with short vertical wavelengths. Assuming that wave energy is constant with height and that atmospheric density decreases with height as exp(-Z/H)

and wave energy is of the form ρv_1^2, so that the velocity amplitude increases with increasing height as exp(Z/2H). At some height the amplitude resulting from this increase becomes sufficiently large to cause either instabilities and turbulent breakdown or interactions with other motions. The wave is said to have come saturated at this point: That is, the amplitude is limited by these instabilities or interactions (Fritts (1984)). This can also occur if the intrinsic frequency changes near a critical layer. A critical layer is a region where the phase velocity of a wave is equal to the mean wind spread. Thus the intrinsic frequency is zero in this case.

SEE ERRATA

6.4 Convective Instability, Shear Instability and Internal Gravity Waves

Hodges (1967) considered the application of the Richardson number to internal gravity wave breaking at heights between 80 km and 110 km and particularly between 80 km and 90 km where the atmosphere is roughly isothermal (mesopause region). Hodges calculated that, for equilibrium conditions, the velocity shear required to produce a Richardson number of 0.08, the critical value for the onset of turbulence given by Townsend (1958), varied from 70 to 90 $ms^{-1}km^{-1}$, a value that is much larger than the shears that are expected to occur due to internal gravity waves. The average vertical wavelength of internal gravity waves is between 10 km and 14 km (a value that is consistent with Kochanski's (1964) observations - further discussion on this point occurs later). The amplitude at, say, 90 km is obtained from the variance profiles of motions with periods of less than 13 hours (figures 6.1 and 6.2) and has a value of about 60 ms^{-1}. When the standard deviation of a sine wave is calculated, the value obtained is $\frac{1}{\sqrt{2}}$ times the ~~amplitude~~ of the sine wave. Thus the value of 60 ms^{-1} must be

multiplied by $\sqrt{2}$ to give the amplitude. In this case the resulting amplitude is 90 ms^{-1}. The observed shear then has a maximum value of about 20 $ms^{-1}km^{-1}$. Even given the possibility that the maximum amplitude is still being underestimated due to periods when little wave activity is present and thus the variance is small, this value of wave shear is considerably less than the 70 to 90 $ms^{-1}km$ required, suggesting that velocity shear instability is unlikely to be as important as convective instability in considering amplitude restrictions on internal gravity waves. The inclusion of vertical shear of zonal wind in equation 6.1 reduces the value of vertical wave wind shear required to produce breaking when the vertical shear of the wave has the same sign as the vertical shear of the zonal wind. However, the maximum vertical shear of zonal wind (the zonal wind is given in table 8.2) is still only about 10 $ms^{-1}km^{-1}$ and is usually considerably less than the 70 to 90 ms^{-1} required for velocity shear instability. Thus, including a vertical shear of zonal wind does not alter the conclusions drawn about the likelihood of convective instabilities dominating shear instabilities.

Hodges (1967) calculated the values of ϕ_1 (see equation 6.7) for which the value of the Richardson number was a minimum. These minimum values occurred when ϕ_1 was an odd multiple of $\pi/2$. When ϕ_1 is $\pi/2$ the velocity shear is zero, suggesting that velocity shear is not important in trying to find the causes of wave instability (see also Fritts and Rastogi(1985)). Thus, when the magnitude of the velocity shear is minimised, the magnitude of the temperature shear is maximised : the conditions in which convective instability is most likely to occur. So convective instability is expected to dominate over velocity shear instability.

The problem of which type of instability is most likely to restrict the amplitude of internal gravity waves has been reconsidered more recently, both on a theoretial basis (e.g. Fritts (1982)) and on an experimental (as opposed to observational) basis (e.g. Thorpe (1978, 1981), Koop (1981) and Koop and McGee (1984) - the latter reference as summarised by Fritts (1984)).

Fritts and Geller (1976) calculated that, on approaching a critical layer from below, there was a larger region where wave instability resulted from the Richardson number being less than ~~a~~ ¼, ~~of~~ than the region that resulted from the Richardson number being less than zero. However, a later theoretical study by Fritts (1982) suggests that the region in which the Richardson number is less than ¼ evolves almost simultaneously with the region in which the Richardson number is less than zero and that the two regions are almost identical thereafter. Koop (1981) conducted an experimental study of wave induced instabilities in a mean flow and found that low Richardson numbers caused convective instabilities and overturning in a form similar to that discussed by Orlanski and Bryan (1969). Koop and McGee (1984) (as given in Fritts (1984)) observed the dynamical instability of a 2 dimensional internal gravity wave field and found that the range of amplitudes that permits dynamical instability without simultaneously permitting convective instability is small.

Balsley et al. (1983) found considerable difference between the experimental data in summer and winter at Poker Flat (65 N). The winter results were explained by Balsley et al. as being the result of convective instability, but they found that the VHF radar echo characteristics showed a single band in summer at a height that was considerably higher than that predicted by Lindzen (1981) for breaking due to convective

instability. They explained their summer echoes in terms of turbulence caused by shear instabilities of waves with periods near the inertial frequency rather than turbulence caused by convective instability in higher frequency internal gravity waves. This point needs to be considered further.

Fritts and Rastogi (1985) calculated the equation for the Richardson number in a form similar to that used by Hodges (1967), but included terms involving the inertial frequency. Thus the condition that $\omega'^2 >> f^2$ need no longer be applied. Thus Fritts and Rastogi (1985) give the equation

$$R_i = \frac{(1+A_1\cos\phi_1)(1-f^2/\omega'^2)}{A_1^2(\sin^2\phi_1+f^2\cos^2\phi_1/\omega'^2)} \qquad (6.12)$$

where ϕ_1 is defined as $\phi_1 = k\underset{\sim}{x} + mz - \omega' t$. SEE ERRATA SEE ERRATA

For a Richardson number of ¼ and $\phi_1 = \pi$ the amplitude of the wave (A_1) is given by

$$A_1^2 = (4\omega'^2/f^2)(1-f^2/\omega'^2)(1-A_1) \qquad (6.13)$$

The positive root for the amplitude is thus given by

$$A_1^2 = \frac{-\ell}{2} + \tfrac{1}{2}\sqrt{(\ell^2 + 4\ell)}$$

where $\ell \equiv 4(\omega'^2/f^2 - 1)$ (Fritts and Rastogi (1985)).

As f/ω' tends to zero, the critical amplitude for the onset of velocity shear instability tends to the amplitude of convective instability. Thus the regions where velocity shear instability and convective instability can occur are almost exactly the same. The behaviour of the critical amplitude for velocity shear instability has been plotted against f/ω' by Fritts and Rastogi (1985) (see figure 6.1).

The type of instability that dominates in the region where instability is possible can be found by solving the differential of the Richardson number with respect to ϕ_1. As ω increases away from the inertial frequency f, f/ω' becomes small and equation 6.12 tends towards equation 6.7. The

Figure 6.1

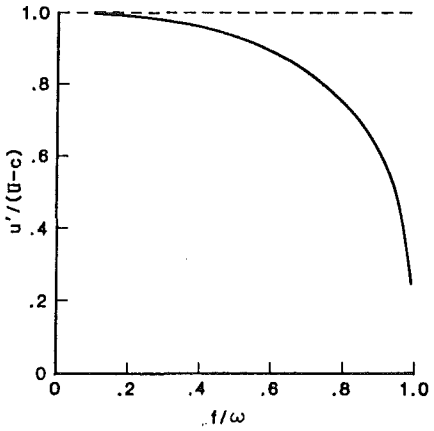

The wave amplitude required to produce velocity shear instability as a function of f/ω. The dotted line represents the amplitude required for convective instability (Fritts and Rastogi (1985)).

differences in phase in the two equations are due to the different defitions of ϕ_1.

Thus, for short period internal gravity waves, convective instability dominates ~~of~~ over velocity shear instability. SEE ERRATA This result is in agreement with laboratory experiments (e.g. Koop (1981), McEwan (1983) and Thorpe (1978)).

6.5 A Test for the Relationship between Shear and Turbulence

A simple test is used to determine whether velocity shear is related to the number of measurements made in an observation period. A high number of readings is assumed to indicate that turbulence is common in the observation period, while a low number of readings is assumed to indicate that turbulence is uncommon in the observation period (see section 6.6). A potential error exists in that data are also rejected when the fading time is very short (<0.5 S), indicating that rapid changes in the reflecting region are occurring. In other words, when a very large amount of turbulence is present.

Turbulence is assumed to occur in the region where internal gravity wave breaking occurs. Thus the method is intended to test whether the presence of a large amount of turbulence is associated with large velocity shears.[2]

Firstly, comparisons were made for a given height so that average temperature and electron density changes do not affect the results. The number of points measured in a month varies considerably with height with the maxima occurring at about 90 km.

At each height the shear of the average velocities was calculated over a period of 3 hours around midday for every day in a month. Thus the vertical shear of horizontal winds due to long period gravity waves, tides, planetary waves and mean winds contributed to the analysis. The resulting data

comprised a maximum of 31 values, the number of days in a month. Half the values were regarded as being "high" and half were regarded as being "low". Thus days of either "high" or "low" shear at a particular height were compared with days when the number of readings at the same height was either "high" or "low".

Coefficients of association (Kendall and Stuart (1967)) were then calculated. For a set of values

		Factor A	
		low	high
Factor B	low	a	b
	high	c	d

the coefficient of association is determined by

$$Q = \frac{ad-bc}{ad+bc} \tag{6.14}$$

and the variance of the coefficient of association is defined by

$$\mathrm{Var}Q = \tfrac{1}{4}\left(1-Q^2\right)^2 \left(\frac{1}{a} + \frac{1}{b} + \frac{1}{c} + \frac{1}{d}\right) \tag{6.15}$$

Coefficients of association of between -0.50 and -0.60 were obtained at Birdlings Flat. The actual values of these coefficients were: -0.62 ± 0.08 and Birdlings Flat in January 1981; -0.52 ± 0.10 at Birdlings Flat in June 1981; -0.56 ± 0.04 in October 1981 at Birdlings Flat; -0.37 ± 0.02 at Arrival Heights in January 1984. The uncertainties in these measurements are the standard deviations: 95% confidence intervals are given by multiplying these values by 1.96 in a normal distribution is assumed. Possible reasons for this behaviour are now considered.

6.6 A Justification for Relating the Number of Points to the Turbulence Level

The assumption that the number of echoes indicates the turbulence needs further consideration.

The number of useful wind measurements depends on the echo strength and the fading time of the received signal. In the latter case, the signal is rejected at times of very high turbulence because the fading time is too short (<½S). The signal is also rejected when the fading time is too large (>8S), which occurs when the amount of turbulence present is small.

The echo strength is related to the amount of turbulence present in the following way. The peak power received by the receiver is given by Hocking (1983) as

$$P_R = \frac{P_T G_T V \sigma e_T e_R A_R}{4\pi z^4} \qquad (6.16)$$

where P_T is the transmitter peak power,

G_T is the transmitter array gain

V is the volume defined by the locus of the half power points of the radar between the ground and the back-backscattering region

e_T is the efficiency of the transmitter,

e_R is the efficiency of the receiver

A_R is the effective area of the receiving array

and z is the height at which the scattering occurs.

The cross section of the backscatter (σ) is defined by Hocking as

$$\sigma = 0.00654\ \pi^{4/3}\ C_{NR}^2 \lambda^{-1/3} \qquad (6.17)$$

where λ is the wavelength of the radar signal

and C_{NR}^2 is the refractive index structure constant measured by the radar. This value of C_{NR}^2 is related to the refractive index structure constant for turbulence C_{NT}^2 by

$$\overline{C}_{NT}^2 = \overline{C}_{NR}^2 / F \qquad (6.18)$$

where F represents the fraction of the volume within the radar volume that is filled with turbulence.

If turbulence exists at a critical value of the Richardson number R_i(critical) (Hocking suggests $R_i = \frac{1}{4}$), the turbulent energy dissipation rate (ε_{turb}) is given by Hocking as

$$\varepsilon_{turb} = [C_{NT}^2 (a^2 \alpha' R_i(\text{critical}) \omega_B^2 M_e^2)^{-1}]^{3/2} \qquad (6.19)$$

where a and α' are constants

ω_B is the Brunt frequency

and M_e is the refractive index gradient given by

$$M_e = \frac{\partial n}{\partial N}\left[\frac{N}{T}\left(\frac{dT}{dz} + \Gamma\right) - \frac{dN}{dz} - (1.4\times10^{-4})N\right] + \frac{\partial n}{\partial \nu_m}\frac{\partial \nu_m}{\partial z} \qquad (6.20)$$

for the mesosphere, where

n is the refractive index,

N is the electron density,

T is the temperature

Γ is the adiabatic lapse rate

and ν_m is the collision frequency of electrons with neutral particles.

The direct relationship between turbulence and the refractive index structure constant for turbulence is going to depend upon whether M_e is constant over the period range. Certainly planetary waves have much less effect on the temperature gradient than shorter period motions in the mesosphere. Changes in electron density are a potential source of error. Also, the value of F, the fraction of the volume within the radar volume that is filled with turbulence, varies according to the level of internal gravity wave activity (assuming that the turbulence is formed by internal gravity wave breaking). The errors introduced by fluctuations in these quantities tend to reduce the value of the coefficient of association between the number of readings measured in a certain time and the

velocity shear, if in fact such a relationship exists. For a particular height the other quantities given in equations 6.14 and 6.15 are constant.

6.7 Problems with the Analysis

Apart from these problems with the physical relationship between the number of readings made and the amount of turbulence present, a much more serious problem arises due to the nature of the data. Ideally, in trying to do an analysis of "high" and "low" values of shear with "high" and "low" values of the number of readings taken in a given time at a given height there should not be a strong component of shear which has a period that is shorter than the sampling period. However, in the data which was analysed, a large high frequency component of the shear caused by internal gravity waves existed.

Test data for a given height were used to determine the effect of the velocity shears caused by short period internal gravity waves on the relationship between the shear of long period motions and the number of points in the "observation" period. A sine wave with a period of half the "observation" period and an amplitude of 40 ms^{-1} was used to simulate the effect of internal gravity waves. The vertical wavelength of this sine wave was 12 km. A second run of test data for another height were calculated. The short period sine component had a phase shift corresponding to a vertical wavelength of 12 km and the second run had a different mean velocity that gave rise to a mean shear shift of 10 ms^{-1} between the two runs. A small random component with a maximum value of 1 ms^{-1} was added. The resulting data pair were sampled at random intervals. Mean velocities over the "observation" periods were calculated and thus the shears over the "observation" periods were estimated.

Mathematically this can be expressed by defining the

first term as

$$a_1 = A\cos(kz_1-\omega t) + B_1 + R_1 \qquad (6.21a)$$

and the second term as

$$a_2 = A\cos(kz_2-\omega t) + B_2 + R_2 \qquad (6.21b)$$

SEE ERRATA

where A is the amplitude of the sine wave

B_i is the mean wind

and R_i is the random component.

The average of a_1 over each of m "observation" periods is subtracted from the average of a_2 over the same period in this model

$$\frac{1}{n}(\Sigma a_1-\Sigma a_2) = \frac{1}{n}\left(\sum_{i=1} A\left(-2\sin\left(k_z\left(\frac{z_1+z_2}{2}\right) - \omega t_i\right)\sin k_z\left(\frac{z_1 z_2}{2}\right)\right)\right.$$
$$\left. + n(B_1-B_2) + \sum_{i=1}^{n}(R_{1i}-R_{2i})\right). \qquad (6.22)$$

where n is the number of observations in each of the m observation periods.

The root mean square amplitude is obtained by averaging over the m "observation" periods.

When n = 1 the magnitude of the first term is just the root mean square of the amplitude of $\sin\left(k_z\left(\frac{z_1+z_2}{2}\right)-\omega t_i\right)$ namely

$$\left|-\frac{2}{\sqrt{2}} A\sin\left(k_z\left(\frac{z_1+z_2}{2}\right)\right)\right| \qquad (6.23)$$

As n gets larger the expected value of the first term on the left hand side of equation (6.22) tends to zero as $\int_{t=0}^{2\pi}\sin\omega t dt = 0$. Thus the existence of shears of motions with periods less than the "observation" period gives rise to a negative association between the number of points in the observation period and the shear.

The test data were run with the number of points varying from 1 to 3, which is too small a number of values for Birdlings Flat where values of 1 to 8 would be more appropriate, but about correct for Arrival Heights. When

these test data were used the coefficient of association was calculated to be Q = -0.60 ± 0.25. Test data for a number of values ranging from 1 to 8 were also analysed. The resulting coefficient of association was -0.39 ± 0.08, where the uncertainty figure is the standard deviation and 95% confidence intervals are given by multiplying this value by 1.96.

The shear for motions with periods greater than the sampling frequency may have been underestimated, although the much longer vertical wavelengths of planetary waves and tides (Hirota (1984)) tends to reduce the vertical shear created by these motions. SEE ERRATA

Earlier it was found that a large apparent negative association occurs between the number of points in a time interval and the average shear over this time interval when ther e is a large component of shear that has a period of less than the sampling period. The number of points found in the 3 hour averages of wind data around midday varied from 2 to 12 with the average number of data peresent being of the order of 5 at Birdlings Flat and about 3 in January 1984 at the most useful altitudes at Arrival Heights.

Thus, conclusions cannot be drawn from these analyses about the degree of shear that exists when turbulence is greatest.

6.8 Variance Profiles and Convective Instability

A simple convective instability model will now be described. Comparison will be made with the observed variance profiles to see if the model is consistent with the observations.

Fritts (1984) used the adiabatic energy equation

$$\theta_1 = \left(- \frac{\partial \theta_o}{\partial z} / ik_x(u_o - c_x) \right) w_1 \qquad (6.24)$$

and assumed that the critical condition for wave breaking was a Richardson number of 0

$$\frac{\partial}{\partial z}(\theta_o+\theta_1) < 0 \qquad (6.25)$$

to develop condition for wave breaking in terms of the velocity amplitudes of the waves.

In equations (6.24) and (6.25) θ is the potential temperature defined as (Houghton (1978)) SEE ERRATA

$$\theta = T\left(\frac{P_o}{P}\right)^{\kappa} \qquad (6.26)$$

where k_x is the horizontal wave number

u_o the mean zonal wind

c_x the horizontal phase velocity

W_1 the vertical perturbation velocity

T the temperature

P the pressure

P_o the base pressure

and κ is a contant defined as $(c_p-c_v)/c_p = 0.288$ in dry air.

Fritts also assumed that $\nabla.V = 0$ (assumption of incompressibility) so that for two dimensional waves

$$u_1 \approx - \frac{k_{zreal}}{k_{xreal}} w_1$$

where $K_z = k_{zreal} + c/2H$ is the vertical wavenumber ~~and~~ SEE ERRATA

and K_z is assumed to vary only very slowly with height.

SEE ERRATA Equation (6.24) is differentiated with respect to z and the differentials of terms other than perturbations are regarded as negligible (Fritts (1984)). The following equation results for the real terms

$$\frac{\partial}{\partial z}(\theta_1)_{real} = -\frac{\partial \theta_o}{\partial z}\frac{k_{zreal} w_1}{k_x(u_o-c)} \qquad (6.28)$$

Using equation 6.22 gives

$$\frac{\partial}{\partial z}(\theta_1) = u_1 \frac{\partial \theta_o}{\partial z} / (u_o-c) \qquad (6.29)$$

Equations (6.29) and (6.25) were then used by Fritts to obtain the condition for wavebreaking due to convective

Figure 6.2

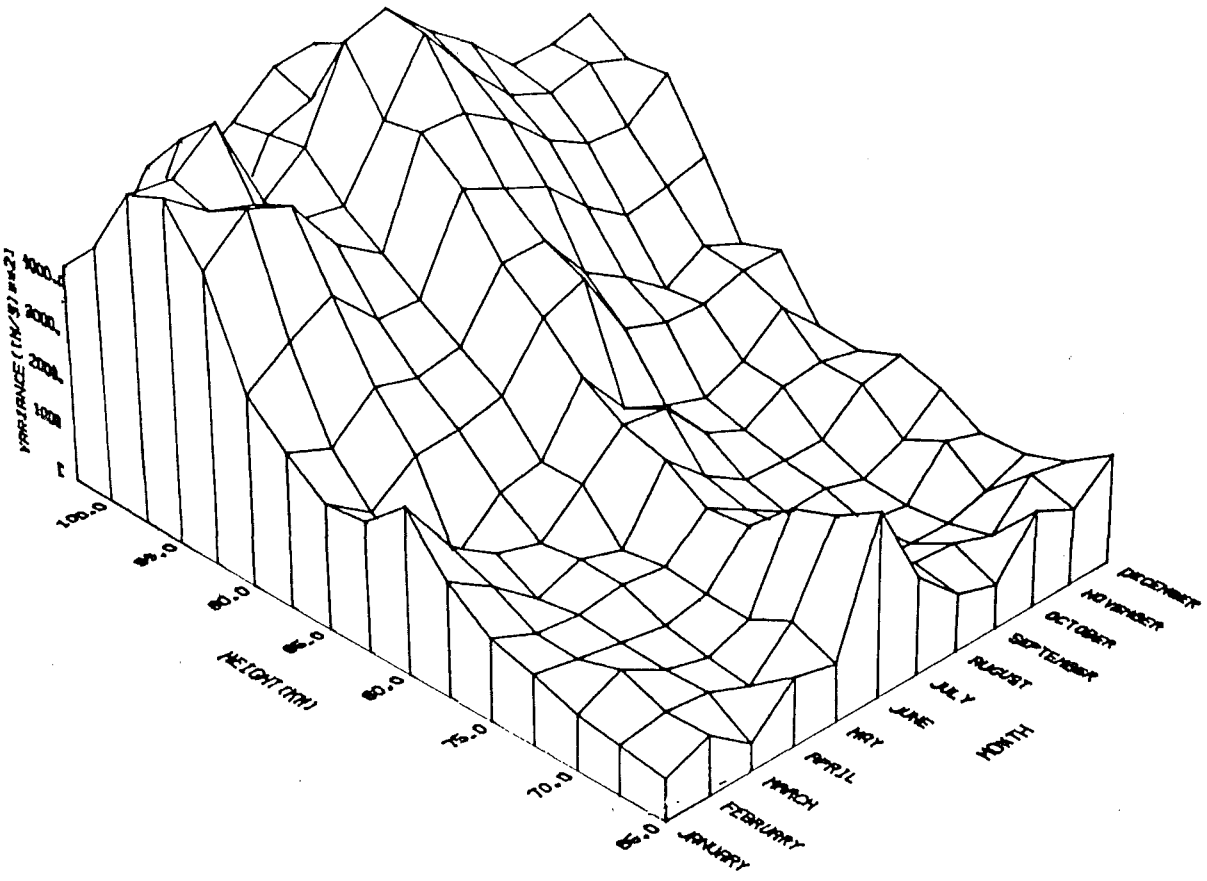

The variance due to short period motions over Birdling's Flat in 1981. A 3 hour filter is used to isolate these motions.

Figure 6.3

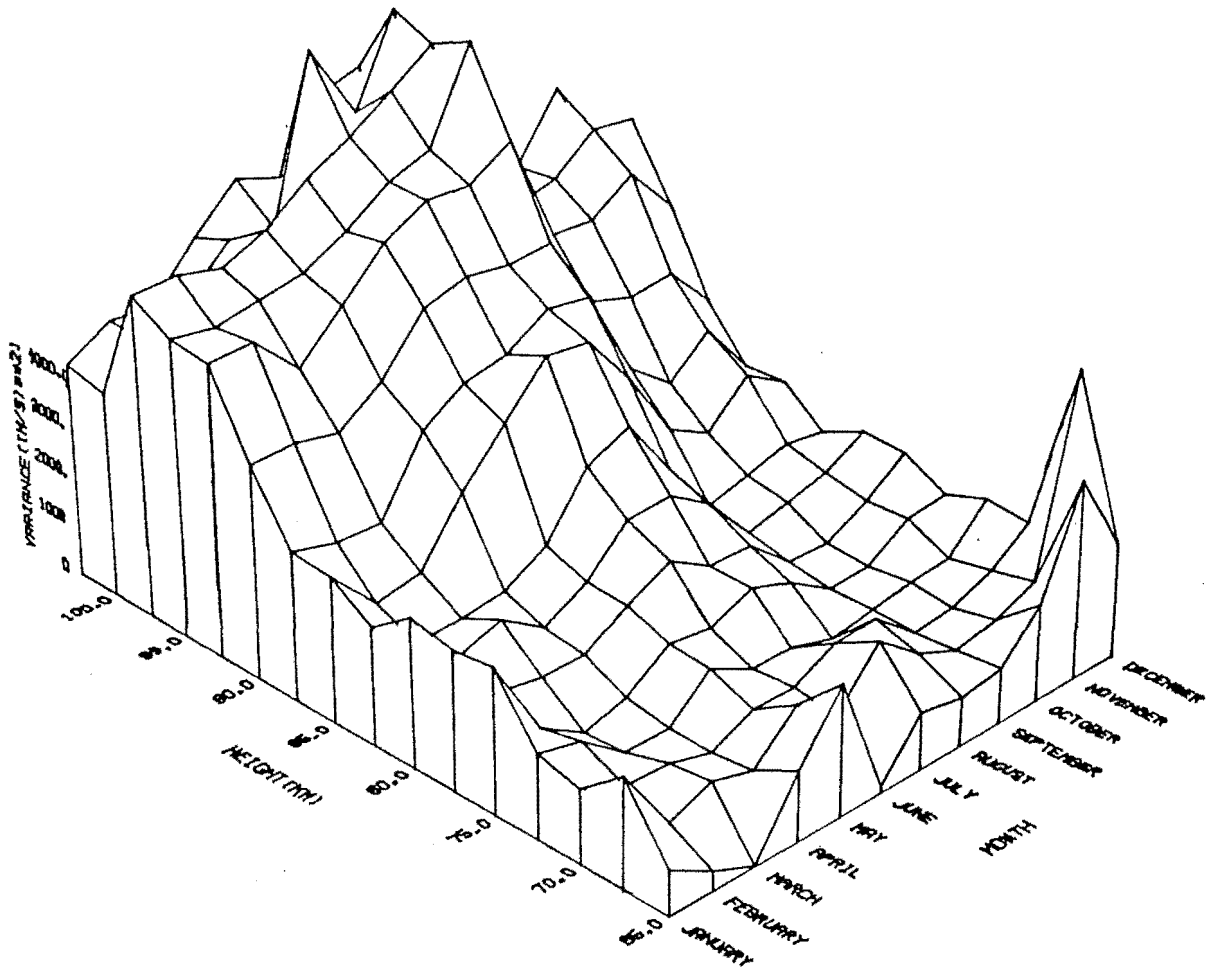

The variance due to short period motions over Birdling's Flat in 1982. A 3 hour filter is used to isolate these motions.

Figure 6.4

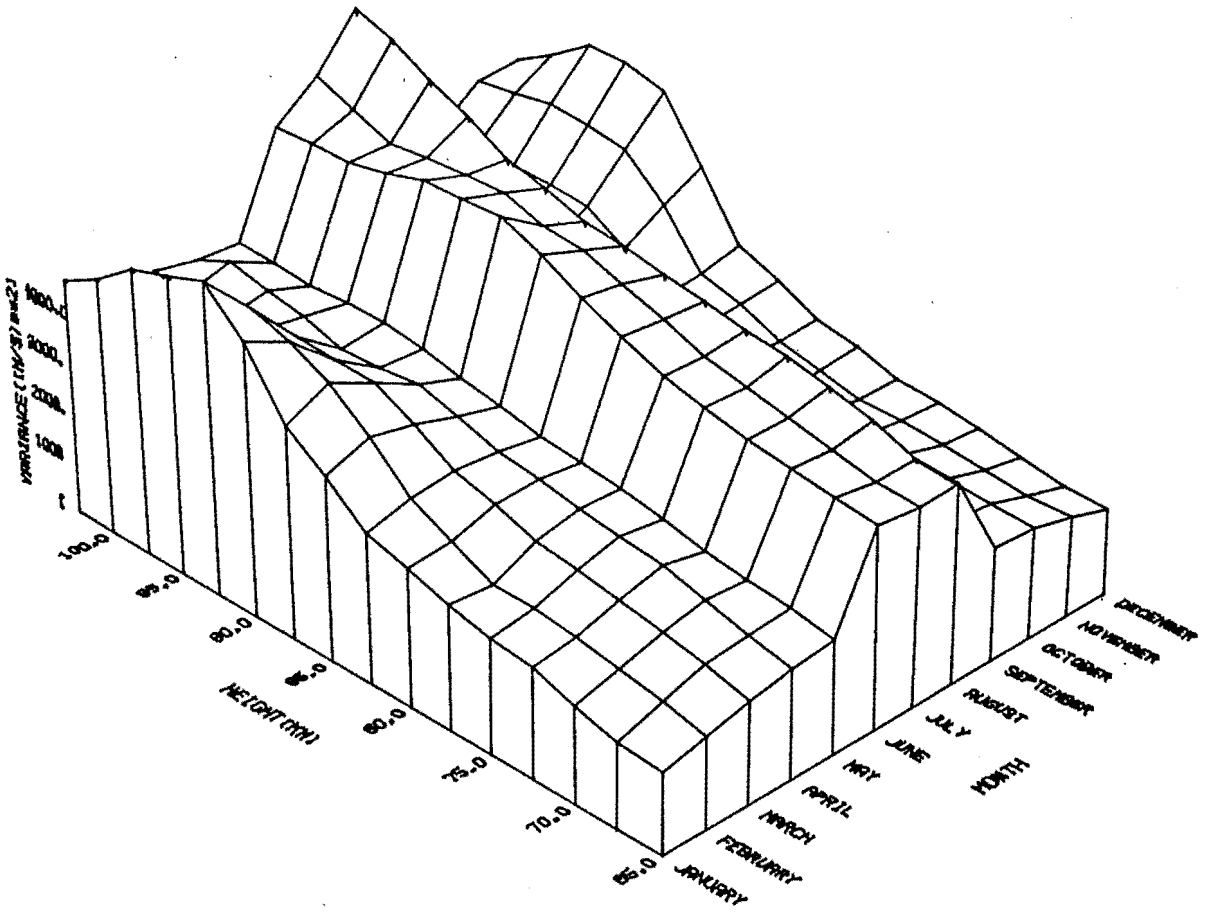

Simulated variances using a convective instability model. The temperatures are for 45N. The units are m^2/s^2.

instability

$$|u_1| > |c-u_o| \qquad (6.30)$$

For a single wave unstable regions occur when the total velocity due to the internal gravity wave motion, $|u_o| + |u_1|$, exceeds the phase velocity. In this case the horizontal displacement of particles by the wave is greater than or equal to half the wavelength. Hence turbulence is produced.

In 2 dimensions the dispersion equation is (Lindzen (1981)

$$|k^2_{zreal}| = \omega_B^2/(c-u_o)^2 - \frac{1}{4H^2} \qquad (6.31)$$

Equations (6.30 and (6.31) shows that the maximum value of the velocity amplitude squared that can occur before the wave becomes unstable is

$$|u_1|^2 = \frac{\omega_B^2}{|K_z^2|} \qquad (6.32)$$

where $K_z = k_{zreal} + i/2H$.

It has previously been assumed that the vertical wavenumber varies only slowly with height near the point where breaking occurs. The destruction of the internal gravity waves ultimately involves those waves approaching critical levels in Lindzen (1981) model and the vertical wavelength becomes small as a wave approaches a critical layer.

Equation (6.32) is used to construct a set of monthly variance profiles (figure 6.4) that can be compared with figures 6.2 and 6.3; the observed variance profiles for 1981 and 1982 respectively. Whilst the agreement between the observed variance profiles and the model variance profiles is only fair, the gross features of the observed variance profiles are reflected in the model variance profiles. The variance increases with height in each month with pronounced peaks

being found at heights between 90 km and 95 km in summer. When a constant vertical wavelength is assumed, the variance is greater at heights over 90 km in summer, because the temperature shears are bigger above the mesopause in summer. There is a minimum in winter at these heights if the same vertical wavelength is used. Therefore a different vertical wavelength must be assumed in June, July and August to reconcile the model with the observed variances. The vertical wavelengths used were 16 km in winter and 12 km in the rest of the year. The jusitification for this is considered later. Another problem which can cause inaccuracies in the model is considered first.

The model profiles (figures 6.4 to 6.6) were constructed using COSPAR(CIRA(1972)) data. This tends to be indicative of the northern hemisphere atmosphere rather than the southern hemisphere atmosphere, as is discussed in chapter 3. Thus the theoretical profiles reflect the temperature conditions that occur at 45 N not the conditions that occur at 45 S. The temperature data of Sehra and Hariharn (1981) indicate that southern hemisphere middle latitude winter temperatures may be as much as 15 K colder at heights of 75 km than northern hemisphere middle latitude winter temperatures. The difference is much smaller in summer (see figure 3.1). To account for this effect temperatures have been estimated from the contour plots given by Sehra and Hariharn (1981) (and are therefore fairly inaccurate) and are substituted for the COSPAR(CIRA(1972)) data at heights below 80 km in June, July and August. Uncertain-times in determining the temperatures from the contour plots are large (approximately ± 5 K), but the use of southern hemisphere temperature data below 80 km does produce theoretical profiles (figure 6.5) that are more like the observed variance profiles (figure 6.2 and 6.3) than the profiles that are constructed using

Figure 6.5

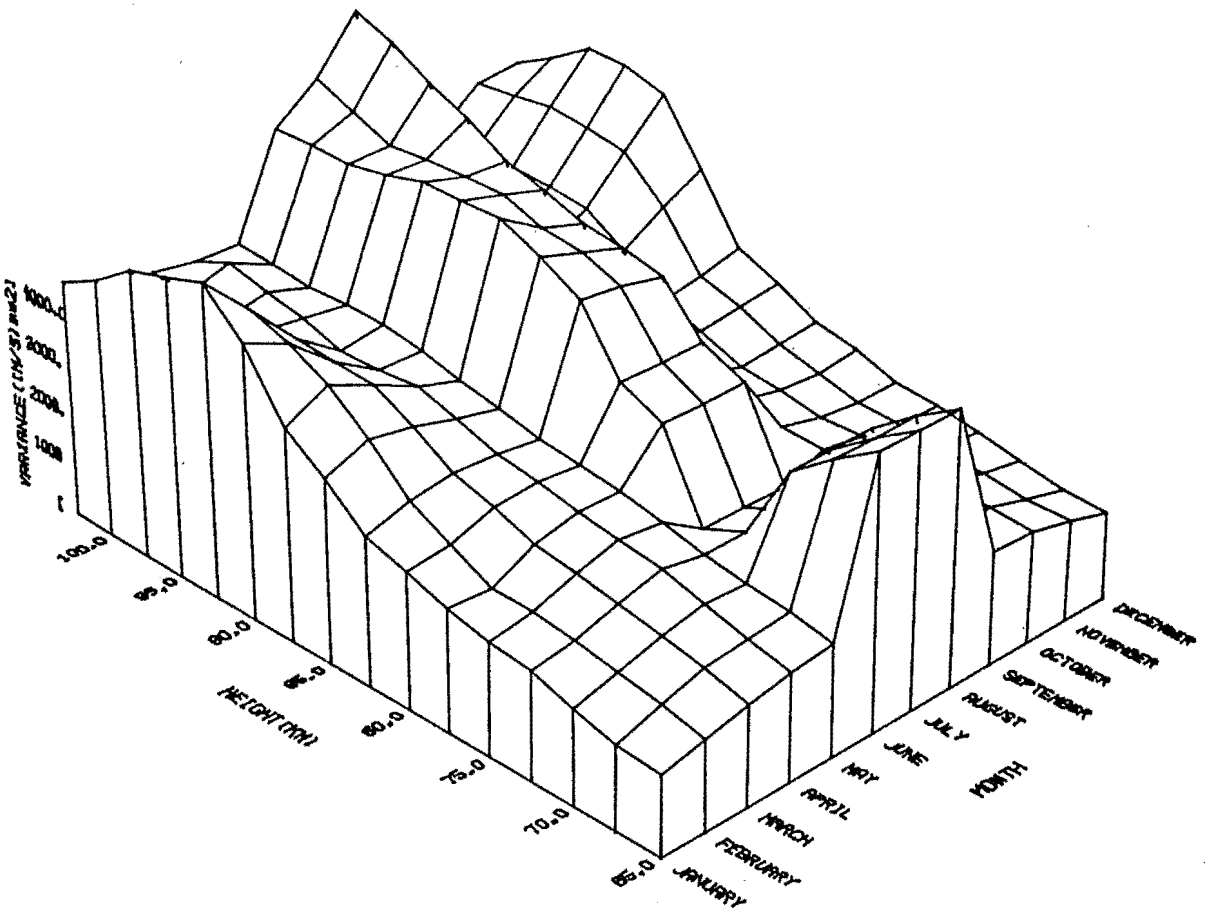

The same as for the previous figure,except that the temperatures below 80km in winter are for 45S.

northern hemisphere temperature data (figure 6.4). The use of more southern hemisphere data would produce more accurate model profiles, but the temperatures are also expected to vary from year to year as the variance profiles vary from year to year (see figures 6.2 and 6.3) indicating that the temperature profiles are changing from year to year.

The other variable that appears in equation (6.3) apart from the Brunt-Väisalä frequency, is the vertical wavenumber K_z. This is given by $K_z = k_{zreal} + i/2H$. The scale height H is a measure of temperature and is affected by the temperature alterations used to produce figure 6.4. The real part of the vertical wavenumber is affected by changes in the vertical wavelength. A monochromatic wave breaks at some height depending on the conditions for instability and may then come to a critical layer at some greater altitude. For a spectrum of waves with varying horizontal phase velocities, these heights of breaking and arriving at a critical level occur at different heights. Obviously the variance profiles measure the amplitude of the spectrum of waves, not the amplitudes of individual waves. Thus the behaviour of the variance profiles with height reflects the behaviour of the amplitudes of the dominant modes, which are those near breaking, not those near critical layers where the amplitude is much attenuated (e.g. see Fritts (1984) for variations in amplitude between the height of breaking and the height at which a critical layer is reached). Smaller vertical wavelengths should have their amplitudes restricted at lower heights than larger vertical wavelengths, so that the vertical wavelength of the waves with the maximum amplitude should increase with increasing height (Weinstock (1982)). Weinstock (1984) produced graphs that gave the vertical wavelength of maximum amplitude increasing from roughly 8 km, with half power points at 6 km and 12 km,at heights

of 60 km to about 14 km, with half power points at 11 km and 17 km at heights of 100 km. These figures are very approximate as each of the spectra given by Weinstock showed a wide spread of vertical wavelength.

Although there are difficulties in determining whether the wavelength varies with height in observational data due to the restricted range of height observations, the values of vertical wavelength are those observed in the mesosphere and lower thermosphere. Observations in these regions commonly show vertical wavelengths of between 8 km and 14 km (e.g. Hines (1960), Vincent (1984)). Chanin and Hauchecorne (1981) used LIDAR techniques that have better vertical resolutions than techniques that use radio frequencies, and thus their data should resolve shorter vertical wavelengths better than radio frequency techniques. Their results also indicated vertical wavelengths of between 8 km and 14 km. Other studies using LIDAR technqieues (Chanin and Hauchecorne (1983)) find shorter vertical wavelengths are also present.

Weinstock (1984) made theoretical calculations of the variation of wave amplitude with vertical wavelength for various heights up to 100 km. The data that Weinstock used came from long term averages of meteorological rocket network data averaged over the whole of the northern hemisphere. These data were given by Justus (1967) and Justus and Woodrum (1973).

Following the values given by Weinstock (1984) the vertical wavelength is assumed to vary between 8 km at heights of 65 km and 14 km at 102.5 km in all seasons except winter (see figure 6.7). The values used in winter are 12 km at heights of 65 km and 18 km at 102.5 km. The results of such an analysis are given in figure 6.6. The values of variance in this model are far closer to those of the observed profiles

Figure 6.6

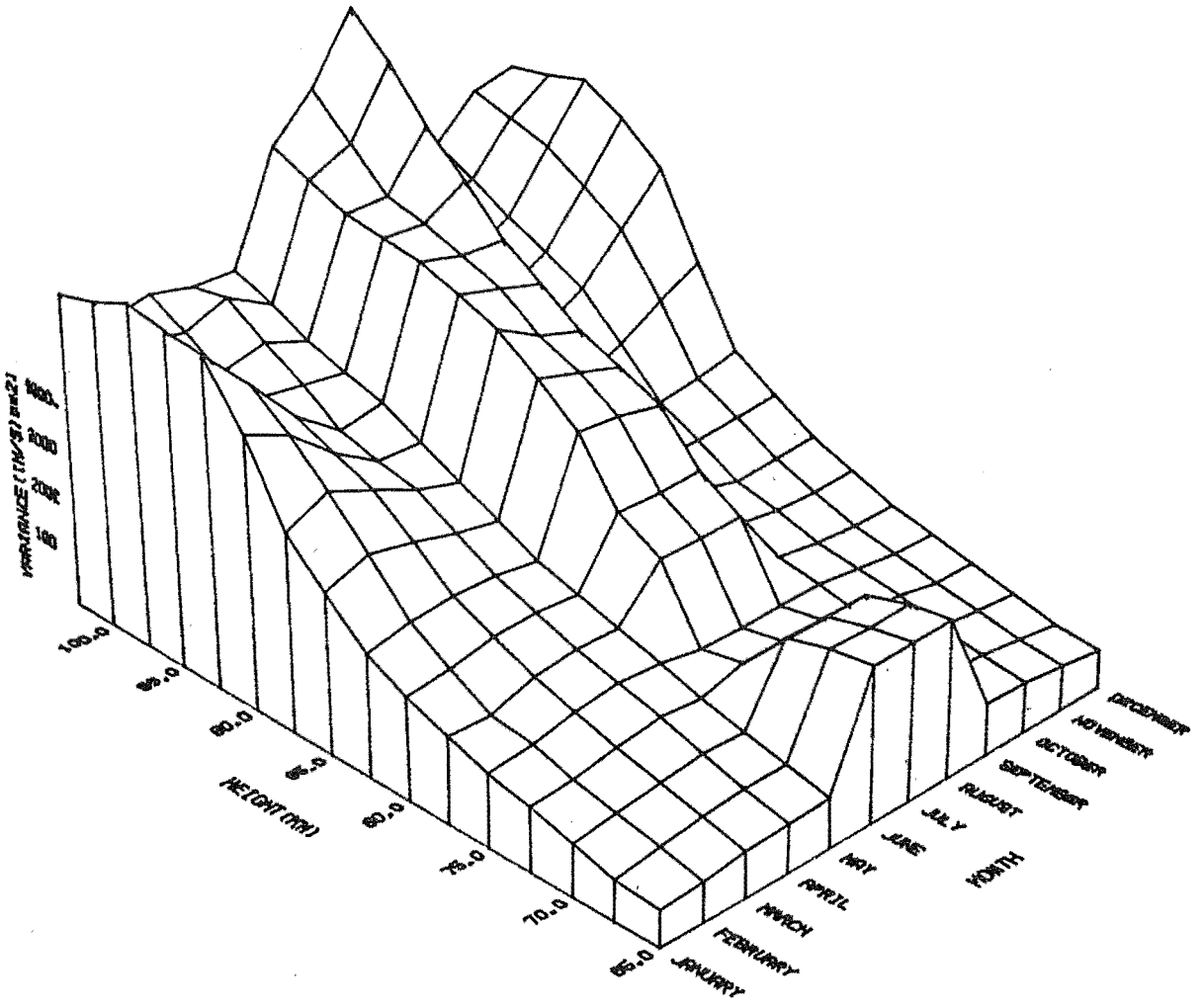

The same as for the previous figure,except that the vertical wavelength varies with height.

Figure 6.7

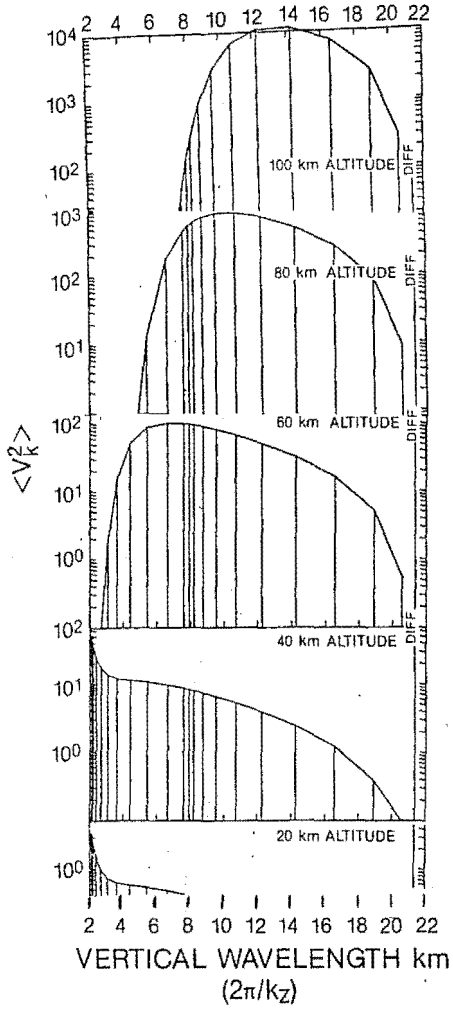

Wave amplitude squared as a function of vertical wavelength (Weinstock (1984)).

(see figures 6.2 and 6.3) than those given in figures 6.4 and 6.5.

One other point still has to be considered. This is the different value of the vertical wavelength used in winter. Support for the possibility that the average vertical wavelength varies with season is found by Ball (1981) who found that the average vertical wavelength was considerably greater in autumn than it was in the rest of the year at Adelaide. However, this does not aid the assumption that the maximum vertical wavelength is found in winter at Birdlings Flat. Manson and Meek (1980) found that the average vertical wavelength in the 80 km to 100 km height range in winter was 17 km for north-south motions and 18 km for east-west motions. In summer the values that they obtained were 13 km and 19 km respectively. The average of these values suggests that for one particular middle latitude station the vertical wavelengths of internal gravity waves are longer in winter than in summer.

Note that, apart from using the vertical wavelength at the point of breaking and thus artificially creating a wave spectrum, the arguments in this section have essentially concerned the saturation of monochromatic waves. The conditions for breaking (equation 6.32) have been derived assuming that no wave-wave interaction occurs. Fritts and Dunkerton (1984) used a monochromatic wave model, but included self-acceleration by the wave and quasi-linear wind accelerations. They found saturation amplitudes that were larger than those given by equation (6.32). Fritts (1985) included a spectrum of interacting waves and found the amplitudes to be less than those that are found for a monochromatic wave, the model assumed in this section.

6.9 Changes in amplitude with vertical wavelength

Vincent (1984) assumed that internal gravity waves at Adelaide were circularly polarised, so that the upward propagating and downward propagating waves could be separated into their Fourier components using the method developed by Gonella (1972) and Mooers (1973) and applied to the oceans by Leaman and Sanford (1975).

Vincent (1984) found a distribution such that the power was proportional to the vertical wavelength squared for most of the spectrum. For wavelengths greater than some cut-off point the power was roughly constant. This distribution is in agreement with the model of wave saturation developed earlier in chapter 6 where the wave amplitude is restricted to a value determined by considerations of turbulence production.

Given Vincent's (1984) work, it should be possible to develop similar results for Birdlings Flat, to see whether similar spectral behaviour occurs there. Furthermore, the possibility of changes in the cut-off wavelength over a year can also be investigated. This should permit a more accurate determination of the vertical wavelength than can be used in equation 6.16 to find the distribution of maximum wave amplitude with height.

The methods used to remove tides and trends are the same as those used by Vincent (1984).

In order to use the method used by Vincent (1984) the internal gravity wave vector should be of sufficiently low frequency for the Coriolis force to have a significant effect. In such a case the meridional velocity will lag the zonal velocity for upward travelling waves and lead the zonal velocity for downward propagating waves. This technique will not work for shorter period waves where the wave will not be circularly polarised. Nor will it

work if the anisotropic behaviour described in chapter 8 also applies to the longer period internal gravity waves.

The longest averaging interval used for the internal gravity waves was 6 hours. The vertical profiles for these 6 hour periods are shown in figure 6.8. One feature that immediately becomes apparent in these profiles is that, above about 80 km, the zonal and meridional wave velocities usually have opposite signs. The amplitudes are 180 degrees out of phase. This corresponds more to linear or strongly elliptical polarisation, rather than circular polarisation. Therefore, it is likely that the method of Leaman and Sanford (1975) cannot be applied to internal gravity wave data of these periods at Birdlings Flat.

The individual vertical profiles have been constructed both for data averaged over 6 hours and for data averaged over 4 hours. The particular data displayed in the plots included (figures 6.6 and 6.7) are mesospheric and lower thermospheric winds measured from Birdlings Flat in July 1981. The plotting routines used (NCAR (1981)) use splines to smooth the plots. Therefore, care should be taken when studying the plots as this smoothing tends to emphasize the wavelike nature of the plots. However, the use of linear interpolations in the presentation of these graphs also assumes information about the graphs. In this case the wave like nature of the curves is underestimated. The use of splines to fit a curve is certainly as valid as the use of linear interpolation. Such additional information is not assumed at any stage in the quantitative treatment of these data.

The profiles (figures 6.8 and 6.9) do not include data from 65 km or 67.5 km. The data from these heights are scarce; very few points occur in a time scale of either

4 or 6 hours, although the rate does vary from day to day. Consequently, insufficient data exists to accurately estimate the averages at these heights.

The four 6 hourly averaged profiles (figure 6.7) have several features in common. Firstly, the signs of the zonal (u) velocity and the meridional (v) velocity are mainly opposite. In other words, the waves are usually found in the northwest and the southeast quadrants. Secondly, the "sense" of the zonal and meridional velocities is not the same. In other words, the zonal velocity tends to increase in the opposite sense to the meridional velocity. Lastly, the motion seems to be wavelike, even taking the effect of fitting a curve into account. Although several waves may be present in some profiles, they can be visually separated into their individual components. The vertical wavelengths vary from about 9 km, the minimum wavelength detectable with a 4.5 km pulse width up to at least 15 km. Furthermore, the amplitude is in some way dependent on the vertical wavelength. In general, as the vertical wavelength increases, the amplitude of the wave also increases.

The 4 hourly averaged profiles of the wind data behave similarly to the 6 hourly averaged profiles. The sign of the zonal velocity is usually opposite to that of the meridional velocity at heights above 80 km. The zonal velocity also tends to increase in the opposite sense to the meridional velocity at heights greater than 80 km. So the waves must tend to be oriented along a northwest-southeast line above 80 km. Amplitudes are smaller below 80 km than above.

Averaging the data for each height over the month gives residues of less than 1 ms^{-1}. Thus there is little or no average over time remaining. However, the appearance of many

Figure 6.8

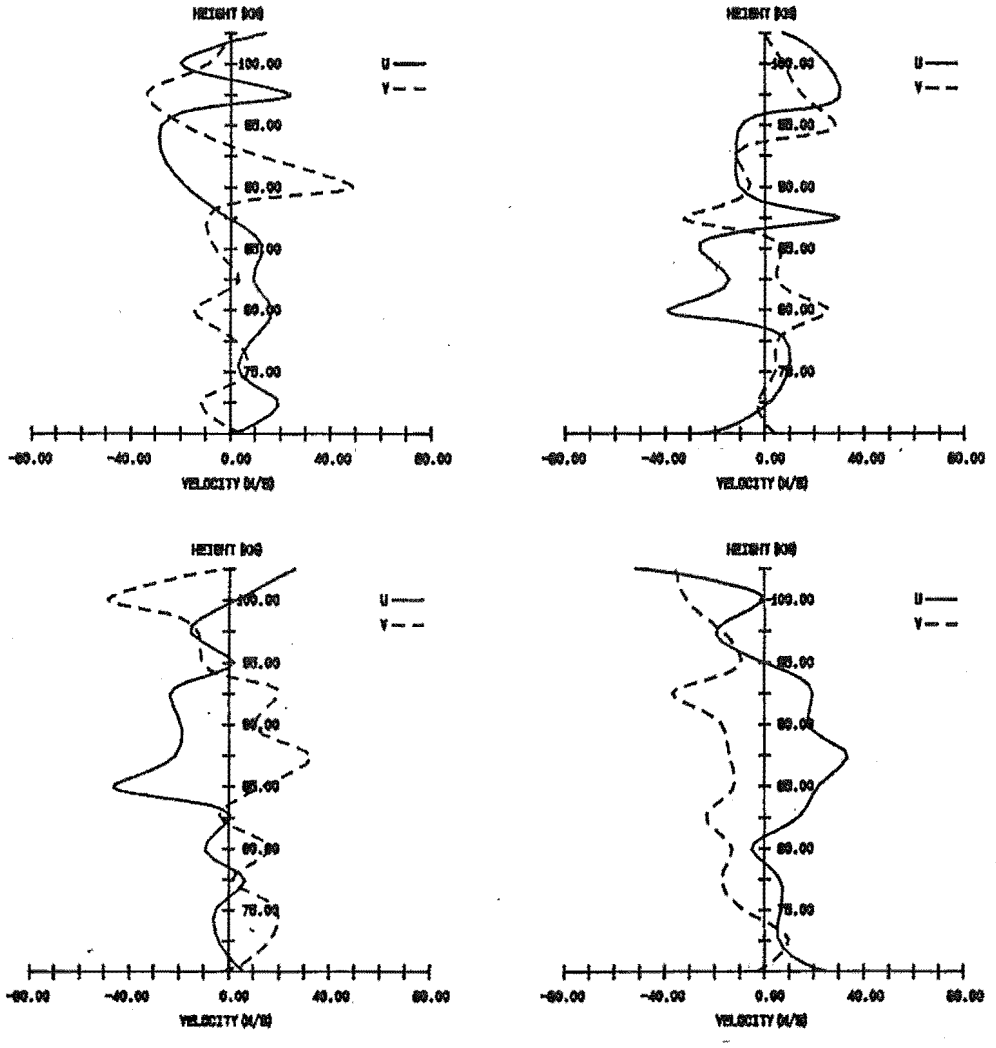

Drift profiles that have been averaged over a period of 6 hours. The measurements were made at Birdlings Flat in July 1981.

Figure 6.9

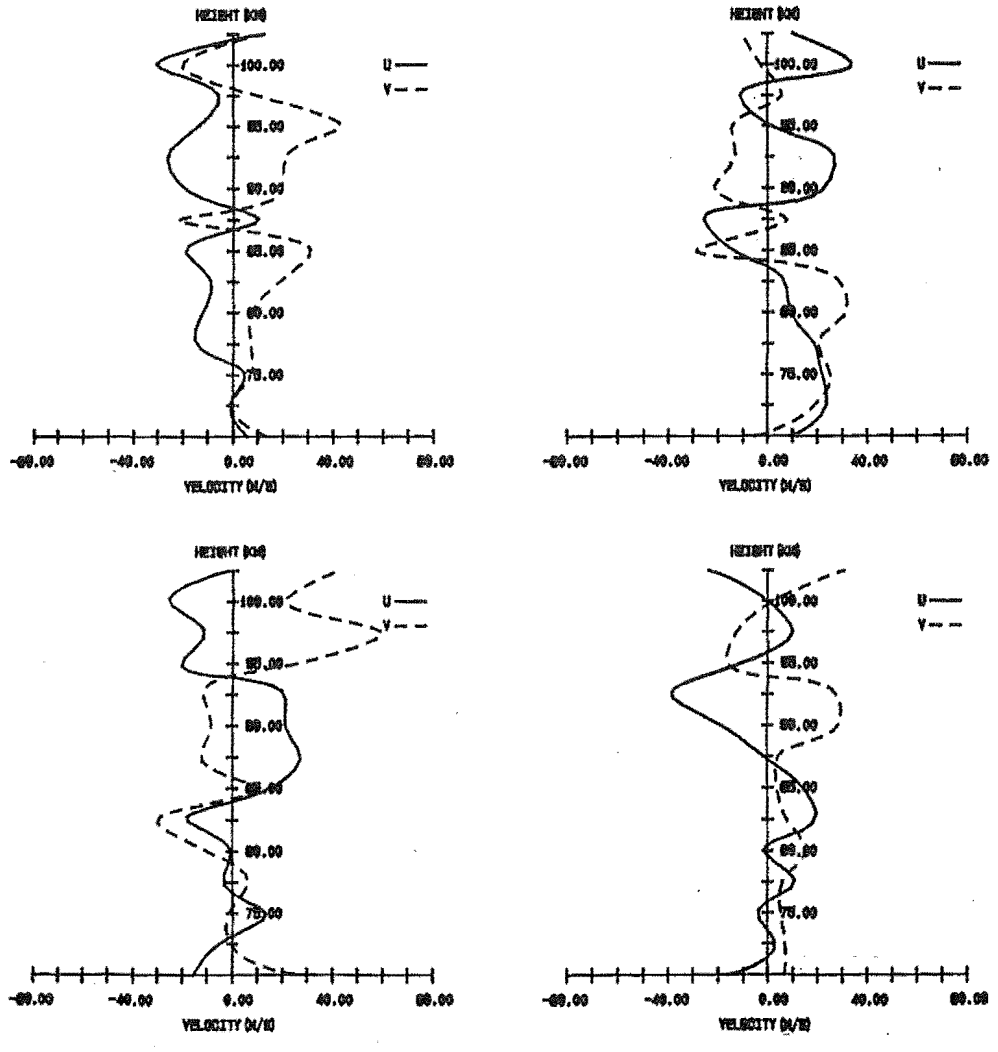

Drift profiles that have been averaged over a period of 4 hours. The measurements were made at Birdlings Flat in July 1981.

of the profiles suggests that some average with height remains. The amplitudes of any waves that are present are expected to change with height, that is, the data are not stationary, it is inappropriate to subtract the averages with height from the data.

The two sets of profiles are very similar. Even the maximum amplitudes appear to be approximately the same. This suggests that, for these periods, there is little change of wave amplitude with frequency. This point is important in determining the frequency range over which the theory determined in the previous chapter is relevant. This point needs to be considered further later in the chapter.

These mean profiles (figures 6.8 and 6.9) are for data that have had tidal motions removed and are averaged over periods of 4 hours and 6 hours. Thus, only long period internal gravity waves contribute to these profiles. The behaviour of waves with these periods cannot necessarily be regarded as being typical of the behaviour of shorter period internal gravity waves. The Coriolis force can be expected to be important even if no other differences occur.

Short period internal gravity waves are not strongly affected by rotational effects (Hines (1974, p.32), Fritts and Rastogi (1985)). Internal gravity waves are affected by rotational effects if their period is sufficiently large. When a rotating atmosphere is assumed, the dispersion equation in the absence of zonal winds becomes (Gossard and Hooke (1975, p.112)

$$K_z^2 = \frac{(\omega_B^2-\omega^2)k_x^2}{(\omega^2-f^2)} \qquad (6.33)$$

where f is the inertial frequency

ω_B is the Brunt-Väisalä frequency SEE ERRATA

ω is the frequency

and k_x and K_z are the horizontal and vertical wavenumbers respectively.

If $\omega_B^2 >> \omega^2 >> \Omega^2$ this is just the familiar form

$$K_z^2 = \frac{\omega_B^2}{c_x^2} \tag{6.34}$$

and rotational effects are minor.

At heights above 80 km the long period motions in figures 6.6 and 6.7 are more characteristic of motions that are eliptical, oriented along a 45^o angle to the axes, than of motions affected by rotational effects.

Any source mechanism that produces these long period waves must be varying over a relatively long period. This should limit the number of possible wave sources and may thus affect both the number of waves produced and the possible structures of these waves. Single wave-like structures are very clear in figures 6.8 and 6.9. Therefore, it is likely that the profiles have been caused by very few waves. Obviously, this assertion is qualitative and needs some quantitative backing. This will be considered later.

The profiles also suggest that the amplitude of any particular wave varies with height. This will tend to cause confusion when wave amplitudes are being calculated.

Various analysis techniques were tried in an attempt to obtain wave amplitude variations with height. These all involved the analysis of amplitude in the vertical wavenumber (cf with frequency) domain. No set of readings that were measured in one run covered a sufficiently large range of heights to permit analysis. Therefore, averages had to be used. When these averages are made the data comes from different times at different heights and thus possible from different wave activity. If the period over which the averages are made is too short (too few points at any height)

then the uncertainty resulting from the averaging will be very large (assuming that the uncertainty is related to the variance and the number of points used in the usual way). Hence, the largest time intervals that are practicable should be considered. The waves that are studied will have much longer periods than those considered earlier in Chapter 6 and in Chapter 8, and thus the expected wave behaviour may be different. The variation of wave amplitude with frequency is discussed later in this chapter and it will be shown that at least one major change in wave behaviour may occur as the frequency varies.

Probably the simplest method of analysis that may be applicable to these data (apart from amplitude estimation by eye) is the use of Fourier analysis techniques. The individual u_1 and v_1 profiles were Fourier analysed both for data that had been approximately "normalised" by dividing the individual points by the square root of the variance that height and for data that was not "normalised". This "normalisation" may not be entirely appropriate. The variance profiles were calculated for motions with much shorter periods. Also there is no certainty that the behaviour of individual waves can be compared with the averaged behaviour of all waves. If a wave has not reached saturation amplitude at lower heights then a variance profile of saturated wave most certainly will not reflect the behaviour of individual waves.

The u_1^2 and v_1^2 profiles were then combined to obtain a Fourier spectrum. Unfortunately, the Fourier analysis of a spectrum containing few waves will underestimate the amplitude of waves with wavelengths that do not correspond to any of the Fourier coefficients as a number of different Fourier periods must be used to reconstruct the wave. That is, leakage occurs, thus the amplitude tends to be "smeared" over a

number of coefficients. If leakage is significant, an estimate of the amplitude at any vertical wavelength cannot be accurately obtained. Thus the spectrum of amplitude with vertical wavelength is incorrect. Another problem is that the lengths of the data series are small (14 pts.).

These failings prevented any useful data from being obtained from the Fourier analysis. Attempts were therefore made to solve the problem of obtaining the amplitude of a wave with an unknown vertical wavelength by using other spectral analysis techniques. The Blackman and Tukey method is unsuitable for analysing short data series. The usefulness of the maximum entropy method in the analysis of short data series has been discussed in Chapter 4. A major problem with the use of MEM analysis is the difficulty in estimating the optimum filter length. When the height profiles were analysed using MEM analysis the 3 criteria discussed in chapter 4 (FPE, AIC and VAT) sometimes disagreed. In particular, the Akaike information criteria (AIC) showed minima for these time series that did not occur at the same filter length as the minima of the other criteria. Therefore,reliance was placed on the final prediction error (FPE) criteria and the criterion autoregressive transfer function (CAT). However, confusion over the optimum filter length may have occurred for some of the profiles. In these cases the filter length tended to be overestimated rather than underestimated. Thus the number of peaks in the spectrum may have been overestimated.

Fifty-two profiles of 4 hour mean motions were obtained in July 1981. At other times data was missing at some height. Of the fifty-two profiles, 35% had more than 1 vertical wavelength present, 29% had none or 1 vertical wavelength and

the remainder could not be analysed because the values of the prediction criteria increased with increasing filter length up to the maximum possible filter length. The distribution of the number of spectral peaks with vertical wavelength in July are given in table 6.1 (see figure6.10)).

TABLE 6.1 THE DISTRIBUTION OF THE NUMBER OF SPECTRAL PEAKS WITH VERTICAL WAVELENGTH IN JULY

Vertical wavelength range (km)	8-10	10-12	12-14	14-16	16-18		
Number of waves	9	2	8	6	1		
Vertical wavelength range (km)	18-20	20-22	22-24	24-26	26-28	28-30	>30
Number of waves	3	5	1	0	1	1	3

The pulse width of the signal corresponds to a height resolution of 4.5 km. Thus spectral peaks with periods of less than 9 km have not been independent samples. Hence, the results in the 8 km and 10 km range need to be treated with caution.

Whilst definite conclusions cannot be drawn from so few data, some points are worth noting. Firstly, the number of waves present decreases with increasing vertical wavelength on average. A second effect is also worth noting. This is the small number of results in the 10 km to 12 km band especially, but also in the 16 km to 18 km band.

Figure 6.10

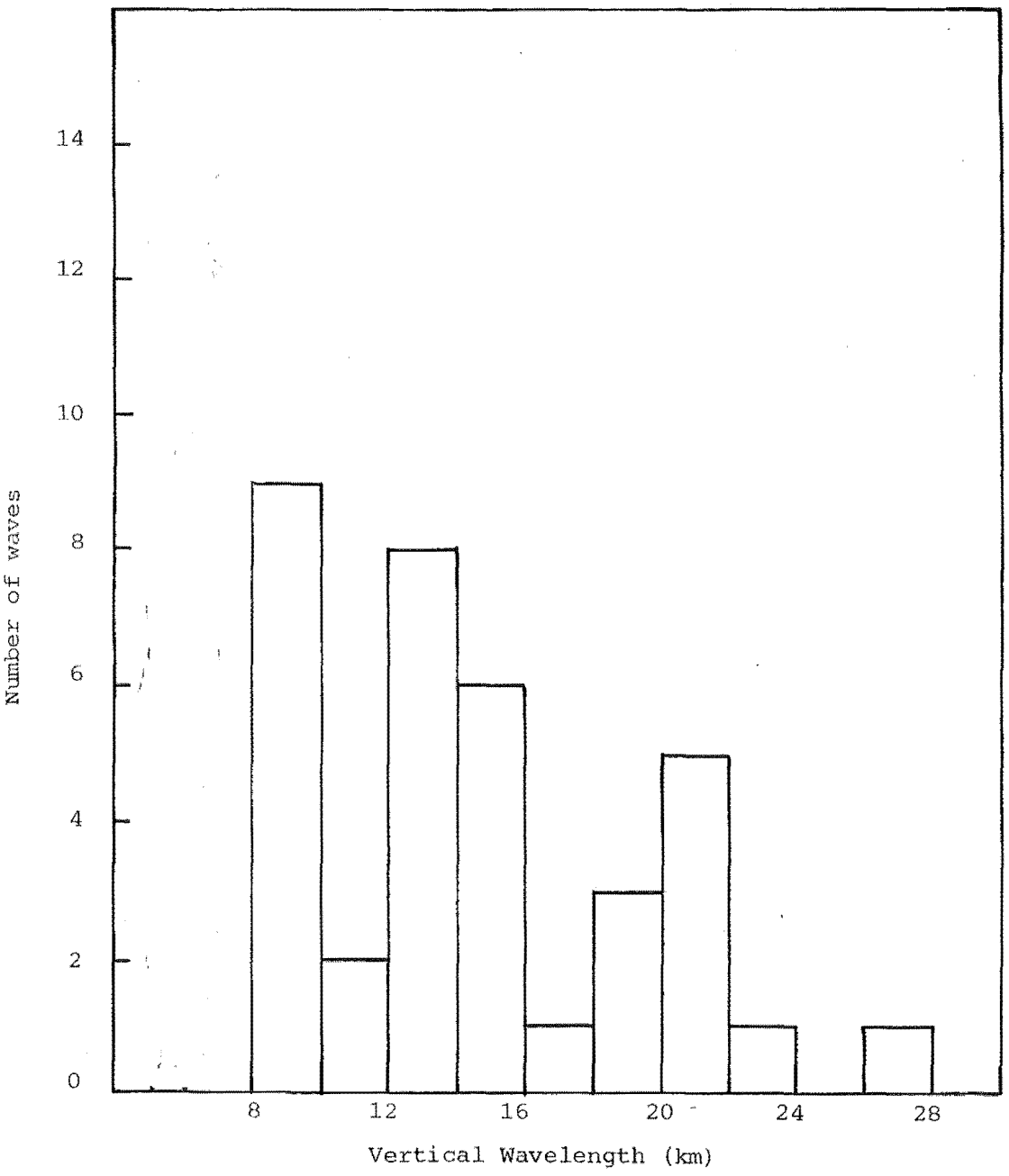

The distribution of the number of spectral peaks with vertical wavelength in July 1981.

The analysis of the power of the spectral peaks did not produce results that were even remotely in agreement with visual observations of the spectra. In visual observations (see figures 6.8 and 6.9) of profiles where more than one wave is apparent there is a clear tendency for motions with small vertical wavelengths to have much smaller amplitudes than motions with longer vertical wavelengths (10 km to 20 km). When the MEM analysis was done, no consistent trend was apparent either when all profiles in which more than one wave was present was considered or when all waves were considered. These latter data were analysed using the definition of the peak power of MEM spectral analysis given by Lacoss (1971). The peak power is given by

$$P_p = \frac{\alpha^2 N_i^2 \Delta}{4} \qquad (6.35)$$

Where α is the amplitude, N_i is the length of the filter, and Δ is the interval between points. The values for the amplitude were adjusted to account for variations in the filter length N_i. When test data were used in MEM analysis the frequencies of the cosine terms were in agreement with the input data, but the slope of the graph was not consistent with the amplitude function of the input data. With the added complications of variations of amplitude with height, a short data series and possible variations of vertical wavelength with height, this method did not produce any useful means of determining amplitude changes with changes in vertical wavelength.

One other method of finding the relationship between the vertical wavelength and the amplitude of the waves was considered. The test data used in the MEM spectral analysis showed that, even for such short data series, the method gave a good estimate of the vertical wavelengths that were present.

Even assuming that added problems will occur when real data is analysed, the wavelengths obtained should be reasonably close to those which exist in the mesosphere and lower thermosphere. These known wavelengths can possibly be used to make harmonic analyses of the profiles. In fact, the data series are not long enough and the amplitude is too variable to make the use of this technique possible.

Attempts to confirm the prediction made by the model used in the last chapter about the variation of wave amplitude with vertical wavelength were unsuccessful due to a combination of problems with both the data used and with the analysis techniques.

166.

6.10 Wave energy

An obvious development from the calculated variances is to make calculations of the overall kinetic energy by multiplying the variance by the corresponding value of the density (obtained from CIRA (COSPAR(1972))).

These energies are displayed in figures 6.11,6.12 and 6.13. In general, the energy decreases rapidly as the height increases up to 80 km. The decrease is then much less as the height increases to 90 km: in some months apparent increases are recorded in this height range. These increases probably represent fluctuations due to uncertainties in the calculation of the variance. One of the largest increases is found in March 1981 when the errors are largest due to the small amount of data that existed. The decrease in variance from 90 km to 97.5 km is almost linear. If the line that includes 90 km and 99 km was extended, no energy would remain above some height between 100 km and 105 km. However, the energy decreases more slowly above 100 km.

Figure 6.11

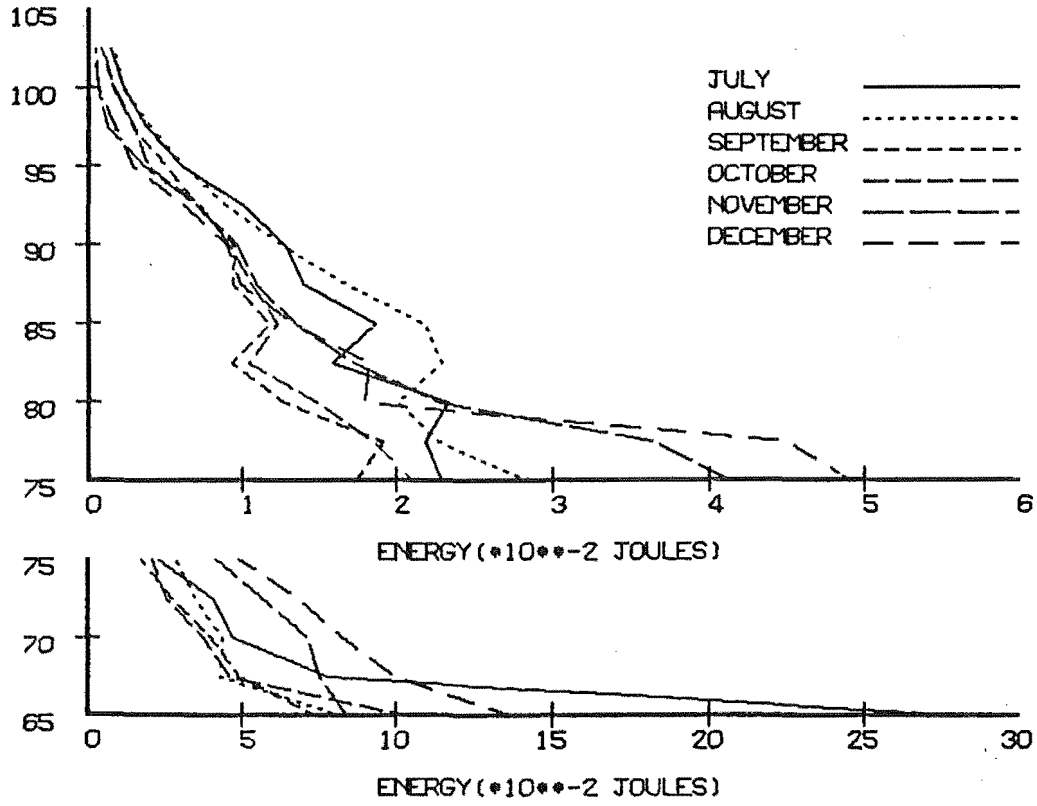

THE ENERGIES OF SHORT PERIOD MOTIONS
IN THE SECOND HALF OF 1980.

Figure 6.12

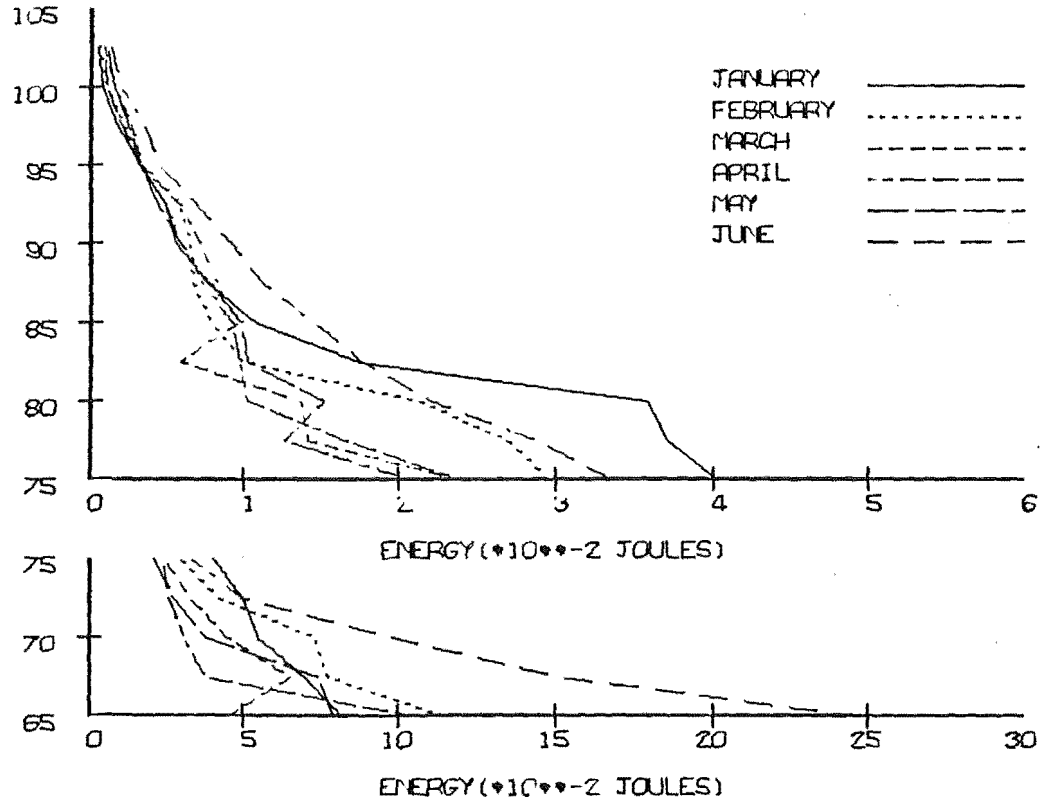

THE ENERGIES OF SHORT PERIOD MOTIONS
IN THE FIRST HALF OF 1981.

Figure 6.13

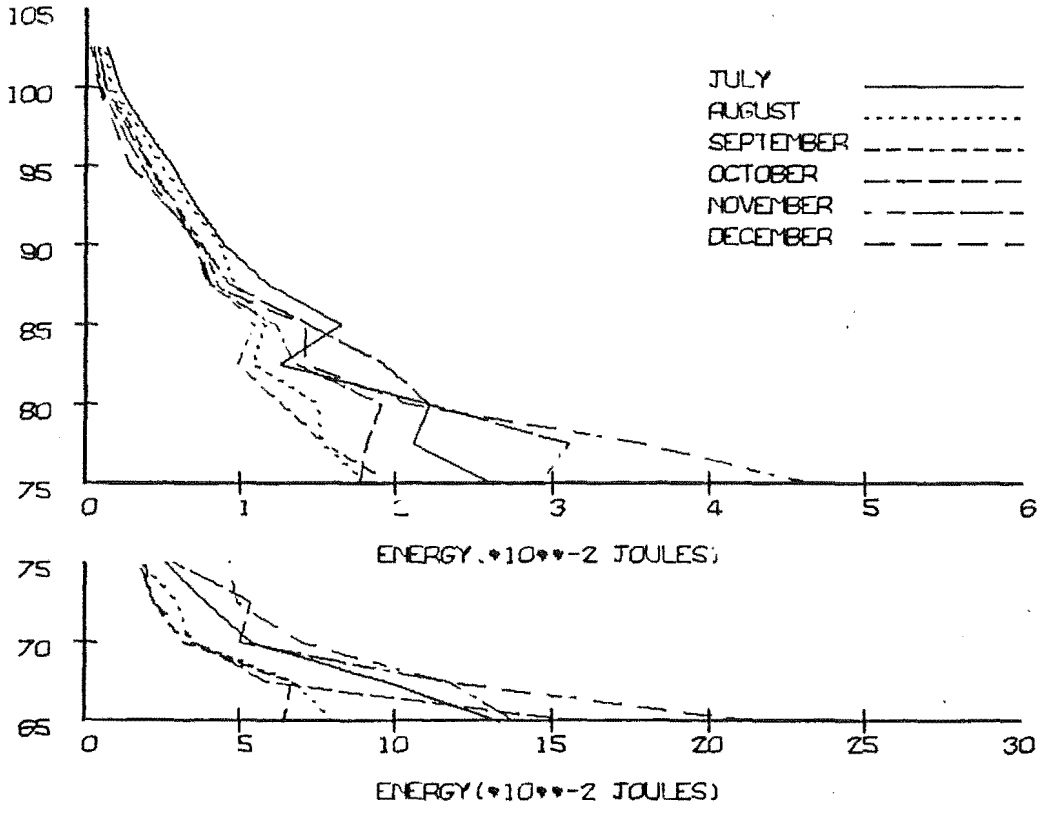

THE ENERGIES OF SHORT PERIOD MOTIONS
IN THE SECOND HALF OF 1981.

If this energy loss is due to wave breaking, then the greatest relative additions of energy from internal gravity waves occur at heights below 80 km and between 90 km and 100 km. Relatively much less energy is lost by internal gravity waves at heights between 80 km and 90 km.

Given the large temperature increase that occurs above 100 km it is worthwhile investigating whether the amplitude restrictions due to instabilities will in fact restrict the amplitude of internal gravity waves. To avoid making any assumption about the temperature structure of the atmosphere, the amplitude can be calculated by assuming that no energy is lost. Thus using density measurements given in the CIRA(COSPAR(1972)) standard atmosphere the expected velocity amplitude can be calculated if no energy is lost. Thus using density measurements given in the CIRA(COSPAR(1972)) standard atmosphere the expected velocity amplitude can be calculated if no energy is lost. Table 6.2 lists the amplitude divided by the amplitude at a height 2.5 km lower.

TABLE 6.2 THE RATIO OF EXPECTED VELOCITY AMPLITUDES DERIVED USING ρV^2 = CONSTANT

Height(km)	95	97.5	100	102.5	105	107.5	110	112.5	113
Ratio V_i/V_{i-1}	1.27	1.25	1.27	1.26	1.24	1.23	1.22	1.22	1.19

Height(km)	117.5	120	122.5	125	127.5	130
Ratio V_i/V_{i-1}	1.18	1.17	1.16	1.15	1.14	1.12

The ratio V_i/V_{i-1} decreases above 100 km where the subscript i refers to a particular height. Lack of data above 102.5 km prevented comparisons being made with experimental data at those heights. However, velocity amplitude decreases, or at most very slightly increases, up to 102.5 km suggesting that energy is being lost up to those heights. Lack of suitable wind data made it difficult to calculate the expected behaviour of the wave amplitude with increasing height for a wave breaking mode, but an estimate was made for those heights which suggested that the expected amplitudes would decrease slightly with increasing height or would at most increase somewhat less than if no energy was lost. Thus, without other energy restricting mechanisms, wave breaking would be expected to continue, at least up to heights of about 120 km or 130 km.

Given that the turbopause is seen to occur between about 100 km and 110 km (e.g. see Hines (1974) Chapter 1), it is clear that either the turbulence is not created by the wave instabilities above this region or that if it is created it is immediately dissipated. Note too that Barat (1969) saw ranges of height where turbulence was not present below the height at which turbulence ceased to occur.

Several studies have been made of the height at which the turbopause does occur. Blamont and de Jager (1961) found a typical value of 102 km in five rocket probes which showed the turbopause varying from 96 km to 112 km. Kampe et al. (1962) found that the turbopause occurred at heights between 100 km and 104 km. As has previously been mentioned, Barat (1968) found turbulence occuring in one profile below 96 km and between 104 km and 111 km, but not between 96 km and 104 km nor above 111 km. In another profile no turbulence was seen.

SEE ERRATA

The reasons for the existence of the turbopause have not been fully explained. The aim of this section was to determine

whether the cessation of turbulence could be explained by any wave breaking model. To this end both temperature shear and velocity shear models were considered. In neither case was breaking expected to cease at a height near the observed turbopause. However, results such as Barat's (1968) results do give some support to a model involving wave generation of turbulence, but the cessation of turbulence does not appear to be primarily a breaking phenomenon.

Stewart (1959) suggested that decreasing Reynolds' number meant that turbulence would not exist above 120 km. The Reynolds' number is defined as

$$Re = VL/\eta_m \qquad (6.36)$$

Where V and L are the characteristic velocity of the turbulence and the characteristic length of the gross shear system respectively while η_m is the molecular kinematic viscosity. Due to a lack of suitable data, Stewart used several approximations in calculating this limit.

Hines (1974 p.32) found that the minimum scale size of motion increases with height. Limitations on the possible size of turbulent shear may cause the turbopause to be lower than the value calculated by Stewart (1959).

The variation in the height of the turbopause which may be seasonal (Blamont and de Jager (1961)) and the effects of this change on models of the cuase of the turbopause are subjects that need further study. As more velocity data becomes available at turbopause heights, this should become possible.

6.11 Variances for Longer Period Motions

Up to this point in this chapter discussion has been concerned with motions with periods of less than 3 hours. The variances of these motions can be compared with the variances of motions with other periods to compare the relative magnitudes of motions. Using the period ranges discussed in Chapter 3, variance profiles are calculated for motions with periods of more than 1 day (figure 6.14), tidal motions for periods between 8 and 24 hours (figure 6.16) and motions with periods between 5 and 8 hours (figure 6.15).

Motions with periods of more than 1 day are particularly strong at heights below 85 km in winter (figure 6.14). Ignoring the values at 65 km, where the small number of points make the data unreliable, the variance in winter is large for heights up to 75 km or 80 km, corresponding to the strong winter planetary wave activity that exists in the stratosphere and is dying out in the mesosphere (see Chapter 2). Another peak in variance is found between 75 km and 90 km. This peak probably corresponds to the local propagation of the 5-day wave (Geisler and Dickinson (1976)) and/or the 2-day wave that is particularly strong in summer (Kingsley et al. (1978), Muller and Nelson (1978), Craig et al. (1980) etc.). Apart from these peaks the variance is generally low at other heights and times, although there is a small apparent increase in variance at heights above 95 km. The variances of planetary wave motions are considerably smaller than the variances of internal gravity waves at heights above 80 km.

The variances for motions with periods of between 5 hours and 8 hours are both fairly uniform,that is not showing any noticeable trends, and relatively small (mostly r.m.s. amplitudes of less than 30 to 35 ms^{-1} and often considerably less - see figure 6.15). The only conclusion that can be drawn from figure 6.15 is that the behaviour of these motions

Figure 6.14

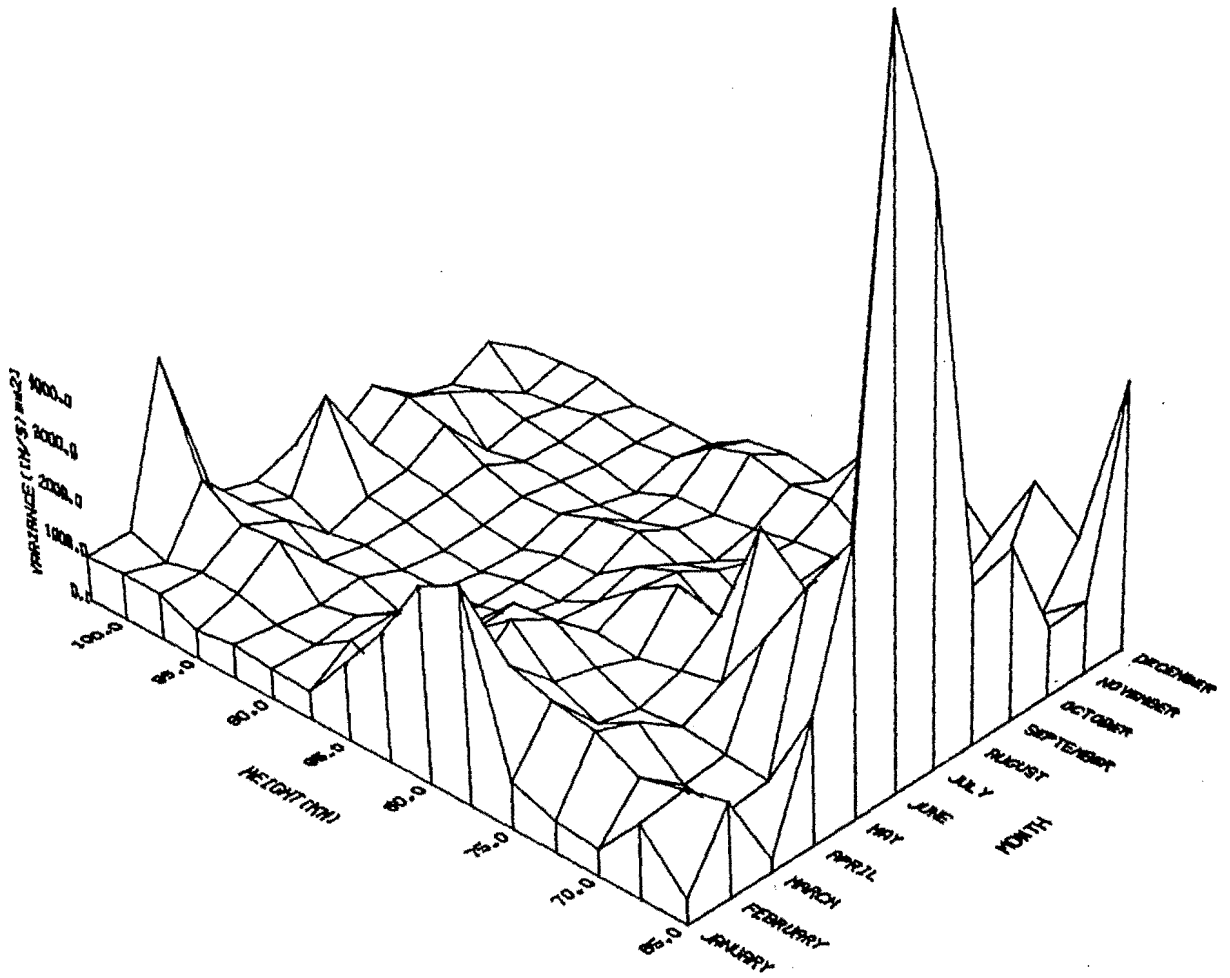

The variance of motions with periods greater than 1 day at Birdlings Flat in 1981(m^2/s^2).

Figure 6.15

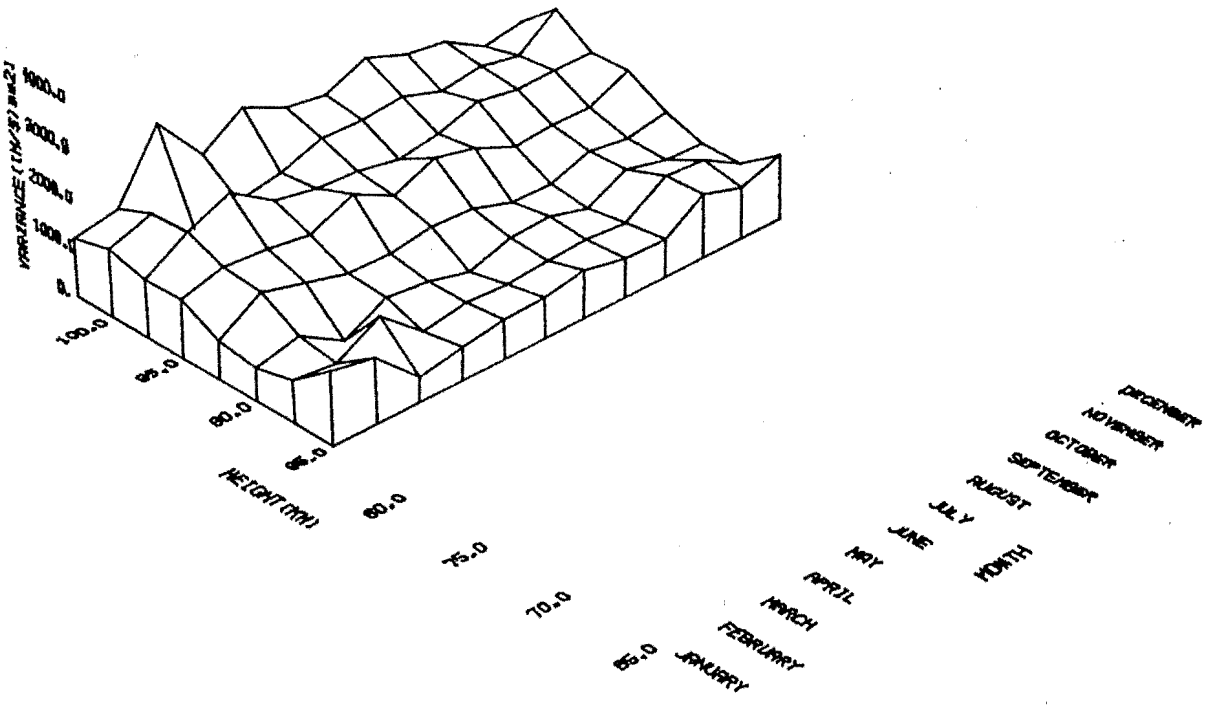

The variance of motions with periods between 5 and 8 hours at Birdlings Flat in 1981(m^2/s^2).

differs considerably from the behaviour of motions with periods of less than 3 hours. Thus convective wavebreaking of the type discussed earlier in this chapter is unlikely to be the mechanism that controls the amplitudes of these motions as there are no height or seasonal variations similar to those seen in figures 6.2 and 6.3, the variance plots for motions with periods of less than 3 hours.

Fritts and Rastogi (1985) expected saturation amplitudes ~~to be smaller~~ for frequencies close to the inertial frequency SEE ERRATA to be significantly smaller than saturation amplitudes for high frequencies. In the former case velocity shear instability is expected to be important. However, at frequencies such that $f/\omega \approx \frac{1}{2}$, corresponding to a period of about 8½ hours at Birdlings Flat the amplitude given by Fritts and Rastogi (1985) is only reduced to 90% of the amplitude that occurs for convective instability. The limited amplitudes in figure 6.15 relative to figures 6.2 and 6.3 are possibly due to an absence of waves with inertial frequencies between 5 and 8 hours reaching saturation amplitudes at every height for much of the time. In this case the variances are expected to be much reduced. The 5 to 8 hour period range includes the ter-diurnal tide. However, the amplitude of this tide is sufficiently small not to be of fundamental significance for the meteorology of the stratosphere and mesosphere (Holton (1975, p.163).

The data in the 5 to 8 hour period range and the 8 to 24 hour period range are restricted to heights above 85 km because of the analysis limitations discussed in chapter 3.

The last period range graphed is the 8 to 24 hour period range (figure 6.16). As the ter-diurnal tide is expected to be small compared with the diurnal and semi-diurnal tides (Holton (1975), Chapman and Lindzen (1970), this period range is expected to be dominated by the diurnal and semi-diurnal

Figure 6.16

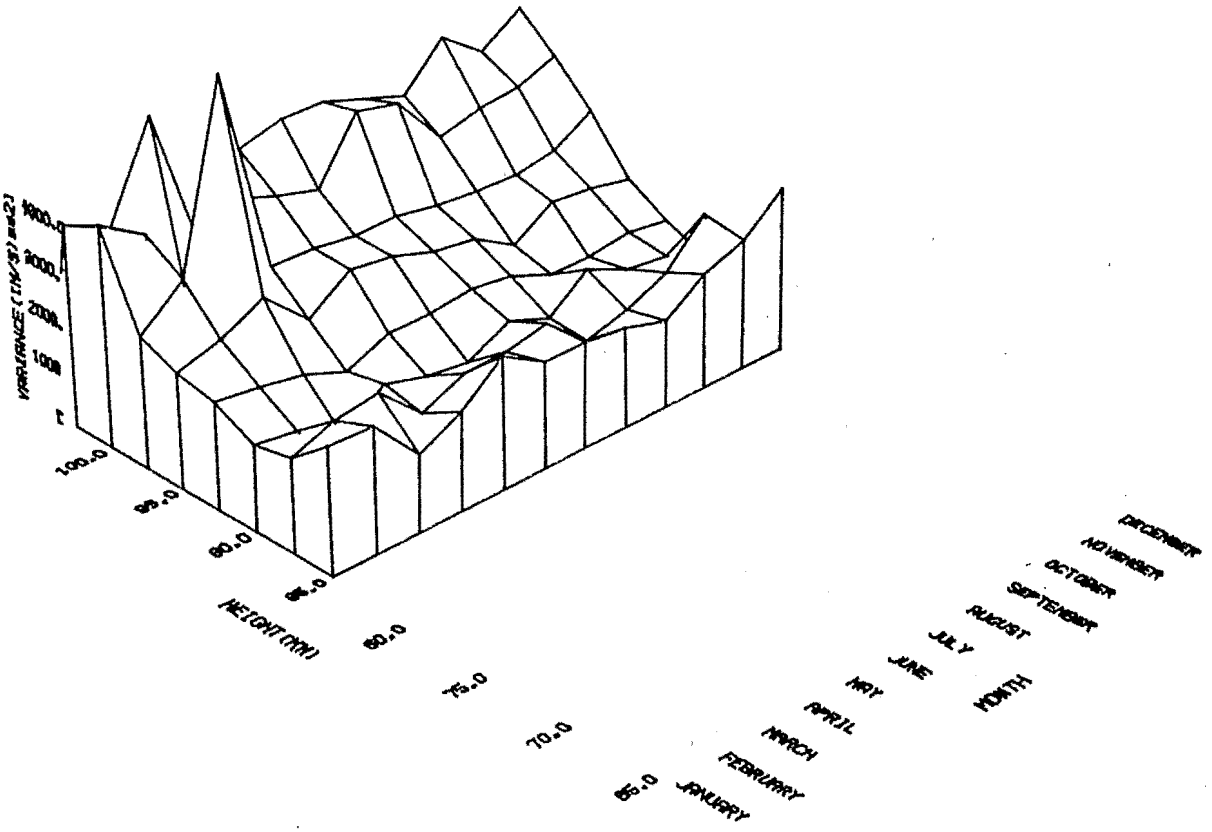

The variance of motions with periods between 8 and 24 hours at Birdlings Flat in 1981(m^2/s^2).

tides. Whilst a detailed discussion and analysis of tidal motions is outside the scope of this thesis, a brief discussion of the expected and observed behaviour of the tides is necessary to interpret the variance profiles for this period range, and to be able to copare these variances with those for other period ranges. This in turn is applicable to the discussion of the relative importance of tides and internal gravity waves in the meridional transport of zonal momentum which is undertaken in the next chapter.

Forbes (1984) presented theoretical predictions of the amplitudes of both the semi-diurnal and diurnal tides at a latitude of 42^{o} (and others). In the range of 85 km and 100 km the diurnal tide is expected to have a maximum value of between 30 and 40 m/s at a height of 95 km. The semi-diurnal tide is expected to have a maximum amplitude of about 40 to 45 ms^{-1} in the 85 km to 95 km height range with the variance increasing upwards from 85 km to 100 km.

Many observations of the variations of tidal amplitudes with height have been made. ~~For instance, Aso and Vincent (1982) made a study of data from Adelaide, Townsville and Kyoto.~~ SEE ERRATA Manson et al. (1981) found that the diurnal tide had an amplitude of about 20 ms^{-1} in summer and a similar amplitude in winter. The semi-diurnal tide had amplitudes of up to 30 ms^{-1} in summer with the peak amplitude occurring at about 98 km, while the maximum winter value was about 20 ms^{-1} for all heights between 90 km and 100 km. Glass and Spizzichino (1974) found that diurnal tides had amplitudes of up to 35 ms^{-1} and that the semi-diurnal tide had amplitudes of up to 30 ms^{-1} at Garchy. Smith (1981) made extensive calculations for the tides at Birdlings Flat. Smith found that in winter the amplitudes of the semi-diurnal tide were between 10 and 20 ms^{-1} as was the diurnal tide. The diurnal tide was considerably stronger

in summer, having amplitudes of more than 30 ms^{-1}. The amplitude increased with height.

Figure 6.16 can be interpreted with the help of these data. The amplitudes between 30 ms^{-1} and 40 to 45 ms^{-1} for most data at heights below 100 km. At 100 km and 102.5 km the variance is larger, especially in summer. The summer value is possibly a result of the large value for the amplitude of the diurnal tide as described by Smith (1981). The increases in variance with height above 90 km are consistent with theoretical predictions for the increase in tidal amplitude for the semi-diurnal tide.

The variances of motions with periods of less than 3 hours are larger than the variances of tides for heights between 85 km and 95 km. The variances of motions with periods of less than 3 hours are much larger than the variances of motions with periods between 5 and 8 hours at heights between 85 km and 102.5 km. Internal gravity wave variances also dominate planetary wave variances above 75 km.

6.12 Afterword

The primary aim of this chapter has been to determine whether the variance profiles of motions with periods of less than 3 hours can be explained by a fairly simple wave breaking model. Given that the possible physical variations of the Brunt-Vaisala frequency and the vertical wavenumber are taken into account, the similarities between the theoretical and observed variances are sufficiently great to suggest that the observed variance profiles can be explained solely in terms of a wavebreaking model.

One important consequence of the breaking of internal gravity waves in the mesosphere and lower thermosphere is the production of drag on the mean flow which is able to balance

the momentum budget. This drag is primarily caused by the changes in the vertical transport of horizontal momentum that occur between the height of breaking and the height at which the wave reaches a critical layer.

Vertical velocities are not obtainable from Birdlings Flat at present. Hence, values of the vertical transport of horizontal momentum could not be calculated. However, in the course of investigating the behaviour of internal gravity waves, a pronounced tendency for the wave vectors to be aligned in the northwesward and southeastward quadrants at heights above 80 km was found. Possible reasons for this alignment are discussed in Chapter 8. In Chapter 7, the relationship of this alignment to the meridional transport of zonal momentum is considered.

SEE ERRATA

CHAPTER 7

THE MERIDIONAL TRANSPORT OF ZONAL MOMENTUM

7.1 Introduction

In the last chapter internal gravity wave breaking was used to explain the variance profiles obtained. Non-conservation of momentum due to wave dissipation leads to a drag on the prevailing winds.

In this chapter the effects of this orientation on the meridional transport of zonal momentum are considered. The development of equations for momentum transport is given. Calculations of this transport at Birdlings Flat and Arrival Heights are made. Finally rough estimates of the accelerations caused by changes in the meridional transport of zonal momentum are made and these accelerations are compared with the accelerations caused by the mean winds.

The term $\overline{u_1 v_1}$ has sometimes been used to indicate the behaviour of the meridional transport of zonal momentum. In fact, the poleward transport of zonal momentum across a ring of unit width in the meridional direction is given by Palmen on Newton (1969) as:

$$M_\phi = \frac{2\pi R^2 \cos^2\phi}{g} \int_{P_2}^{P_1} (\Omega R \cos\phi \bar{v} + \bar{u}\bar{v} + \overline{u_1 v_1}) dP$$

Thus comparisons of $\overline{u_1 v_1}$ as an indication of the meridional transport of zonal momentum are only valid if the same pressure range is considered and if the same latitutde is also studied.

7.2 General Discussion of Momentum and Momentum Transport in the Atmosphere

The transport of zonal momentum by eddies is of great importance to theories of general circulation. Consequently, the study of this phenomenon has a relatively long history.

The first "modern" treatment of this transport was done by Jeffreys (1926). Both Jeffreys (1926) and Starr (1948) were concerned with the problem of how zonal momentum was transported from the source region at the earth's surface near the equator to the region where momentum is transferred from the atmosphere to the earth's surface in the middle latitudes. Momentum is transferred from the earth's surface to the atmosphere near the equator because westward winds are moving in the opposite sense to the earth's rotation. In the middle latitude the eastward winds are moving in the same direction as the earth's rotation and hence momentum is transferred from the atmosphere to the earth's surface.

Thus, there must be a net transport of momentum from the equator to the middle latitudes if the circulation system is to remain stable.

One more factor affecting the transfer of momentum is the westward winds that occur near the poles. These transfer momentum from the surface to the atmosphere. However, it can be shown that their influence is small. Oort and Peixóto (1983) give the angular momentum of the atmosphere unit mass as:

$$M = M_{\Omega} + M_{r} \tag{7.4}$$

where $M_{\Omega} = \Omega R^2 \cos^2\phi$ represents the angular momentum that is present if the atmosphere is in solid rotation with the earth and $M_r = uR\cos\phi$ is the angular momentum relative to the rotating earth. This second term is the important one in determining the circulation. From M_r it is apparent that the contribution of the westward winds near the poles to the relative angular momentum budget is small compared with that of the mid-latitude eastward winds and the equatorial westward winds.

The eastward winds are sufficiently strong to lead to a superrotation of the atmosphere as a whole relative to the

solid earth of about +6 m s^{-1} (Peixóto and Oort (1984)).

The problem that was investigated by Jeffreys (1926) and Starr (1948) amongst others was how angular momentum was transferred from the main source region near the equator to the sink region in the middle latitudes. Horizontal momentum may be transferred either by the direct advection of air that has either positive or negative angular momentum, or by the advection of angular momentum (Starr (1948)). The first case requires a net transfer of mass across a line of latitude. Except for short period changes and seasonal effects this does not occur. Therefore, the north-south transportation of angular momentum must be the result of the advection of relative angular momentum without implying the mean transport of mass over a latitude line over all heights.

The obvious candidate for transferring relative angular momentum is the meridional winds. However, meridional winds are not strong enough to cause the necessary amount of relative angular momentum transport, except possibly in the tropcis (Starr (1948), Peixóto and Oort (1984)). In fact, the meridional winds near the earth's surface are sufficiently weak to cause some doubt about the direction in which they are transferring momentum (Lorenz (1967)).

Thus another mechanism must be sought to explain the transport of momentum from the source to the sink regions. Starr (1948) proposed that relative angular momentum was transported by eddies at mid-tropospheric heights. At this point it is worth noting that while internal gravity waves can transport and redistribute momentum, they do not possess momentum (McIntyre (1973), (1981)).

One consideration in the implementation of Starr's (1948) model is that momentum must be transported from ground level up to the height at which it is transported polewards in

the troposphere near the equator and downwards again in the middle latitudes. The downward transfer of momentum in the mddle latitudes is accomplished by cyclonic disturbances.

(Starr (1948), Palmén and Newton (1969, Chapter 1)) indicate that both eddies and the general circulation are important. Newell et al. (1972, p.149) explain that the upward transport of total angular momentum results from Hadley or Ferrel cells transporting Ω (absolute) angular momentum. Furthermore, they found that in the equatorial troposphere the vertical flux of relative angular momentum due to eddies is small compared with the transportation due to Hadley or Ferrel cells.

Starr's (1948) and Jeffrey's (1926) proposals that the horizontal transport of momentum is accomplished by large scale eddies has been confirmed by observational studies by Buch (1954) and Starr and White (1951) amongst others in the northern hemisphere and by Obasi (1963) in the southern hemisphere. They found poleward transport of zonal angular momentum from the equator to the middle latitudes in both hemispheres at mid-tropospheric heights.

Essentially, the previous discussion has been undertaken to emphasize the nature of and the reasons for momentum transport in the atmosphere and to introduce the theoretical development needed to discuss momentum transport.

7.3 Meridional Transport of Zonal Momentum in the Middle Atmosphere

At any height where the transport of momentum is considered a global network of stations is needed to calculate the total momentum transport properly. Both standing eddies and changes in momentum transport with latitude are important in understanding the total picture of momentum transport and the effect of this transport on the general circulation. Such a network was available at tropospheric heights by the 1940's

and 1950's, but there is still no such network available near the mesopause. However, the current availability of relatively long time series in the mesosphere means that estimates can be made of the contributions of the various transient eddy components to the momentum budget.

Furthermore, information is available about the momentum transport due to stationary waves and travelling planetary waves in the mesosphere from satellite derived radiances.

Satellite derived radiances are available with poor height resolution up into the mesosphere using the 15 μm bands of CO_2 (Gille et al. (1980). Above 80 km CO_2 is not in local thermodynamic equilibrium, so that the temperatures obtained by inversion techniques may be slightly in error (Drummond et al. (1980)).

Labitzke (1980) has found evidence of stationary planetary waves up to heights of 90 km in the northern hemisphere winter (zonal wavenumber 1, amplitude of ~ 3K) and with much smaller amplitudes in both the summer and the southern hemisphere. Thus, in any determination of the transport of momentum by transient or travelling waves, it should be remembered that some transport occurs due to the presence of quasi-stationary waves.

There have been a number of studies of momentum transport above the tropopause. Newell (1963) used meteorological rocket network data measured at heights between ~ 30 km and ~ 60 km to determine values of the covariance between the meridional and the zonal wind components of transient eddies at several North American stations ranging in latitude from 28.33 N (Cape Canaveral, Florida) to 64.00 N (Fort Greely, Alaska). Newell found large positive values of $\overline{u_1 v_1}$ in winter and smaller positive values in summer (Murgatroyd et al. (1965)). Murgatroyd et al. (1965) converted Newell's (1963) values of $\overline{u_1 v_1}$ into

values for the transport of relative momentum showing strong northward transport of positive zonal momentum in winter. Newell's technique was such that the total contribution of $\overline{u_1 v_1}$ from all transient eddies (Planetary waves, tides and gravity waves) was measured.

Hartmann (1976) used Nimbus 5 selective chopper radiometer radiances to study planetary wave momentum transport up to heights of about 55 km. Hartmann found that the maximum transport by stationary planetary waves occurred at a height of about 50 km at about latitude 45.

Crane et al. (1980) also calculated planetary wave velocities from satellite derived radiances using geostrophic wind calculations, but they used Nimbus 6 pressure modulator radiometer data which allowed readings to be taken to pressures of 0.03 mb (up to ~ 70 km). The other heights that they used were 0.3 mb (~ 55 km), 3 mb (~ 40 km) and 30 mb (~ 25 km). Crane et al studied the values of $\overline{u_1 v_1}$ which is equivalent to the momentum flux of transient planetary wave eddies, and found that $\overline{u_1 v_1}$ was poleward at all heights and seasons except for the polar regions. The magnitude of $\overline{u_1 v_1}$ was as great as 400 $m^2 s^{-2}$ at 0.3 mb (55 km) at 50 N in winter. At 0.03 mb (70 km) the magntidue of $\overline{u_1 v_1}$ had a maximum value of about 100 $m^2 s^{-2}$. SEE ERRATA

Hunt (1981) used a model atmosphere and also found poleward momentum transport in the middle atmosphere.

Geostrophic winds for heights of up to 0.4 mb (50-55 km) were used by Hamilton (1982). Hamilton found that zonal wavenumber one dominated the momentum flux due to transfer of planetary waves. The value of $\overline{u_1 v_1}$ was highest at 0.4 mb and indicated that positive zonal momentum was transported northward from September until May with the summer results being more doubtful.

Other studies of momentum transport have included Elford's (1979) study of the accelerations resulting from momentum transport due to tides and the estimate of Smith and Lyjak (1985) of the acceleration that is needed to balance the momentum budget. This is discussed further later.

7.4 The Theoretical Background of Momentum Transport

The small amount of theoretical background needed to determine momentum transport can be derived from the definition of angular momentum (M) given by Oort and Peixoto (1983):

$$M = \Omega R^2 \cos\phi + uR\cos\phi \qquad (7.2)$$

where Ω is the angular frequency of the earth's rotation, ϕ is the latitude, R is the earth's radius and u is the zonal velocity.

The time rate of change of angular momentum is given by Newell et al. (1977, p.132) as:

$$\frac{\partial M}{\partial t} + \frac{1}{R\cos\phi}\left[\frac{\partial (Mu)}{\partial \lambda} + \frac{\partial}{\partial \phi}(Mv\cos\phi)\right] + \frac{\partial}{\partial p}(Mw + gR\cos\phi\tau_\lambda) \qquad (7.3)$$

The meridional flux is $J_\phi = Mv$ where v is the meridional velocity so that

$$J_\phi = \Omega R^2 \cos^2\phi v + uvR\cos\phi \ . \qquad (7.4)$$

The time averaged value of J_ϕ is given by

$$\bar{J}_\phi = \Omega R^2 \cos^2\phi \bar{v} + R\cos\phi(\overline{uv}) \qquad (7.5)$$

If the hemispheric coverage is available the zonally averaged form of equation 7.5 is SEE ERRATA

$$[\bar{J}_\phi] = \Omega R^2 \cos^2\phi [\bar{v}] + R\cos\phi([\overline{uv}]) \qquad (7.6)$$

Lorenz (1967, p.79) gives the expansion of any term of the type $[\overline{xv}]$ as

$$[\overline{xv}] = [\bar{x}][\bar{v}] + [\overline{x^*v^*}] + [\overline{x_1 v_1}] + [\overline{x_1^* v_1^*}] \qquad (7.7)$$

As no direct information is available about the deviation of stationary waves from the zonal average ([u*v*]) discussion is restricted to the terms $[\bar{u}]$ $[\bar{v}]$, $[\overline{u_1^* v_1^*}]$ and $[\overline{u_1 v_1}]$ and the various components of the latter two cases.

The probable importance of standing waves has been considered previously. The maximum value of $\overline{u^* v^*}$ apparently occurs at about 55 km and decreases above this height (from Hartmann (1976), Crane et al. (1980)). Thus, this component is relatively less important near the mesopause than near the stratopause. Furthermore, stationary waves are less important in the southern hemisphere than in the northern hemisphere (Harwood (1976)) so that the exclusion of stationary waves should not affect the momentum budget markedly near the mesopause.

The terms $\overline{u_1 v_1}$ and $\overline{u_1^* v_1^*}$ cannot be differentiated when only one longitude is being used. Henceforth, $\overline{u_1 v_1}$ will be used to cover both terms.

The equation for momentum flux used by Murgatroyd et al. (1965, p.90)

$$\text{Flux}_\phi = \frac{2\pi R^2 \cos^2 \overline{u_1 v_1}}{g} \qquad (7.8)$$

is equivalent to the relevant term in the integral of equation 7.5 a unit pressure height range is used as the mass element dm is defined as $dm = a^2 \cos\phi d\lambda d\phi dp/g$.

7.5 Values of Momentum Transport

The values of $\overline{u_1 v_1}$ for various motions are given in the following figures: motions with periods of less than 3 hours are given in figure 7.1 ; motions with periods between 5 and 8 hours are given in figure 7.2 ; motions with periods between 8 and 24 hours are given in figure 7.3 ; motions with periods of more than 1 day are given in figure 7.4 ; the values of $\overline{u_1 v_1}$ for all transient motions are given in figure 7.5. Negative signs indicate southward transport of positive zonal momentum.

(a) *Motions with periods of less than 3 hours*

From figure 7.1 it can be seen that the southward transport of positive zonal momentum by short period motions (< 3 hours) is less than 100 m^2s^{-2} in most months at heights below 80 km. Some larger values of southward transport do occur below 80 km, especially in winter. Maximum values of southward transport occur at heights between 90 and 100 km in winter. In this case the magnitude of $\overline{u_1v_1}$ can exceed 600 m^2s^{-2}. In summer magnitudes of more than 400 m^2s^{-2} can occur.

Values of $\overline{u_1v_1}$ are given only at heights of 85 km and above for both the 5 to 8 hour and 8 to 24 hour period ranges. The shortage of night-time wind measurements below 85 km did not allow sufficiently long time series of 2 hourly averages to be constructed below this height (see Chapter 3).

(b) *Motions with periods between 5 and 8 hours*

The magnitude of $\overline{u_1v_1}$ for the 5 to 8 hour averages (figure 7.2) reached values of a little over 100 m^2s^{-2}. The direction of the transport of positive zonal momentum was mostly southward. Lower magnitudes than 100 m^2s^{-2} were commonly found throughout the year.

(c) *Motions of tidal periods*

The values of $\overline{u_1v_1}$ for the tidal periods (8 to 24 hours) were commonly around -200 m^2s^{-2} throughout the year for heights between 85 and 100 km (figure 7.3) although one more intense period of southward transport occurred at a height of about 95 km in late summer and early autumn. Elford (1979) found values of momentum transport at 35 S for the 24 hr and 12 hr tides of between -100 m^2s^{-2} in summer at 35^oS but no momentum flux in winter.

Figure 7.1

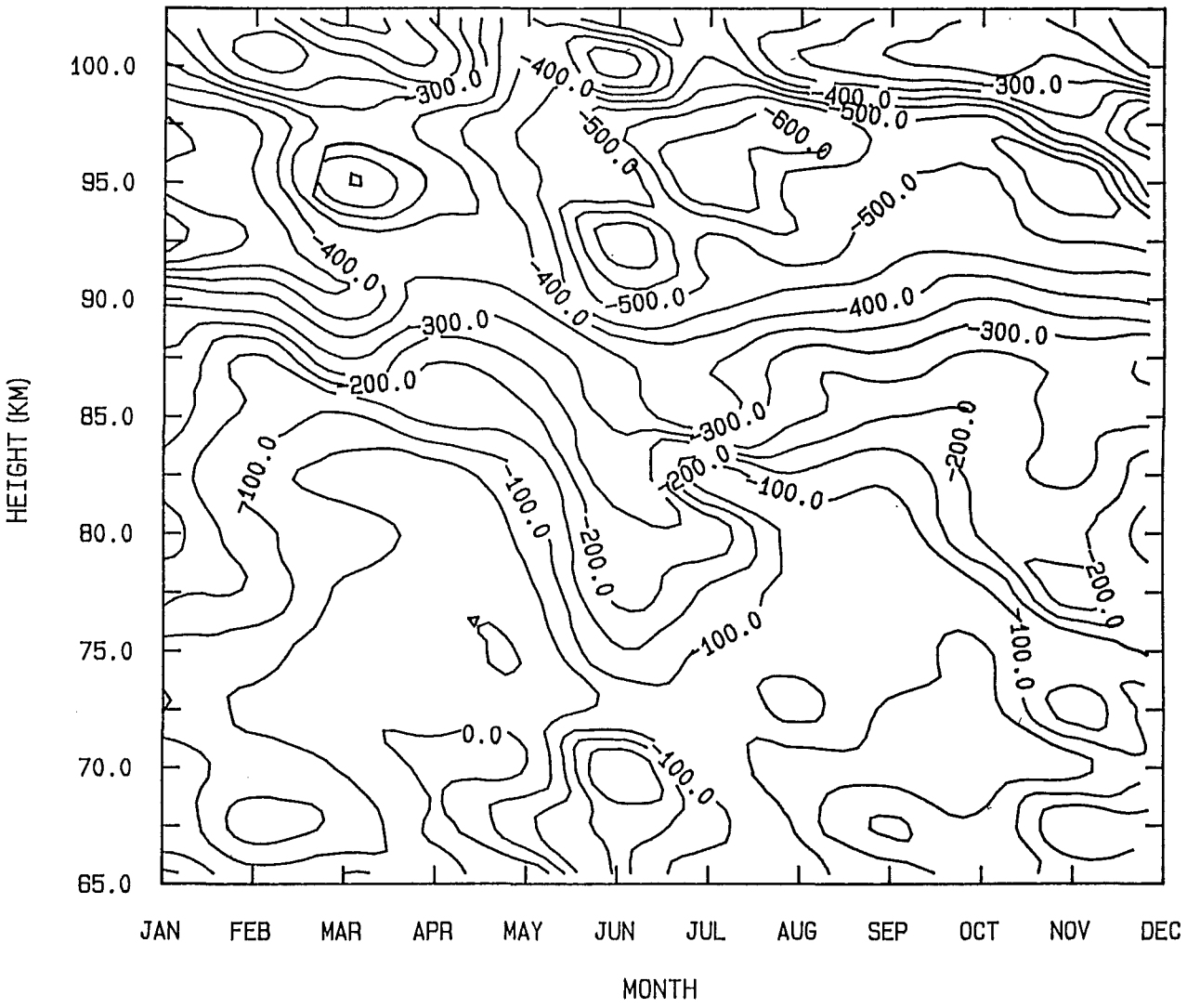

The meridional transport of zonal momentum by motions with periods of less than 3 hours in 1981($m^2.s^{-2}$). Negative values indicate southward transport of positive zonal momentum.

Figure 7.2

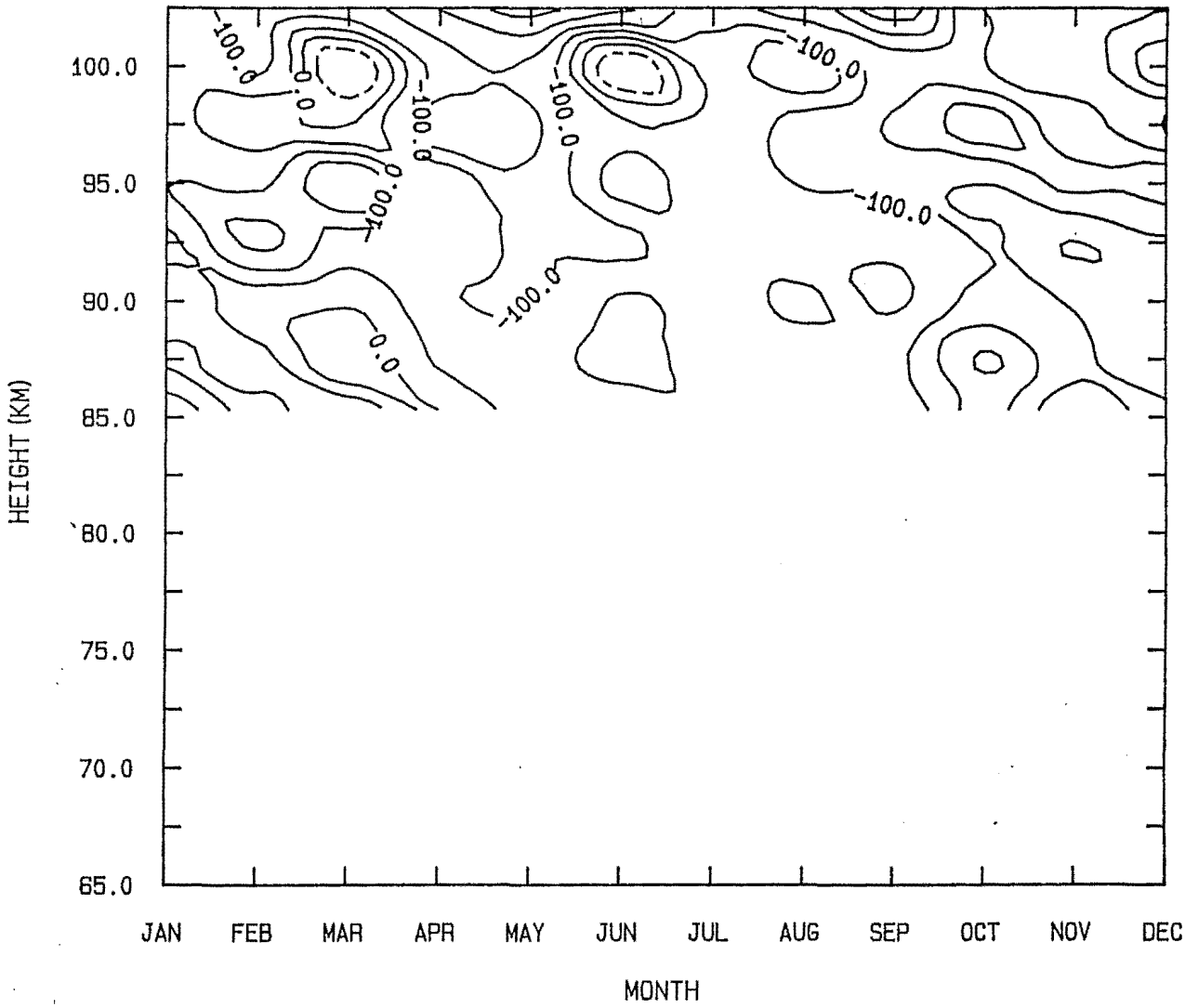

The meridional transport of zonal momentum by motions with periods of between 5 hours and 8 hours in 1981($m^2.s^{-2}$). Negative values indicate southward transport of positive zonal momentum.

Figure 7.3

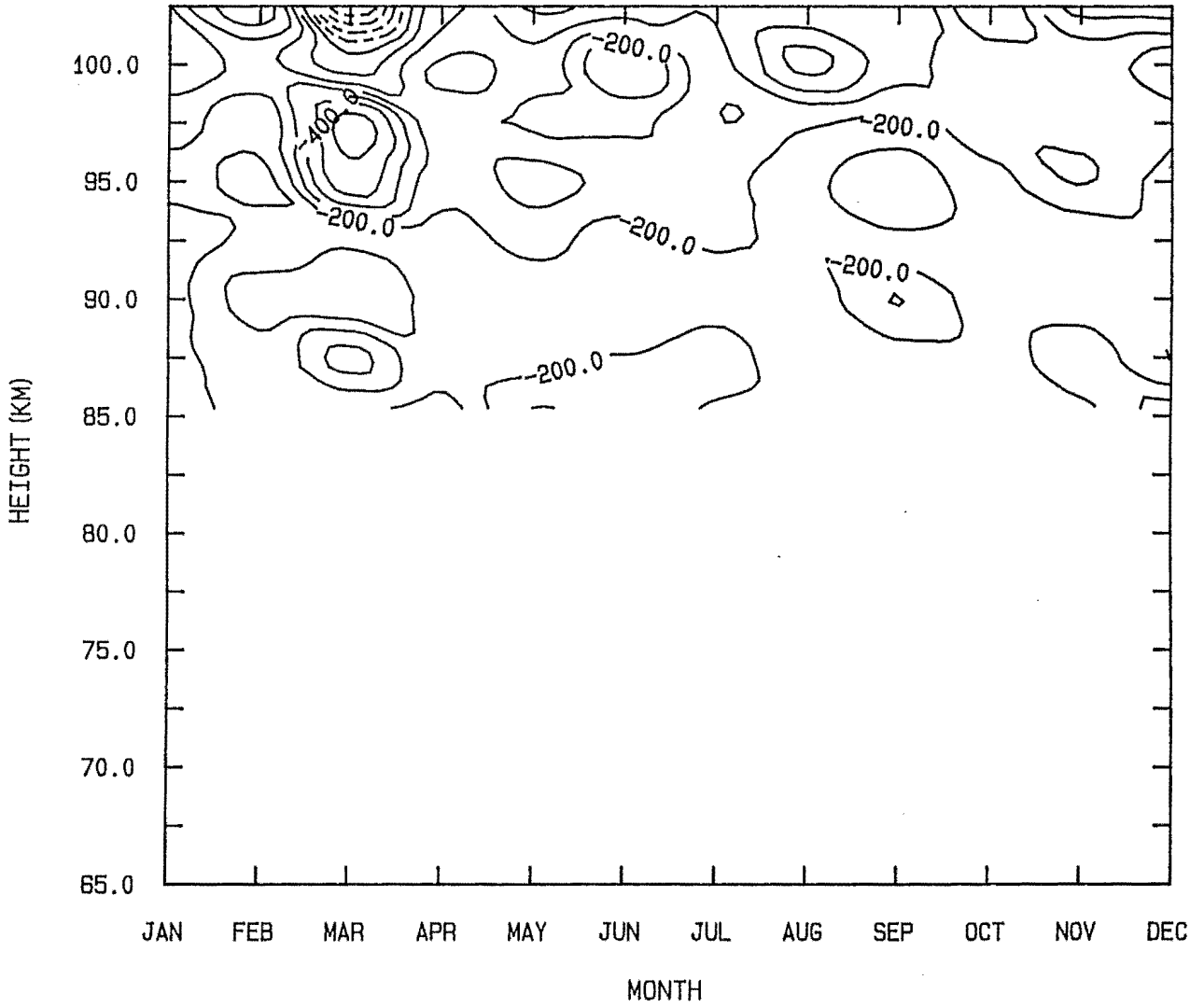

The meridional transport of zonal momentum by motions with periods of between 8 hours and 1 day in 1981($m^2.s^{-2}$). Negative values indicate southward transport of positive zonal momentum.

(d) *Planetary waves*

The values of $\overline{u_1 v_1}$ for motions with periods of greater than 1 day at 65 km were excluded because of the small number of data available at this height. There were mostly fewer than 20 points available at this height compared with about 30 at other heights, thus there was a considerable random variability from month to month at 65 km. The magnitude of $\overline{u_1 v_1}$ is more than 300 $m^2 s^{-2}$ in a southward direction at heights of less than 75 km in the middle of winter (figure 7.4). However, the value of $\overline{u_1 v_1}$ does not often exceed 100 $m^2 s^{-2}$ at heights above 85 km except in late summer and early autumn.

(e) *All motions*

Overall the study of positive zonal momentum transport by transient motions shows a distinct southward trend at almost all heights in each month (figure 7.5).

The magnitude of this transport is less than 400 $m^2 s^{-2}$ below 77.5 km except in winter where the large amplitude of planetary waves contributes to enhanced transport. Maximum magnitudes of $\overline{u_1 v_1}$ for the sum of all transient motions typically occur between 90 km and 100 km at which heights magnitudes of over 800 $m^2 s^{-2}$ occur.

7.6 Correlation Coefficients and Significance

The $\overline{u_1 v_1}$ calculations for momentum transport allow correlation coefficients to be calculated. The significance of these correlations is tested using the equation given in Chapter 3.

The correlation coefficients for motions with periods of less than 3 hours are given in table 8.1. The significance of these correlation coefficients is discussed in Chapter 8.

Figure 7.4

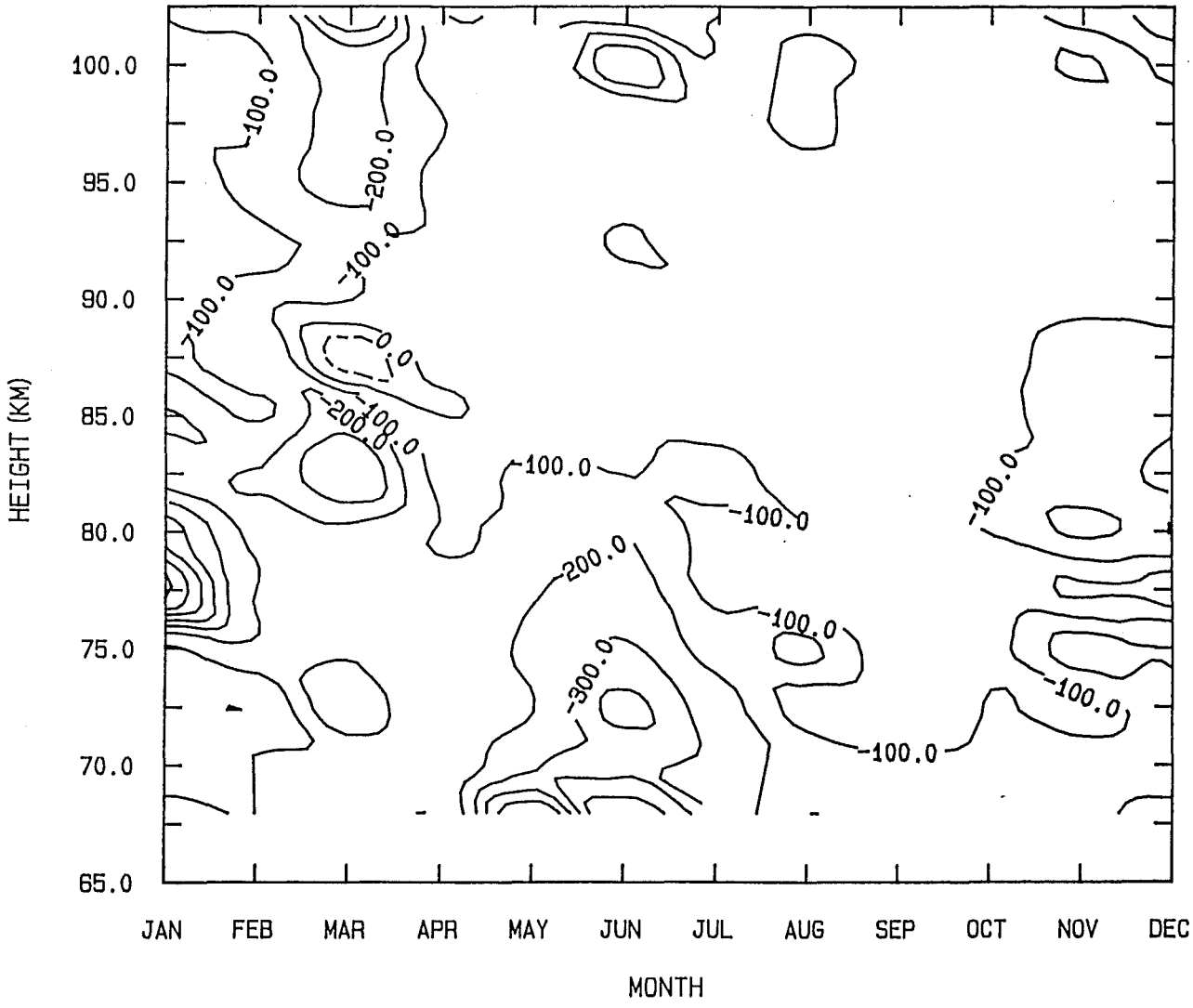

The meridional transport of zonal momentum by motions with periods of greater than 1 day in 1981($m^2.s^{-2}$). Negative values indicate southward transport of positive zonal momentum.

Figure 7.5

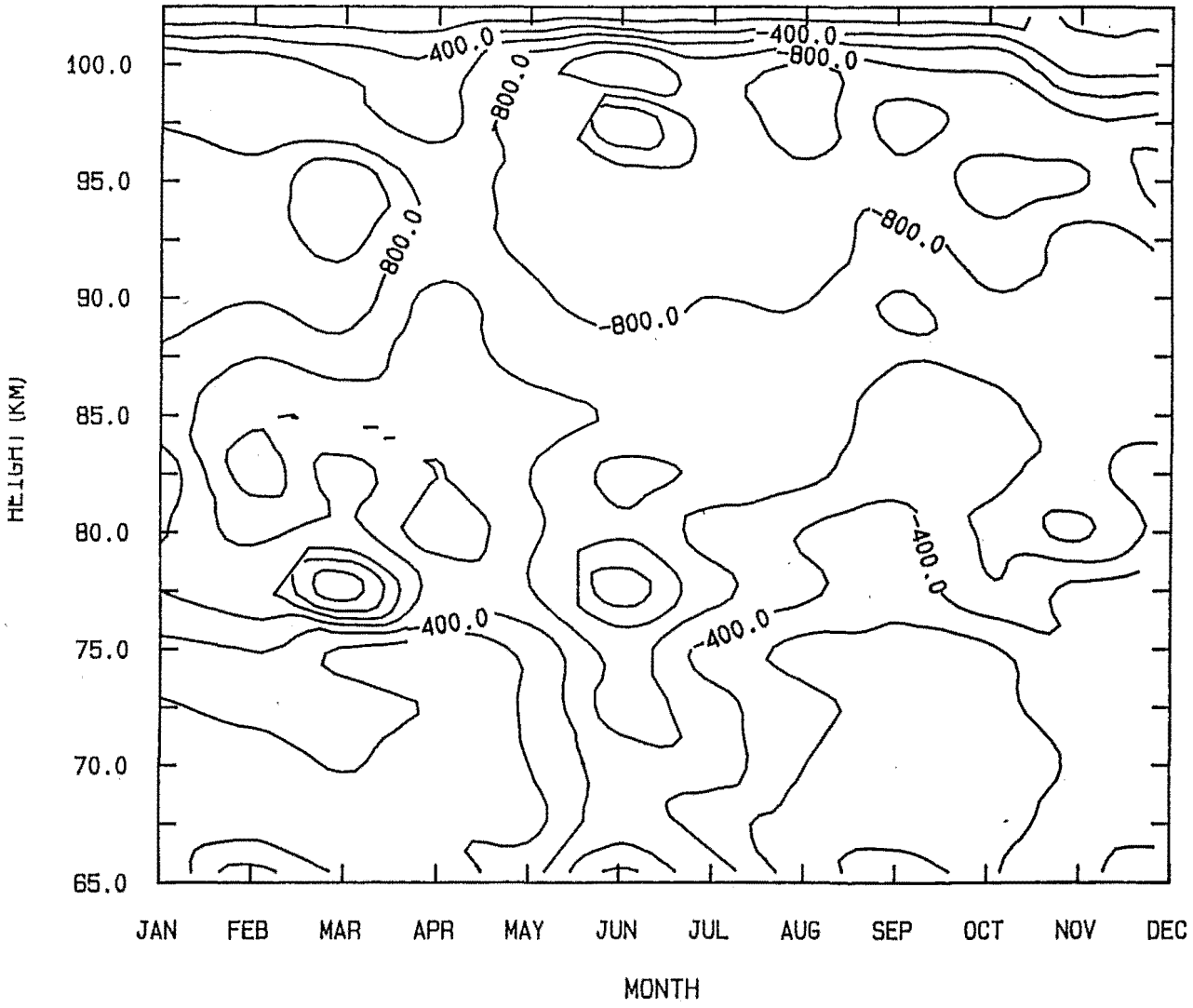

The meridional transport of zonal momentum by all transient motions in 1981($m^2.s^{-2}$). Negative values indicate southward transport of positive zonal momentum.

(a) *Motions with periods between 5 and 8 hours*

In the majority of cases the correlation coefficients that occur for motions with periods of between 5 and 8 hours are significantly less than zero (table 7.1). There does not appear to be any pattern to the correlation coefficients that are not significantly different from zero, except that the small number of data in March leads to large uncertainties.

(b) *Tidal periods*

Similarly for motions with periods of between 8 and 24 hours most correlation coefficients are significantly less than zero (table 7.2). However, there are several correlations at 85 km that are not significantly different from zero.

(c) *Planetary waves*

The situation is not so clear for motions with periods greater than 1 day (table 7.3). The small number of points used means that the uncertainties are large. In a large number of cases these large uncertainties mean that the correlation is not significantly different from zero at the 95% level. However, in the majority of cases the correlation coefficients are significantly less than zero.

(d) *All motions*

The overall correlation for all transient motions is significantly less than zero throughout the year at all heights from 75 km upwards with the exception of the correlation coefficients at 102.5 km in March (table 7.4). Maximum values for the correlation coefficients are normally found at heights between 85 km and 95 km (with several exceptions). From the calculations made earlier in this chapter, it can be seen that this is the region in which momentum transport by internal gravity waves is strongest.

For tables 7.1 to 7.4 see

APPENDIX III

7.7 Comparisons of the Momentum Transport for Different Period Ranges

The analysis of the motion into separate period ranges allows the relative importance of the various components of motion to the meridional transport of positive zonal momentum to be determined. Averages of momentum transport over 10 km height ranges in all four seasons are given in the following tables.

TABLE 7.5 Values of $\overline{u_1 v_1}$ for motions with periods of less than 3 hours ($m^2 s^{-2}$) in 1981 at Birdlings Flat

Height (km)	Summer	Autumn	Winter	Spring
65-67	- 82	- 16	-101	- 74
75-85	-151	- 61	-185	-160
85-95	-345	-295	-444	-375
95-102.5	-334	-295	-476	-369

TABLE 7.6 Values of $\overline{u_1 v_1}$ for motions with periods of between 5 and 8 hours ($m^2 s^{-2}$) in 1981 at Birdlings Flat

Height (km)	Summer	Autumn	Winter	Spring
85-95	- 85	- 73	- 72	-101
95-102.5	- 94	-125	- 80	-134

TABLE 7.7 Values of $\overline{u_1 v_1}$ for motions with periods of between 8 and 24 hours ($m^2 s^{-2}$) in 1981 at Birdlings Flat

Height (km)	Summer	Autumn	Winter	Spring
85-95	-178	-201	-185	-171
95-102.5	-268	-323	-259	-243

TABLE 7.8 Values of $\overline{u_1 v_1}$ for motions with periods of more than 1 day ($m^2 s^{-2}$) in 1981 at Birdlings Flat

Height (km)	Summer	Autumn	Winter	Spring
67.5-75	- 90	-234	-219	-102
75-85	-200	-154	-130	-113
85-95	- 97	- 73	- 73	- 71
95-102.5	- 80	-145	-134	- 85

TABLE 7.9 Values of $\overline{u_1 v_1}$ for all transient motions ($m^2 s^{-2}$) in 1981 at Birdlings Flat

Height (km)	Summer	Autumn	Winter	Spring
65-75	-235	-185	-497	-193
75-85	-493	-454	-575	-423
85-95	-721	-648	-776	-682
95-102.5	-732	-781	-905	-775

These tables supplement the contour plots (figures 7.1 to 7.5). The relative importance of the various components of motion at Birdlings Flat can also be deduced from those tables.

Several points should be noted concerning the values of $\overline{u_1 v_1}$ for the various period ranges given in tables 7.5 to 7.8.

The first is that planetary waves dominate over internal gravity waves in the lowest height range (65 km to 75 km) in winter and autumn. The values of the $\overline{u_1 v_1}$ are low for both period ranges in spring and summer compared with the winter and autumn values for planetary waves.

The second point is that internal gravity waves dominate the meridional transport of zonal momentum at heights between 85 km and 95 km. The magnitudes of the values of $\overline{u_1 v_1}$ for other period ranges are much lower.

Thirdly, the less than 3 hour period range and the 8 to 24 hour period range are the most important period ranges for heights above 95 km. The tides become relatively more important in this height range compared with the 85 km to 95 km height range.

The overall picture can be gained from the comparison of the values of $\overline{u_1 v_1}$ for the various period ranges with the values of $\overline{u_1 v_1}$ for all transient motions (table 7.9). Motions with periods of more than 1 day dominate the southward transport of zonal momentum at heights between 65 km and 75 km in autumn, account for over half the transport in this height range in spring and almost half the transport in this height range in winter and summer. Thus at these heights planetary waves dominate the meridional transport of angular momentum by waves: a situation similar to that which occurs lower in the atmosphere (see earlier in this chapter for references). Motions with

periods of less than 3 hours dominate the meridional transport of zonal momentum at heights between 85 km and 95 km, especially in winter and autumn.

7.8 Accelerations Due to the Meridional Transport of Zonal Momentum

Changes in the transport of momentum cause accelerations of the mean flow.

The change of angular momentum M in a fixed zonal ring of air of mean density ρ with unit width and depth is given by Palmén and Newton (1969, p.16) as

$$\frac{\partial M}{\partial t} = -\frac{\partial}{\partial y}\left(2\pi R^2\cos^2\phi\,(\Omega R\cos\phi + \bar{u})\rho\bar{v}\right. + 2\pi R^2\cos^2\phi\rho\overline{u_1v_1}) - \frac{\partial}{\partial z}\left(2\pi R^2\cos^2\phi\,(\Omega R\cos^2\phi + \bar{u})\rho\bar{w}\right. + 2\pi R^2\cos^2\phi\rho\overline{u_1w_1}) \quad . \tag{7.9}$$

Where ϕ is the latitude, R is the radius of the earth, Ω is the angular velocity of the earth, y is in the meridional direction so that $y = R\phi$, z is in the vertical direction and u, v, w and t are as used elsewhere.

This can be written as an acceleration (Elford (1979))

$$\frac{\partial\bar{u}}{\partial t} = \bar{v}\left(2\Omega\sin\phi - \frac{1}{R\cos\phi}\,\frac{\partial}{\partial\phi}\,(\bar{u}\cos\phi)\right) - \bar{w}\,\frac{\partial\bar{u}}{\partial z} - \frac{1}{R\cos^2\phi}\,\frac{\partial}{\partial\phi}\,(\overline{u_1v_1}\cos^2\phi) - \frac{1}{\rho}\,\frac{\partial}{\partial z}(\rho\overline{u_1w_1}) \tag{7.10}$$

The acceleration due to the mean flow is determined by the first 3 terms of equation (7.10), while the remaining terms give zonal acceleration due to horizontal and vertical transport by transient motions.

In this work, where information is available about $\overline{u_1v_1}$, interest is centred on the fourth term in equation (7.10): meridional changes in the meridional transport of zonal momentum.

A very rough estimate of this term in the southern hemisphere can be made by comparing $\overline{u_1 v_1}$ values from Birdlings Flat with $\overline{u_1 v_1}$ values from Arrival Heights.

There are several points that ought to be considered at this stage.

The first is that Arrival Heights has approximately the same longitude as Birdlings Flat (166.7 E and 172.7 E respectively).

Secondly, the difference in latitudes between Birdlings Flat and Arrival Heights is large (the latitudes are 43.8 S and 77.8 S respectively). The use of a latitude difference in determining the gradient of $\overline{u_1 v_1}$ over latitude assumes that $\overline{u_1 v_1}$ varies linearly with latitude between the two points. Apart from information about planetary waves (e.g. Smith and Lawrence (1985) and Hamilton (1983), which, from the figures given earlier, are of minor importance to momentum transport above a height of about 80 to 85 km, and deductions from the known characteristics of tides (Elford (1979)) there is apparently no information available about how the meridional transport of zonal momentum varies with latitude near the mesopause. Newell et al. (1972, p.148) have produced meridional profiles of the dominant planetary wave momentum transport in the troposphere which do not show linear variations with latitude in the middle latitudes (see figure 7.6). However, in the absence of more stations, there is no option but to treat the variation as linear. The mean value of $\overline{u_1 v_1}$ must go to zero at the poles assuming symmetry.

A third point worth considering is that the characteristic of internal gravity waves may vary considerably depending on their source. The two locations are sufficiently far apart for this to be a major source of error, especially between 85 km and 95 km where, from the tables given earlier,

Figure 7.6

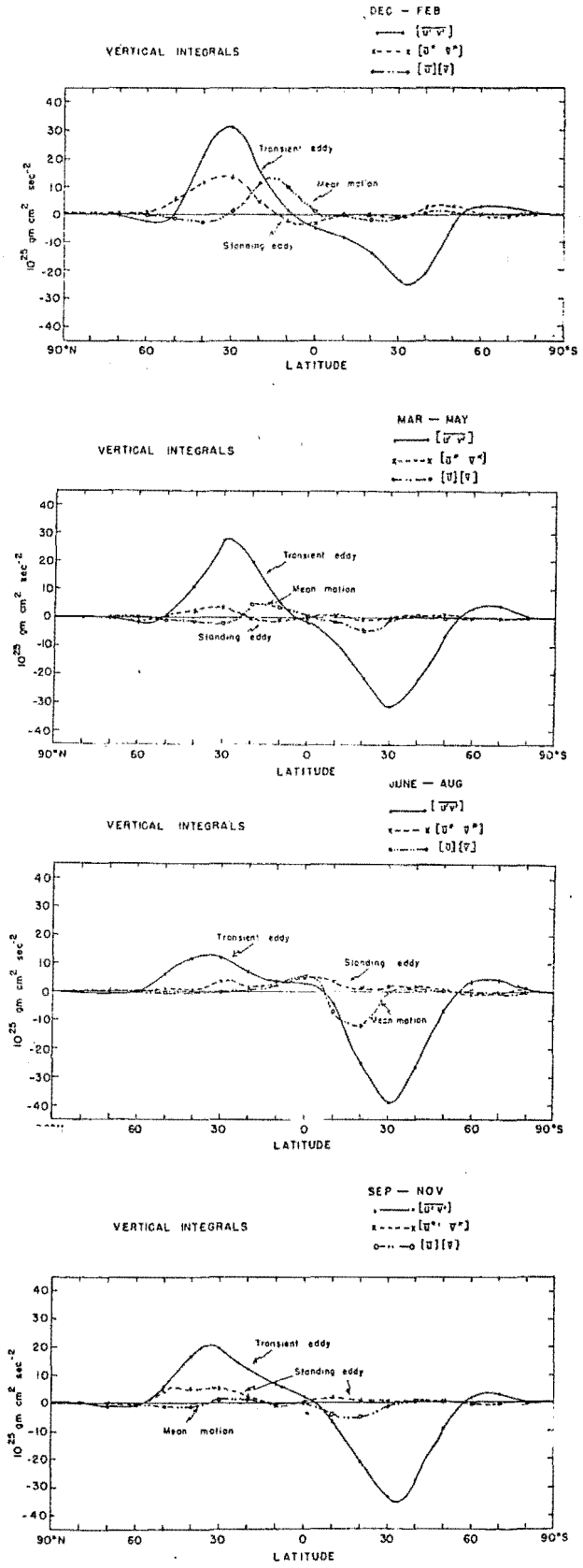

:iations in the total vertical integral of $\overline{u_t v_t}$ ($\overline{u'v'}$) with :itude (Newell et al. (1972)).

internal gravity waves are a major source of momentum transport at Birdlings Flat.

A fourth factor lies in the data from Arrival Heights. Fewer usable readings are available than there are at Birdlings Flat. The method used to calculate the contribution from components with periods between 5 and 8 hours and 8 and 24 hours requires that there should be a nearly continuous (at most 2 gaps) series of 2 hour averages containing at least (2N+1) points, where N is the number of points in the cut-off of the Behannon and Ness (1966) filter. Sufficient time series of this length were not available through much of the year (table 3.3 gives a randomly selected day in October). Furthermore, removing averages from the data used to construct the averages is a large source of error when few data are available. Thus instead of analysing the contribution of the individual period ranges to the acceleration of the mean flow, the accelerations due to all transient motions for heights between 75 and 85 km and 85 and 95 km are calculated.

As Arrival Heights data were available from December 1982, the Birdlings Flat data used also came from after this date. The data used came from April, July and October 1983 and January 1984. Thus each season is represented. Unfortunately, the July 1983 data is probably not representative of typical winter data in so far as the mean zonal wind jet in the mesosphere at Birdlings Flat is very weak.

The terms involving the mean wind in equation (7.10) are

$$\bar{a}_m = 2\Omega\bar{v}\sin\phi + \frac{\bar{u}\bar{v}}{R}\tan\phi - \frac{\bar{v}}{R}\frac{\partial\bar{u}}{\partial\phi} - \bar{w}\frac{\partial\bar{u}}{\partial z} \qquad (7.11)$$

where $\bar{a}_m$ denotes the acceleration due to the mean winds. This expression can be evaluated using the mean winds given in tables 7.13 and 7.14 that existed at the time that the observations of the momentum transport were made. This

TABLE 7.10 (a) The number of readings used at each height for each hour at Arrival Heights on October 11 1983. Values for hours 0 to 11

	Hour											
Height (km)	0	1	2	3	4	5	6	7	8	9	10	11
67	0	0	0	0	0	0	0	0	0	0	0	0
69	0	0	0	0	0	0	0	0	0	0	0	0
71	0	0	0	0	0	0	0	0	0	0	0	0
73	0	0	0	0	0	0	0	0	0	0	0	0
75	0	0	0	0	0	0	0	0	0	0	0	0
77	0	0	0	0	0	0	0	0	0	0	1	0
79	0	0	0	0	0	0	0	0	0	0	1	1
81	0	0	0	0	0	0	0	0	0	0	1	1
83	0	0	0	0	0	0	0	0	0	0	0	0
85	0	0	0	0	1	1	0	1	0	0	0	1
87	0	0	1	0	0	0	1	0	0	0	0	0
89	0	0	1	0	0	0	1	0	0	0	0	0
91	0	1	0	0	1	0	1	0	0	0	1	0
93	0	0	0	0	0	0	0	0	0	0	0	0
95	0	0	0	0	0	0	0	1	0	0	0	0
97	0	0	0	0	1	0	0	0	0	0	0	0

TABLE 7.10 (b) The number of readings used at each height for each hour at Arrival Heights on October 11 1983. Values for hours 12 to 23

	Hour											
Height (km)	12	13	14	15	16	17	18	19	20	21	22	23
67	0	0	0	0	0	0	0	0	0	0	0	0
69	0	0	0	0	0	0	0	0	0	0	0	0
71	0	0	0	0	0	0	0	0	0	0	0	0
73	0	0	0	0	0	0	0	0	0	0	0	0
75	0	0	0	0	0	0	0	0	0	0	0	0
77	0	1	0	0	0	0	0	0	0	0	0	0
79	1	1	1	1	0	0	0	0	0	0	0	0
81	0	0	0	1	0	0	0	0	0	0	0	0
83	0	0	0	0	1	1	0	0	0	0	0	0
85	0	0	1	1	1	0	1	1	0	0	0	0
87	0	0	0	0	1	0	0	0	0	0	0	0
89	0	0	0	0	0	0	0	0	0	0	0	0
91	1	0	0	0	0	0	0	0	1	0	1	1
93	0	0	0	0	0	0	0	0	1	0	0	0
95	0	0	0	0	0	0	0	0	0	0	0	0
97	0	0	0	0	0	0	0	0	0	0	1	1

TABLE 7.11 Total $\overline{u_1 v_1}$ for all transient motions at Birdlings Flat in 1983/84 ($m^2 s^{-2}$)

Height (km)	April	July	October	January
75-85	-412	-625	-212	-425
85-95	-707	-713	-449	-587

TABLE 7.12 Total $\overline{u_1 v_1}$ for all transient motions at Arrival Heights in 1983/84 ($m^2 s^{-2}$)

Height (km)	April	July	October	January
75-85	-154	-292	-176	- 87
85-95	-222	-229	-294	-147

TABLE 7.13 The mean winds at Birdlings Flat in 1983/84 (eastward and northward winds are positive, units are ms^{-1})

	April		July		October		January	
Height (km)	75-85	85-95	75-85	85-95	75-85	85-95	75-85	85-95
mean zonal wind	29	3	17	10	7	-3	-32	6
mean meridional wind	-10	2	-1	-4	-7	1	11	5

TABLE 7.14 The mean winds at Arrival Heights in 1983/84 (eastward and northward winds are positive, units are $m\,s^{-1}$)

	April		July		October		January	
Height (km)	75-85	85-95	75-85	85-95	75-85	85-95	75-85	85-95
mean zonal wind	10	1	16	13	-6	2	-21	-20
mean meridional wind	2	-1	-2	-2	-3	2	-2	6

analysis is crude due to the large size of the horizontal and vertical grids. The mean winds used are the average of those at Birdlings Flat and Arrival Heights, $\frac{\partial \bar{u}}{\partial z}$ is the difference between the zonal winds in the 75-85 km and the 85-95 km height range and $\bar{w}$ is estimated from the continuity equation assuming that there is no variation in density with time, that $\bar{u}$ is constant with longitude and that density varies only with height.

$$\frac{1}{R\cos\phi}\frac{\partial}{\partial\phi}(\bar{v}\cos\phi) + \frac{\partial}{\partial z}(\rho\bar{w}) = 0 \qquad (7.12)$$

TABLE 7.15 The average values of mean vertical wind obtained from this equation for 1983/84 using the Birdlings Flat and Arrival Heights data

	April		July		October		January	
Height (km)	75-85	85-95	75-85	85-95	75-85	85-95	75-85	85-95
$\bar{w}$ ($x10^{-2} ms^{-1}$)	-2.47	0.55	-0.69	-0.89	-1.33	0.05	2.70	0.60

The strength of stationary planetary waves in the mesosphere was discussed earlier in this chapter and thus the validity of the assumption that $\bar{u}$ does not vary with longitude was considered. It is unlikely that stationary waves are very important in the southern hemisphere middle latitude mesosphere.

The value of $\bar{w}$ as in January 1984 in the 75 km to 85 km height range is considerably larger than the value calculated by Norton (1983) for December 1982. Norton found values of $\bar{w}$ at this height of about 0.9 cm/s when the ~~max~~ jet in the meridional wind was assumed to be constant in height with changing latitude and about 1.5 cm/s when it was assumed to vary. The meridional jet is observed to be lower at Birdlings Flat than at Arrival Heights. Norton (1983) considered both the case when the height of the meridional jet was constant with latitude and the case when the jet varied with latitude. In the 85 km to 95 km height range Norton found that the value of vertical velocity was 0.6 cm/s upwards when the height of the meridional jet was assumed not to vary and 0.6 cm/s downwards when it was assumed to vary in December 1982.

SEE ERRATA

The low values of downward vertical velocity in July compared with say the 4 cm s^{-1} given by Ebel (1974) for mid-winter at 40 N may be explained by postulating the existence of a sudden warning in the stratosphere (e.g. see Schoeberl (1978)). The decrease in the strength of the zonal wind from the lowest height measured up to 80 km compared with the values in 1981 and 1982 (figures 2.6 and 2.7) is consistent with the existence of a sudden warming. The lower value of subsidence in July is consistent with Labitzke's (1972) description of the features of a sudden warming in the stratosphere: the warming of the stratosphere is coupled with a cooling in the mesosphere.

Once the vertical wind has been calculated, the acceleration due to the mean winds can be estimated using

equation (7.11).

TABLE 7.16 Accelerations due to the mean winds (units are m s^{-1} day^{-1})

	April		July		October		January	
Height (km)	75-85	85-95	75-85	85-95	75-85	85-95	75-85	85-95
$\bar{a}_m$ (ms^{-1} day^{-1})	41	-6	16	31	54	-14	-48	-47

These accelerations are positive (eastward) in winter and negative (westward) in summer as expected. The acceleration is smaller than expected in July due to the unusual wind regime that existed in that month.

The $2\Omega\bar{v}\sin\phi$ (Coridis) term, corresponding to changes in the momentum, contributes the majority of the acceleration to the mean flow throughout the year.

The acceleration due to the meridional transport of zonal momentum by waves can be calculated using tables 7.1 and 7.2 and equation (7.10).

The relevant term in this equation for this acceleration (a_{xy}) is

$$a_{xy} = \frac{-1}{R\cos^2\phi} \frac{\partial}{\partial\phi} (\overline{u_1 v_1}\cos^2\phi)$$
$$= \frac{2\tan\phi}{R} \overline{u_1 v_1} - \frac{1}{R} \frac{\partial \overline{u_1 v_1}}{\partial\phi} \qquad (7.13)$$

These accelerations are given in the following table.

TABLE 7.17 Zonal accelerations due to the meridional transport of zonal momentum by waves (units are ms^{-1} day^{-1})

Height (km)	75-85	85-95	75-85	85-95	75-85	85-95	75-85	85-95
a_{xy} (ms^{-1} day^{-1})	22	30	26	30	9	18	18	25

All of the accelerations due to the meridional transport of zonal momentum are in the same direction in table 7.17.

Elford (1979) found that the values of $\overline{u\,v}$ for tides at Adelaide were negligible in winter, but the values were negative in summer. The resulting accelerations were positive in summer: thus acting in the opposite direction to the accelerations due to the mean winds, thus reducing the net acceleration.

It is clear that the accelerations given in table 7.17 do not act in such a way as to balance the accelerations due to the mean winds that are given in table 7.16. In winter the sign of the acceleration due to changes in the meridional transport of angular momentum with latitude is the same as the sign of the acceleration due to the mean winds. Thus, the drag resulting from changes in the meridional transport of zonal momentum with latitude serves to increase the acceleration of the mean flow. In summer the sign of the acceleration due to changes in the meridional transport of zonal momentum with latitude is opposite to the sign of the acceleration due to the mean winds. However, the magnitudes of the accelerations due to the $\overline{u_1 v_1}$ terms are only half the magnitudes of the accelerations due to the mean winds. There are also large net deficits in April and October.

The maximum observed rate of change of the mean zonal flow in the middle latitudes at 90 km near mid-winter is

2 ms^{-1} day^{-1} (Elford (1979)). The changes in the meridional transport of zonal momentum with latitude do not produce sufficient drag to balance the accelerations in the mean flow caused by the mean winds in any season. In winter the changes in horizontal momentum transport act to increase the accelerations due to the mean winds. Thus, as expected, the accelerations must be limited by the vertical transport of zonal momentum by internal gravity waves (e.g. Fritts (1984), Holton (1982, 1983), Lindzen (1981)).

Lindzen (1981) made calculations of the accelerations caused by the vertical transport of zonal momentum by using

$$-\frac{1}{\rho_o}\frac{d}{dz}\left(\rho_o \overline{u_1 w_1}\right) \approx \frac{-k_x}{2H}\left.\frac{(u_o-c_x)^3}{\omega_B\left(1+k_y^2/k_x^2\right)3/2}\right|_{\text{evaluated at } z = z_{break}} \qquad (7.14)$$

Lindzen found accelerations of 135 ms^{-1} day^{-1} in summer and -102 ms^{-1} day^{-1} in winter for a single wave. Schoeberl (1985) suggested that these accelerations are exaggerations of the actual accelerations that occur as the effects of interactions between the mean flow and the internal gravity waves have not been taken into account in this analysis. Vincent and Reid (1983) calculated $\overline{u_1 w_1}$ from observations at heights between 80 km and 90 km and found values between 10 ms^{-1} day^{-1} and 20 ms^{-1} day^{-1} for 3 days.

Smith and Lyjak (1985) used satellite data to calculate the residual gravity wave drag. They found a residual of 20-25 ms^{-1} day^{-1} at 0.1 mbar (65 km). Schoeberl et al. (1983) used a numerical model and by varying the parameters found that the accelerations needed varied between 27 ms^{-1} day^{-1} and 178 ms^{-1} day^{-1}. Apruzese et al. (1982), who also used numerical modelling, required zonal accelerations of about 40 ms^{-1} day^{-1} at 80 km in the middle latitudes. Adding the values for the acceleration

given in tables 7.16 and 7.17 give required accelerations of around $-40\ ms^{-1}\ day^{-1}$ between 75 km and 85 km in the middle of winter in 1983 and about $+30\ ms^{-1}\ day^{-1}$ for the same height in summer in 1983. These values are in agreement with the values given by Apruzese et al. (1982).

Without knowing the value of the drag induced by this transport in the region studied in this thesis, the net acceleration cannot be calculated.

Although changes in the meridional transport of zonal momentum must be considered in calculating the momentum budget, drag due to changes in the vertical transport of zonal momentum is the main mechanism by which internal gravity waves can balance the momentum budget.

One assumption that has been made in this chapter is that the variation of $\overline{u_1 v_1}$ is fairly steady with latitude. The accelerations produced by the use of this assumption seem realistic. However, in the region above 80 km where internal gravity waves dominate $\overline{u_1 v_1}$ this assumption is dependent on whether the existence of non-zero values of $\overline{u_1 v_1}$ is a local or a global phenomena. Thus the cause of the anisotropy of internal gravity waves is of importance to this problem. In the next chapter investigations into the possible causes of the anisotropy are undertaken. In particular, reasons why the anisotropy is weak below 80 km, but strong between 80 km and 95 km are considered.

CHAPTER 8

ANISOTROPIES IN THE MESOSPHERE

8.1 Introduction

Graphs of internal gravity wave variance plotted against height have been included in chapter 6. One of the points that needed explaining in these graphs was that the general shape of the profiles was fairly regular throughout the year. A possible explanation of this and other features has been discussed in chapters 6 and 7. However, in the course of attempting to explain the various features of the variance plots, it seemed necessary to study the profiles at a more basic level. The method chosen was to plot scatter diagrams of the zonal and meridional velocities of the individual points that exist after filtering has occurred.

Vincent and Ball (1977) tried a similar method but did not present a comprehensive set of results. No generalisations could be made from those data. However, Ball (1981) tested wave amplitude over a range of directions throughout the year, but found no consistent pattern over the whole analysis. Vincent (1984) (private communication to Murphy (1984)) suggests that there might be a northeast-southwest alignment at Adelaide.

A set of monthly scatter diagrams from a period of 2½ years from June 1980 to December 1982 have been analysed. Various months have been included in this chapter to demonstrate the overall behaviour of the monthly scatter diagrams. Other analyses have been made to indicate various features that occur in the scatter diagrams. Various explanations for the observed behaviour are discussed.

If internal gravity waves move in one particular direction then momentum will also be carried preferentially in one direction. Thus internal gravity waves can directly affect the circulation of the mesosphere as well as the indirect mechanism of producing drag from turbulence caused by internal gravity wave breaking. Other consequences of the observations are also discussed.

8.2 Scatter diagrams of internal gravity wave amplitudes

In this section the scatter diagrams mentioned in section 8.1 are described. Also, further analyses of the data are made to highlight certain features of the scatter diagrams.

The scatter diagrams are of eastward and northward wind velocities that occur in the data after the 3-hourly means have been subtracted from the raw data. The scatter diagrams that have been presented include all heights from 65 km to 102.5 km. Originally, plots for each month of the 2½ year period were made. However, the large number of plots had to be reduced to a more manageable number so only a few representative months, and months with unusual features, are included. The months of January, April, July and October 1981 have previously been used as representative months in this thesis, so they are also used in this chapter.

The spring and autumn months have features that are common to all months so discussion will start with the months of April 1981 and October 1981.

The April 1981 data are graphed in figure 8.1. The scatter is fairly large at 65 km and no concentration appears to occur near the origin. Up to a height of 80 km the points are apparently grouped in an isotropic manner. There is little increase in amplitude from 65 km to 85 km. The

For figures 8.1 to 8.4 see

APPENDIX IV

usual maximum amplitude (not including the odd widely scattered point) is restricted to a value that is somewhat less than 50 m/s. The maximum amplitude increases as the height increases from 82.5 km to about 92.5 km. The diagrams are first noticeably anisotropic at 85 km and this anisotropy increases as the height increases up to 90 km. Alignment occurs along a line that is roughly that of the northwest-southeast axis for all heights at which the anisotropy can be seen. The anisotropy apparently lessens as the height increases from 92.5 km to 100 km. At 100 km and 102.5 km it is difficult to detect any anisotropy. The maximum usual velocities occur in the 90 km to 95 km height ranges. Maximum velocities that commonly occur are about 120 m/s. This can be compared with the rejection point given in chapter 3 of at least 200 m/s.

The scatter diagrams of the October 1981 data behave in a similar fashion (figure 8.2). There is no strong concentration of points near the origin at 65 km. The maximum amplitude remains fairly constant at heights between 67.5 km and 77.5 km, with this maximum having a magnitude of about 50 m/s. The scatter diagram for 77.5 km shows weak anisotropy. From 80 km to 85 km the amplitude increases along the major (northwest and southeast) axis but apparently not in other directions. The amplitude continues to increase up to heights of either 92.5 km or 95 km. The anisotropy becomes less apparent at 97.5 km. At 102.5 km there is little evidence of anisotropy. The major axis of the anisotropic behaviour continues to occur along the northwest-southeast axis over the whole height range in which the anisotropy is present.

Some small differences occur between the July 1981 scatter diagrams (figure 8.3) and the scatter diagrams of

the two months that have previously been discussed. The points on the scatter diagram appear to be evenly spread from the origin to the maximum amplitude at both 65 km and 67.5 km. The maximum amplitude decreases slightly from 65 km to 70 km. Between 70 km to 75 km the maximum amplitude changes very little. The amplitude increases from 75 km until maximum values occur at 92.5 km. At 75 km and 77.5 km there is a westnorthwest and eastsoutheast orientation of the anistropy. A similar orientation occurs at these heights in July 1980. At 80 km the orientation of the major axis of the anistropy is aligned approximately along the northwest-southeast axis, but no anisotropy is apparent at 82.5 km. The anisotropy appears again at 85 km, with the orientation of the major axis at this and at higher heights occurring along a northwest-southeast axis. The anisotropy becomes stronger as the height increases from 85 km to 90 km. At 90 km the velocities are larger in the northwest quadrant than they are in other quadrants. Similar behaviour occurs at other heights near 90 km. This is considered further later in this chapter. The anisotropy decreases above 90 km. At heights of 100 km and 102.5 km no anisotropy is apparent. The maximum amplitude has also decreased greatly as the height has increased from 95 km to 102.5 km. There is no concentration of points near the origin at 100 km and 102.5 km, the points apparently being distributed homogeneously from the origin out to the maximum amplitude. In the other scatter diagrams that have so far been considered, the points tend to be concentrated near the origin at 100 km and 102.5 km as they are at other heights. This lack of concentration at the greatest heights at which data has been measured also occurs in other winter months. However, this effect and a similar one at 65 km may be caused by the smaller amount of data

occurring at these heights.

The last month considered is January 1981 (figure 8.4). In January very few points exist at 65 km. The scatter diagram appears isotropic at 67.5 km. At heights between 70 km and 77.5 km there is a tendency for data to be aligned along a north-south axis. The data have a similar alignment at the same heights in December 1981 and January 1982. Below 80 km the maximum velocity commonly seen is between 50 m/s and 60 m/s. As the height increases from 80 km to 92.5 km or 95 km the maximum amplitude also increases. A northwest-southeast orientation of the data is apparent in every scatter diagram in this height range. There is a tendency for the largest velocities to be seen in the northwest quadrant at heights between 87.5 km and 95 km. Above 95 km the anisotropy decreases. The scatter diagrams of the data measured at 100 km and 102.5 km appear isotropic. The amplitude decreases from a maximum at 92.5 km or 95 km as the height increases up to 102.5 km.

The visual anisotropy that is apparent in the scatter diagrams can be confirmed by calculating the value of $\overline{u_1 v_1}$, the covariance of the zonal and meridional velocities of the filtered data. If the scatter diagrams are isotropic, then the calculated value of $\overline{u_1 v_1}$ should be approximately zero. If $\overline{u_1 v_1}$ is positive the scatter diagrams should be asymmetric in favour of the northeast and southwest quadrants. If $\overline{u_1 v_1}$ is negative the scatter diagrams should be asymmetric in favour of the northwest and southeast quadrants. Figures 8.5 and 8.6 are diagrams of $\overline{u_1 v_1}$ in the first 6 months of 1981 and the last 6 months of 1981 respectively. Two points are immediately obvious. Firstly, the magnitude of $\overline{u_1 v_1}$ is small at heights of less than 80 km in all months. This is only partially due to the smaller amplitudes in this region.

The last statement will be elaborated on later in this chapter. Secondly, $\overline{u_1v_1}$ rapidly becomes more negative between the heights of 85 km and 95 km in every month studied. This is in agreement with the observed scatter of the scatter diagrams (figures 8.1 to 8.4). Several other features of the $\overline{u_1v_1}$ diagrams (figures 8.5 and 8.6) are notable. Throughout the year the sign of $\overline{u_1v_1}$ is negative at almost every height. The few exceptions occur at low heights where the magntidue of $\overline{u_1v_1}$ is small. Any alignment along axes does not affect the value of $\overline{u_1v_1}$ as the product along an axis will always be zero. Hence, there is no increases in the value of $\overline{u_1v_1}$ at those heights where such an alignment is seen in the scatter diagrams: between heights of 75 km and 80 km in January and December.

Up to this point various diagrams have been presented to show that there is apparently a favoured alignment of the data above 80 km. However, no attempt has been made to show that this alignment is statistically significant, and if so whether the alignment is significant in certain months or over a certain range of heights.

The significance of the anisotropy can be tested by converting the value of $\overline{u_1v_1}$ into a correlation function. A good approximation to the correlation function can be made by using values already presented. The value of $\overline{u_1v_1}$ can be divided by the variance. This technique underestimates the correlation by a factor of 2 if alignment occurs along either the positive or negative line oriented at 45 degrees to the zonal and meridional axes. As the alignment that does occur is along such a line, the value of $\overline{u_1v_1}$ divided by the variance can be multiplied by 2 to obtain a good approximation of the correlation at zero lags. The significance was tested by assuming 99.9% confidence intervals, which were then

Figure 8.5

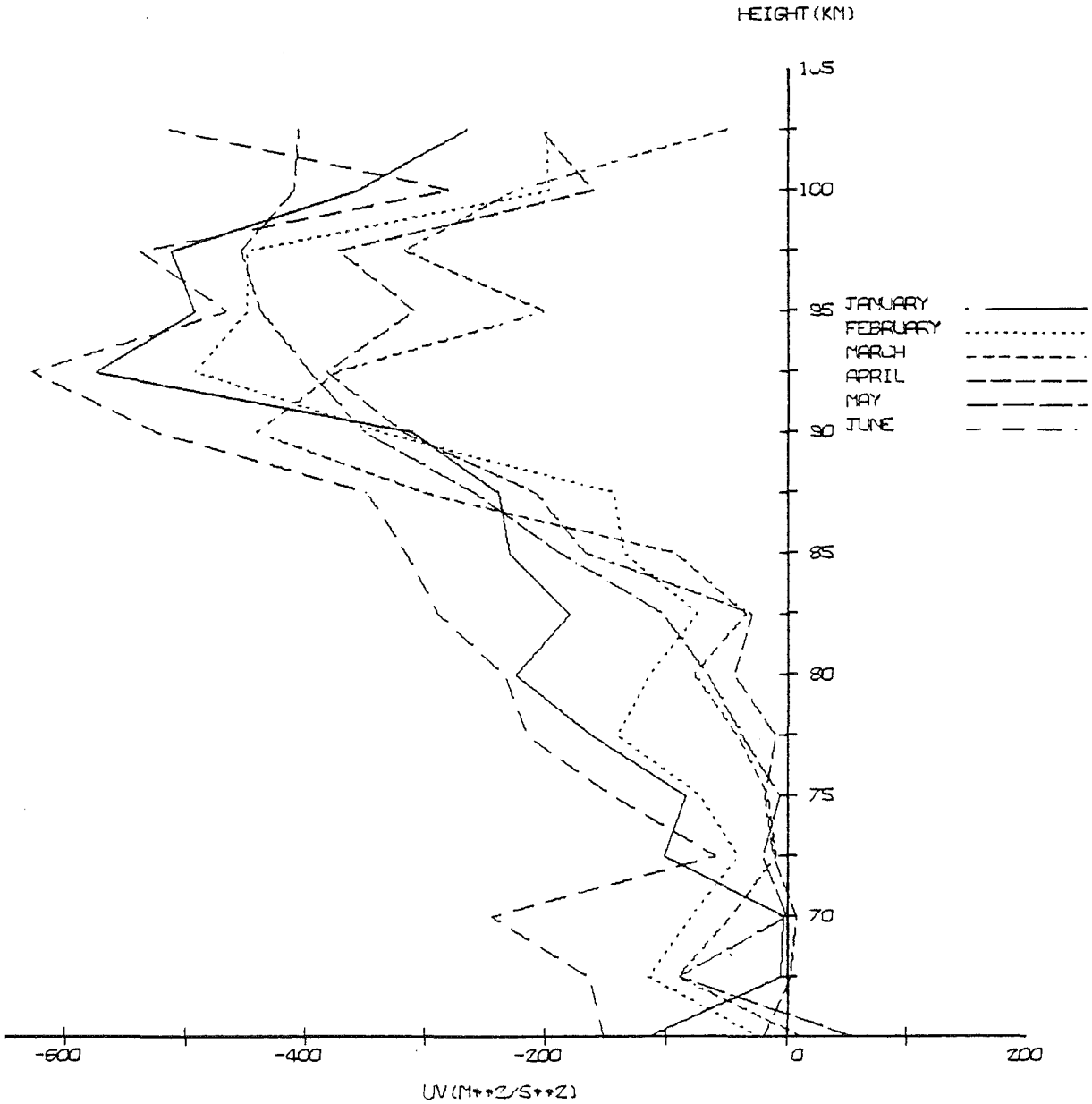

THE PRODUCT OF ZONAL AND MERIDIONAL VELOCITIES FOR VARIATIONS OF LESS THAN 3 HOURS FOR THE FIRST SIX MONTHS IN 1981.

Figure 8.6

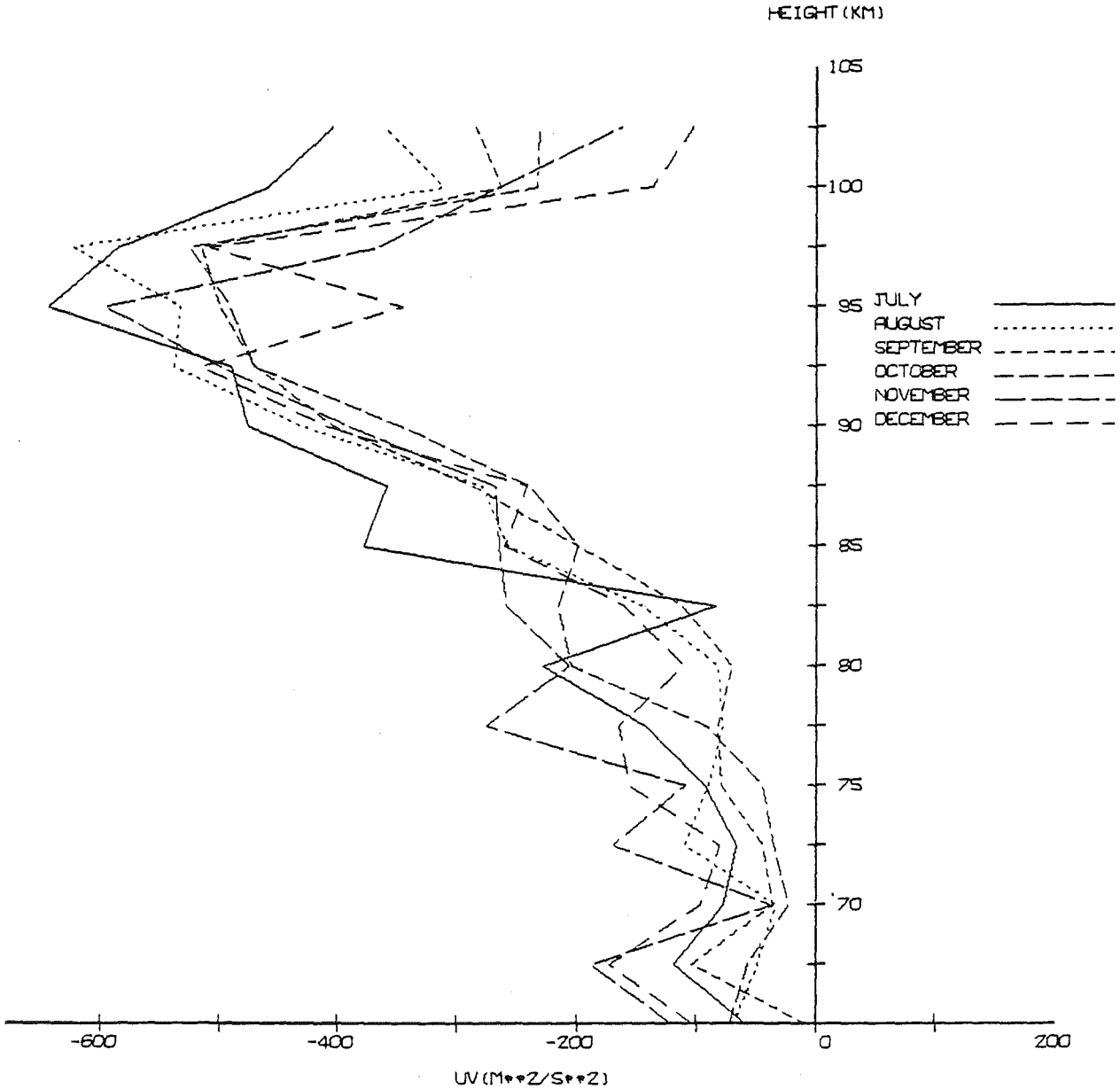

THE PRODUCT OF ZONAL AND MERIDIONAL VELOCITIES FOR VARIATIONS OF LESS THAN 3 HOURS FOR THE SECOND SIX MONTHS IN 1981.

calculated using the techniques used by Jenkins and Watts (1968). If the zero value for the correlation function was outside these confidence limits, the correlation was regarded as significant. The correlations are presented in table 8.1.

In general, these correlations confirm the conclusions drawn about the scatter diagrams, although significant correlations appear at some heights where no anistropy is apparent in the scatter diagrams.

Fewer points were obtained in March than in other months because many days' data were lost when the partial reflection drifts experiment was not working. As a result of this the uncertainties in the correlations obtained in March are larger than the uncertainties of the correlations obtained in other months. Significant correlations occur between the zonal and meridional velocities at all heights between 85 km and 97.5 km in every month other than March. In March, the correlations are significant at 87.5 km, 90 km and 92.5 km, despite the large uncertainties that occur in this month.

In general, correlations are largest at heights near 90 km. Some large correlations do occur at the lowest heights, but these are usually associated with large errors indicating that very few data were used in the correlation calculations.

Significant correlations do occur down to heights of between 70 km and 80 km in summer, winter and spring. These correlations may be associated with apparent alignments along the zonal axis in July, and along the meridional axis in summer. In June, August (see figure 8.7) and spring the alignment seems to be similar to that found in all months at heights between 85 km and 95 km.

The determination of these correlations underestimates

For figure 8.7 see

APPENDIX IV

TABLE 8.1 (a) Correlation coefficient between u_1 and v_1 for periods of less than 3 hours. The uncertainties represent 95% confidence intervals. The data are for the first six months of 1981

Height (km)	January	February	March	April	May	June
65	+0.71 -0.60 -0.30	+0.66 -0.08 -0.60	+0.45 +0.10 -0.50	+0.20 -0.06 -0.19	+0.22 +0.20 -0.25	+0.35 -0.16 -0.31
67.5	+0.24 -0.02 -0.02	+0.21 -0.42 -0.17	+0.23 -0.36 -0.20	+0.15 -0.02 -0.16	+0.18 -0.24 -0.16	+0.22 -0.22 -0.20
70	+0.16 -0.02 -0.16	+0.17 -0.22 -0.16	+0.20 -0.18 -0.19	+0.13 -0.04 -0.13	+0.14 +0.00 -0.14	-0.18 -0.34 -0.16
72.5	+0.14 -0.30 -0.13	+0.18 -0.12 -0.17	+0.22 -0.04 -0.21	+0.14 -0.04 -0.14	+0.12 -0.08 -0.11	+0.19 -0.12 -0.18
75	+0.16 -0.20 -0.15	+0.21 -0.22 -0.19	+0.25 -0.06 -0.25	+0.14 -0.06 -0.14	+0.12 -0.02 -0.12	+0.20 -0.30 -0.17
77.5	+0.13 -0.28 -0.12	+0.14 -0.32 -0.13	+0.20 -0.16 -0.18	+0.11 -0.02 -0.11	+0.09 -0.14 -0.09	+0.15 -0.34 -0.14
80	+0.17 -0.28 -0.15	+0.17 -0.22 -0.16	+0.27 -0.20 -0.24	+0.14 -0.14 -0.13	+0.11 -0.14 -0.10	+0.15 -0.34 -0.13
82.5	+0.14 -0.28 -0.13	+0.13 -0.20 -0.12	+0.22 -0.14 -0.21	+0.14 -0.06 -0.13	+0.10 -0.20 -0.10	+0.11 -0.36 -0.10

Continued next page ..

TABLE 8.1 (a) (Continued....)

Height (km)	January	February	March	April	May	June
85	+0.09 -0.38 -0.09	+0.09 -0.28 -0.08	+0.17 -0.14 -0.17	+0.10 -0.26 -0.09	+0.08 -0.26 -0.07	+0.09 -0.32 -0.08
87.5	+0.08 -0.32 -0.07	-0.08 -0.22 -0.08	+0.16 -0.34 -0.14	+0.09 -0.26 -0.09	+0.07 -0.30 -0.07	+0.08 -0.30 -0.08
90	+0.06 -0.34 -0.06	+0.06 -0.30 -0.06	+0.11 -0.36 -0.10	+0.07 -0.32 -0.06	+0.05 -0.34 -0.05	+0.06 -0.36 -0.06
92.5	+0.07 -0.40 -0.06	+0.06 -0.30 -0.06	+0.13 -0.24 -0.12	+0.07 -0.30 -0.07	+0.06 -0.34 -0.05	+0.06 -0.38 -0.06
95	+0.08 -0.30 -0.08	+0.07 -0.33 -0.07	+0.16 -0.14 -0.16	+0.08 -0.24 -0.08	+0.07 -0.34 -0.07	+0.09 -0.28 -0.08
97.5	+0.09 -0.32 -0.07	+0.07 -0.28 -0.07	+0.16 -0.18 -0.16	+0.09 -0.28 -0.08	+0.07 -0.30 -0.07	+0.09 -0.28 -0.08
100	+0.08 -0.28 -0.08	+0.09 -0.16 -0.08	+0.18 -0.14 -0.17	+0.10 -0.16 -0.10	+0.09 -0.28 -0.08	+0.12 -0.18 -0.11
102.5	+0.08 -0.24 -0.08	+0.09 -0.18 -0.09	+0.20 -0.04 -0.19	+0.11 -0.16 -o.11	+0.09 -0.28 -0.09	+0.11 -0.32 -0.10

TABLE 8.1 (b) Correlation coefficient between u_1 and v_1 for periods of less than 3 hours. The uncertainties represent 95% confidence intervals. The data are for the second six months of 1981

Height (km)	July	August	September	October	November	December
65	+0.31 -0.12 -0.29	+0.23 -0.24 -0.21	+0.24 -0.04 -0.23	+0.21 -0.16 -0.20	+0.40 -0.32 -0.31	+0.53 -0.18 -0.44
67.5	+0.21 -0.24 -0.19	+0.19 -0.14 -0.18	+0.15 -0.32 -0.14	+0.13 -0.22 -0.12	+0.21 -0.42 -0.18	+0.22 -0.42 -0.18
70	+0.16 -0.20 -0.15	+0.15 -0.14 -0.15	+0.13 -0.16 -0.13	+0.11 -0.10 -0.11	+0.19 -0.14 -0.18	+0.16 -0.28 -0.15
72.5	+0.15 -0.16 -0.14	+0.12 -0.38 -0.11	+0.13 -0.22 -0.12	+0.11 -0.18 -0.11	+0.17 -0.42 -0.14	+0.16 -0.22 -0.15
75	+0.14 -0.24 -0.13	+0.13 -0.34 -0.12	+0.13 -0.28 -0.12	+0.12 -0.20 -0.11	+0.19 -0.34 -0.16	+0.16 -0.32 -0.14
77.5	+0.10 -0.32 -0.09	+0.09 -0.24 -0.09	+0.10 -0.26 -0.10	+0.09 -0.28 -0.08	+0.10 -0.56 -0.08	+0.13 -0.30 -0.12
80	+0.11 -0.34 -0.10	+0.11 -0.18 -0.10	+0.13 -0.20 -0.12	+0.09 -0.42 -0.08	+0.14 -0.20 -0.13	+0.17 -0.24 -0.16
82.5	+0.11 -0.14 -0.11	+0.10 -0.30 -0.10	+0.11 -0.26 -0.10	+0.10 -0.42 -0.09	+0.13 -0.38 -0.11	+0.18 -0.16 -0.17

Continued next page ..

TABLE 8.1 (b) (Continued....)

Height (km)	July	August	September	October	November	December
85	+0.07 -0.34 -0.07	+0.08 -0.34 -0.07	+0.08 -0.28 -0.08	+0.08 -0.28 -0.08	+0.10 -0.34 -0.09	+0.11 -0.34 -0.10
87.5	+0.07 -0.30 -0.06	+0.07 -0.30 -0.07	+0.07 -0.34 -0.07	+0.08 -0.36 -0.07	+0.09 -0.34 -0.09	+0.09 -0.32 -0.08
90	+0.05 -0.34 -0.05	+0.05 -0.34 -0.05	+0.06 -0.36 -0.05	+0.06 -0.36 -0.05	+0.07 -0.38 -0.07	+0.07 -0.38 -0.06
92.5	+0.06 -0.30 -0.06	+0.06 -0.36 -0.06	+0.06 -0.36 -0.06	+0.06 -0.38 -0.06	+0.08 -0.40 -0.07	+0.07 -0.36 -0.07
95	+0.07 -0.32 -0.07	+0.07 -0.32 -0.07	+0.07 -0.34 -0.07	+0.07 -0.34 -0.07	+0.09 -0.40 -0.08	+0.08 -0.24 -0.08
97.5	+0.07 -0.30 -0.07	+0.07 -0.34 -0.07	+0.08 -0.30 -0.07	+0.07 -0.36 -0.06	+0.09 -0.24 -0.09	+0.07 -0.32 -0.07
100	+0.10 -0.26 -0.09	+0.10 -0.24 -0.09	+0.09 -0.24 -0.09	+0.08 -0.20 -0.08	+0.09 -0.24 -0.09	+0.08 -0.12 -0.08
102.5	+0.10 -0.24 -0.10	+0.10 -0.22 -0.09	+0.09 -0.24 -0.09	+0.09 -0.20 -0.08	+0.09 -0.18 -0.09	+0.09 -0.12 -0.09

the effect of anisotropy along the zonal and meridional axes, as the value of $\overline{u_1 v_1}$ is ~~to~~ zero for both of these alignments. SEE ERRATA Therefore, these correlations are best used in demonstrating the reliability of the anisotropies apparently visible in scatter diagrams of data from above 85 km.

In studying the scatter diagrams (figures 8.1 to 8.4 and 8.7) it seemed possible that the major axis of the anisotropy was not symmetrical about the origin. This point can be studied further by dividing the possible angles between the zonal and meridional velocities into 8 sectors and calculating the variance for each sector. The number of points in each sector can be calculated, and the total average power in each sector can be determined by multiplying the variance in each sector by the percentage of the total number of points in that particular sector. This last calculation indicates the relative power in each direction. This calculation was made to see if there were any major differences between the direction where the variance was a maximum and where the total power was a maximum. In practice there was no difference. As the error calculations for the variance follow established methods, it was decided to use variance differences to indicate preferred directions. The analysis is concerned with the values of power along the northwest to southeast axis, as the lack of reflective symmetry about a northeast to southwest axis was noticed at heights at which the alignment along the northwest-southeast axis is most visible. The percentage of points in these two octants (112.5 to 157.5 degrees and 292.5 to 337.5 degrees) is about the same, with each having from 15 to 20% of the total number of points between the heights of 85 km and 97.5 km. Favoured directions also occur when the adjacent sectors are included in the calculations.

Variance plots have been made for the northwest and southeast octants for the second half of 1980, for 1981 and for 1982. Attention is focused on 1981 data. However, mention is made of data from the other 2 years when it contradicts, or when it reinforces, the 1981 data.

The data are divided into 3 groups. Error bars are included where the difference between the variance in the northwest octant may be significantly different from the variance in the southeast quadrant. The error bars represent the 95% confidence intervals for the variance.

The variance plots for January, February, November and December 1981 are given in figure 8.8. There is a significant difference between the variance in the northwest direction and the variance in the southeast direction at all heights above 87.5 km in January. The northwestward variance is larger than the southeastward component above 85 km in the other 3 months, but the difference is significant only above 95 km in December, at 90 km in February and at 92.5 km in November. Below 85 km the southeastward variance appears larger than the northwestward variance at most heights in all 4 months. However, the difference between the northwestward and the southeastward variance exceeds the error bars given by the 95% confidence intervals only at 77.5 km in December. The difference between the southeastward and the northwestward velocity appears to be large at 80 km in January. However, the data consisted of relatively few points, and thus the error in these two values of the variance is large so that no definite conclusions can be drawn about this particular point.

The variance plots in May, June, July and August 1981 (figure 8.9) also show significant differences between the northwestward and the southeastward variances. In May the northwestward variance appears larger than the southeastward

Figure 8.8

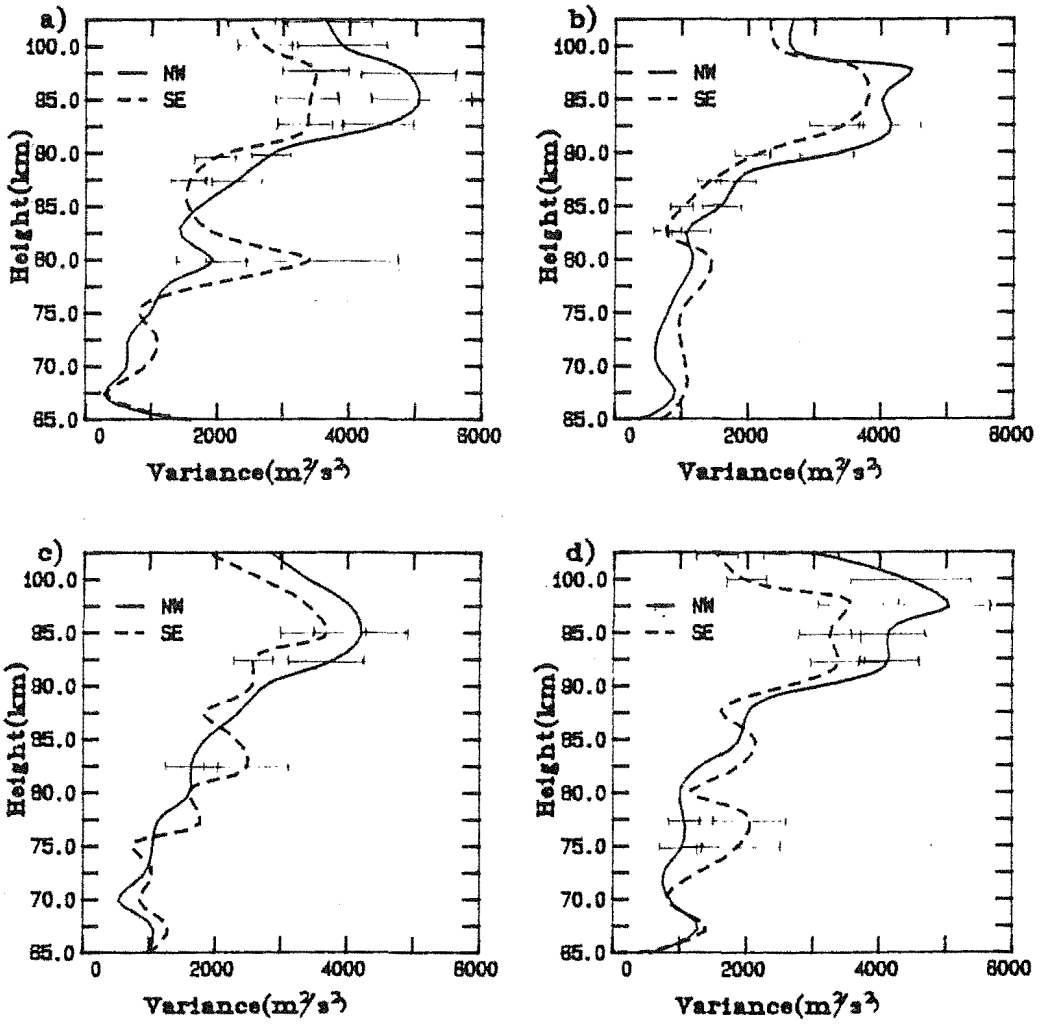

Comparisons of variance between the northwest and southeast octants in 1981. The data are for :a)January; b)February; c)November; d)December.

Figure 3.9

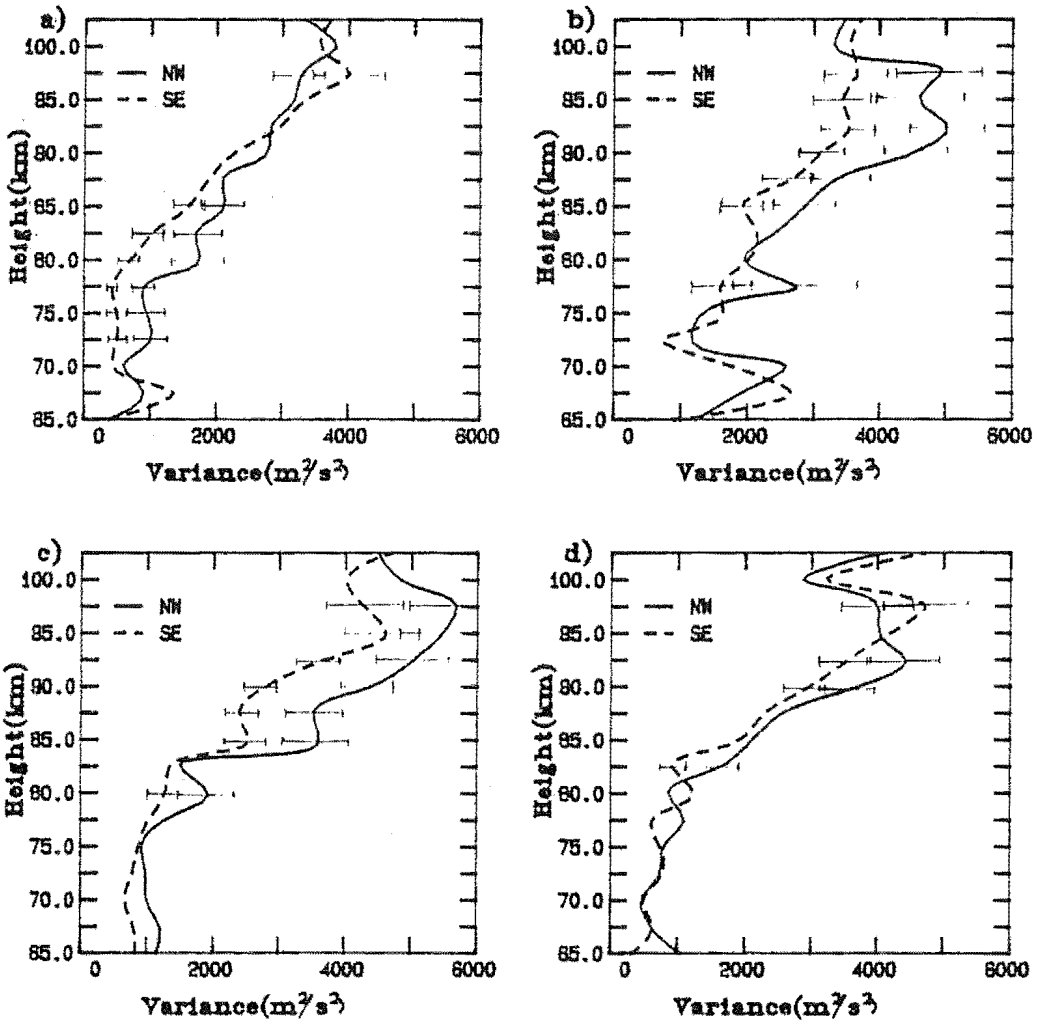

Comparisons of variance between the northwest and southeast octants in 1981. The data are for :a)May; b)June; c)July; d)August.

variance at all heights between 70 km and 92.5 km. The difference between the two variances exceeds the 95% confidence intervals at 72.5 km and between 77.5 km and 82.5 km. These differences may not be so important below 80 km,where little anisotropy is apparent and thus all directions need to be considered, as they are above this height, where the points in the scatter diagrams tend to be aligned along a northwest-southeast line. However a "total power" (that obtained by multiplying the variance in an octant by the percentage of points in that octant) in the northwest octant and the two surrounding octants is from 4/3 to 5/3 times the total power in the southeast octant and the two surrounding octants over the whole height range in which the difference between the variance in the northwest octant and the southeast octant is significant.

The variance plots for June also have a large range of heights for which the northwestward variance is larger than the souteastward variance. This excess occurs for all heights between 82.5 km and 97.5 km. The difference exceeds the 95% confidence intervals at 85 km and at all heights between 90 km and 97.5 km. The height range of this difference roughly coincides with the region for which the anisotropy is closest on the scatter diagrams in June.

The situation is similar in July. The difference exceeds the 95% confidence intervals at all heights between 85 km and 92.5 km and at 97.5 km. The range of heights over which this effect occurs is similar to the range of heights over which it occurs in June. There are no significant differences between the northwestward and the southeastward variances at other heights in June or July 1981.

The magnitudes of the northwestward and the southeastward variances are almost the same over at heights

between 67.5 km and 75 km in August. Although the northwestward variance appears to be larger than the southeastward variance over a range of heights from 82.5 km to 92.5 km, at no height does this difference exceed the corresponding confidence interval.

The spring and autumn variance comparisons are given in figure 8.10. The limited number of data that were obtained in March have been discussed previously. This paucity of data is indicated by the large confidence intervals that are found at all heights in March. No notable trends are apparent in this month. The northwestward and southeastward variances differ by an amount that is less than the 95% confidence intervals at all heights. Although more data are present in October than in March, there are also no significant differences between the two variances in October. However, the situation is different in both April and September. In April the northwestward variances appear larger than the southeastward variances over a range of heights from 70 km to 90 km. The difference between the two variances exceeds the 95% confidence intervals at 75 km, 77.5 km and 85 km. There are no significant differences between the two variances at other heights in April 1981. The September variance comparisons show similar behaviour. The northwestward variance seems to be larger than the southeastward variance at all heights between 67.5 km and 82.5 km. The difference is significant at heights of 72.5 km and 77.5 km.

The features seen in these 1981 profiles need to be considered in relation to the profiles of other years. Figures 8.11 and 8.12 show the variances in 1980. Errors are not included in these diagrams so that the discussion is qualitative and general rather than quantitative and more precise.

Figure 8.10

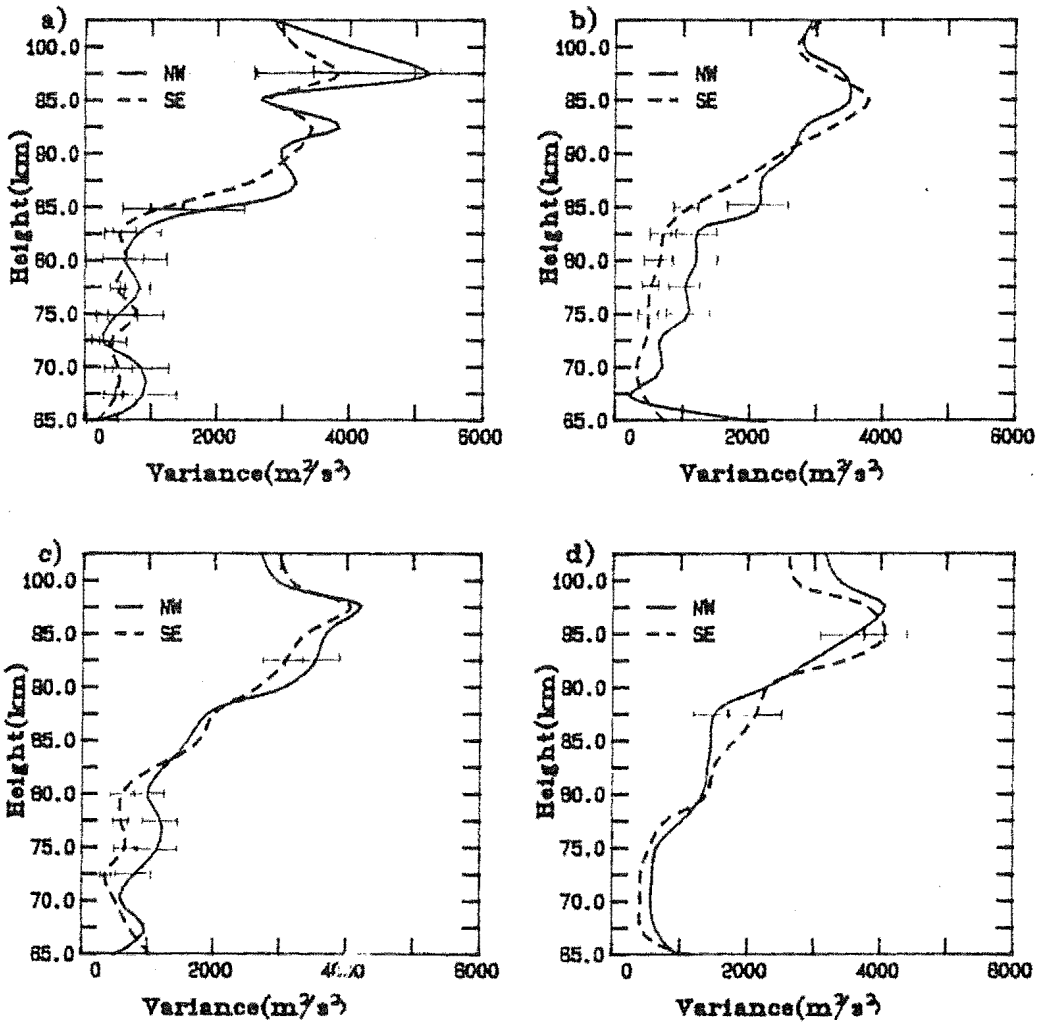

Comparisons of variance between the northwest and southeast octants in 1981. The data are for :a)March; b)April; c)September; d)October.

Figure 8.11

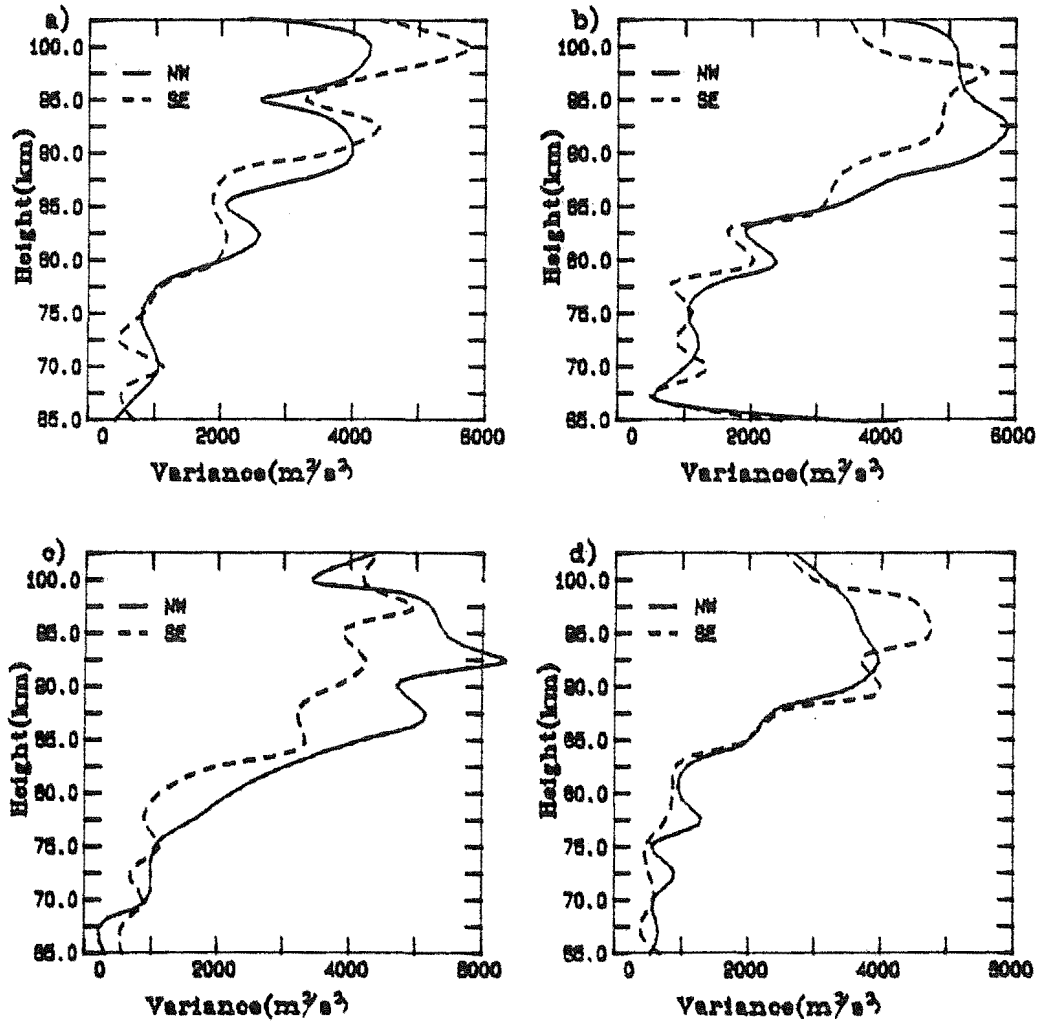

Comparisons of variance between the northwest and southeast octants in 1980. The data are for :a)June; b)July; c)August; d)September.

Figure 8.12

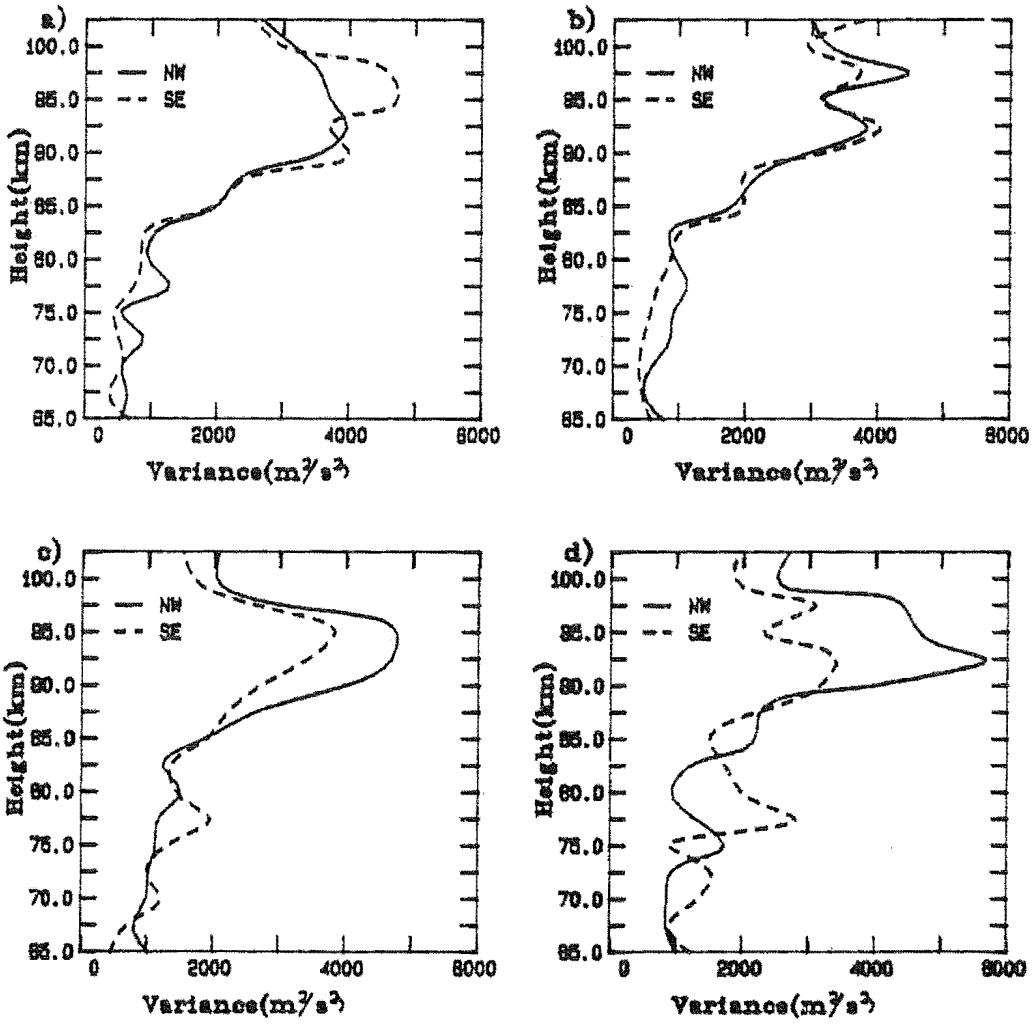

Comparisons of variance between the northwest and southeast octants in 1980. The data are for :a)September; b)October; c)November; d)December.

There is no evidence of any excess of northwestward variance over southeastward variance in June 1980. Except at 100 km, where the southeastward variance is much larger than the northwestward variance, there is little difference between the northwestward and the southeastware variance in June. In July 1980 the northwestward variance is larger than the southeastward variance at all heights from 85 km to 102.5 km at all heights except at 97.5 km. At 90 km and 92.5 km the difference is large. In August 1980 the northwestward variance is larger than the southeastward variance at all heights between 75 km and 97.5 km. The magnitude of the northwestward variance is much the same as the magnitude of the souteastward variance at all heights except 95 km and 97.5 km in September 1980. The southeastward variance is larger than the northwestward variance at 95 km and 97.5 km in September. The magnitude of the two variances is about the same at all heights in October 1980. In November 1980 the northwestward variance appears to be larger than the southeastward variance at all heights from 85 km to 102.5 km. Similaroy, the northwestward variance seems to be larger than the southeastward variance at all heights between 90 km and 102.5 km in December 1980. There is also an excess of southeastward variance over northwestward variance at 77.5 km and 80 km in December.

The behaviour of the variance comparisons in 1982 is similar to the behaviour in 1981. However, the behaviour of the northwestward excess of variance at heights above 80 km in winter is more akin to the behaviour in 1980 than the behaviour in 1981. That is, no excess is apparent in June but excesses do occur in July and August. In other seasons the behaviour of the variance profiels in 1982 is similar to the behaviour in 1981.

8.3 Possible experimental explanations for anisotropic behaviour

The discovery of a preferred direction that was discussed in the last section was unexpected. Consequently, an explanation of this behaviour is needed. Possible explanations include a failure of the drifts experiment, a failure of the analysis of the data or a physical constraint on the data that has been exerted by some dynamical process that has not been completely investigated previously.

There is no point in investigating a possible physical mechanism for this anisotropic behaviour before investigating whether the drifts experiment or the analysis of the experiment has affected the data to cause an anistropy.

The receiving aerials used at Birdlings Flat are set up as a right-angled isoceles triangles with two of the sides oriented along north-south and east-west axes respectively. This orientation could obviously be related to a phenomenon than exhibits an orientation along an axis at 45 degrees to a north-south axis. The simplest method of checking whether the observed anisotropic behaviour is caused by the geometry of the aerials is to use a different geometry. Luckily, such a check was available, but in a different location. A partial reflection drifts experiment has been set up at Arrival Heights. This station has been set up with the aerials arranged in an almost equilateral triangle. Consequently, no obvious alignment is likely with this geometry. However, because of the large difference in the latitudes of the two sites isotropy at Arrival Heights need not imply that the anisotropy at Birdlings Flat is caused by the geometry of the partial reflection drifts experiment.

In practice, anisotropic behaviour was seen at Arrival Heights in both November and December 1983 (the November data

are given in figure 8.13. An approximately northwest-southeast orientation was seen in all the November data from 79 km to 93 km. However, the actual angle that the "principal axis" made with the east-west and north-south axes varied somewhat over this range of heights. The most usual axis along which the data were oriented was a northnorthwest-ward-southsoutheastward axis. No orientation was apparent at 95 km. An orientation of the data towards the northwest and southeast quadrants was also apparent in December at heights of between 79 km and 83 km. The data at 85 km appear to be isotropic, but an orientation towards the northwest and southeast quadrants occurs between 87 km and 91 km. The angle of the orientation alters a little over this interval. No orientation is apparent at 93 km. Above this height an orientation may occur, but the large spread of data makes such an orientation somewhat indefinite.

Therefore, it has been confirmed that the distribution of the zonal and meridional velocity vectors of internal gravity waves behave in an anisotropic manner at Arrival Heights. The conjecture that the anisotropic behaviour of the velocity vectors of internal gravity waves at Birdlings Flat is caused by the geometry of the drifts experiment can thus almost certainly be rejected.

The possibility that the preferred direction of the data is caused by the analysis procedure is more difficult to disprove. The set of procedures used to filter the drifts to extract motions that have periods of less than 3 hours can be tested by plotting the raw wind data (figure 8.14). This scatter diagram is affected by prevailing winds and motions with periods longer than 3 hours. The prevailing wind alters the position of the "centre" of the scatter diagram. The direction and magnitude of this displacement

For figure 8.13 see

APPENDIX IV

Figure 8.14

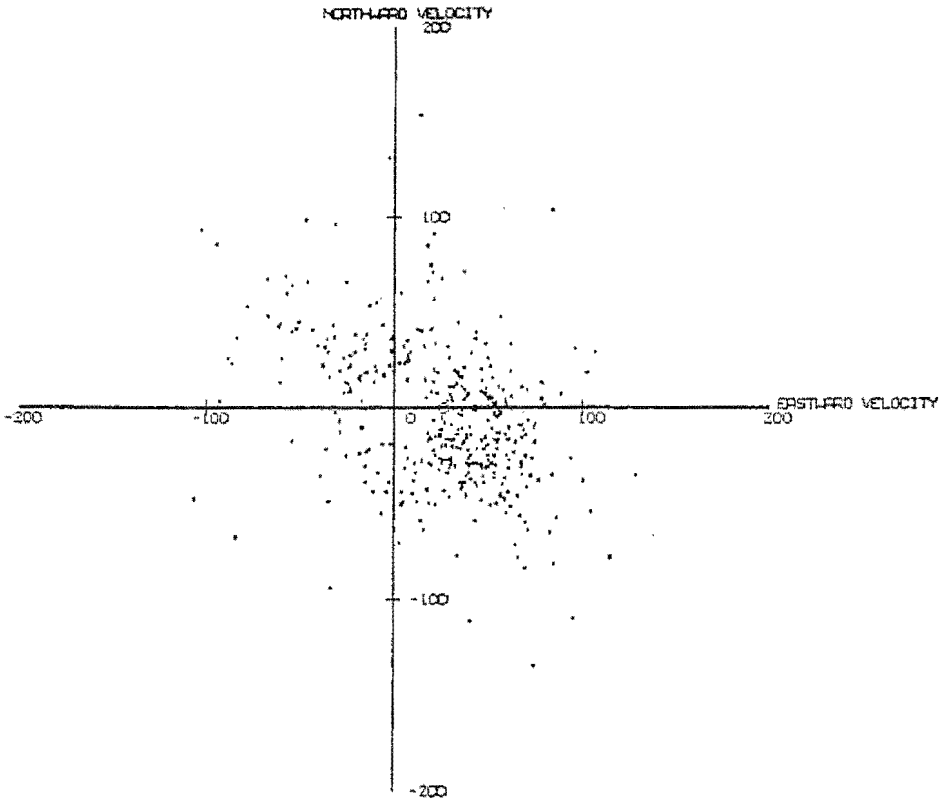

INDIVIDUAL DRIFT READINGS AT BIRDLINGS FLAT
FOR PERIODS OF LESS THAN 3 HOURS IN
JULY 1981 AT AN ALTITUDE OF 80.0KM FOR NO FILTER.

varies greatly with height and month. Long period waves will tend to make the scatter diagrams appear to be more circular.

Despite this variety of effects, the data still show a tendency to be along a northwest-southeast line. This tendency is apparent at all heights at which the tendency existed in the filtered data. The amplitudes apparent in these plots are not much larger than the amplitudes that occur in the data that has been filtered to remove 3 hour means. These results show the importance of internal gravity wave contributions to the total variance. These results also demonstrate that the observed anisotropy in the filtered data is not likely to have been caused by the algorithms used to do the filtering.

The other possible experiment or analysis related cause involves the process of analysing the correlations to obtain the drifts. The behaviour of the anisotropy with height is the strongest argument against this explanation. The anisotropy is not apparent at all heights. The lowest height at which the anisotropy becomes apparent varies over the year. For example, the anisotropy is not visible below 82.5 km in April, yet a preferred direction appears between 70 km and 80 km in July. This behaviour suggests a physical explanation of the phenomenon rather than a fault in the analysis. The procedures used are the same in any month so, if the anisotropy is caused by the analysis, the behaviour would be expected to be the same in each month. The suggestion that the anisotropic behaviour is caused by either the experiment itself or the analysis of the experimental data can almost certainly be rejected.

8.4 Possible dynamical explanations of the anisotropic behaviour

1. *Magnetic effects*

One possible cause of the anisotropy is a preferred orientation due to the effect of the earth's magnetic field. The reasons for rejecting this hypothesis are primarily based on the nature of the anisotropy.

The first point that needs to be made in this argument is that charged particles act as tracers for the neutral atmosphere in the D-region (Gossard and Hooke (1975)). Neutral particle densities are larger at D-region heights than they are in other higher inospheric regions. Magnetic and electric effects are thus not strong enough to cause charged particles to move separately from neutral particles.

When magnetic effects are included in the dispersion equation for internal gravity waves (Appendix I) the following equation arises (Hines (1974)):

$$\left\{\omega^4 - \omega^2c^2(k_h^2 + k_z^2) + (\gamma-1)g^2k_h^2 + ig\gamma\omega^2k_z\right\}$$

$$- \left[\sigma_1B_o^2/(\omega\rho_o)\right]\left\{2i\omega^4 - \gamma g\omega^2(k_z-k_\zeta \sin I) - i\omega^2c^2(k_h^2+k_z^2+k_\zeta^2)\right.$$

$$\left. + i(\gamma-1)g^2(k_x^2\sin^2 I+k_y^2)\right\} + \left[\sigma_2B_o^2/(\omega\rho_o)\right]\left\{(2-\gamma)g\omega^2k_x\cos I\right\} \tag{8.1}$$

The z axis is vertically upwards; the x axis points to magnetic east; the ζ axis points in the direction of B_o; I is the magnetic dip angle; $k_\zeta = k_y\cos I - k \sin I$; g is the acceleration due to gravity; $\gamma = c_p/c_v$; c is the speed of sound; B_o is the magnetic field; ρ_o is the unperturbed density of the neutral gas; σ_1 is the Pedersen conductivity; σ_2 is the Hall conductivity.

The relationship between dipole co-ordinates and

geographic co-ordinates is given in Appendix II.

The quantities in the { } brackets are all of roughly the same order of magnitude. Therefore, the relative importance of the magnetic terms in the dispersion equation (equation 8.1) is dependent upon the size of the $[\sigma_1 B_o/(\omega\rho_o)]$ and $[\sigma_2 B_o/(\omega\rho_o)]$ terms. The period of the motions can be assumed to be 3 hours. The magnetic field strength is of the order of 10^{-5}Wbm^{-2}. Densities vary from $2\text{x}10^{-4}$kgm^{-3} at 80 km to $4\text{x}10^{-6}$kgm^{-3} at 100 km. The maximum value of the Pedersen and Hall conductivities in the 65 km to 100 km height range occurs at 100 km. These conductivities can be calculated by using the equations given by Matsushita and Campbell (1967). The maximum value of the Hall conductivity is approximately 10^{-2}m^{-3}kg^{-1}s^{-1}C at 100 km. The magnitude of the Pedersen conductivity is about half this value at the same height. Both the Pedersen and the Hall conductivities decrease rapidly with decreasing height below 100 km. The two terms in square brackets can be estimated from these values. The magnitude of the exp expression in the second set of square brakets is about $4\text{x}10^{-4}$ at 100 km, while the magnitude of the expression in the first set of square brackets is about $2\text{x}10^{-4}$. These figures suggest that the magnetic terms are not of sufficiently large magnitude in the D-region to cause the observed anisotropies.

Another problem with assuming that magnetic effects cause the observed anisotropy lies in the height distribution and the preferred direction of this anisotropy. As the density decreases with increasing height and both the Pedersen and Hall conductivities increase with increasing height up to 100 km, the degree of anisotropy should continue to increase with increasing height if magnetic effects cause

the anisotropic behaviour. In practice the correlations decrease in every month with increasing height from 90 km to 92.5 to 92.5 km to 102.5 km.

Lastly, different orientations are sometimes seen at heights of between 70 km and 75 km. If we assume that the wave distribution would be isotropic if the earth's magnetic field is not present, there is no apparent reason why the earth's magnetic field should cause different orientations at slightly different heights.

Magnetic effects are unlikely to be important in a region where neutral particle motions dominate the movement of charged particles. From this argument, and for the reasons discussed above, it is unlikely that magnetic effects play an important part in alignment internal gravity waves in a particular direction.

8.5 Possible dynamical explanations of the anisotropic behaviour

2. *Source related considerations*

The problem of determining a possible source, or sources, for the internal gravity waves seen in the mesosphere is an important one, as the source of the waves and the medium through which they propogate will determine the characteristics of the waves. A variety of tropospheric sources have been proposed. Hines (1974) has detailed a number of these sources: winds blowing over hills and mountains (steady winds produce stationary waves, variable winds produce travelling waves); thermal convective instabilities; thunderstorms; moving squall lines; moving fronts (especially cold fronts); instabilities in general atmospheric circulation under distortion by planetary waves; tropical cyclones; general shear instabilities (e.g. jet

streams); instabilities caused by photochemical variations and water vapour changes of state; non-linear interaction of other gravity waves (including atmospheric tides); explosions; earthquakes; tsunamis; deposition of momentum and/or heat by extraterrestrial auroral and high energy particles; heating and Lorentz forces associated with auroral current systems; eclipses of the sun. In fact, any process that introduces changes in the atmosphere or instabilities on a time scale of minutes to hours may produce internal gravity waves. The actual sources of particular waves that have been observed in the middle and upper atmosphere have seldom been identified.

Many of these possible sources that have been discussed by Hines (1974) are of little relevance to the problem considered here. Any phenomenon that occurs only at irregular intervals cannot produce regular dynamical effects that occur throughout the year. By this reasoning eclipses, earthquakes, tsunamis, explosions and to a lesser extent tropical cyclones can be excluded from the list of probable major sources of the internal gravity waves observed over Birdlings Flat. The most likely major sources of internal gravity waves over Birdlings Flat would be shear due to the tropospheric jet and cold fronts, both of which will produce waves in all seasons. Orography is not important as waves from this source reach the ionosphere at distances of 500 km to 2000 km from the source. A typical calculation of this distance can be found in Hines (1974).

A variety of theoretical studies have been made on the way that shears can produce internal gravity waves. Lindzen and Rosenthal (1976) have developed a theory of wave production by wind shear that has already been mentioned. Other studies include those of Fritts (1982), (1979), Davis

and Peltier (1979) and Lalas and Einaudi (1976) and others.

At first sight a model of the anisotropic behaviour that has been developed from an anisotropic source is an attractive means of explaining the observed anisotropic behaviour. The latitude of the tropospheric jet does not change a great deal over the year and may thus consitute one possible source that will favour the observation of waves coming from one direction. Similarly, most cold fronts tend to be found in roughly the same direction.

However, if the anisotropic behaviour in the mesosphere and lower thermosphere results from a source in the troposphere that causes wave production in a particular direction, then the scatter diagrams should be anisotropic, and in fact anisotropic to the same degree, at all the heights studied, not just those within a particular range of heights (roughly 80 km to 95 km).

Another objection to the notion that the anisotropic behaviour is source related occurs for those months where the alignment does not occur along the same axis at all heights. Apart from the Arrival Heights data that was presented in the experimental-related causes section of this chapter, this effect is also noticeable in some summer months when there is a north-south orientation at about 75 km as well as the common northwest-southeast orientation that is seen throughout the year at heights between 80 km and 95 km. It is difficult to see how a tropospheric source could be anisotropic in such a way that it could produce a north-south orientation at 75 km and a northwest-southeast orientation at greater altitudes.

Another possibility is that the waves observed at these heights are produced by a source that is both local to the heights at which the observations are made (e.g. the mesospheric jet). Apart from the observations that have been

made of wave activity in noctilucent clouds that have been associated with cold fronts in the troposphere, other objections to the idea that the source is local are also apparent. Firstly, if the sources of these waves are other waves, then the problem has merely been shifted to one of why the other waves should act as an anisotropic source. This may be a suitable mechanism but it is not obvious why it should occur. One important feature of the atmosphere is the mesospheric jet. The jet may produce internal gravity waves, but, as the direction of zonal jet changes from being eastward in winter to being westward in summer it is unlikely that it would produce waves with the same preferred direction throughout the year.

It is impossible to eliminate anisotropic sources as being the cause of the anisotropic behaviour of internal gravity waves discussed in this chapter, but from the arguments discussed above it does not seem probable that the effect is directly related to a tropospheric source. The possibility of mesospheric sources such as tidal breaking has not been considered fully and may offer a plausible explanation for this effect.

8.6 Possible dynamical explanations of the anisotropic behaviour

3. *Critical layers*

When mean winds are included in the primitive equations, situations arise in which the phase velocity of the internal gravity wave is equal to the component of the mean wind in the direction in which the wave is travelling, that is, singularities occur. When a wave approaches such a region it is said to have reached a critical layer. Booker and Bretherton (1967) give an equation for the vertical

structure of a wave in a mean wind.

$$\frac{\partial^2 w_1}{\partial z^2} + \left\{ \frac{\omega_B^2}{(u_o - c_x)^2} - \frac{\frac{\partial^2 u_o}{\partial z^2}}{(u_o - c_x)} - k_x^2 \right\} w_1 = 0 \qquad (8.2)$$

W_1 is the vertical velocity; c_x is the horizontal phase speed of the wave $\left(= \frac{\omega}{k_x}\right)$; u_o is the component of the prevailing wind in the direction in which the wave is propagating; k_x is the horizontal wavenumber in the x direction.

It is clear from equation 8.2 that a singularity occurs when the phase speed c_x is equal in magnitude and sign to the component of the prevailing wind in the direction of wave propagation. In this case the vertical wavelength tends to zero and wave energy is dissipated.

The reason for considering critical layers as a possible source of anisotropy comes from studying the mean winds. The anisotropy tends to occur only where the magnitude of the prevailing winds is small (tables 8.2 and 8.3 - note that the errors are approximate and possible overestimates as the total variance has been used rather than the variance in each direction).

A major problem with invoking critical layers as an explanation for anisotropic behaviour over a range of heights and over the period of a year is that the prevailing wind is changing in both magnitude and direction, both with height and over time. This problem can be avoided to a certain extent by assuming that we need only be concerned with the height where the magnitude of the prevailing wind becomes equal to the mean phase speed of the internal gravity waves, and to make a rather unjustified assumption that there is little spread of phase speeds away from this mean. If we consider power spectra at internal gravity wave frequencies then the assumption of a mean phase speed is reasonable as wave power

TABLE 8.2(a) ZONAL WINDS IN THE FIRST 6 MONTHS OF 1981. THE UNCERTAINTIES REPRESENT 95% CONFIDENCE INTERVALS

	Velocity (m/s)					
Height (km)	January	February	March	April	May	June
65	-63 ± 10	-40 ± 13	41 ± 6	29 ± 4	64 ± 8	82 ± 9
67.5	-65 ± 4	-42 ± 6	34 ± 5	34 ± 3	66 ± 5	82 ± 5
70	-66 ± 3	-35 ± 4	34 ± 4	35 ± 3	62 ± 4	71 ± 4
72.5	-68 ± 3	-30 ± 5	31 ± 4	37 ± 3	53 ± 3	61 ± 4
75	-72 ± 3	-23 ± 5	29 ± 6	41 ± 4	53 ± 3	45 ± 4
77.5	-70 ± 4	-16 ± 4	29 ± 4	47 ± 3	54 ± 2	36 ± 4
80	-44 ± 6	-3 ± 6	13 ± 10	39 ± 4	36 ± 4	9 ± 5
82.5	-29 ± 5	16 ± 4	20 ± 7	26 ± 4	29 ± 4	13 ± 4
85	1 ± 4	22 ± 3	6 ± 6	21 ± 3	16 ± 3	13 ± 3
87.5	20 ± 3	22 ± 3	9 ± 6	11 ± 4	8 ± 3	15 ± 3
90	20 ± 2	20 ± 2	4 ± 4	9 ± 2	8 ± 2	13 ± 2
92.5	18 ± 3	15 ± 3	-4 ± 5	3 ± 3	8 ± 2	11 ± 3
95	24 ± 4	14 ± 4	-9 ± 7	-1 ± 4	3 ± 3	13 ± 4
97.5	25 ± 3	16 ± 4	-3 ± 7	0 ± 4	-1 ± 3	12 ± 4
100	32 ± 4	15 ± 4	-5 ± 8	-2 ± 4	4 ± 4	12 ± 5
102.5	35 ± 4	19 ± 4	-9 ± 9	1 ± 4	-1 ± 4	12 ± 5

TABLE 8.2(b) ZONAL WINDS IN THE SECOND 6 MONTHS OF 1981. THE UNCERTAINTIES REPRESENT 95% CONFIDENCE INTERVALS

	Velocity (m/s)					
Height (km)	July	August	September	October	November	December
65	91 ± 9	48 ± 7	38 ± 5	13 ± 5	2 ± 7	-31 ± 14
67.5	60 ± 6	28 ± 5	37 ± 4	23 ± 3	-10 ± 5	-54 ± 5
70	45 ± 4	20 ± 4	30 ± 3	26 ± 2	-17 ± 4	-61 ± 4
72.5	32 ± 4	20 ± 3	28 ± 2	27 ± 2	-17 ± 4	-72 ± 3
75	29 ± 4	22 ± 4	30 ± 3	25 ± 2	-19 ± 4	-70 ± 4
77.5	22 ± 3	25 ± 3	29 ± 2	15 ± 2	-19 ± 4	-69 ± 3
80	23 ± 4	26 ± 3	17 ± 3	3 ± 3	-23 ± 5	-53 ± 5
82.5	26 ± 4	22 ± 4	20 ± 3	-4 ± 3	-28 ± 4	-33 ± 5
85	24 ± 3	18 ± 2	11 ± 3	-12 ± 3	-22 ± 4	-11 ± 4
87.5	20 ± 3	13 ± 3	11 ± 2	-7 ± 3	-10 ± 4	6 ± 3
90	22 ± 2	13 ± 3	9 ± 2	-4 ± 2	0 ± 3	13 ± 2
92.5	16 ± 3	8 ± 3	5 ± 2	-4 ± 2	4 ± 4	12 ± 3
95	14 ± 3	4 ± 4	5 ± 3	-6 ± 3	8 ± 4	22 ± 3
97.5	15 ± 3	3 ± 4	6 ± 3	0 ± 3	15 ± 4	29 ± 3
100	15 ± 5	2 ± 5	6 ± 4	7 ± 3	26 ± 3	37 ± 3
102.5	11 ± 5	0 ± 5	3 ± 4	9 ± 4	26 ± 3	38 ± 3

TABLE 8.3(a) MERIDIONAL WINDS IN THE FIRST 6 MONTHS OF 1981. THE UNCERTAINTIES REPRESENT 95% CONFIDENCE INTERVALS

	Velocity (m/s)					
Height (km)	January	February	March	April	May	June
65.0	-2 ± 10	2 ± 13	-21 ± 6	-18 ± 4	-20 ± 8	-36 ± 9
67.5	1 ± 4	0 ± 6	-18 ± 5	-18 ± 3	-20 ± 5	-27 ± 5
70.0	4 ± 3	2 ± 4	-19 ± 4	-15 ± 3	-18 ± 4	-27 ± 4
72.5	8 ± 3	5 ± 5	-17 ± 4	-16 ± 3	-22 ± 3	-20 ± 4
75.0	12 ± 3	5 ± 5	-18 ± 6	-21 ± 4	-23 ± 3	-24 ± 4
77.5	15 ± 4	6 ± 4	-28 ± 4	-20 ± 3	-23 ± 2	-21 ± 4
80.0	13 ± 6	1 ± 6	-11 ± 10	-13 ± 4	-11 ± 4	-8 ± 5
82.5	12 ± 5	-8 ± 4	-13 ± 7	-11 ± 4	-7 ± 4	-8 ± 4
85.0	7 ± 4	-10 ± 3	-8 ± 6	-8 ± 3	-5 ± 3	-11 ± 3
87.5	1 ± 3	-5 ± 3	-12 ± 6	-2 ± 4	-4 ± 3	-9 ± 3
90.0	-1 ± 2	-5 ± 2	1 ± 4	-1 ± 2	-3 ± 2	-9 ± 2
92.5	-4 ± 3	-1 ± 3	3 ± 5	-1 ± 3	-2 ± 2	-8 ± 3
95.0	-8 ± 4	4 ± 4	6 ± 7	1 ± 4	3 ± 3	-9 ± 4
97.5	-8 ± 3	5 ± 4	11 ± 7	5 ± 4	6 ± 3	-9 ± 4
100.0	-14 ± 4	1 ± 4	12 ± 8	10 ± 4	12 ± 4	-4 ± 5
102.5	-15 ± 4	-4 ± 4	18 ± 9	6 ± 4	14 ± 4	-2 ± 5

TABLE 8.3(b) MERIDIONAL WINDS IN THE LAST 6 MONTHS OF 1981. THE UNCERTAINTIES REPRESENT 95% CONFIDENCE INTERVALS

	Velocity (m/s)					
Height (km)	July	August	September	October	November	December
65	-25 ± 9	-9 ± 7	-11 ± 5	-16 ± 5	-18 ± 7	-2 ± 14
67.5	-30 ± 6	-8 ± 5	-12 ± 4	-14 ± 3	-7 ± 5	-7 ± 5
70	-24 ± 4	-11 ± 4	-9 ± 3	-11 ± 2	-5 ± 4	-1 ± 4
72.5	-19 ± 4	-7 ± 3	-11 ± 2	-11 ± 2	-3 ± 4	6 ± 3
75	-17 ± 4	-5 ± 4	-12 ± 3	-8 ± 2	-3 ± 4	6 ± 4
77.5	-11 ± 3	-9 ± 3	-10 ± 2	-10 ± 2	2 ± 4	7 ± 3
80	-4 ± 4	-9 ± 3	-6 ± 3	-4 ± 3	4 ± 5	11 ± 5
82.5	-10 ± 4	-6 ± 4	-6 ± 3	0 ± 3	7 ± 4	15 ± 5
85	-9 ± 3	-4 ± 2	1 ± 3	6 ± 3	5 ± 4	11 ± 4
87.5	-10 ± 3	-4 ± 3	0 ± 2	7 ± 3	8 ± 4	9 ± 3
90	-12 ± 2	-5 ± 3	1 ± 2	3 ± 2	4 ± 3	3 ± 2
92.5	-8 ± 3	-6 ± 3	0 ± 2	7 ± 2	3 ± 4	2 ± 3
95	-6 ± 3	-2 ± 4	0 ± 3	7 ± 3	-4 ± 4	-4 ± 3
97.5	-4 ± 3	-4 ± 4	1 ± 3	4 ± 3	-7 ± 4	-6 ± 3
100	-5 ± 5	0 ± 5	-2 ± 4	-1 ± 3	-12 ± 3	-10 ± 3
102.5	-1 ± 5	2 ± 5	1 ± 4	-1 ± 4	-13 ± 3	-13 ± 3

falls off rapidly with decreasing wave period for periods less than about 2 hours. An estimate of the mean phase speed for waves with periods near 3 hours can be made from the values of horizontal wavelength and period given by Vincent and Reid (1983). The phase speed is then of the order of 10-20 m/s. If the wave sources are such that the waves are observed to be coming from all directions, then the effect of a critical layer might be to reduce the number of large amplitude wind vectors along an axis, but not to eliminate all large amplitude vectors in the region of this axis.

Furthermore, given that the combination of zonal and meridional winds would decide the direction from which waves would be removed, the consistency in the direction of the axis along which the wave vectors tend to occur throughout the year is very difficult to explain.

Critical layers cannot be eliminated as the cause of the observed anisotropy, but the arguments presented above make it very difficult to reconcile the nature of critical layers with the observed characteristics of the anisotropy.

8.7 Possible Dynamical Explanations of the Anistropic Behaviour :

4. *Critical Layers Revisited-Wave Refraction*

Recently, Dunkerton and Butchart (1984) proposed a mechanism which could cause internal gravity wave vectors to be aligned along particular axes. This theory involved the refraction of the wave train by the zonal wind.

For waves with zero phase speed, the intrinsic frequency of the wave is just $k_h.u_o$. These waves reach critical layers when $\frac{k_h}{|k_h|}.u_o = 0$. Thus waves orthogonal to the mean flow are removed from the spectrum.

There are several objections to the idea of this

mechanism being responsible for the observed anisotropies of the internal gravity wave vectors.

Firstly, Dunkerton and Butchart expected this behaviour to occur in the stratosphere due to amplitudes and directions of the zonal wind in this region and thus there is no reason why anisotropies should not be present at, say, 70 km. SEE ERRATA

The second objection is that the prevailing wind varies in both magnitude and direction with both height and month. Thus, the observed anisotropies should vary in direction with both height and month : this does not occur.

The advantage of an explanation using critical layers is that the relationship between the strength of the prevailing wind and the phase speed becomes important. While it does not seem likely that the mechanism suggested by Dunkerton and Butchart (1984) is directly responsible for the observed anisotropies, there is a possibilty that critical layers and other mechanisms which cause dissipation may be important.

8.8 Possible Dynamical Explanations of the Anistropic Behaviour :

5. *Waves Forced by Mountains*

One particular potential source needs to be considered in more detail. This is winds blowing over mountains. When the wind is steady the phase speeds of the resulting waves is zero. The waves have an intrinsic frequency due to the velocity of the wind that forces the waves.

These waves are often seen over the Canterbury Plains. Cherry (1971) recorded some of the parameters of these waves. The wind speeds that force the waves is commonly between 10 and 20 ms^{-1}. The resulting waves have horizontal wavelengths of 10 km or less. Similar wavelengths have been seen over the Rockies (Lilly (1978)). This corresponds to periods of between 8 and 16 minutes, and, for an isothermal atmosphere at 200 K, vertical wavelengths of between 12 km and 24 km. These values will be the same in the mesosphere if it is assumed that the

horizontal wind speed at the point of observation is the same as that at ground level : a reasonable assumption at 85 km in winter.

The Southern Alps are roughly aligned along a line running along a northeast-southwest axis. Winds blowing over these mountains act as a wave source for waves with amplitudes aligned along a northwest-southeast axis.

There are some major objections to such waves being the cause of the observed alignment in the atmosphere above Birdlings Flat.

The first objection is that even in the troposphere these waves can be seen entirely across the plains. Thus it is improbable that these waves could not be observed below 80 km, but could be seen above this height.

The second objection is that internal gravity waves with zero phase speed are removed from the wave spectrum by a critical layer in the lower sttatosphere in summer (Lindzen (1981)). Therefore, no alignment of wave velocity vectors along the preferred northwest-southeast axis should be seen in summer. In fact, the tendency to alignment in summer seems as strong as in any other season.

A third problem with relating the observed alignment of short period motions to waves produced by mountains is found when the frequency of occurrence of conditions that can produce lee waves is considered.

The data in table 8.4 give the number of day in each month of 1981 when winds from the northwest quarter occurred at midday at Christchurch Airport. If the anisotropy that is found near the mesopause is related to lee waves, then the frequency of occurrence of days when northwesters are present should be connected to the strength of the anisotropy.

TABLE 8.4 The frequency of occurrence of northwesterly winds at Christchurch Airport. The data are for noon. The year is 1981

Month	Jan	Feb	Mar	Apr	May	Jun	Jul	Aug	Sep	Oct	Nov	Dec
Number of days of Northwesterlies	3	1	3	3	2	2	2	2	8	5	4	5

Northwesterlies are most common in spring. They are least apparent in winter (ignoring February). Thus any anisotropic effect due to lee waves should be more apparent in spring. This is not seen in the scatter diagrams. Furthermore, the number of days of northwesterlies in a month is low, the frequency varying from a maximum of 27% in September 1981 to a minimum of 4% in February 1981. This, coupled with the large values of short period winds seen on each day, suggests that any lee wave induced directional effect can cause only minor changes to an otherwise isotropic internal gravity wave spectrum.

~~Finally the anisotropies are also seen at Arrival Heights, which requires a similar mechanism for the production of the anisotropies there.~~ SEE ERRATA

8.9 Possible Dynamical Explanations of the Anisotropic Behaviour :

6. *Wave Breaking and Dissipation*

Internal gravity wave breaking is an important dynamical feature of the mesospher and therefore must be considered as a possible cause for the observed anisotropy.

The first association that can be checked is whether the formular giving the critical amplitude for wave-breaking has any parameters that could lead to anisotropies. Equation 6.32 is

$$u_1^2 = \omega_B^2 / (k_{z\,real}^2 + 1/4H^2)$$ SEE ERRATA

Neither the Brunt-Väisalä frequency ω_B nor the scale height H vary with direction. The vertical wavelength might vary with direction due to either directional changes in the source mechanism or in the medium through which the internal gravity waves propagate. In the former cases the arguments previously discussed in the sections about sources and mountain waves are applicable. In the latter case the arguments concerning refraction and critical layers apply.

Both critical layers and breaking cause dissipation, which leads to interactions between the internal gravity waves and the mean flow. That is, momentum carried by the waves is transferred to the mean flow in regions where dissipation occurs. Andrews and McIntyre (1976, 1978) and Boyd (1976) have studied the accelerations of the mean flow caused by the meridional transport of zonal momentum by planetary waves. Andrews and McIntyre (1976) found that mean flow accelerations caused by these waves occurred when dissipation was present. Boyd (1976) found that in the absence of critical surfaces, dissipation, thermal heating and non-harmonic time dependence there is no mean flow wave interaction. This is reflected in the values of $\overline{u_1 v_1}$ found for planetary waves.

In the presence of critical layers the vertical flux of zonal momentum decreases (Fritts (1984)). If the internal gravity wave is totally absorbed by the critical layer, then this flux must become zero (e.g. see Jones and Houghton (1971)). Thus zonal momentum is transferred by internal gravity waves to the mean flow only if dissipation occurs (Jones (1967), Schoeberl (1985), Bretherton (1969)).

The existence of non-zero values of $\overline{u_1 v_1}$ means that the meridional transport of zonal momentum by internal gravity waves exists. If dissipation is related to the existence of a non-zero value of $\overline{u_1 v_1}$ then the anisotropies should occur at lower heights

in winter than in summer as wave breaking occurs at lower heights in winter (Lindzen (1981)). This does occur. However, there is little other evidence to either suggest that the requirements of momentum transport cause the alignment or the mechanism by which such an alignment could occur. Furthermore, there is no apparent mechanism by which such an orientation can occur for small scale waves.

8.10 Momentum considerations

In this chapter the variations of the zonal and meridional wave velocities have been considered, especially with respect to the changes in the product $\overline{u_1 v_1}$. Clearly this discussion has relevance to the momentum that is being carried by the internal gravity waves

If internal gravity waves are isotropic throughout the height region considered (65 km to 102.5 km) then $\overline{u_1 v_1}$ is zero everywhere in this region. If the waves are anisotropic then $\rho\overline{u_1 v_1}$ is not zero and the sign of $\rho\overline{u_1 v_1}$ is dependent on the orientation of the anisotropy. However, if the waves are aligned along either the zonal or meridional axes, the value of $\overline{u_1 v_1}$ is zero, even though the internal gravity waves are transporting momentum horizontally.

A non-isotropic wave source in the troposphere would mean that $\rho\overline{u_1 v_1}$ would be non-zero at all heights. In this case the $\overline{u_1 v_1}$ profiles would be expected to exhibit behaviour similar to that of the variance profiles discussed in chapter 6. Although there are similarities between the $\overline{u_1 v_1}$ profiles (figures 8.5 and 8.6) and the variance profiles (figures 6.3 to 6.26), the ratio of the maximum value of $\overline{u_1 v_1}$ to the minimum value of $\overline{u_1 v_1}$ is far greater than the ratio of the maximum variance to the minimum variance.

Figure 8.15

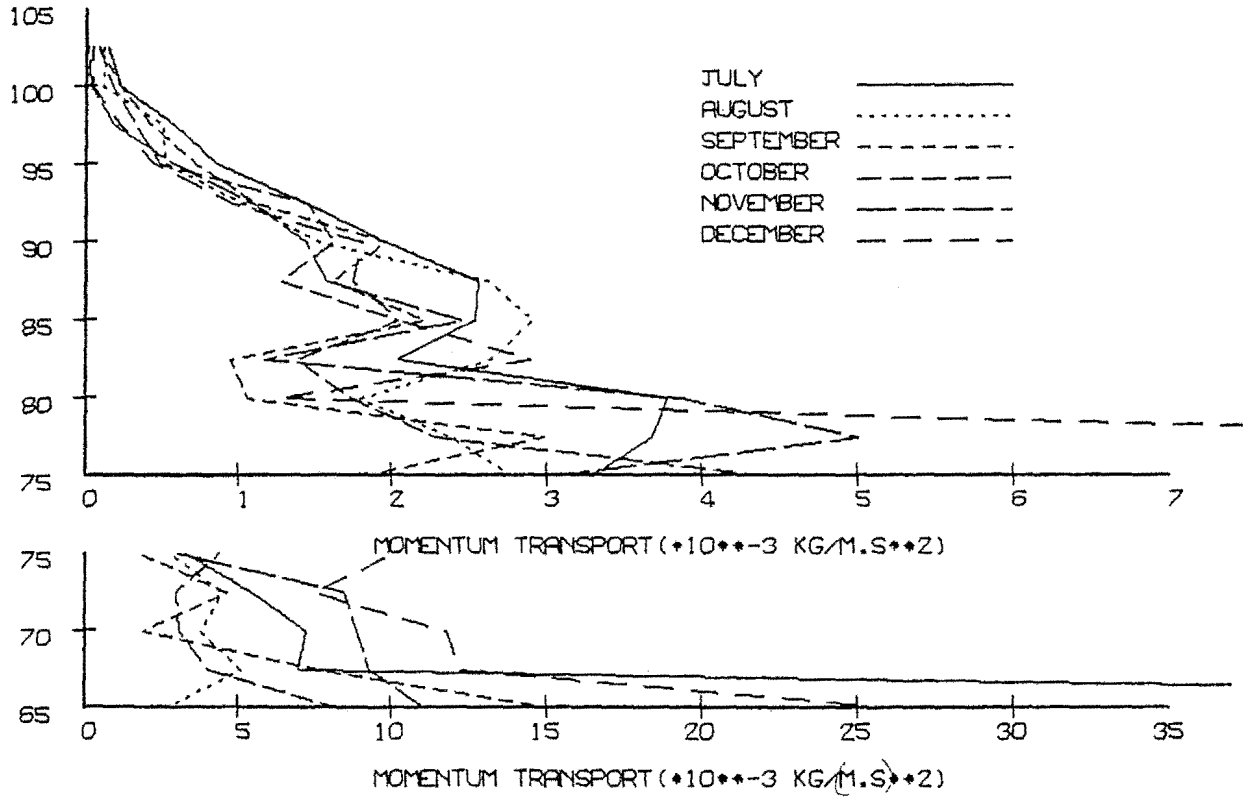

VARIATIONS IN THE HORIZONTAL TRANSPORT OF HORIZONTAL MOMENTUM IN 1980.

Figure 8.16

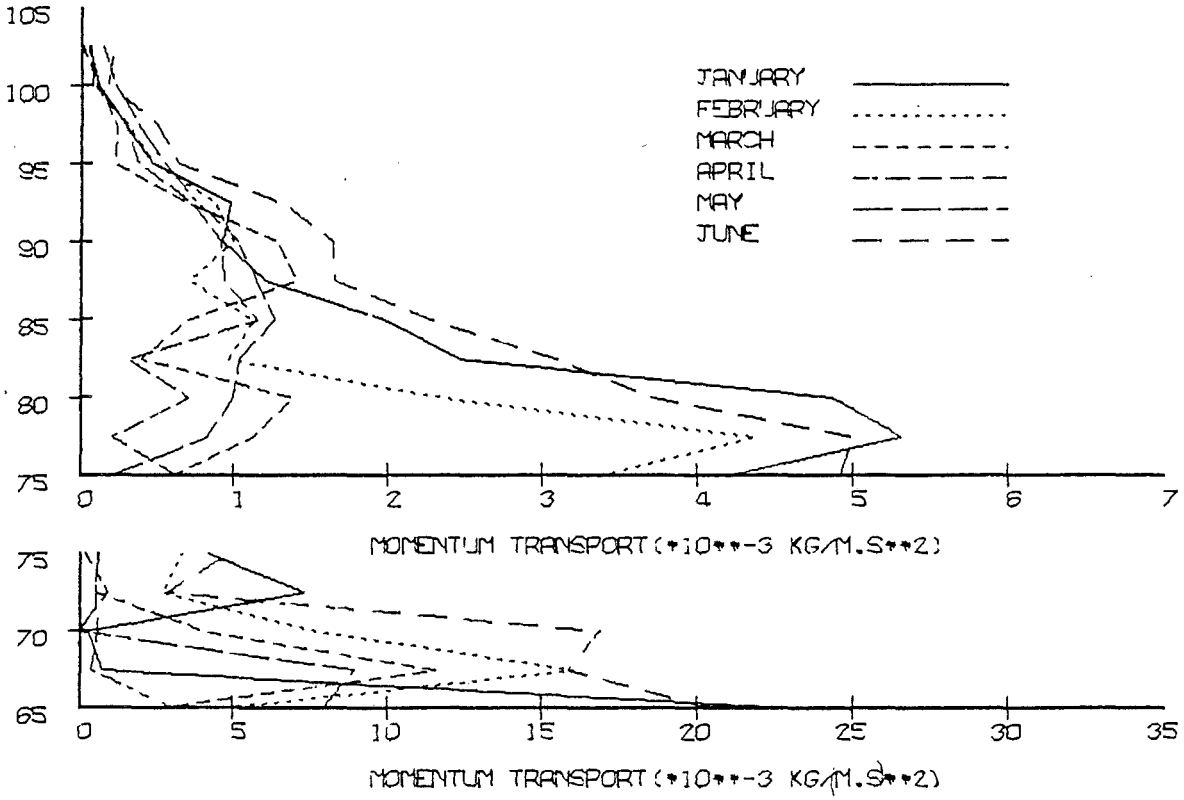

VARIATIONS IN THE HORIZONTAL TRANSPORT OF HORIZONTAL MOMENTUM IN 1981.

Figure 8.17

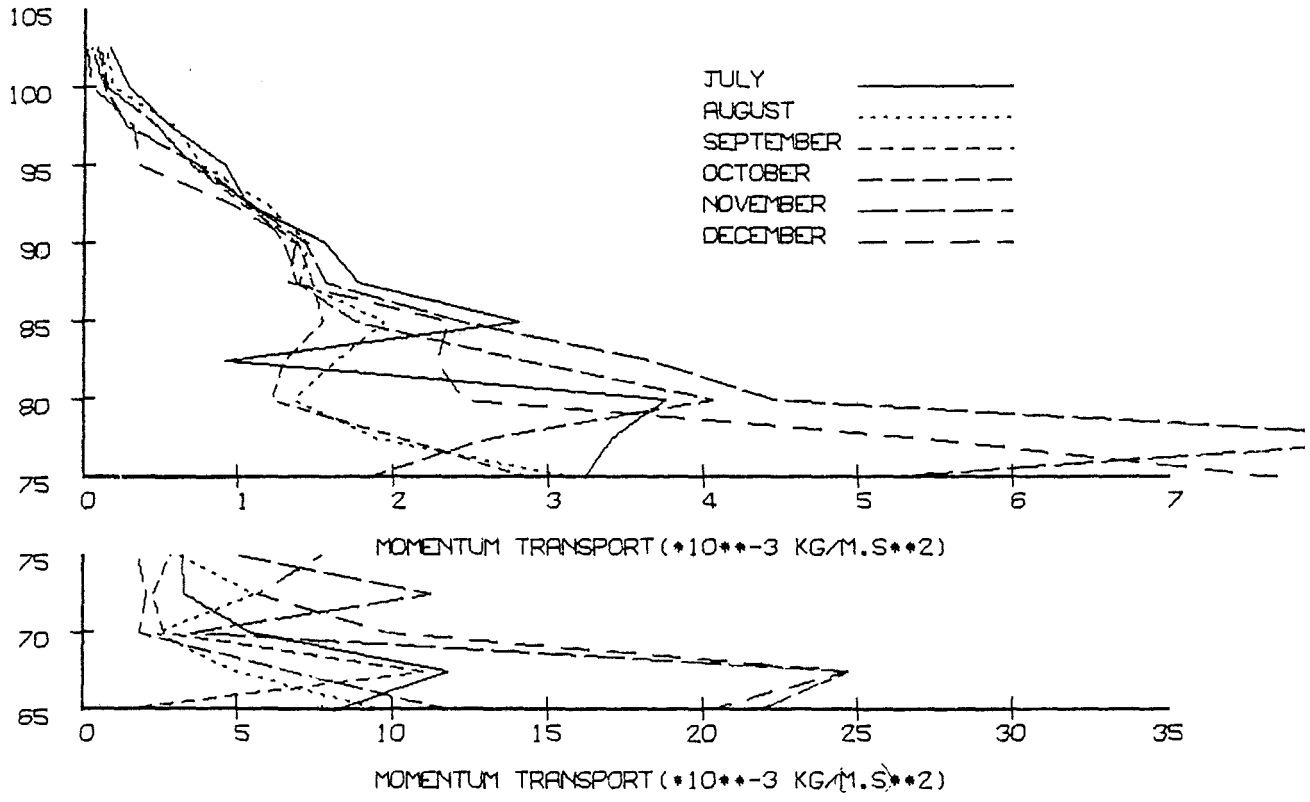

VARIATIONS IN THE HORIZONTAL TRANSPORT OF HORIZONTAL MOMENTUM IN 1981.

The graphs of the horizontal transport of horizontal momentum (figures 8.15 to 8.17) show that, in most months, there is relatively little change in the value of $\rho\overline{u_1 v_1}$ as height increases from 75 km to 90 km, the difference in most cases being less than 2 or 3 times compared with order of magnitude changes in the density in the same height range. Thus, this horizontal transport of horizontal momentum becomes relatively more important with increasing height up to 90 km. Unfortunately, as the phenomenon is a horizontal one and only one measurement is made for each height, information is not available about the amount of momentum that these internal gravity waves lose to the mean flow.

8.11 Afterword

The previous sections show that, on their own, none of the mechanisms invoked provided a convincing explanation of the observed anisotropic behaviour of internal gravity waves at heights above about 80 km

The system is complicated by the existence of two separate regions. The approximate situation is that the internal gravity waves are isotropic at lower levels, while they are strongly anisotropic between 80 km and 95 km. One problem is deciding which behaviour is abnormal. That is, is it usual for the u-v scatter diagrams to be isotropic or is it abnormal? Could the isotropic behaviour of these plots be concealing an underlying anisotropy or is the anisotropy suddenly "turned on" near 80 km? These questions can be regarded as asking whether the cause of the effect is passive and masked, or whether the effect is the result of some dynamic activity near the height at which it is observed to occur. An example of a

passive cause is a dominant tropospheric source such as cold front shear or jet stream shear that comes from one particular direction. However, the problem of deciding why this effect would be hidden below about 80 km would remain Also, the increasingly isotropic nature of the u-v plots near 100 km would also defy explanation. This last point is easier to explain in terms of an active cause such as critical layers, where the amplitudes of waves in one direction have been severely restricted at a particular height, but once the restriction has been removed the wave amplitudes grow in an exponential manner until amplitudes large enough to cause breaking or some other amplitude restricting mechanism to occur. This argument obviously favours a critical layer type of approach as does an apparent connection with the zonal wind. However, the problems with assuming that critical layers cause the anisotropies have already been discussed.

Another problem is the apparent anisotropies that occur at lower heights. It is quite possible that these effects are caused by some entirely different mechanism.

Clearly, much work needs to be done, both to understand the cause of this effect and to determine whether it is merely local or whether it is on a much larger scale.

Ignoring possible causes for the moment, it is worthwhile to consider the possible effects of these anisotropies. The internal gravity waves are oriented in one particular direction over a range of heights from about 80 km to about 95 km. Furthermore, there seems to be a tendency for the U-V vectors to occur in the northwest quadrant rather than in the southeast quadrant in both summer and winter. Thus, there will be some horizontal transport of

both energy and horizontal momentum. If the anisotropy occurs over a large area then it may be important in terms of both the energy balance and the circulation near the mesopause. The problem of particle transport and hence any possible relationship to the winter anomaly is a more complex one as particle transport is not a first order effect of wave motion. The winter anomaly is the anomalously high absorption of radio waves that occurs in the winter months. For example, see Offermann (1979).

Clearly, there is a possibility that the anisotropy is local, but fairly common. In such a case the anisotropies need not have major effects on either the circulation or on the energy balance. A fuller knowledge of the effects of the anisotropies will be gained when more is known about the possible cause.

CHAPTER 9

CONCLUSIONS

In the last few years a lot of attention has been focussed on the breaking of internal gravity waves in the mesosphere. Lindzen (1981) pointed out that internal gravity wave amplitudes were large enough to permit wave breaking to occur at heights of above 70 km in summer and at even lower heights in winter. Holton (1982) stressed the potential importance of internal gravity wave breaking in simultaneously balancing the momentum and energy budgets in the mesosphere. This thesis has been undertaken primarily to study the nature of this internal gravity wavebreaking in terms of the way that it affects the observations of the mean behaviour of internal gravity waves.

No individual motion can be studied entirely in isolation from the other motions of the atmosphere. The possibility of direct wave-wave interaction does exist (e.g. Spizzichino (1969), and changes in background temperatures and wind velocities can affect wave characteristics.

Spectral analyses have been made, using maximum entropy method techniques, so that the regular motions that were present in individual months could be studied. A 4-day wave is present in the July 1981 data. This wave can probably be identified with the zonal wavenumber one planetary wave that was discussed by Venne and Stanford (1979). In the January 1981 data a 5-day wave is found. This is probably the $H_{\frac{1}{2}}$ free mode. A 2-day wave is also present. References to these modes can be found in Salby (1984). Waves with periods of 5 days are also found in April and October data. Comparisons have been made between those wind

results and other results that were found using satellite derived radiances and f-min measurements.

Analyses of the variances of motions with periods longer than a day from which mean winds have been removed show that the variances of such motions are small compared with the variances of internal gravity waves, especially above 80 km.

Internal gravity wave variance profiles have been calculated for 2½ years from June 1980 to December 1982 at Birdlings Flat. The similarities between all of these profiles over this period of time is striking. In all months the variance increases with height to a peak value of heights of between 92.5 km and 95 km.

The first attempts at discovering the causes of the behaviour of those variance profiles involved explaining the sudden increase in variance that occurs above 80 km in terms of removing the restrictions on the wave amplitude that happen below 80 km. However, the variance does not increase at heights greater than about 92.5 km or 95 km. Thus any restriction would need to be reimposed at a height of around 95 km. A better assumption would be that the amplitude was restricted at all heights, but because of variations in some parameters, amplitude increases could happen above 80 km. Therefore stability conditions have been invoked as a possible explanation of the variance profiles.

A common method of determining the stability of a fluid is to use a Richardson number criterion. Instabilities must occur if the Richardson number is zero, as a fluid element that is moving upwards would be expected to continue doing so in this case: that is, convective instability occurs. However, turbulence may also occur in fluids with small positive Richardson numbers. Thus the observed amplitude

restrictions may be related to the occurrence of these Richardson numbers. The mean atmosphere is stable throughout the middle atmosphere and in the lowest parts of the thermosphere. However, Richardson numbers are smaller in regions of temperature decrease, such as the mesosphere, than they are in regions of temperature increase, such as the stratosphere or the lower thermosphere. Thus the maximum amplitudes of waves that can exist before turbulence is produced are expected to be considerably smaller in the mesosphere than in the lower thermosphere. Even without determining the relevant Richardson number it is clear that variances can be expected to be larger above 80 km to 85 km than they are below this height. Thus a Richardson number approach promises to give some sort of explanation of the observed variance profiles.

A model that purports to explain the observed variances must explain the overall shape of the variance profiles as well as the maximum values of the variance. The major features of the variance profiles are: There is a maximum of variance found in winter with a secondary maximum in summer; in summer, spring and autumn there is little increase in variance between 65 km and 80 km, while there is a steady increase in variance above this height up to 95 km.

The convective instability model invoked in Chapter 6 fairly accurately explained these features of the variance profiles provided that several assumptions were made. The first assumption is that significant differences can occur between southern hemisphere temperatures and northern hemisphere temperatures in the mesosphere. There is some support for this assumption (Sehra and Hariharn (1981). A corollary to this is that mean temperatures change from year to year. The second assumption is that the dominant vertical wavelength

increases slightly with height. Some theoretical support is available for this assumption (Weinstock (1984)). The third assumption is that a larger dominant vertical wavelength is found in winter than in summer. This last assumption has the least experimental theoretical support, although there is some experimental evidence of changes in vertical wavelength with season (e.g. Ball (1981)). If this last assumption is not made the model fails to explain the pronounced variance peak that is found in winter and an alternative mechanism for explaining the variance profiles must be found.

One of the predictions made by this model is that, at a given height, the amplitude is proportional to the vertical wavelength when the waves are saturated. Unsuccessful attempts were made to test this assumption. One problem was that too few data were available in any particular profile. Another was that difficulties were encountered in removing trends from the data.

Estimates of wave energies showed decreases from 65 km to 102.5 km. Comparisons of variance between motions with periods of less than 3 hours and motions with other periods demonstrated the importance of internal gravity waves at heights between 85 km and 95 km.

The strong anisotropy in internal gravity wave velocity vectors above 70 km to 80 km that is discussed in Chapter 8 suggests that the meridional transport of zonal momentum is potentially important in balancing the momentum budget. The availability of data from both Arrival Heights and Birdlings Flat means that estimates of mean vertical winds can be made and that accelerations due to the mean winds can be calculated. These accelerations must be balanced in some way. No method of calculating the vertical flux of zonal momentum was available from the data used, but calculations of the meridional

transport of zonal momentum were made. Accelerations could be estimated using Arrival Heights and Birdlings Flat data as the two places have about the same longitude, although the large latitude difference mean that these are only rough estimates.

The flux of zonal momentum is poleward throughout the year and as the magnitude of the momentum flux decrease from Birdlings Flat to Arrival Heights the accelerations are always eastward at heights between 75 km and 95 km. This acts to balance the mean wind accelerations in summer but increases them in winter. Furthermore in summer the magnitude of the acceleration due to the meridional flux of zonal momentum is much smaller than the magnitude of the acceleration due to the mean wind. Thus, not unexpectedly, the vertical flux of zonal momentum due to internal gravity waves is more important in balancing the momentum budget than the overall meridional flux of zonal momentum.

In the course of investigating changes in variance with height scatter,diagrams were made of the velocity vectors of motions from which 3 hourly averages had been removed. Originally, this exercise was designed to see how the maximum amplitude varied with height. It was believed that the velocity field would be isotropic at every height or anisotropic in one particular direction at all heights. The second case would indicate that the waves were being produced by an anisotropic tropospheric source. If this second case occurred, the preferred direction might be variable over the course of a year, depending on what the source was. Instead of either of these monthly sets of patterns occurring, the scatter diagrams are in the main isotropic over a period of 2½ years at heights below about 75 km to 80 km in winter and below about 80 km to 85 km

in the rest of the year. Above these heights the points on the u-v scatter diagrams are very noticeably aligned along a northwest-southeast line in all months at Birdlings Flat, up to a height of about 97.5 km or 100 km. As height increases above 95 km the scatter diagrams appear more isotropic, but this varies throughout the year.

These results were put on a quantitative basis by determining the correlations between the eastward and northward components of motion of vectors that had had 3 hourly averages removed. This technique was usable because the alignment above 80 km is along an axis that is oriented at 45 degrees to the north-south and east-west axes. Sometimes there are alignments along a north-south axis at lower heights (near 75 km) in summer. These alignments can not be seen in correlation analyses as the northward and eastward wind vectors are independent in this case and thus no correlation occurs. Similarly, the east-west alignments that occasionally occurred in winter cannot appear in the correlation analysis.

All of these results are sufficiently unexpected to require an explanation.

The first thing that needs to be tested is the possibility that the alignment is caused by a bias in either the experiment or the analysis. The behaviour of the scatter diagrams is the strongest argument against this objection. If such a bias occurs then the height at which it occurs would have to vary with season; the amount of bias would have to vary with height and the bias would have to cease at a height of around 100 km. Thus, experimental or analytical bias is not a very plausible option.

Physical explanations can be considered.

The first of these is that the alignment of the internal gravity waves is being caused by magnetic effects. As charged particles act as tracers for the neutral atmosphere in the D-region (Gossard and Hooke (1975)), the relevant equations must be calculated for all particles. When the appropriate values of Pedersen and Hall conductivities, density and the strength of the earth's magnetic field are substituted into the acoustic/internal gravity wave dispersion equation, it can be seen that the magnetic terms have little effect. Furthermore, if the alignment is caused by magnetic effects, the anisotropy should become more noticeable with increasing height. This does not occur. Therefore, magnetic effects can be ruled out as a probable cause of the observed alignment.

The breaking of internal gravity waves does not seem to cause the alignment directly, and no explanation based on wave breaking can conform to the observed pattern of the alignment.

The best explanations for this phenomenon seem to involve considerations about either the source of the waves or critical layers. However, both explanations suffer from problems that are not easy to reconcile with the observed behaviour of the anisotropy.

If the anisotropy is caused by tropospheric sources, an explanation is needed as to why the effect is not visible below about 80 km. One possible explanation for this might be that there is a dominant isotropic source that disappears due to wave breaking below 80 km, while the smaller amplitude anisotropic sources produces waves that only become apparent

at greater altidudes. There is no information available to justify such a complex explanation. Another possibility is that there is a mesospheric source for these waves. This source must be found in one particular location throughout the year. The mean dynamics of this region change with the seasons, and so there is no apparent reason why such a source would remain in the same position. Furthermore, on one occasion at least internal gravity waves seen in noctilucent clouds at 83 km have been associated with a tropospheric source, namely cold front shear (Hines (1974)). So some internal gravity waves that have been seen at around 80 km have come from a tropospheric source.

Similarly, there are arguments against critical layers being the cause of the observed anistropies. For instance, the prevailing wind varies considerably throughout the year, so there seems to be little chance that critical layers could produce an alignment along one particular axis throughout the year.

However, there is an apparent association between the height at which the zonal wind changes from westward to eastward, or from a strong eastward value to a weak eastward value, and the height at which the alignment is first noticeable. Unfortunately, the analogy with trapped planetary waves (e.g. Charney and Drazin (1961), Dickinson (1968)) does not appear to be a good one.

Clearly, the problem of the cause of the observed phenomenon has not been solved. A parallel problem is whether the effect is local or widespread. While Arrival Heights data does show some preference for waves to be aligned in one particular direction that is similar to that observed at Birdlings Flat, there is no particular reason to assume

that the alignments are part of an effect that is continuous from Antarctica through to New Zealand and possibly beyond.

The alignments in the data may represent two separate local effects.

However, if the alignment occurs over large regions there are obviously going to be implications about the energy and momentum budgets near the mesopause. Anisotropic wave motion will lead to the preferential dumping of momentum in one direction. Energy will also be carried horizontally through the atmosphere. There may possibly be influences on particle transport too, but as this is not a first order process, it is not necessarily a consequence of the anisotropy.

Clearly, a lot more work needs to be done, particularly on finding out more about the alignments that have been seen in the data.

Sed haec prius fuere - Catullus

APPENDIX I

TABLE 3.1 (a) The number of readings used at each height for each hour on April 11, 1981. Values for hours 0 to 11

	Hour											
Height (km)	0	1	2	3	4	5	6	7	8	9	10	11
65	0	0	0	0	0	0	0	0	0	1	2	1
67.5	0	0	0	0	0	0	0	0	0	0	0	1
70	0	0	0	0	0	0	0	0	0	3	0	0
72.5	0	0	0	0	0	0	0	0	0	0	1	0
75	0	0	0	0	0	0	0	0	0	0	2	0
77.5	0	0	0	0	0	0	0	0	0	0	0	0
80	0	0	0	0	0	0	0	0	0	1	0	0
82.5	0	0	0	0	0	0	0	1	0	1	0	1
85	0	0	0	0	0	0	0	1	0	0	0	1
87.5	0	2	1	2	0	1	0	3	1	1	1	1
90	2	3	2	2	7	2	2	4	4	0	1	2
92.5	3	2	1	1	8	3	3	8	1	1	2	4
95	1	0	1	2	1	2	2	1	1	1	5	2
97.5	0	0	1	0	2	3	2	1	3	6	5	1
100	0	2	0	1	1	0	0	0	1	4	3	1
102.5	0	2	0	1	1	0	1	2	5	1	0	1

TABLE 3.1 (b) The number of readings used for each hour at each height on April 11, 1981. Values for hours 12 to 23

	Hour											
Height (km)	12	13	14	15	16	17	18	19	20	21	22	23
65	3	3	0	0	0	0	0	0	0	0	0	0
67.5	3	4	5	2	0	0	0	0	0	0	0	0
70	1	4	5	4	1	0	0	0	0	0	0	0
72.5	1	1	2	2	2	0	0	0	0	0	0	0
75	0	1	0	0	2	0	0	0	0	0	0	0
77.5	0	0	0	1	0	0	0	0	0	0	0	0
80	0	0	0	1	0	0	0	0	0	0	0	0
82.5	1	1	3	2	1	2	0	0	0	0	0	0
85	1	3	1	2	1	1	2	0	0	0	0	0
87.5	1	0	0	0	3	1	3	1	1	0	2	0
90	1	0	0	2	0	3	2	0	2	1	0	2
92.5	0	0	0	1	2	1	2	2	5	4	2	2
95	1	0	0	0	2	0	2	1	1	1	0	3
97.5	1	0	0	0	2	0	2	1	1	1	0	3
100	3	6	3	2	0	1	1	0	2	1	0	0
102.5	2	6	3	1	3	2	1	0	0	1	0	1

TABLE 3.2 (a) The number of readings used for each hour at each height on July 11, 1981. Values for hours 0 to 11

	Hour											
Height (km)	0	1	2	3	4	5	6	7	8	9	10	11
65	0	0	0	0	0	0	0	0	0	0	0	0
67.5	0	0	0	0	0	0	0	0	0	0	0	0
70	0	0	0	0	0	0	0	0	0	0	0	2
72.5	0	0	0	0	0	0	0	0	0	0	2	2
75	0	0	0	0	0	0	0	0	0	4	3	2
77.5	0	0	0	0	0	0	0	0	2	10	5	0
80	0	0	0	0	0	1	0	1	2	1	2	0
82.5	0	0	0	0	0	0	0	1	0	1	1	0
85	1	2	1	3	2	2	3	0	3	0	0	0
87.5	1	1	0	2	2	3	3	2	3	1	0	1
90	4	3	2	4	4	1	3	1	6	1	1	3
92.5	1	2	4	6	7	3	3	1	3	2	0	3
95	4	1	3	1	2	2	1	1	1	1	2	1
97.5	0	2	2	3	1	0	0	3	1	0	0	0
100	0	0	1	1	0	0	1	0	2	3	0	1
102.5	1	1	1	0	2	1	0	2	2	1	1	1

TABLE 3.2 (b) The number of readings used for each hour at each height on July 11, 1981. Values for hours 12 to 23

	Hour											
Height (km)	12	13	14	15	16	17	18	19	20	21	22	23
65	0	0	0	0	0	0	0	0	0	0	0	0
67.5	1	0	1	0	0	0	0	0	0	0	0	0
70	3	3	3	0	0	0	0	0	0	0	0	0
72.5	2	5	3	0	0	0	0	0	0	0	0	0
75	0	3	1	2	0	0	0	0	0	0	0	0
77.5	1	0	2	2	3	0	0	0	0	0	0	0
80	1	1	1	2	4	1	0	0	0	0	0	0
82.5	1	0	1	4	3	0	0	1	0	0	0	1
85	1	0	0	1	0	0	3	2	1	1	0	1
87.5	0	1	1	1	0	0	0	1	3	1	1	2
90	1	1	1	1	0	4	2	6	7	6	3	2
92.5	0	0	0	0	0	2	4	2	4	2	3	2
95	1	0	1	0	0	3	6	1	3	2	2	0
97.5	2	0	0	0	2	4	0	1	2	5	0	0
100	0	1	0	1	1	1	1	2	2	4	0	0
102.5	3	0	1	0	1	0	1	1	0	0	2	0

TABLE 3.3 (a) The number of readings used for each hour at each height on October 11, 1981. Values for hours 0 to 11

	Hour											
Height (km)	0	1	2	3	4	5	6	7	8	9	10	11
65	0	0	0	0	0	0	0	0	0	0	1	0
67.5	0	0	0	0	0	0	0	0	0	0	2	1
70	0	0	0	0	0	0	0	0	0	0	1	2
72.5	0	0	0	0	0	0	0	0	0	0	2	3
75	0	0	0	0	0	0	0	0	0	0	3	4
77.5	0	0	0	0	0	0	0	0	3	0	5	5
80	0	0	1	0	0	0	0	0	0	0	3	3
82.5	0	0	0	0	1	1	1	0	0	0	0	2
85	0	0	1	1	2	0	0	2	1	0	1	1
87.5	1	0	0	1	2	1	4	0	0	0	0	0
90	4	1	0	1	3	2	3	3	1	0	4	0
92.5	1	2	0	2	4	4	3	3	3	0	1	0
95	1	0	2	4	1	2	3	2	1	0	1	0
97.5	4	2	1	2	2	3	6	0	0	0	1	1
100	0	0	0	2	2	3	0	0	1	0	2	1
102.5	0	0	1	0	0	1	3	1	1	0	1	2

TABLE 3.3. (b) The number of readings used for each hour at each height on October 11, 1981. Values for hours 12 to 23

	Hour											
Height (km)	12	13	14	15	16	17	18	19	20	21	22	23
65	2	0	3	0	1	0	0	0	0	0	0	0
67.5	0	2	3	3	3	0	0	0	0	0	0	0
70	4	6	6	4	5	1	0	0	0	0	0	0
72.5	3	4	3	6	7	1	0	0	0	0	0	0
75	7	1	2	4	4	1	0	0	0	0	0	0
77.5	6	7	8	6	1	1	0	0	0	0	0	0
80	1	2	2	2	0	1	1	0	0	0	0	0
82.5	1	1	1	2	0	0	0	0	0	1	0	0
85	1	3	2	1	2	0	1	0	0	0	0	0
87.5	0	1	1	2	3	2	3	0	1	0	0	0
90	2	1	2	3	5	6	5	4	2	0	0	0
92.5	2	1	1	1	1	1	3	3	0	1	0	1
95	1	0	2	1	1	3	4	2	0	1	0	1
97.5	1	2	1	0	0	2	3	1	1	4	0	0
100	0	3	0	1	1	1	1	1	1	1	0	1
102.5	0	1	0	3	1	2	1	1	1	1	0	1

TABLE 3.4 (a) The number of readings for each hour at each height on December 22, 1981. Values for hours 0 to 11

	Hour											
Height (km)	0	1	2	3	4	5	6	7	8	9	10	11
65	0	0	0	0	0	0	0	0	0	0	0	0
67.5	0	0	0	0	0	0	0	0	1	0	1	2
70	0	0	0	0	0	0	0	0	0	2	2	2
72.5	0	0	0	0	0	0	0	0	0	0	1	0
75	0	0	0	0	0	0	0	0	0	0	0	0
77.5	0	0	0	0	0	0	0	0	0	0	0	1
80	0	0	0	0	0	0	0	0	3	0	1	0
82.5	0	0	1	0	0	0	0	1	2	1	1	1
85	1	1	3	1	1	2	1	3	1	0	2	3
87.5	1	6	2	2	1	0	1	5	0	1	0	0
90	3	4	2	1	4	3	2	3	0	2	0	1
92.5	2	8	4	5	1	1	2	1	0	2	1	1
95	1	5	1	4	2	2	0	0	1	0	3	1
97.5	0	3	1	1	1	2	2	1	1	1	4	2
100	0	0	2	1	0	0	0	1	3	0	3	2
102.5	0	0	0	3	0	0	3	1	0	3	5	3

TABLE 3.4 (b) The number of readings for each hour at each height on December 22, 1981. Values for hours 12 to 23

	Hour											
Height (km)	12	13	14	15	16	17	18	19	20	21	22	23
65	0	0	0	0	0	0	0	0	0	0	0	0
67.5	0	0	0	0	0	0	0	0	0	0	0	0
70	1	0	0	0	1	0	0	0	0	0	0	0
72.5	1	0	0	0	3	0	0	0	0	0	0	0
75	0	0	0	0	1	0	0	0	0	0	0	0
77.5	0	0	0	0	4	0	0	0	0	0	0	0
80	0	0	0	0	2	4	1	1	0	0	0	0
82.5	0	0	0	0	2	2	2	0	0	0	0	0
85	0	0	0	0	1	3	2	1	3	1	0	0
87.5	0	0	0	0	0	0	6	2	2	0	0	0
90	0	0	0	0	2	4	3	5	4	1	3	4
92.5	0	0	0	0	1	3	4	0	2	3	5	6
95	0	0	0	0	2	1	2	2	1	3	0	1
97.5	0	0	0	0	1	5	0	3	2	1	2	1
100	1	0	0	0	1	2	0	0	1	0	0	4
102.5	0	0	0	0	3	1	0	0	0	0	1	0

APPENDIX II

DIPOLE AND GEOGRAPHIC CO-ORDINATES

This section follows Davies (1969).

The relationship between dipole co-ordinates (Φ, the latitude, and Λ, the longitude) and the corresponding geographic co-ordiantes (ϕ,λ) at a point P are given by

$$\sin\Phi = \sin\phi\sin\phi_o + \cos\phi\cos\phi_o\cos(\lambda-\lambda_o) \qquad \text{(II.1)}$$

$$\sin\Lambda = \frac{\cos\phi\sin(\lambda-\lambda_o)}{\cos\Phi} \qquad \text{(II.2)}$$

where ϕ_o and λ_o are the geographical latitude and longitude of the north pole (ϕ_o = 78.3N, λ_o = 291.0E).

APPENDIX III

TABLE 7.1 (a) Correlation coefficients for motions with periods between 5 and 8 hours. The uncertainties represent 95% confidence intervals. The data are for the first six months of 1981 at Birdlings Flat

Height (km)	January	February	March	April	May	June
85	+0.42 -0.39 -0.30	+0.44 -0.12 -0.40	+1.50 -0.79 -0.21	+0.45 +0.03 -0.46	+0.23 -0.32 -0.20	+0.34 -0.47 -0.24
87.5	+0.34 -0.23 -0.29	+0.24 -0.33 -0.21	+0.82 +0.15 -1.09	+0.29 -0.41 -0.23	+0.19 -0.39 -0.16	+0.27 -0.17 -0.24
90	+0.23 -0.47 -0.18	+0.22 -0.12 -0.21	+1.03 -0.08 -0.89	+0.21 -0.44 -0.17	+0.14 -0.62 -0.11	+0.24 -0.36 -0.20
92.5	+0.32 -0.21 -0.28	+0.20 -0.49 -0.16	+1.01 -0.41 -0.51	+0.26 -0.30 -0.22	+0.17 -0.49 -0.14	+0.22 -0.45 -0.17
95	+0.26 -0.33 -0.22	+0.23 -0.28 -0.20	+1.44 -0.58 -0.41	+0.23 -0.22 -0.21	+0.19 -0.34 -0.16	+0.28 -0.12 -0.26
97.5	+0.27 -0.19 -0.24	+0.23 -0.04 -0.23	+0.81 +0.00 -0.81	+0.23 -0.49 -0.18	+0.20 -0.47 -0.16	+0.28 -0.16 -0.26
100	+0.31 -0.23 -0.27	+0.24 -0.26 -0.21	+0.48 +0.51 -1.39	+0.31 -0.44 -0.21	+0.22 -0.44 -0.18	+0.29 +0.21 -0.33
102.5	+0.33 -0.21 -0.29	+0.29 -0.37 -0.23	+1.13 -0.19 -0.79	+0.34 -0.48 -0.24	+0.22 -0.49 -0.17	+0.29 -0.44 -0.22

TABLE 7.1 (b) Correlation coefficients for motions with periods between 5 and 8 hours. The uncertainties represent 95% confidence intervals. The data are for the second six months of 1981 at Birdlings Flat.

Height (km)	July	August	September	October	November	December
85	+0.25 -0.27 -0.22	+0.34 -0.37 -0.26	+0.27 -0.34 -0.23	+0.41 -0.52 -0.26	+0.34 -0.24 -0.29	+0.33 -0.37 -0.26
87.5	+0.21 -0.42 -0.17	+0.24 -0.40 -0.19	+0.21 -0.53 -0.16	+0.24 -0.64 -0.16	+0.26 -0.39 -0.21	+0.31 -0.33 -0.25
90	+0.20 -0.37 -0.17	+0.19 -0.51 -0.15	+0.22 -0.30 -0.19	+0.21 -0.45 -0.17	+0.22 -0.49 -0.17	+0.25 -0.34 -0.21
92.5	+0.22 -0.29 -0.19	+0.21 -0.41 -0.17	+0.23 -0.32 -0.20	+0.22 -0.42 -0.18	+0.27 -0.23 -0.24	+0.24 -0.38 -0.20
95	+0.26 -0.18 -0.23	+0.26 -0.28 -0.22	+0.23 -0.41 -0.19	+0.20 -0.36 -0.17	+0.20 -0.57 -0.15	+0.22 -0.48 -0.17
97.5	+0.26 -0.22 -0.23	+0.33 -0.35 -0.26	+0.21 -0.39 -0.17	+0.16 -0.60 -0.12	+0.24 -0.32 -0.21	+0.29 -0.13 -0.27
100	+0.24 -0.16 -0.23	+0.28 -0.03 -0.28	+0.26 -0.35 -0.21	+0.23 -0.25 -0.20	+0.30 -0.22 -0.26	+0.29 -0.35 -0.23
102.5	+0.27 -0.30 -0.23	+0.27 -0.33 -0.22	+0.25 -0.60 -0.17	+0.25 -0.22 -0.23	+0.29 -0.22 -0.26	+0.35 -0.27 -0.29

TABLE 7.2 (a) Correlation coefficients for motions with periods between 8 and 24 hours. The undertainties represent 95% confidence intervals. The data are for the first six months of 1981

Height (km)	January	February	March	April	May	June
85	+0.37 -0.45 -0.26	+0.41 -0.23 -0.34	+1.27 -0.34 -0.64	+0.45 -0.12 -0.40	+0.19 -0.48 -0.16	+0.32 -0.47 -0.23
87.5	+0.29 -0.48 -0.21	+0.24 -0.26 -0.21	+1.43 -0.57 -0.42	+0.29 -0.32 -0.24	+0.18 -0.36 -0.16	+0.23 -0.42 -0.19
90	+0.21 -0.54 -0.16	+0.21 -0.14 -0.20	+0.96 -0.10 -0.80	+0.21 -0.28 -0.49	+0.17 -0.41 -0.15	+0.23 -0.33 -0.20
92.5	+0.26 -0.51 -0.19	+0.20 -0.37 -0.17	+0.88 -0.29 -0.57	+0.24 -0.37 -0.20	+0.16 -0.49 -0.14	+0.22 -0.30 -0.19
95	+0.25 -0.30 -0.21	+0.22 -0.10 -0.21	+1.07 -0.81 -0.18	+0.20 -0.45 -0.16	+0.16 -0.48 -0.13	+0.24 -0.42 -0.19
97.5	+0.24 -0.35 -0.20	+0.22 -0.17 -0.20	+0.90 -0.39 -0.50	+0.24 -0.34 -0.20	+0.21 -0.27 -0.19	+0.27 -0.27 -0.23
100	+0.28 -0.35 -0.23	+0.23 -0.25 -0.21	+1.11 -0.16 -0.81	+0.31 -0.33 -0.25	+0.23 -0.30 -0.20	+0.30 -0.01 -0.30
102.5	+0.30 -0.29 -0.25	+0.25 -0.52 -0.18	+0.60 -0.38 -1.29	+0.36 -0.25 -0.30	+0.22 -0.41 -0.18	+0.30 -0.31 -0.25

TABLE 7.2 (b) Correlation coefficients for motions with periods between 8 and 24 hours. The uncertainties represent 95% confidence intervals. The data are for the second six months of 1981

Height (km)	July	August	September	October	November	December
85	+0.23 -0.37 -0.19	+0.33 -0.29 -0.27	+0.24 -0.42 -0.20	+0.43 -0.20 -0.36	+0.31 -0.29 -0.26	+0.30 -0.42 -0.23
87.5	+0.19 -0.45 -0.16	+0.22 -0.44 -0.18	+0.21 -0.43 -0.18	+0.30 -0.34 -0.24	+0.25 -0.36 -0.21	+0.29 -0.34 -0.24
90	+0.19 -0.40 -0.16	+0.22 -0.46 -0.16	+0.21 -0.60 -0.12	+0.30 -0.38 -0.18	+0.25 -0.44 -0.17	+0.29 -0.55 -0.15
92.5	+0.19 -0.41 -0.16	+0.20 -0.39 -0.17	+0.22 -0.30 -0.19	+0.22 -0.36 -0.18	+0.25 -0.31 -0.21	+0.23 -0.39 -0.19
95	+0.22 -0.38 -0.19	+0.25 -0.22 -0.23	+0.24 -0.11 -0.23	+0.20 -0.28 -0.18	+0.19 -0.56 -0.15	+0.23 -0.34 -0.20
97.5	+0.22 -0.43 -0.18	+0.31 -0.33 -0.25	+0.21 -0.26 -0.19	+0.18 -0.45 -0.15	+0.22 -0.41 -0.18	+0.26 -0.31 -0.22
100	+0.23 -0.24 -0.20	+0.23 -0.50 -0.18	+0.23 -0.42 -0.19	+0.22 -0.25 -0.19	+0.28 -0.25 -0.24	+0.28 -0.15 -0.26
102.5	+0.25 -0.28 -0.22	+0.25 -0.34 -0.21	+0.29 -0.42 -0.22	+0.24 -0.10 -0.23	+0.25 -0.43 -0.20	+0.31 -0.39 -0.24

TABLE 7.3 (a) Correlation coefficients for motions with periods of more than 1 day. The uncertainties represent the 95% confidence intervals. The data are for the first six months of 1981.

Height (km)	January	February	March	April	May	June
67.5	+0.41 -0.62 -0.22	+0.42 -0.26 -0.34	+0.66 -0.67 -0.25	+0.41 -0.51 -0.26	+0.31 -0.62 -0.19	+0.45 -0.06 -0.43
70	+0.42 -0.12 -0.38	+0.40 -0.33 -0.30	+0.66 -0.57 -0.32	+0.37 -0.48 -0.25	+0.34 -0.48 -0.24	+0.40 -0.40 -0.29
72.5	+0.41 -0.41 -0.37	+0.40 -0.02 -0.39	+0.60 -0.66 -0.25	+0.39 -0.39 -0.29	+0.28 -0.64 -0.18	+0.41 -0.39 -0.30
75	+0.41 -0.37 -0.30	+0.40 -0.37 -0.30	+0.62 -0.71 -0.22	+0.33 -0.61 -0.20	+0.25 -0.71 -0.14	+0.31 -0.70 -0.17
77.5	+0.27 -0.73 -0.15	+0.39 -0.37 -0.29	+0.66 -0.26 -0.48	+0.40 -0.38 -0.29	+0.22 -0.75 -0.12	+0.37 -0.54 -0.24
80	+0.38 -0.46 -0.27	+0.38 -0.41 -0.28	+0.67 -0.35 -0.44	+0.41 -0.22 -0.35	+0.33 -0.53 -0.22	+0.38 -0.53 -0.24
82.5	+0.41 -0.46 -0.35	+0.36 -0.41 -0.24	+0.21 -0.35 -0.06	+0.40 -0.22 -0.34	+0.33 -0.53 -0.23	+0.39 -0.53 -0.27

continued on next page..

TABLE 7.3 (a) (continued...)

Height (km)	January	February	March	April	May	June
85	+0.36 -0.54 -0.23	+0.38 -0.44 -0.27	+0.35 -0.84 -0.11	+0.40 0.00 -0.40	+0.34 -0.49 -0.24	+0.38 -0.48 -0.26
87.5	+0.35 -0.56 -0.22	+0.29 -0.66 -0.17	+0.36 +0.48 -0.65	+0.40 -0.20 -0.34	+0.38 -0.27 -0.31	+0.38 -0.51 -0.25
90	+0.34 -0.59 -0.21	+0.25 -0.73 -0.14	+0.63 -0.54 -0.32	+0.35 -0.52 -0.23	+0.28 -0.64 -0.18	+0.41 -0.38 -0.30
92.5	+0.41 -0.11 -0.37	+0.35 -0.54 -0.23	+0.55 -0.67 -0.24	+0.32 -0.60 -0.20	+0.30 -0.61 -0.19	+0.39 -0.07 -0.41
95	+0.41 -0.31 -0.32	+0.31 -0.63 -0.19	+0.53 -0.70 -0.22	+0.38 -0.44 -0.27	+0.32 -0.55 -0.21	+0.43 -0.17 -0.37
97.5	+0.41 -0.30 -0.32	+0.39 -0.39 -0.29	+0.58 -0.63 -0.26	+0.37 -0.47 -0.26	+0.28 -0.64 -0.18	+0.42 -0.16 -0.37
100	+0.40 -0.06 -0.38	+0.38 -0.43 -0.27	+0.65 -0.47 -0.37	+0.40 -0.17 -0.35	+0.34 -0.50 -0.23	+0.34 -0.61 -0.20
102.5	+0.35 -0.56 -0.11	+0.34 -0.55 -0.22	+0.63 -0.53 -0.33	+0.37 +0.05 -0.39	+0.38 -0.15 -0.34	+0.41 -0.06 -0.39

TABLE 7.3 (b) Correlation coefficients for motions with periods of more than 1 day. The uncertainties represent the 95% confidence intervals. The data are for the second six months of 1981.

Height (km)	July	August	September	October	November	December
67.5	+0.37 -0.43 -0.27	+0.39 -0.31 -0.31	+0.38 -0.47 -0.26	+0.33 -0.51 -0.23	+0.48 -0.25 -0.38	+0.38 +0.25 -0.48
70	+0.34 -0.50 -0.23	+0.34 -0.52 -0.23	+0.39 -0.25 -0.32	+0.32 -0.52 -0.22	+0.35 -0.64 -0.20	+0.41 -0.44 -0.30
72.5	+0.29 -0.61 -0.19	+0.38 -0.39 -0.28	+0.39 -0.22 -0.33	+0.32 -0.53 -0.22	+0.43 -0.44 -0.29	+0.43 -0.49 -0.28
75	+0.35 -0.44 -0.25	+0.27 -0.65 -0.17	+0.39 -0.21 -0.34	+0.34 -0.47 -0.24	+0.26 -0.77 -0.13	+0.42 -0.53 -0.26
77.5	+0.36 -0.34 -0.28	+0.36 -0.41 -0.26	+0.38 -0.05 -0.36	+0.37 -0.29 -0.30	+0.42 +0.07 -0.44	+0.41 +0.14 -0.46
80	+0.37 -0.19 -0.33	+0.34 -0.42 -0.25	+0.33 -0.55 -0.22	+0.31 -0.55 -0.12	+0.24 -0.80 -0.23	+0.39 -0.59
82.5	+0.32 -0.52 +0.22	+0.37 -0.13 -0.33	+0.38 -0.36 -0.29	+0.25 -0.69 -0.15	+0.37 -0.61 -0.21	+0.45 -0.42 -0.31

continued on next page..

TABLE 7.3 (b) (continued....)

Height (km)	July	August	September	October	November	December
85	+0.36 -0.38 -0.27	+0.30 -0.57 -0.20	+0.39 -0.17 -0.34	+0.36 -0.37 -0.27	+0.38 -0.56 -0.24	+0.42 -0.47 -0.28
87.5	+0.29 -0.60 -0.19	+0.25 -0.68 -0.15	+0.38 -0.29 -0.31	+0.36 -0.36 -0.28	+0.32 -0.69 -0.17	+0.32 -0.69 -0.17
90	+0.36 -0.33 -0.29	+0.30 -0.56 -0.20	+0.36 -0.42 -0.26	+0.35 -0.43 -0.25	+0.36 -0.61 -0.21	+0.40 -0.32 -0.26
92.5	+0.28 -0.63 -0.18	+0.30 -0.58 -0.20	+0.35 -0.46 -0.25	+0.33 -0.50 -0.23	+0.42 -0.43 -0.29	+0.45 -0.32 -0.34
95	+0.34 -0.46 -0.24	+0.26 -0.65 -0.22	+0.33 -0.54 -0.24	+0.34 -0.47 -0.13	+0.25 -0.77 -0.24	+0.39 -0.55
97.5	+0.31 -0.57 -0.20	+0.25 -0.69 -0.15	+0.39 -0.21 -0.33	+0.26 -0.67 -0.16	+0.34 -0.63 -0.30	+0.45 -0.22 -0.38
100	+0.35 -0.41 -0.26	+0.30 -0.57 -0.20	+0.35 -0.48 -0.24	+0.37 -0.24 -0.31	+0.41 +0.08 -0.43	+0.33 -0.68 -0.18
102.5	+0.35 -0.40 -0.27	+0.33 -0.47 -0.24	+0.31 -0.60 -0.20	+0.37 -0.30 -0.30	+0.37 -0.58 -0.23	+0.45 -0.28 -0.36

TABLE 7.4 (a) Correlation coefficients for all periods. The uncertainties represent the 95% confidence intervals. The data are for the first six months of 1981

Height (km)	January	February	March	April	May	June
65	+0.60 -0.39 -0.39	+0.54 -0.43 -0.34	+0.39 +0.01 -0.39	+0.16 -0.11 -0.16	+0.19 -0.38 -0.16	+0.20 -0.63 -0.14
67.5	+0.20 -0.19 -0.18	+0.16 -0.48 -0.13	+0.19 -0.36 -0.16	+0.13 -0.12 -0.12	+0.14 -0.34 -0.12	+0.16 -0.43 -0.14
70	+0.13 -0.09 -0.13	+0.14 -0.19 -0.13	+0.17 -0.05 -0.16	+0.10 -0.32 -0.09	+0.11 -0.14 -0.11	+0.14 -0.35 -0.13
72.5	+0.12 -0.25 -0.11	+0.14 -0.06 -0.14	+0.17 -0.33 -0.15	+0.11 -0.10 -0.11	+0.09 -0.25 -0.09	+0.15 -0.32 -0.13
75	+0.13 -0.23 -0.12	+0.16 -0.28 -0.15	+0.19 -0.36 -0.17	+0.11 -0.25 -0.11	+0.10 -0.26 -0.09	+0.13 -0.56 -0.10
77.5	+0.10 -0.30 -0.10	+0.11 -0.35 -0.10	+0.15 -0.34 -0.13	+0.09 -0.11 -0.09	+0.07 -0.34 -0.06	+0.11 -0.47 -0.10
80	+0.14 -0.29 -0.13	+0.12 -0.45 -0.10	+0.14 -0.66 -0.11	+0.10 -0.41 -0.09	+0.08 -0.38 -0.07	+0.10 -0.50 -0.09
82.5	+0.10 -0.45 -0.09	+0.09 -0.44 +0.08	+0.15 -0.51 +0.12	+0.11 -0.22 +0.10	+0.07 -0.36 +0.07	+0.09 -0.46 +0.08

Continued next page ..

TABLE 7.4 (a) (Continued....)

Height (km)	January	February	March	April	May	June
85	+0.07 -0.51 -0.06	+0.07 -0.27 -0.07	+0.12 -0.44 -0.11	+0.08 -0.30 -0.07	+0.06 -0.39 -0.05	+0.07 -0.43 -0.06
87.5	+0.06 -0.44 -0.05	+0.06 -0.29 -0.06	+0.14 -0.23 -0.13	+0.08 -0.28 -0.07	+0.06 -0.33 -0.06	+0.07 -0.34 -0.06
90	+0.04 -0.46 -0.04	+0.05 -0.34 -0.05	+0.09 -0.37 -0.08	+0.05 -0.31 -0.05	+0.04 -0.42 -0.04	+0.05 -0.37 -0.05
92.5	+0.05 -0.42 -0.05	+0.05 -0.34 -0.05	+0.10 -0.37 -0.09	+0.06 -0.31 -0.06	+0.04 -0.42 -0.04	+0.05 -0.40 -0.50
95	+0.06 -0.37	+0.06 -0.35	+0.12 -0.35	+0.06 -0.33	+0.06 -0.37	+0.07 -0.33 -0.06
97.5	+0.06 -0.33 -0.06	+0.06 -0.33 -0.06	+0.12 -0.36 -0.11	+0.07 -0.31 -0.07	+0.06 -0.36 -0.05	+0.07 -0.32 -0.07
100	+0.06 -0.33 -0.06	+0.07 -0.26 -0.07	+0.14 -0.24 -0.13	+0.08 -0.26 -0.08	+0.07 -0.36 -0.06	+0.10 -0.17 -0.09
102.5	+0.06 -0.34 -0.06	+0.07 -0.31 -0.07	+0.16 -0.18 -0.15	+0.09 -0.20 -0.09	+0.07 -0.35 -0.07	+0.09 -0.34 0 -0.08

TABLE 7.4 (b) Correlation coefficients for all periods. The uncertainties represent the 95% confidence intervals. The data are for the second six months of 1981

Height (km)	July	August	September	October	November	December
65	+0.25 -0.21 -0.22	+0.18 -0.27 -0.17	+0.19 +0.07 -0.19	+0.17 -0.15 -0.16	+0.27 -0.54 -0.19	+0.34 -0.59 -0.21
67.5	+0.16 -0.39 -0.14	+0.15 -0.20 -0.14	+0.12 -0.39 -0.11	+0.10 -0.29 -0.09	+0.18 -0.38 -0.15	+0.18 -0.36 -0.16
70	+0.13 -0.26 -0.12	+0.12 -0.26 -0.11	+0.11 -0.20 -0.10	+0.08 -0.26 -0.08	+0.14 -0.36 -0.13	+0.13 -0.29 -0.12
72.5	+0.10 -0.48 -0.09	+0.10 -0.35 -0.09	+0.11 -0.10 -0.10	+0.09 -0.24 -0.08	+0.13 -0.44 -0.12	+0.12 -0.35 -0.11
75	+0.10 -0.48 -0.09	+0.10 -0.39 -0.09	+0.10 -0.31 -0.10	+0.09 -0.30 -0.09	+0.13 -0.50 -0.11	+0.12 -0.35 -0.11
77.5	+0.08 -0.32 -0.08	+0.08 -0.24 -0.07	+0.08 -0.24 -0.08	+0.07 -0.29 -0.07	+0.09 -0.47 -0.08	+0.11 -0.27 -0.10
80	+0.09 -0.40 -0.08	+0.08 -0.37 -0.08	+0.10 -0.32 -0.09	+0.07 -0.44 -0.07	+0.09 -0.57 -0.07	+0.13 -0.42 -0.11
82.5	+0.08 -0.34 -0.08	+0.08 -0.32 -0.08	+0.09 -0.31 -0.08	+0.07 -0.49 -0.07	+0.09 -0.48 -0.08	+0.14 -0.34 -0.12

Continued next page ..

TABLE 7.4 (b) (Continued....)

Height (km)	July	August	September	October	November	December
85	+0.06 -0.39 -0.05	+0.06 -0.41 -0.06	+0.06 -0.34	+0.06 -0.39 -0.06	+0.07 -0.43 -0.07	+0.08 -0.42 -0.07
87.5	+0.05 -0.38 -0.05	+0.06 -0.41 -0.06	+0.06 -0.37 -0.06	+0.06 -0.37 -0.06	+0.07 -0.42 -0.07	+0.07 -0.46 +0.06
90	+0.04 -0.36 -0.04	+0.04 -0.40 -0.04	+0.04 -0.37 -0.04	+0.04 -0.43 -0.04	+0.06 -0.43 -0.05	+0.05 -0.41 -0.05
92.5	+0.05 -0.34 -0.04	+0.05 -0.38 -0.05	+0.05 -0.32 -0.05	+0.05 -0.40 -0.04	+0.06 -0.38 -0.06	+0.06 -0.40 -0.05
95	+0.06 -0.34 -0.05	+0.06 -0.37 -0.05	+0.06 -0.33 -0.06	+0.05 -0.39 -0.05	+0.07 -0.47 -0.06	+0.06 -0.32 -0.06
97.5	+0.06 -0.32 -0.06	+0.06 -0.36 -0.06	+0.06 -0.34 -0.06	+0.05 -0.44 -0.05	+0.07 -0.34 -0.07	+0.06 -0.34 -0.05
100	+0.08 -0.28 -0.07	+0.07 -0.40 -0.07	+0.07 -0.34 -0.07	+0.06 -0.34 -0.06	+0.08 -0.18 -0.08	+0.07 -0.15 -0.07
102.5	+0.08 -0.29 -0.08	+0.08 -0.34 -0.07	+0.07 -0.34 -0.07	+0.07 -0.30 -0.06	+0.08 -0.23 -0.07	+0.07 -0.23 -0.07

APPENDIX IV

Figures 8.1 to 8.4,

8.7 and 8.13

Figure 8.1a)

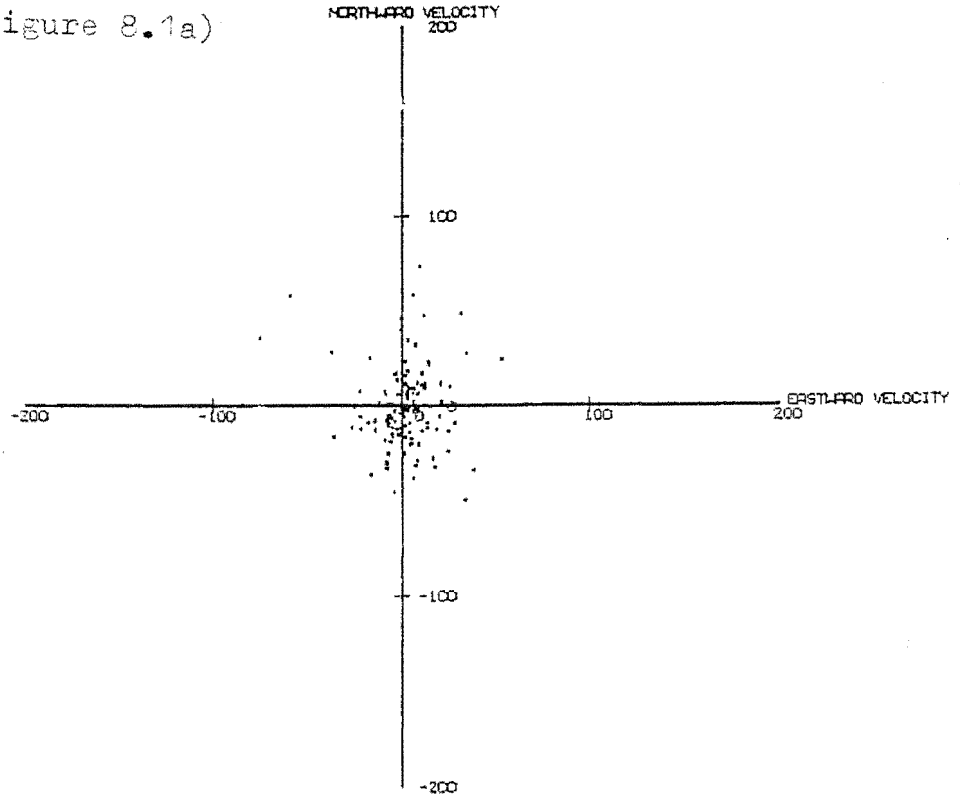

INDIVIDUAL DRIFT READINGS FOR PERIODS OF LESS THAN 3 HOURS IN APRIL 1981 AT 85.0KM.

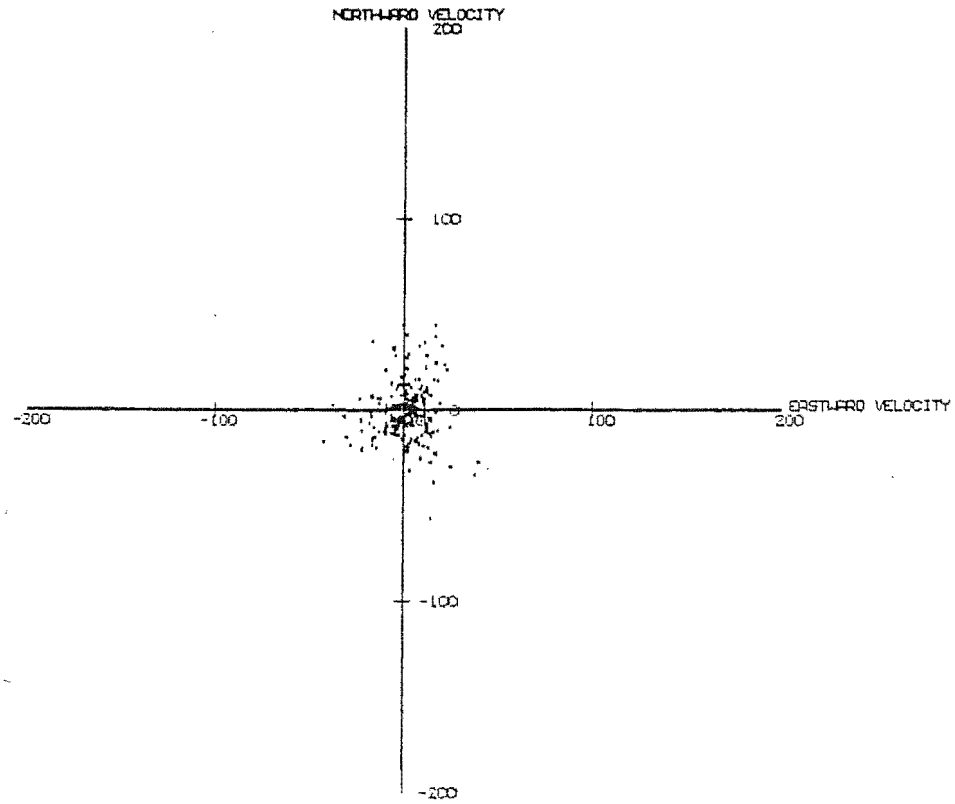

INDIVIDUAL DRIFT READINGS FOR PERIODS OF LESS THAN 3 HOURS IN APRIL 1981 AT 87.5KM.

Figure 8.1b)

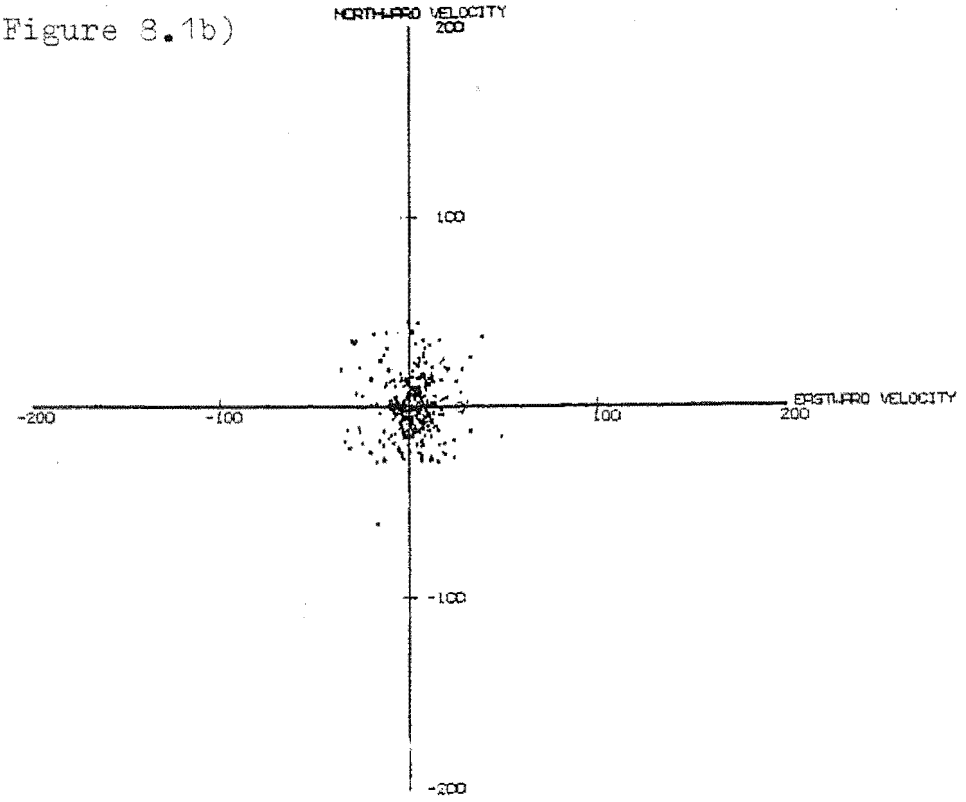

INDIVIDUAL DRIFT READINGS FOR PERIODS OF LESS THAN 3 HOURS IN APRIL 1981 AT 70.0KM.

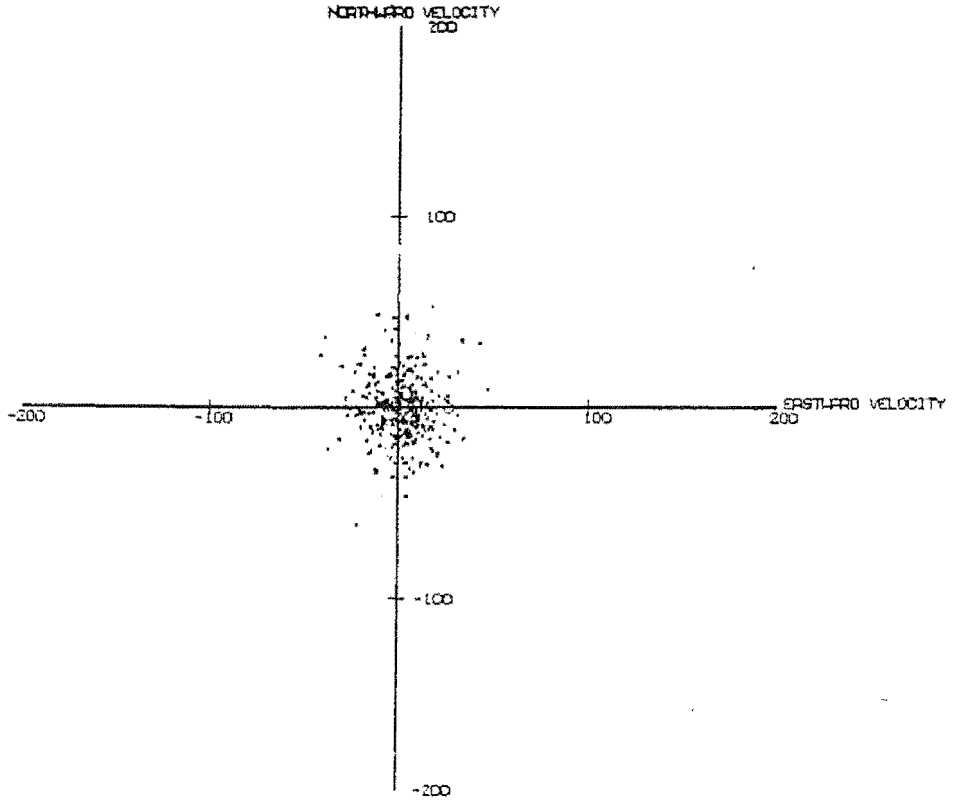

INDIVIDUAL DRIFT READINGS FOR PERIODS OF LESS THAN 3 HOURS IN APRIL 1981 AT 72.5KM.

Figure 3.1c)

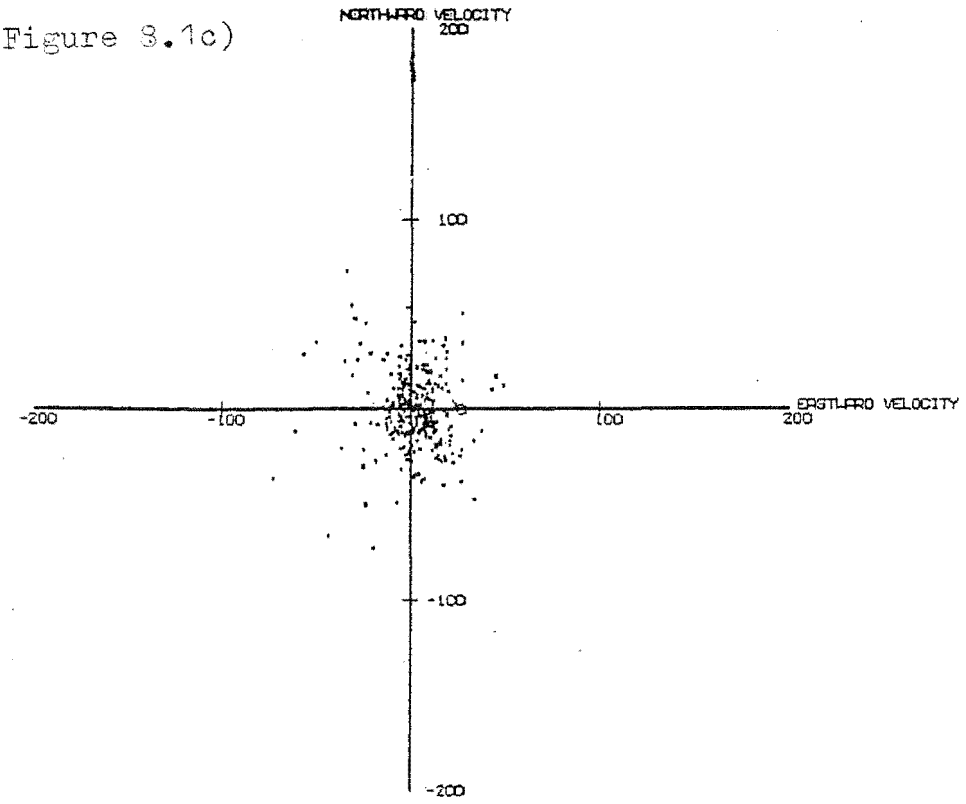

INDIVIDUAL DRIFT READINGS FOR PERIODS OF LESS THAN 3 HOURS IN APRIL 1981 AT 75.0KM.

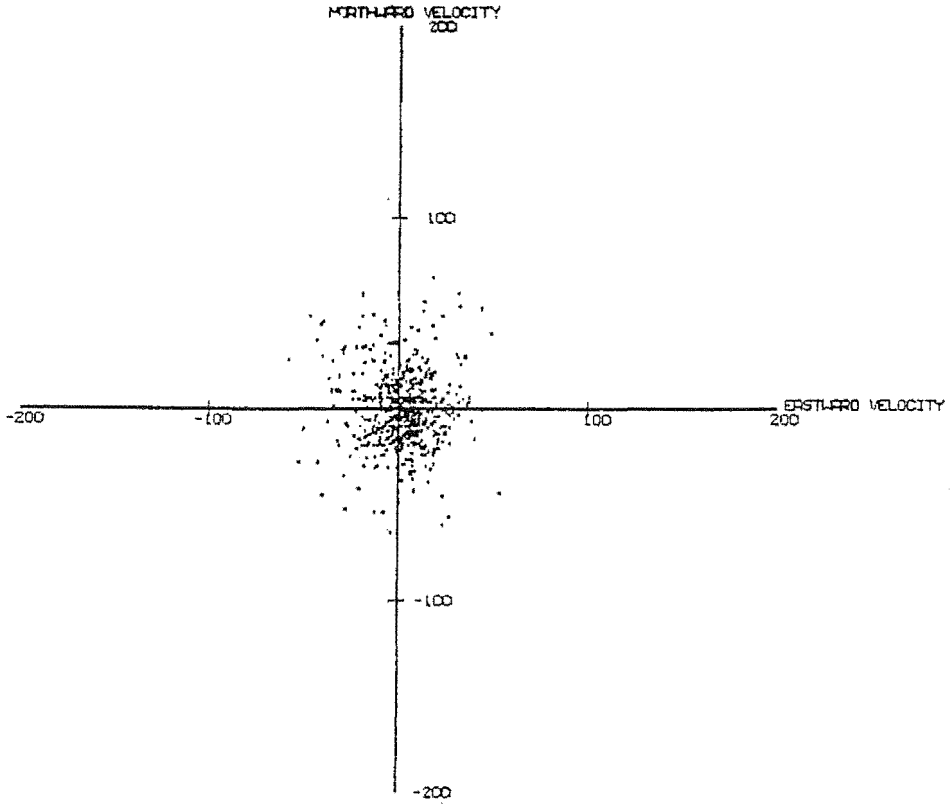

INDIVIDUAL DRIFT READINGS FOR PERIODS OF LESS THAN 3 HOURS IN APRIL 1981 AT 77.5KM.

Figure 8.1d)

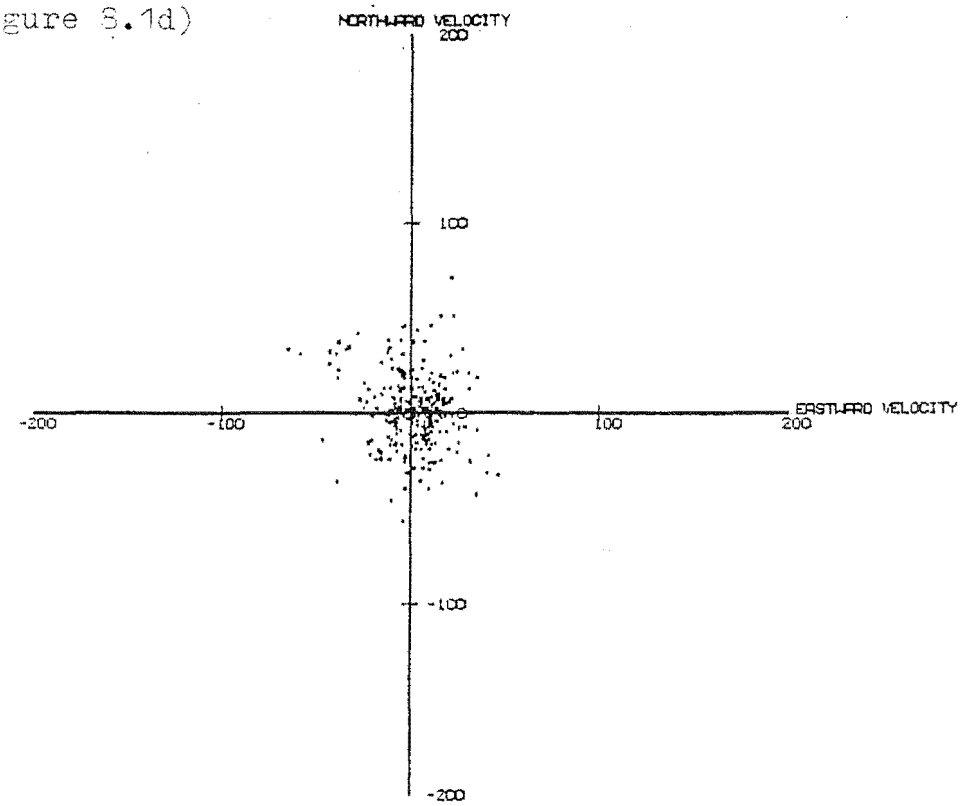

INDIVIDUAL DRIFT READINGS FOR PERIODS OF LESS THAN 3 HOURS IN APRIL 1981 AT 80.0KM.

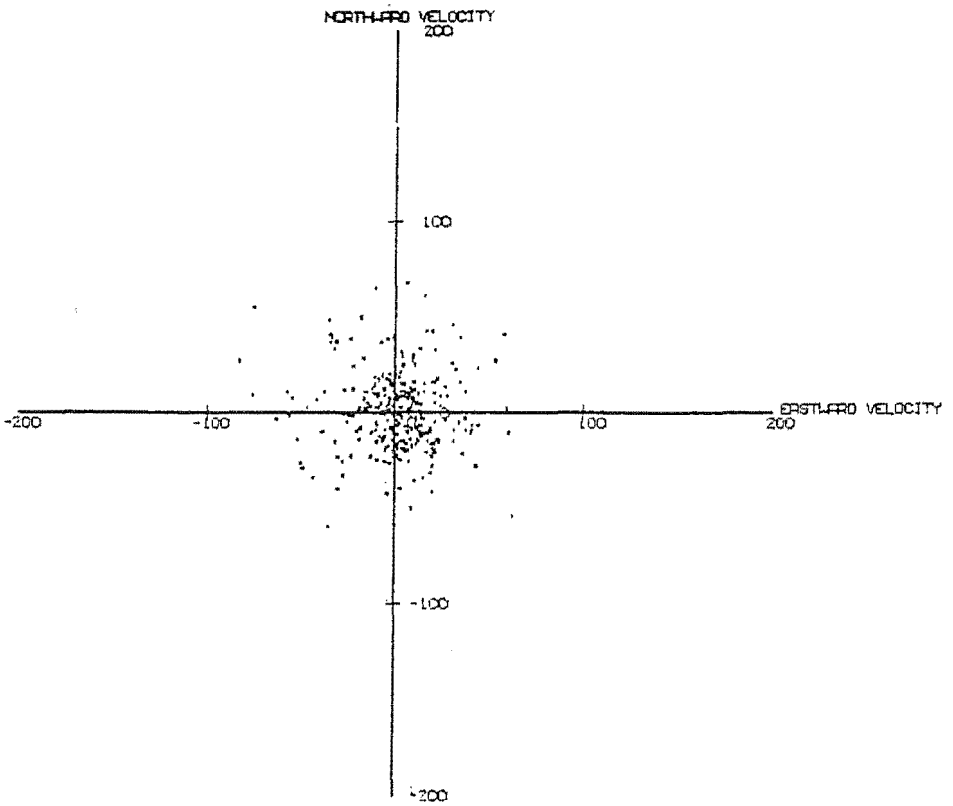

INDIVIDUAL DRIFT READINGS FOR PERIODS OF LESS THAN 3 HOURS IN APRIL 1981 AT 82.5KM.

Figure 8.1e)

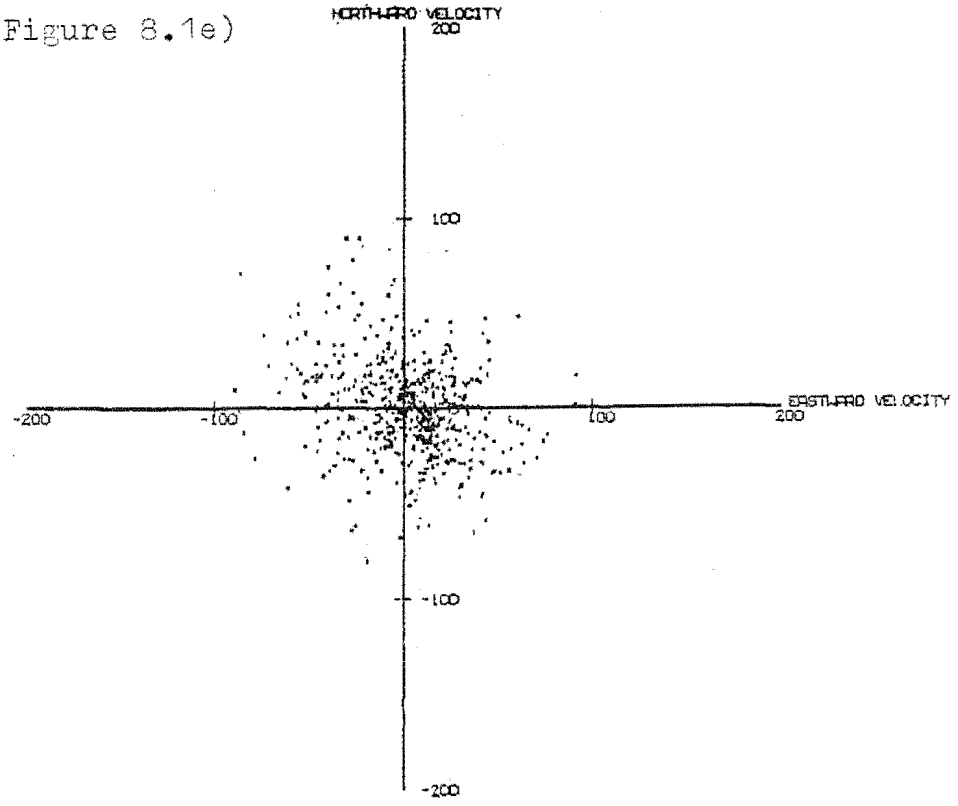

INDIVIDUAL DRIFT READINGS FOR PERIODS OF LESS THAN 3 HOURS IN APRIL 1981 AT 85.0KM.

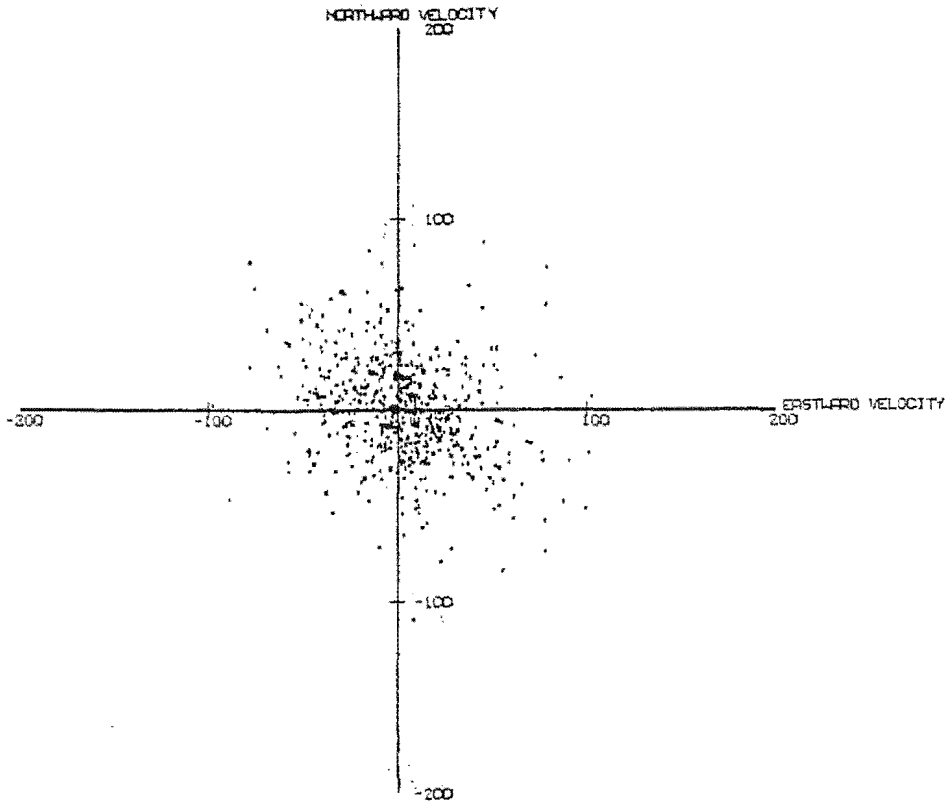

INDIVIDUAL DRIFT READINGS FOR PERIODS OF LESS THAN 3 HOURS IN APRIL 1981 AT 87.5KM.

Figure 8.1f)

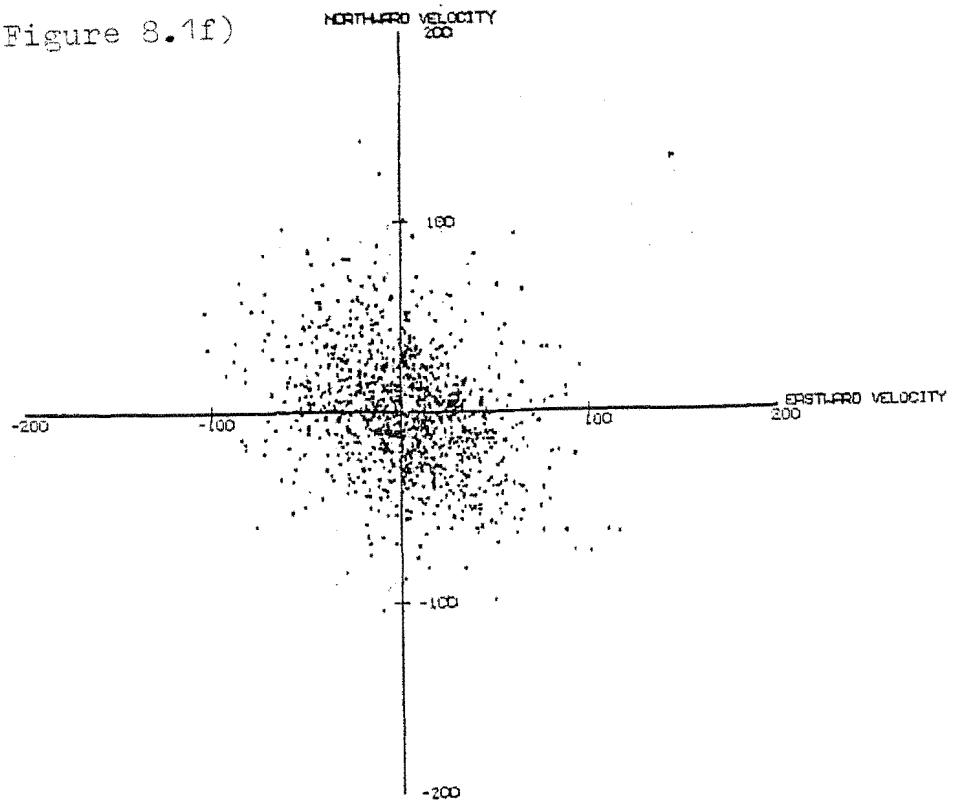

INDIVIDUAL DRIFT READINGS FOR PERIODS OF LESS THAN 3 HOURS IN APRIL 1981 AT 90.0KM.

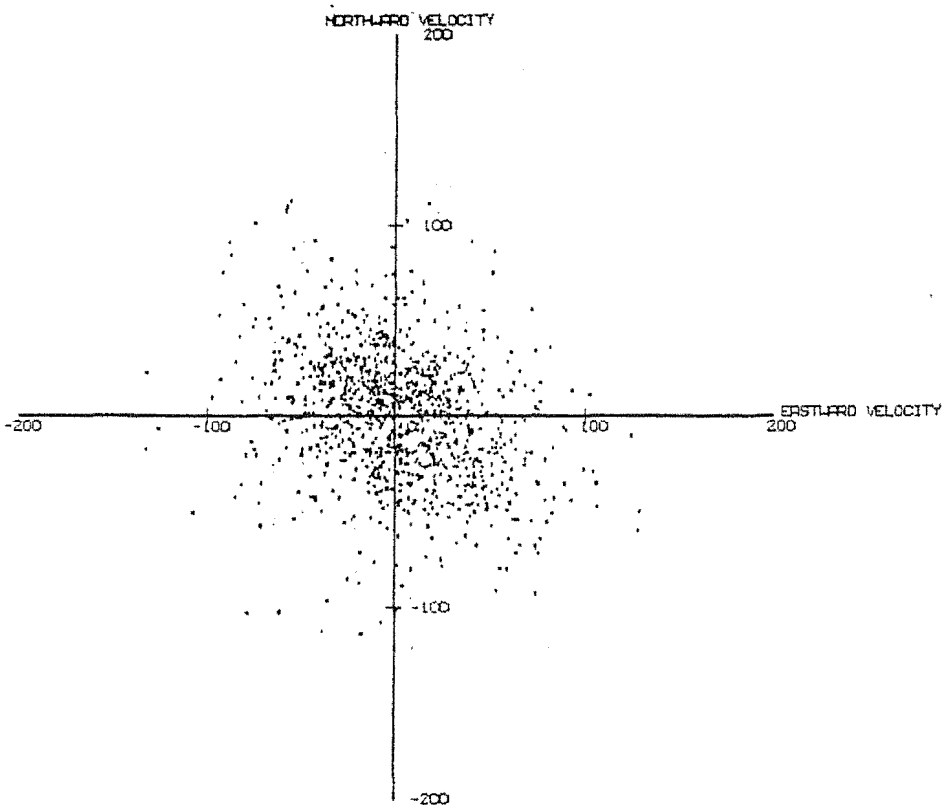

INDIVIDUAL DRIFT READINGS FOR PERIODS OF LESS THAN 3 HOURS IN APRIL 1981 AT 92.5KM.

Figure 8.1g)

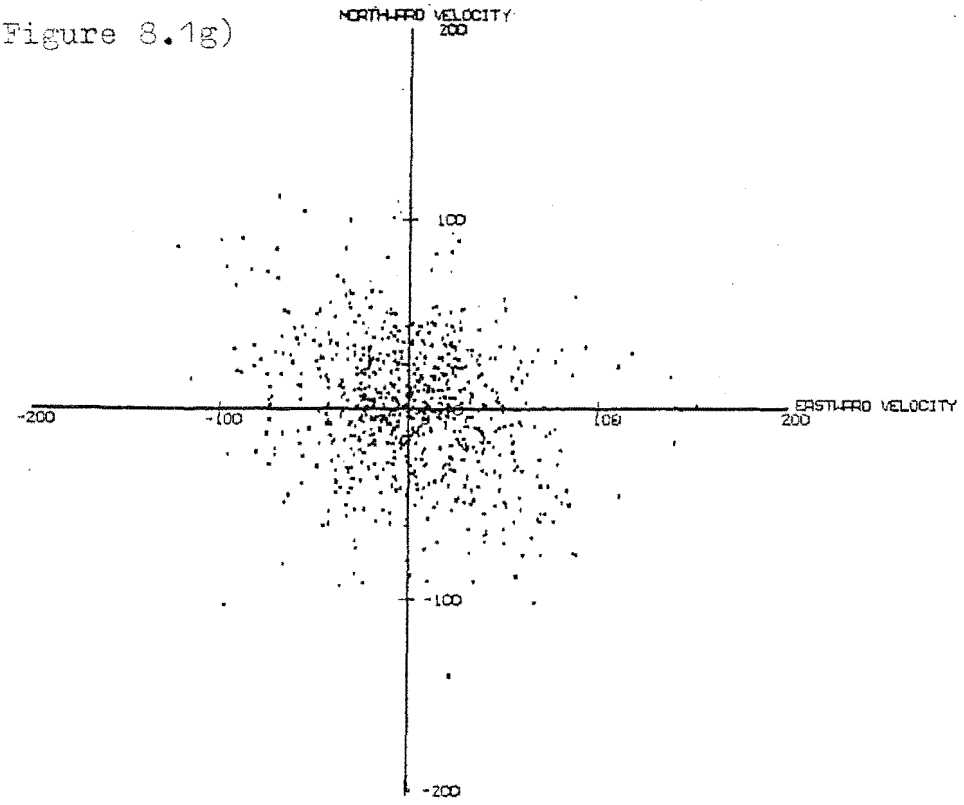

INDIVIDUAL DRIFT READINGS FOR PERIODS OF LESS THAN 3 HOURS IN APRIL 1981 AT 95.0KM.

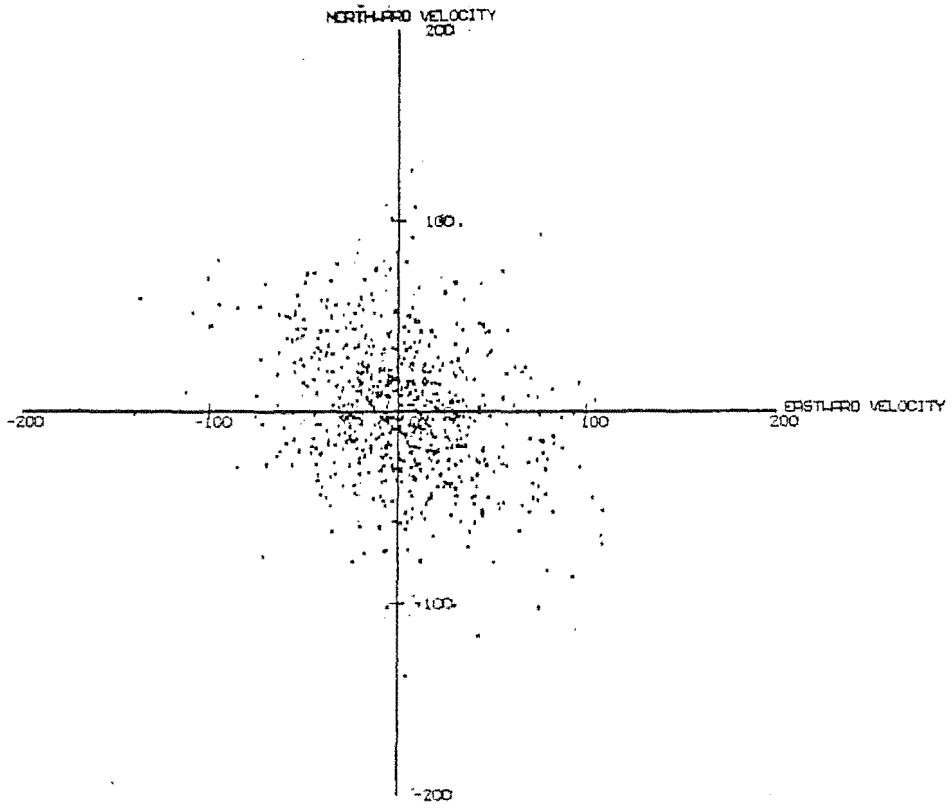

INDIVIDUAL DRIFT READINGS FOR PERIODS OF LESS THAN 3 HOURS IN APRIL 1981 AT 97.5KM.

Figure 8.1h)

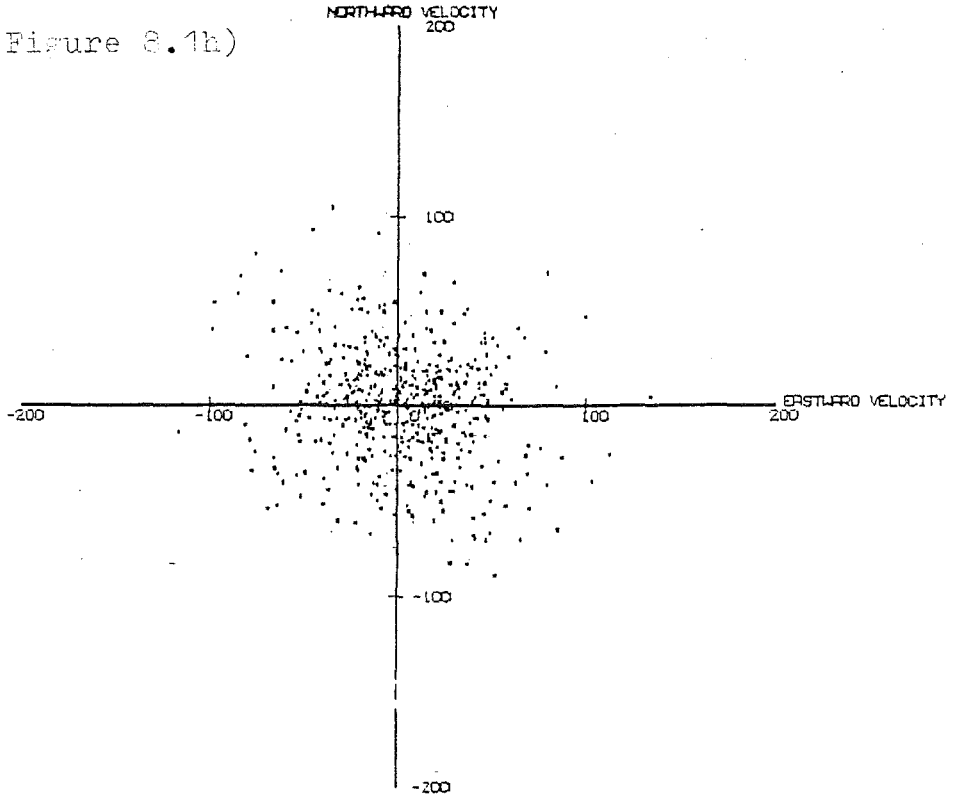

INDIVIDUAL DRIFT READINGS FOR PERIODS OF LESS THAN 3 HOURS IN APRIL 1981 AT 100.0KM.

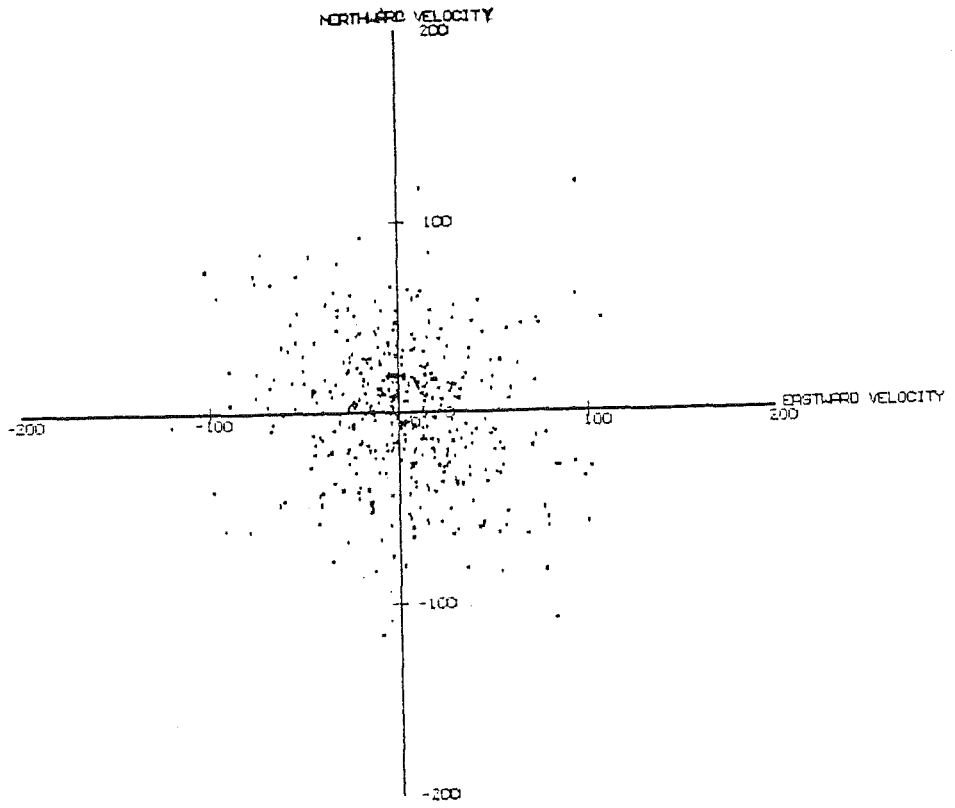

INDIVIDUAL DRIFT READINGS FOR PERIODS OF LESS THAN 3 HOURS IN APRIL 1981 AT 102.5KM.

Figure 8.2a)

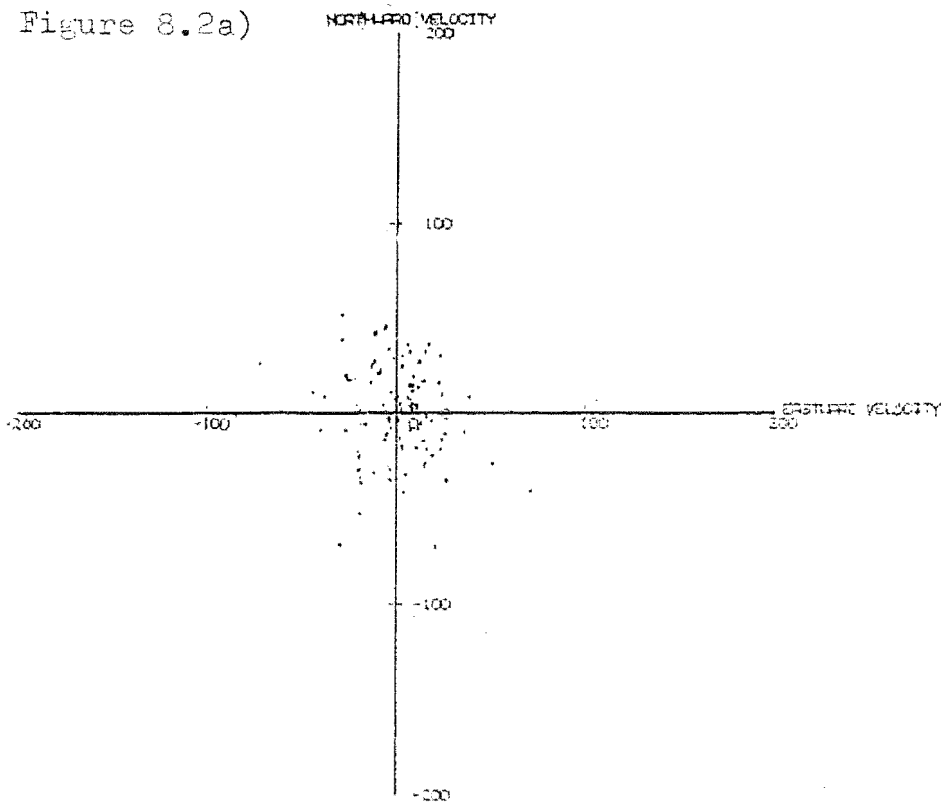

INDIVIDUAL DRIFT READINGS AT BIRDLINGS FLAT FOR PERIODS OF LESS THAN 3 HOURS IN OCTOBER 1981 AT AN ALTITUDE OF 85.0KM

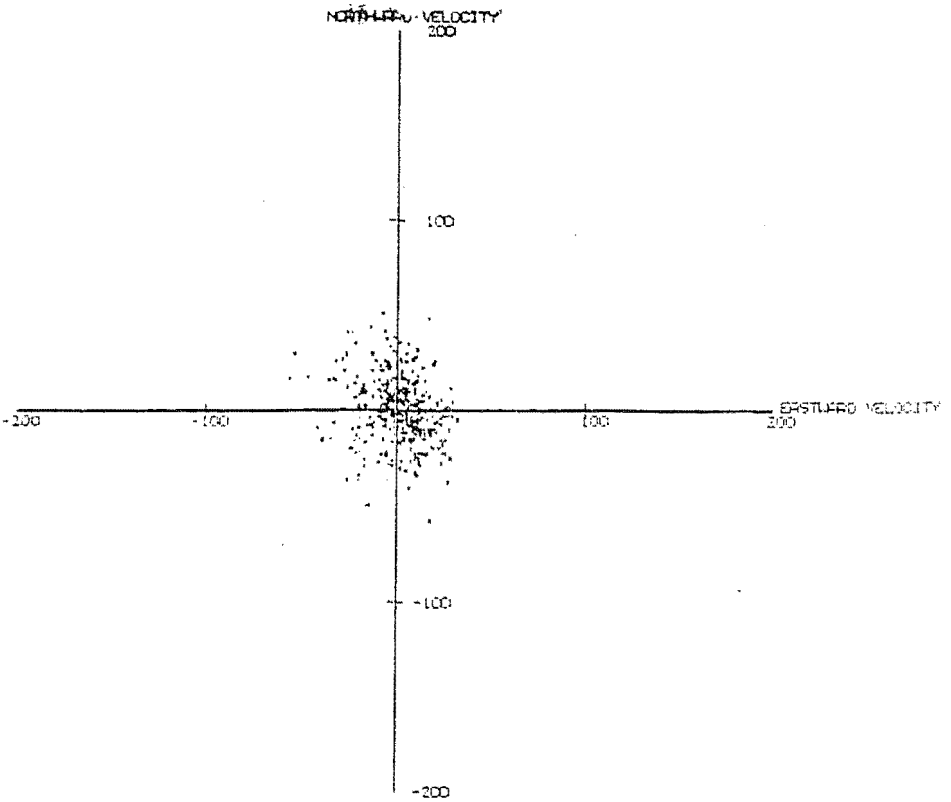

INDIVIDUAL DRIFT READINGS AT BIRDLINGS FLAT FOR PERIODS OF LESS THAN 3 HOURS IN OCTOBER 1981 AT AN ALTITUDE OF 87.5KM.

Figure 8.2b)

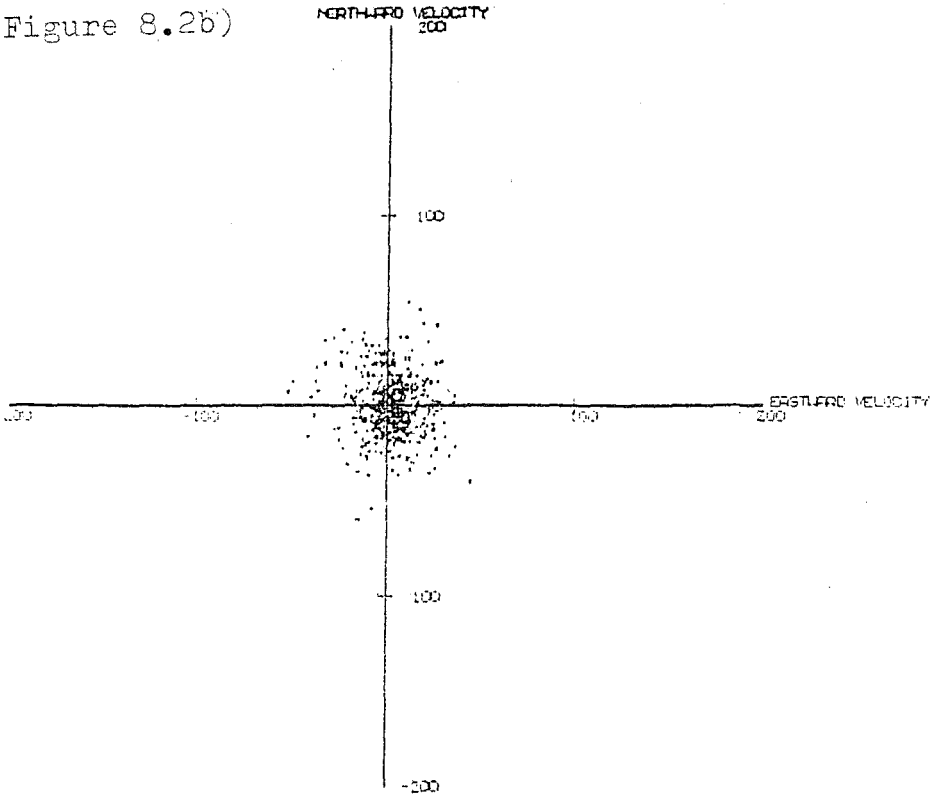

INDIVIDUAL DRIFT READINGS AT BIRDLINGS FLAT FOR PERIODS OF LESS THAN 3 HOURS IN OCTOBER 1981 AT AN ALTITUDE OF 70.0KM.

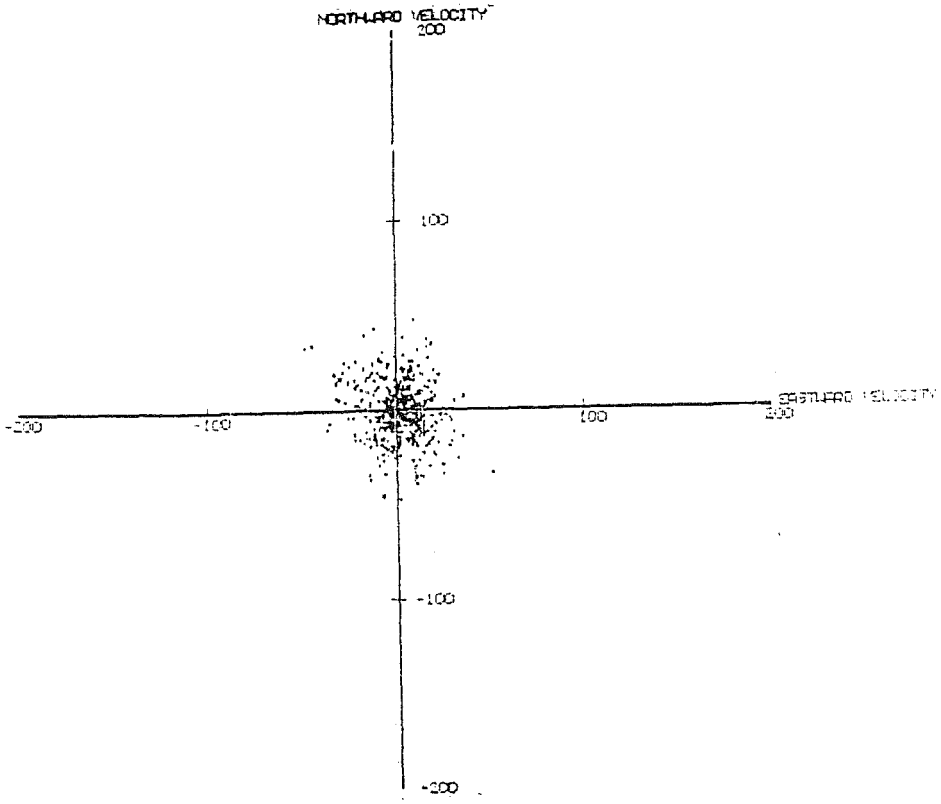

INDIVIDUAL DRIFT READINGS AT BIRDLINGS FLAT FOR PERIODS OF LESS THAN 3 HOURS IN OCTOBER 1981 AT AN ALTITUDE OF 72.5KM.

Figure 8.2c)

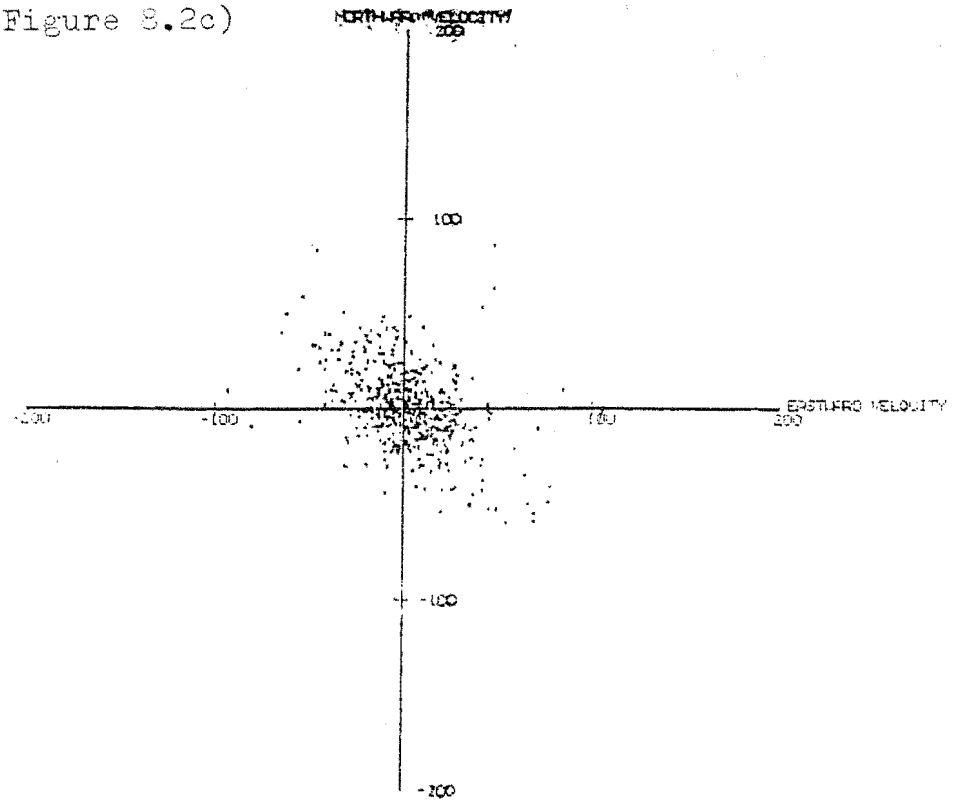

INDIVIDUAL DRIFT READINGS AT BIRDLINGS FLAT FOR PERIODS OF LESS THAN 3 HOURS IN OCTOBER 1981 AT AN ALTITUDE OF 80.0KM.

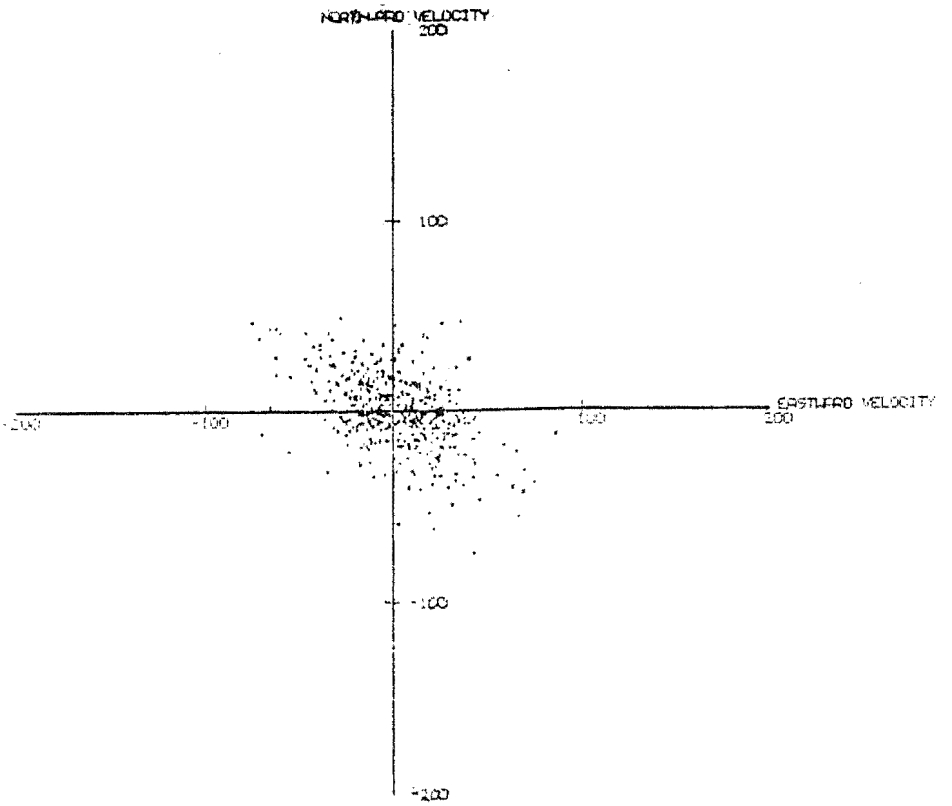

INDIVIDUAL DRIFT READINGS AT BIRDLINGS FLAT FOR PERIODS OF LESS THAN 3 HOURS IN OCTOBER 1981 AT AN ALTITUDE OF 82.5KM.

Figure 8.2d)

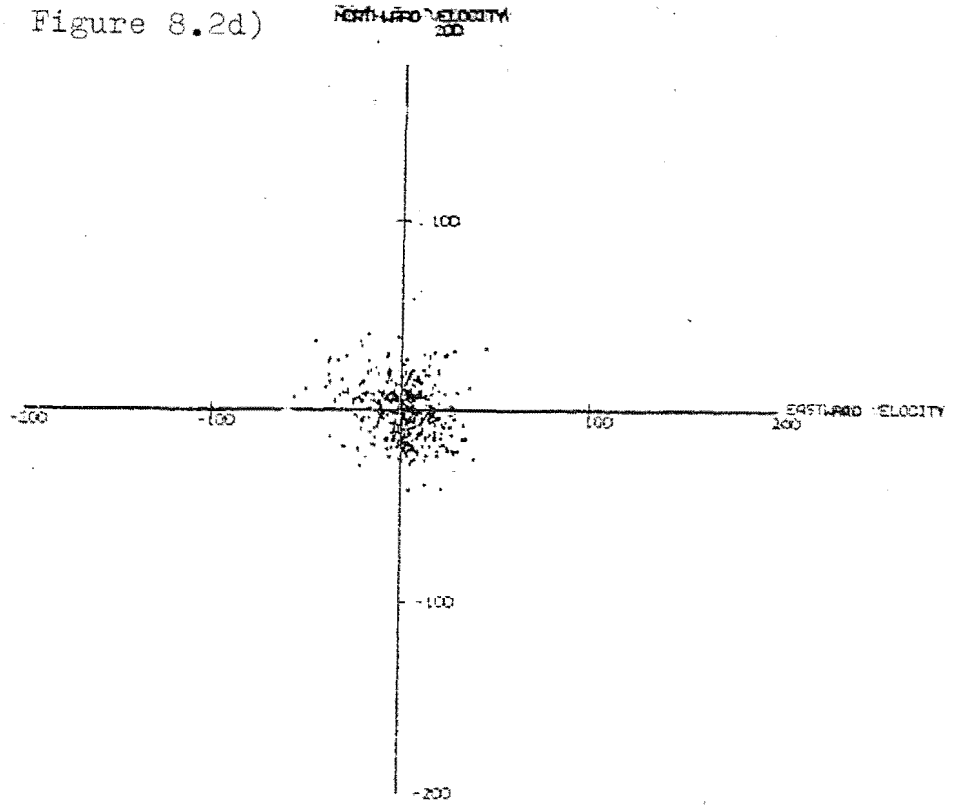

INDIVIDUAL DRIFT READINGS AT BIRDLINGS FLAT
FOR PERIODS OF LESS THAN 3 HOURS IN
OCTOBER 1981 AT AN ALTITUDE OF 75.0KM.

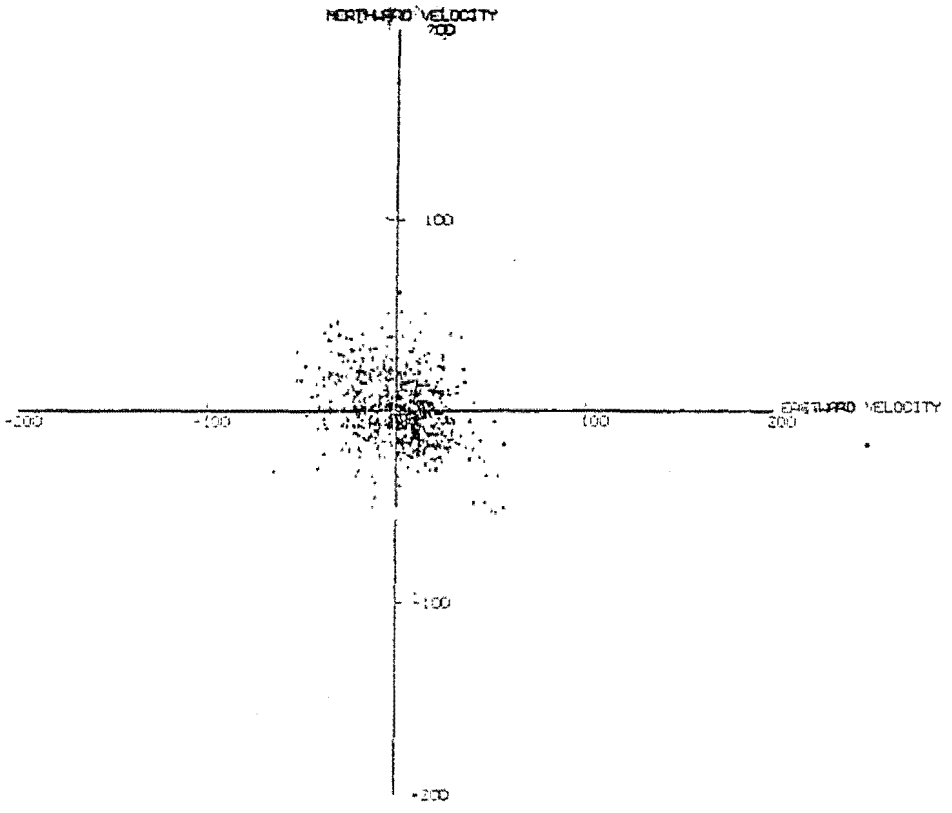

INDIVIDUAL DRIFT READINGS AT BIRDLINGS FLAT
FOR PERIODS OF LESS THAN 3 HOURS IN
OCTOBER 1981 AT AN ALTITUDE OF 77.5KM.

Figure 8.2e)

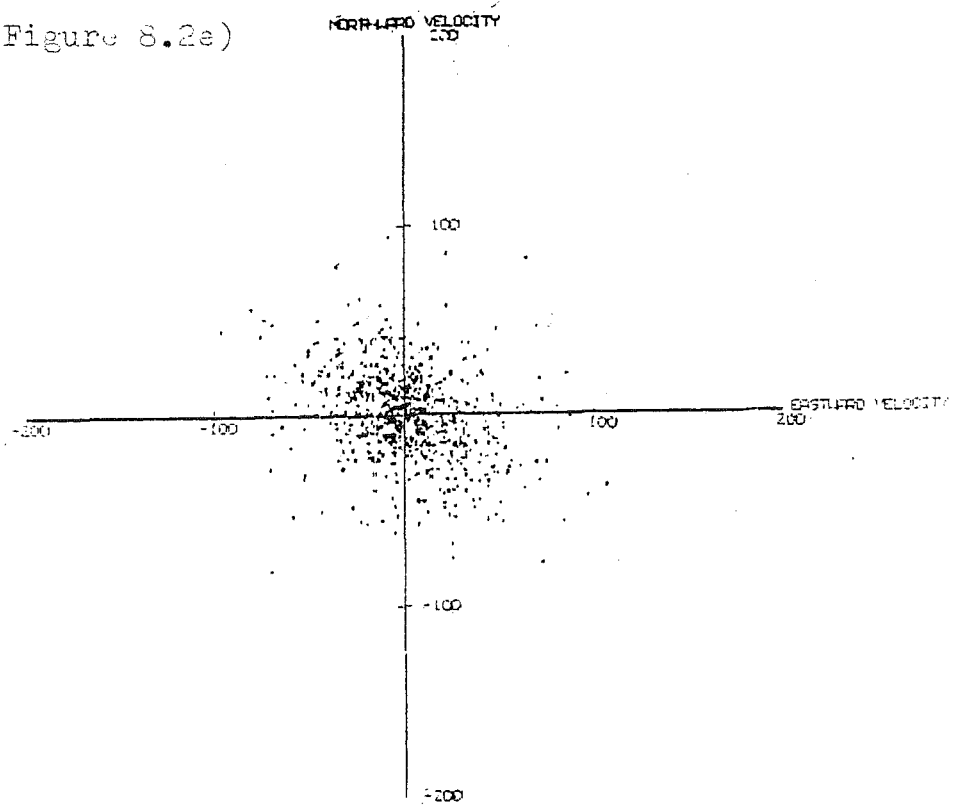

INDIVIDUAL DRIFT READINGS AT BIRDLINGS FLAT FOR PERIODS OF LESS THAN 3 HOURS IN OCTOBER 1981 AT AN ALTITUDE OF 85.00M.

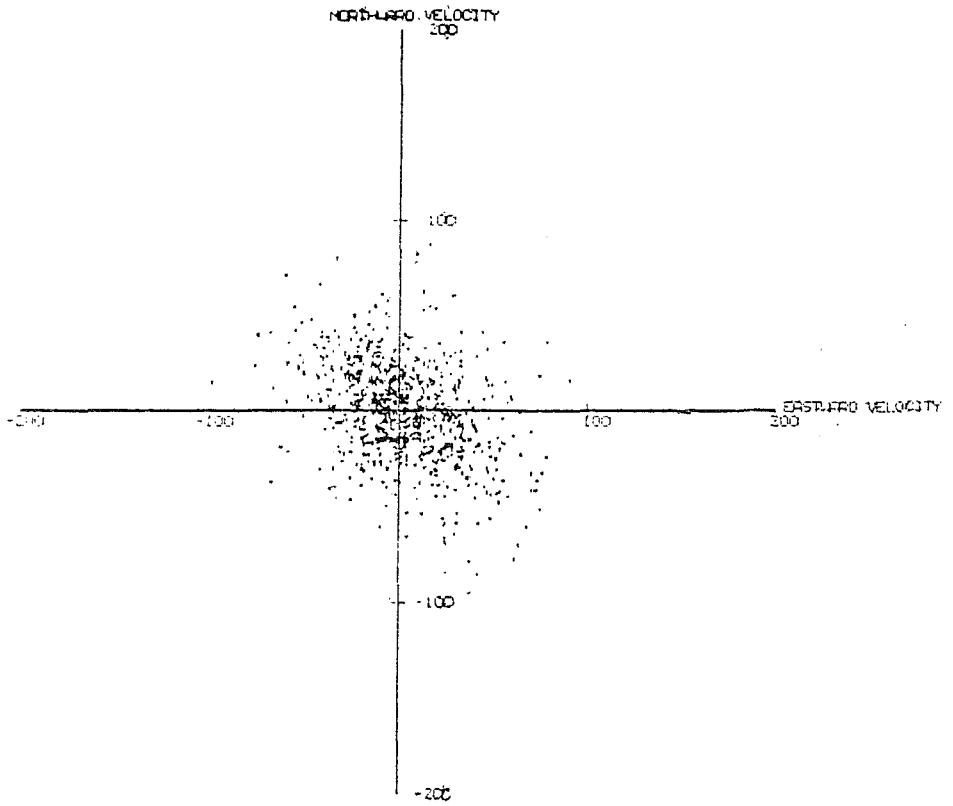

INDIVIDUAL DRIFT READINGS AT BIRDLINGS FLAT FOR PERIODS OF LESS THAN 3 HOURS IN OCTOBER 1981 AT AN ALTITUDE OF 87.50M.

Figure 8.2f)

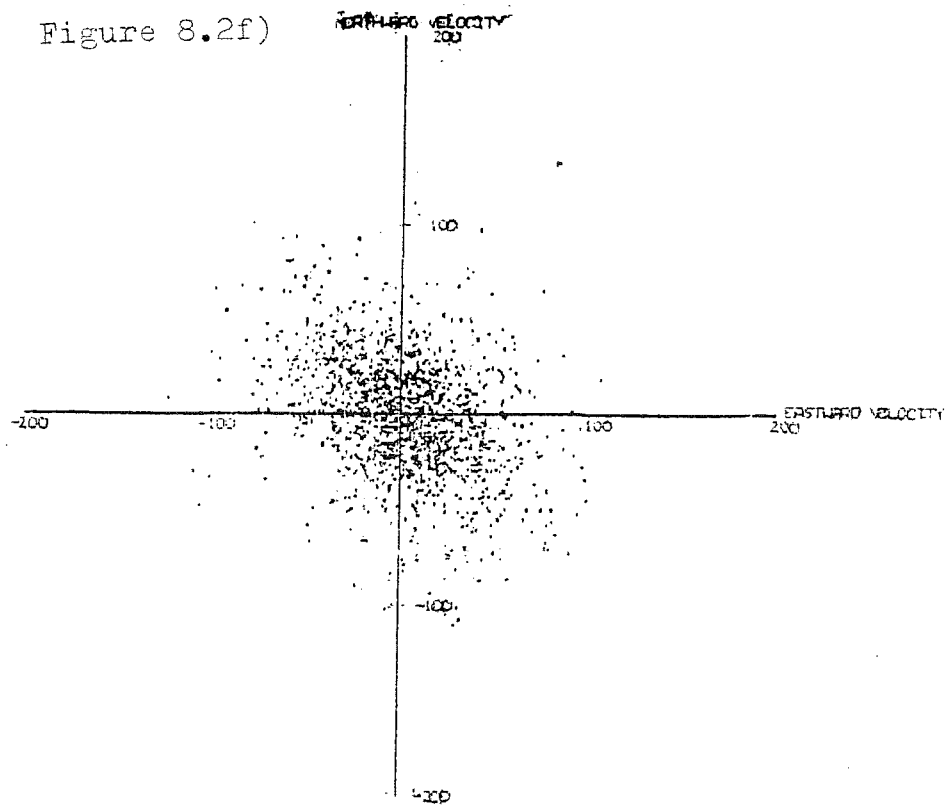

INDIVIDUAL DRIFT READINGS AT BIRDLINGS FLAT FOR PERIODS OF LESS THAN 3 HOURS IN OCTOBER 1981 AT AN ALTITUDE OF 30.0KM.

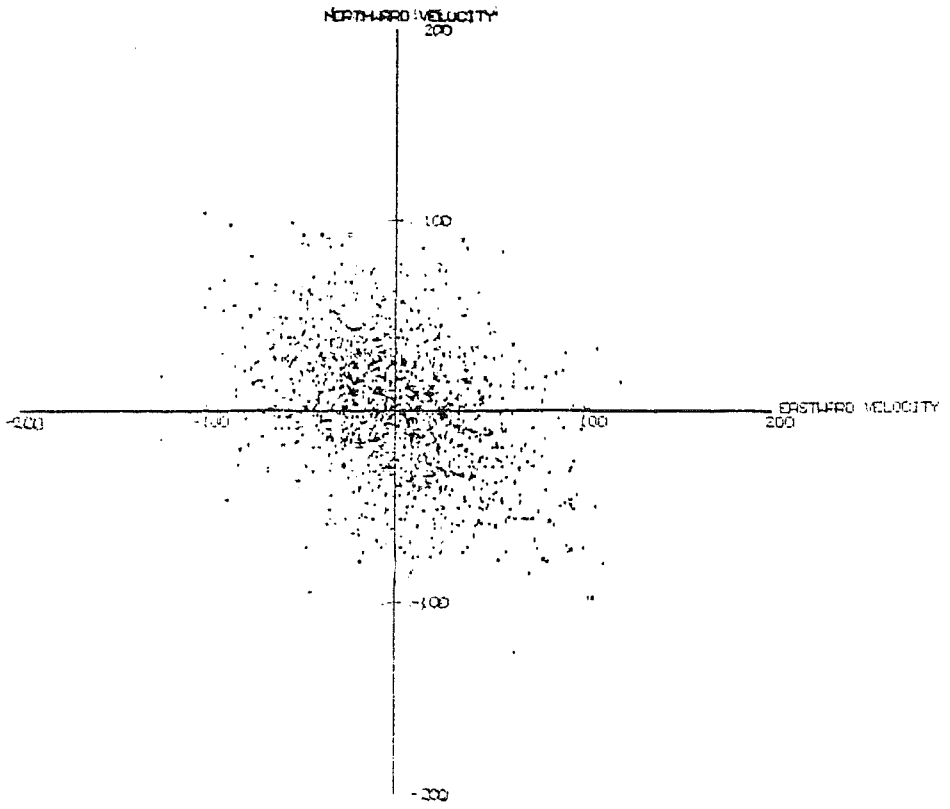

INDIVIDUAL DRIFT READINGS AT BIRDLINGS FLAT FOR PERIODS OF LESS THAN 3 HOURS IN OCTOBER 1981 AT AN ALTITUDE OF 92.5KM.

Figure 8.2g)

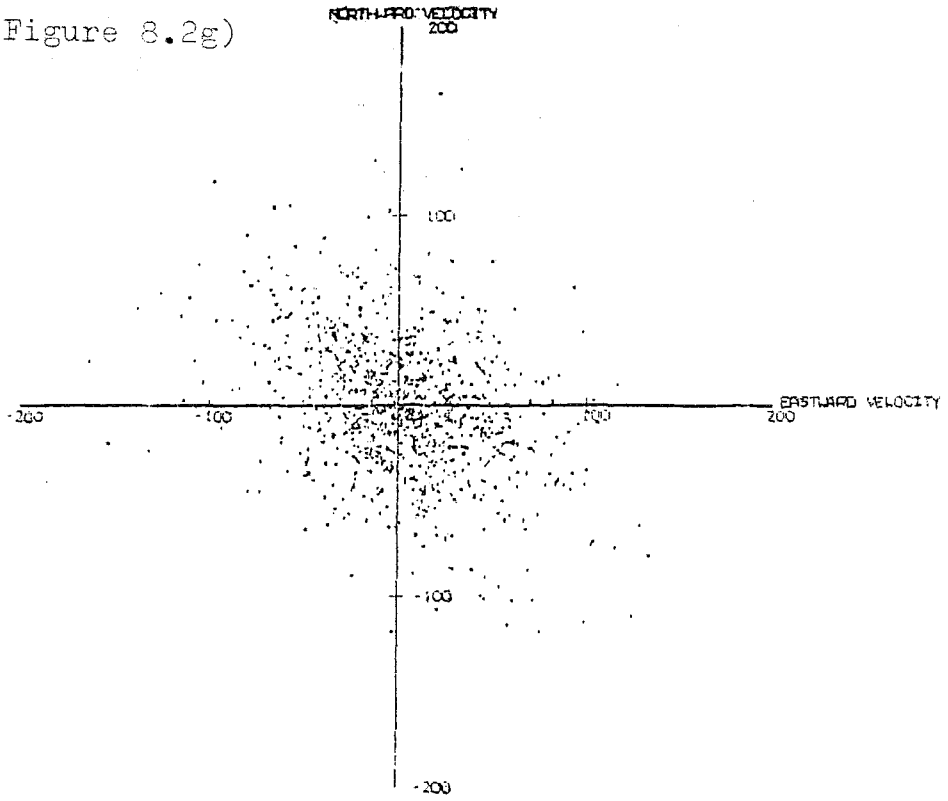

INDIVIDUAL DRIFT READINGS AT BIRDLINGS FLAT
FOR PERIODS OF LESS THAN 3 HOURS IN
OCTOBER 1981 AT AN ALTITUDE OF 95.0KM

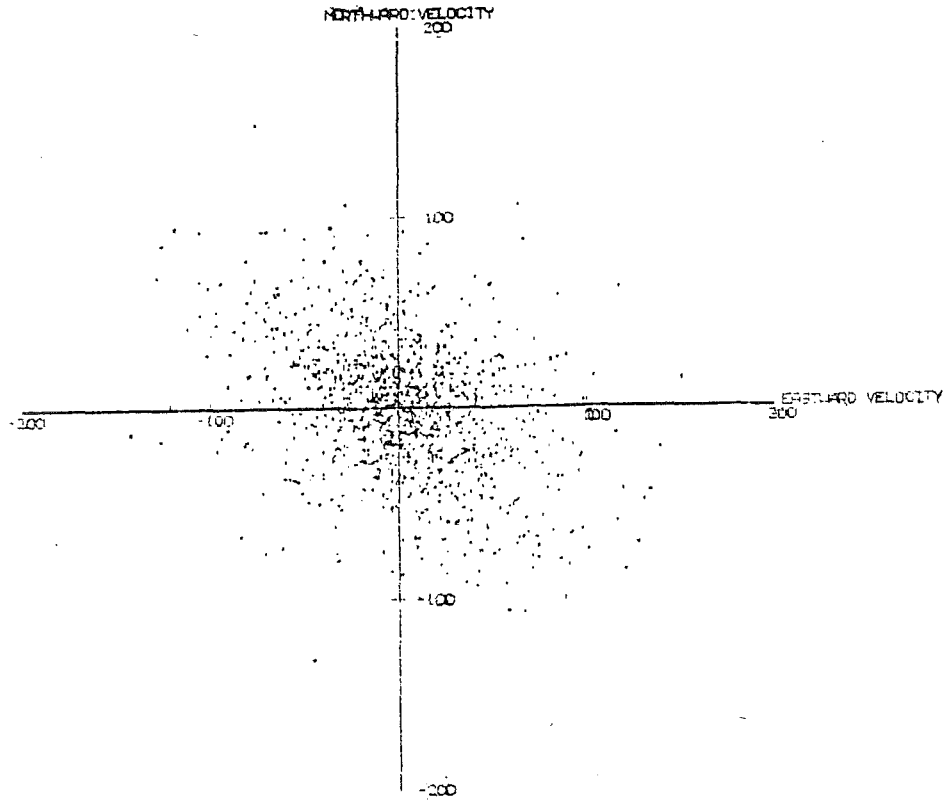

INDIVIDUAL DRIFT READINGS AT BIRDLINGS FLAT
FOR PERIODS OF LESS THAN 3 HOURS IN
OCTOBER 1981 AT AN ALTITUDE OF 97.5KM.

Figure 8.2h)

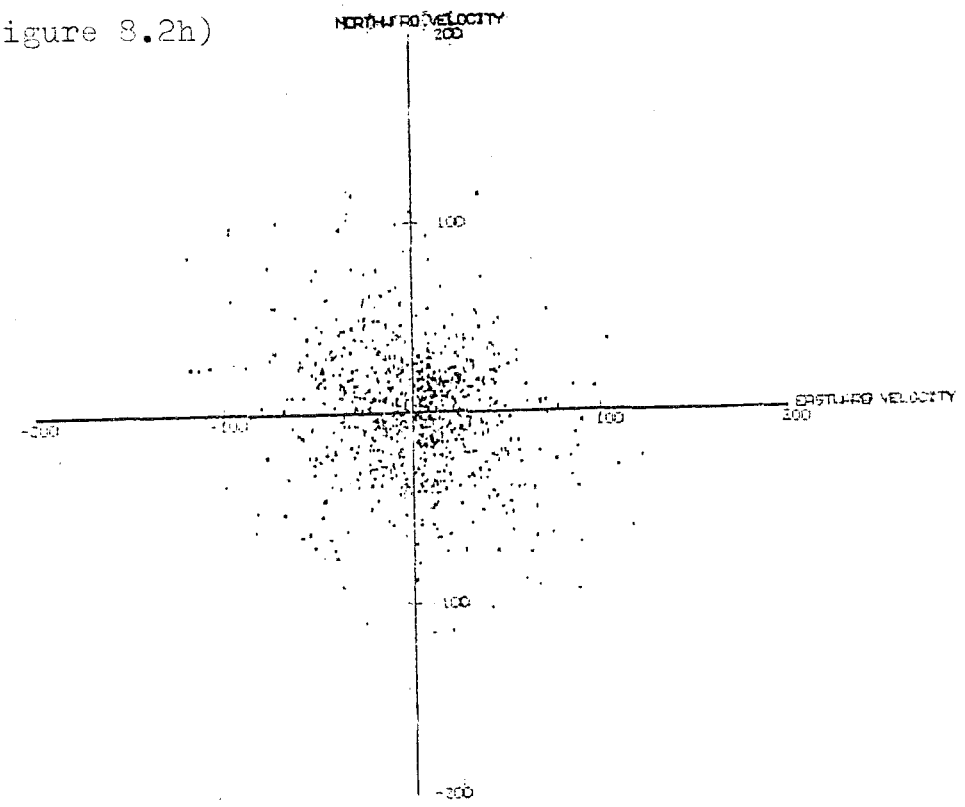

INDIVIDUAL DRIFT READINGS AT BIRDLINGS FLAT FOR PERIODS OF LESS THAN 3 HOURS IN OCTOBER 1981 AT AN ALTITUDE OF 100.0KM.

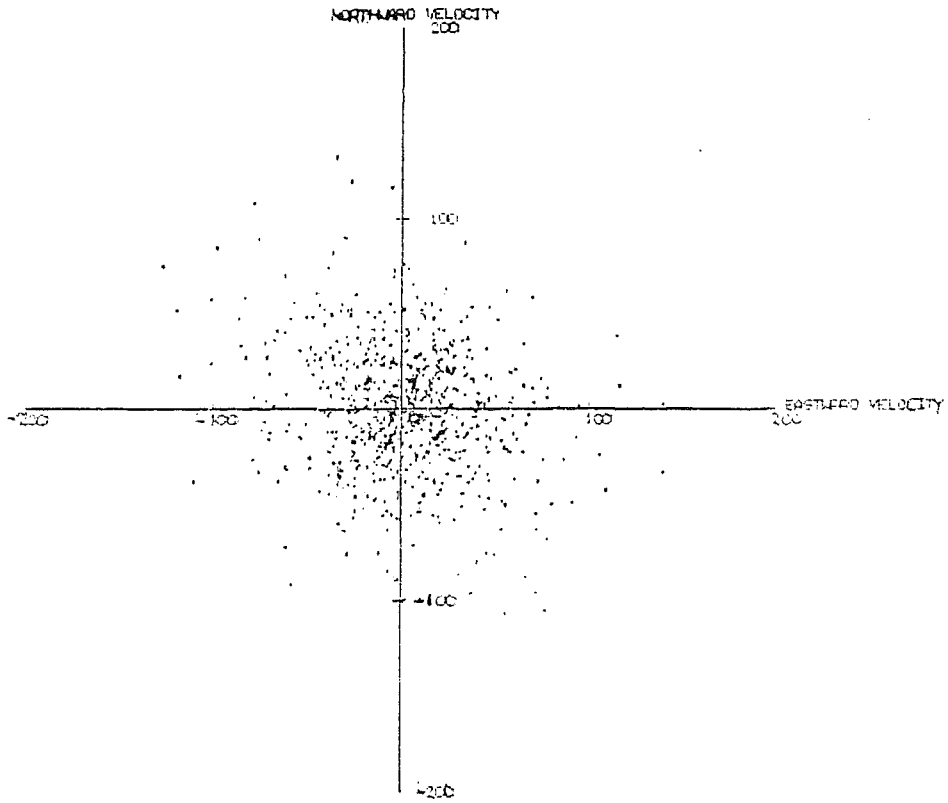

INDIVIDUAL DRIFT READINGS AT BIRDLINGS FLAT FOR PERIODS OF LESS THAN 3 HOURS IN OCTOBER 1981 AT AN ALTITUDE OF 102.5KM.

Figure 8.3a)

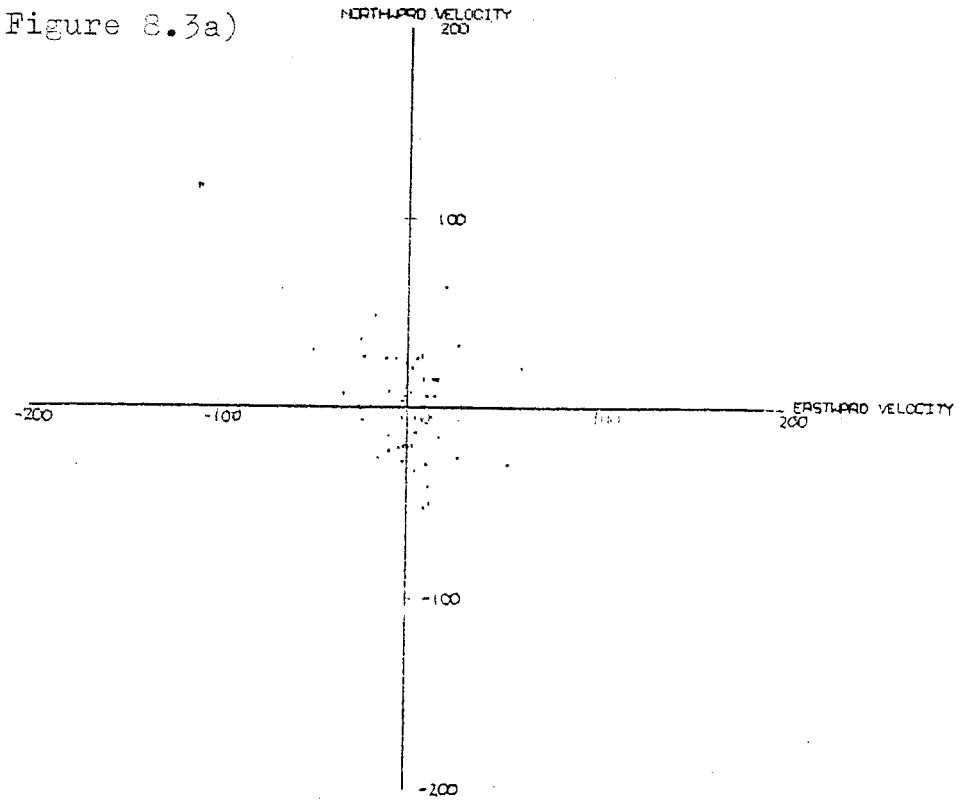

INDIVIDUAL DRIFT READINGS AT BIRDLINGS FLAT
FOR PERIODS OF LESS THAN 3 HOURS IN
JULY 1981 AT AN ALTITUDE OF 65.0KM.

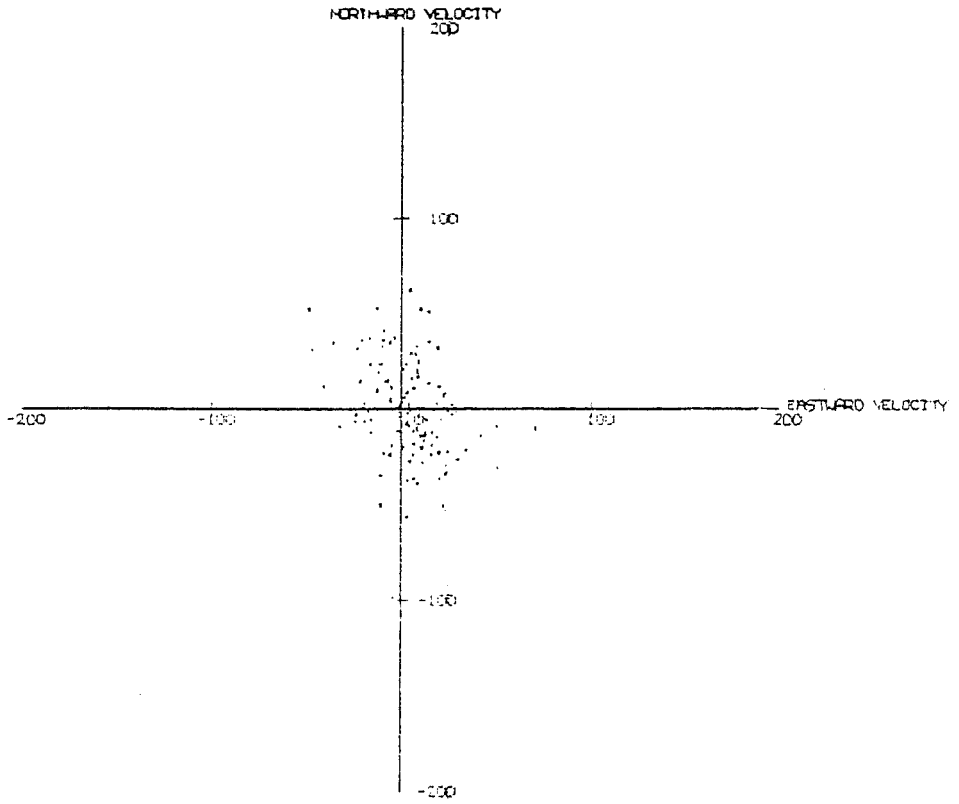

INDIVIDUAL DRIFT READINGS AT BIRDLINGS FLAT
FOR PERIODS OF LESS THAN 3 HOURS IN
JULY 1981 AT AN ALTITUDE OF 67.5KM.

Figure 8.3b)

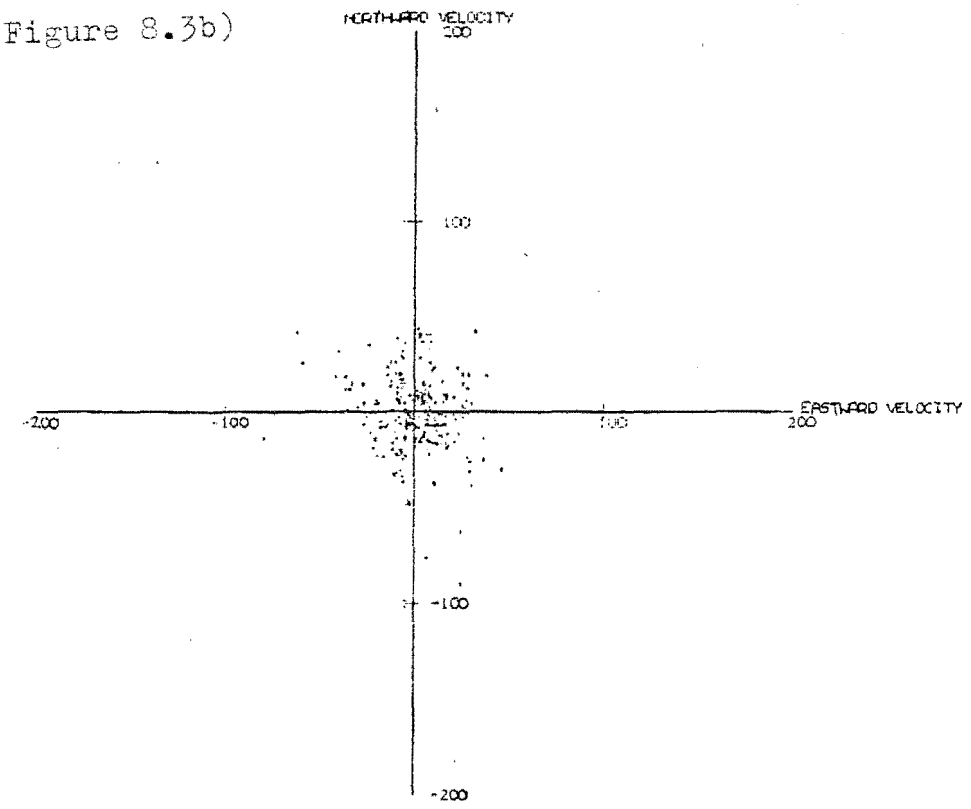

INDIVIDUAL DRIFT READINGS AT SIRDLINGS FLAT
FOR PERIODS OF LESS THAN 3 HOURS IN
JULY 1981 AT AN ALTITUDE OF 70.0KM.

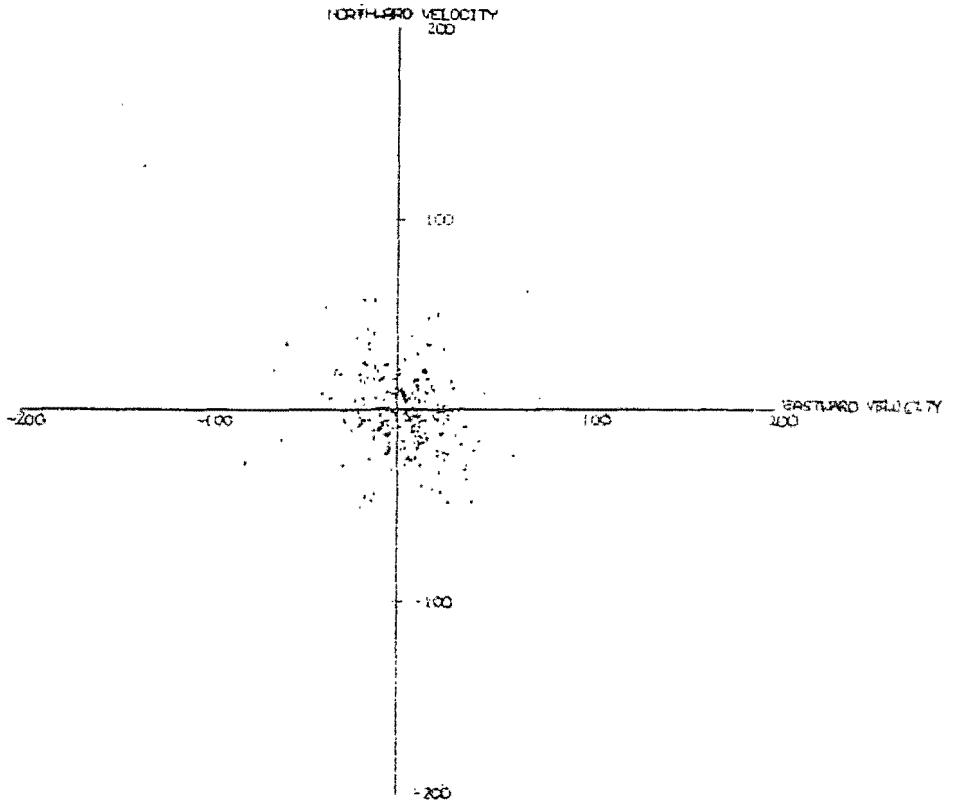

INDIVIDUAL DRIFT READINGS AT SIRDLINGS FLAT
FOR PERIODS OF LESS THAN 3 HOURS IN
JULY 1981 AT AN ALTITUDE OF 72.5KM.

Figure 8.3c)

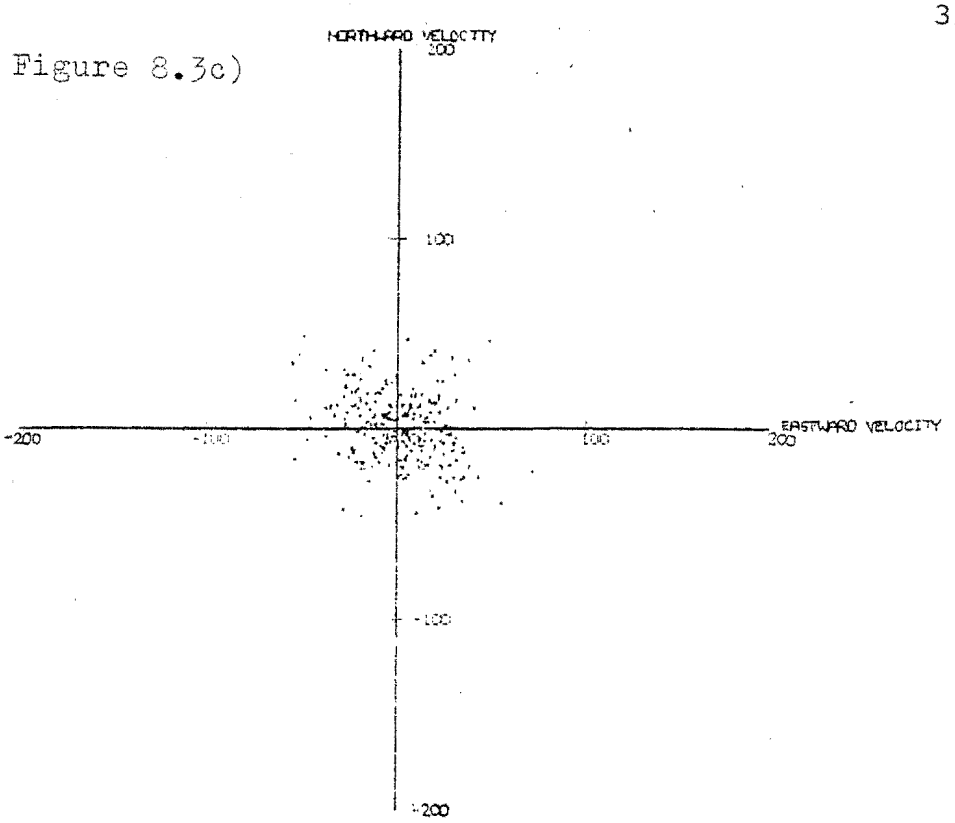

INDIVIDUAL DRIFT READINGS AT BIRDLINGE FLAT
FOR PERIODS OF LESS THAN 3 HOURS IN
JULY 1981 AT AN ALTITUDE OF 75.0km.

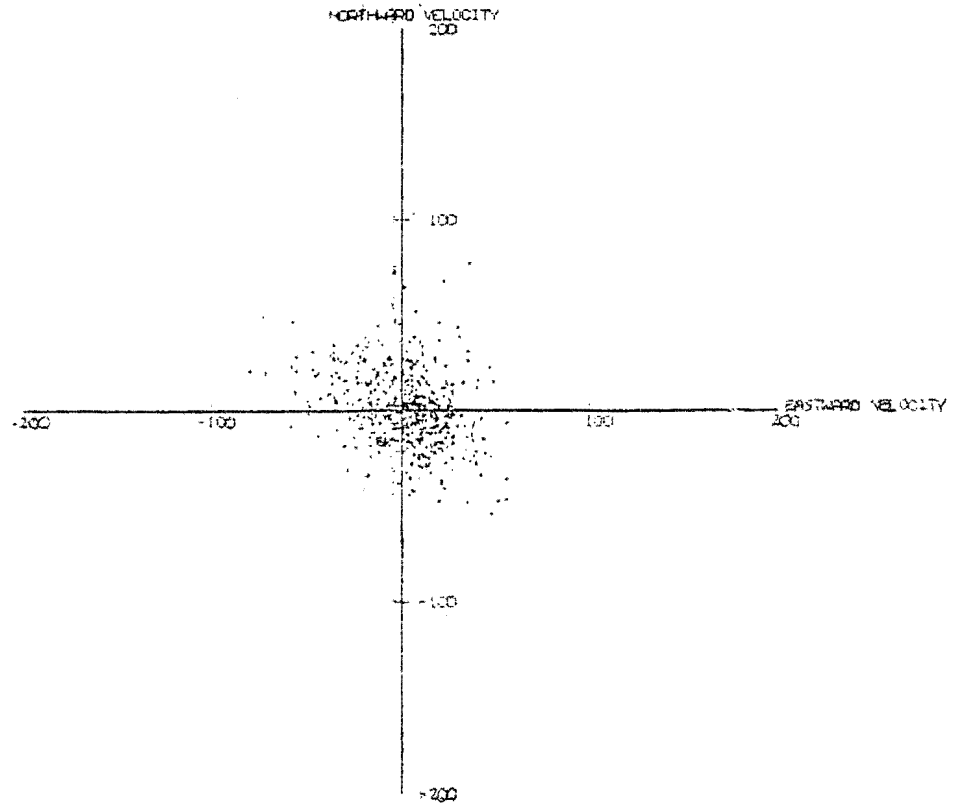

INDIVIDUAL DRIFT READINGS AT BIRDLINGE FLAT
FOR PERIODS OF LESS THAN 3 HOURS IN
JULY 1981 AT AN ALTITUDE OF 77.5km.

Figure 8.3d)

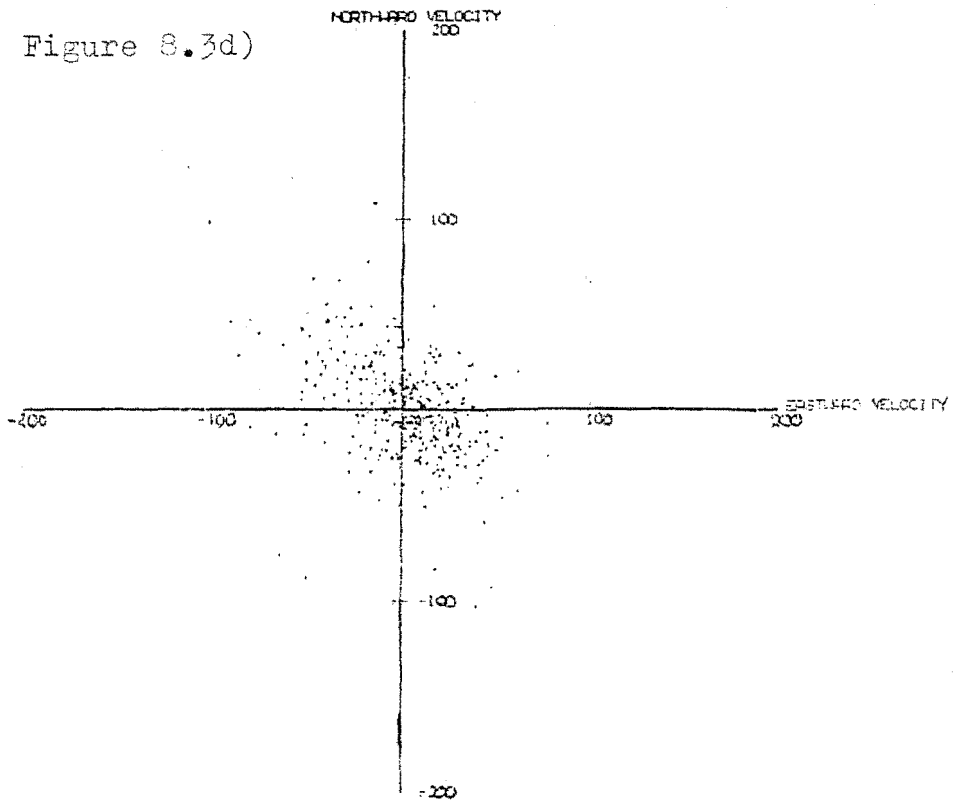

INDIVIDUAL DRIFT READINGS AT BIRDLINGS FLAT FOR PERIODS OF LESS THAN 3 HOURS IN JULY 1981 AT AN ALTITUDE OF 80.0KM.

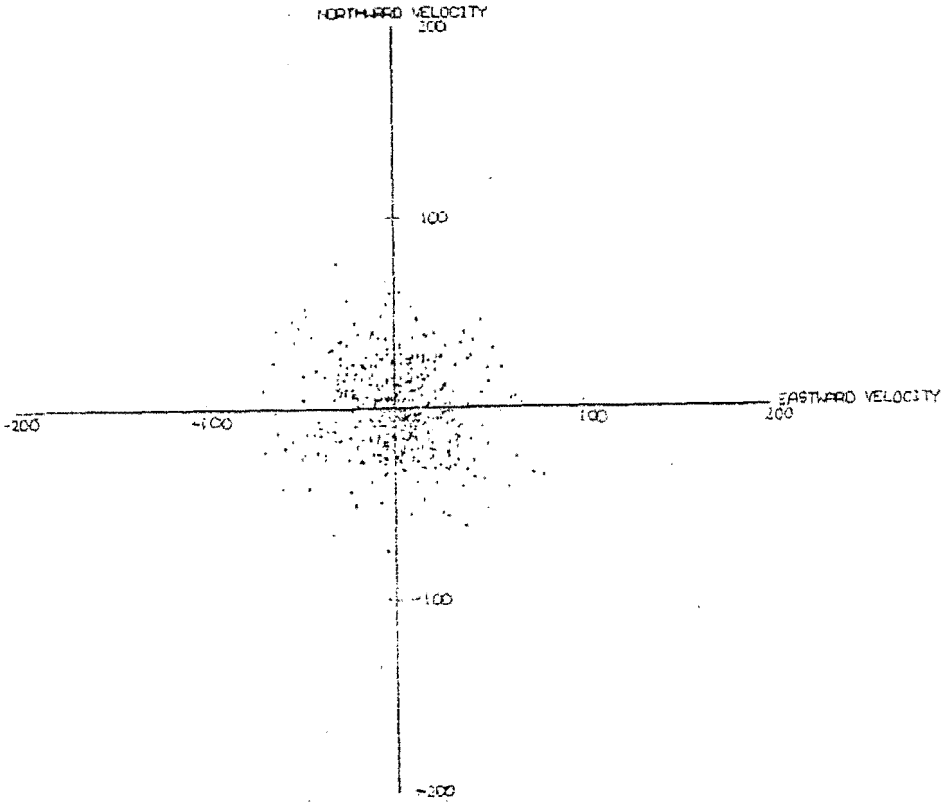

INDIVIDUAL DRIFT READINGS AT BIRDLINGS FLAT FOR PERIODS OF LESS THAN 3 HOURS IN JULY 1981 AT AN ALTITUDE OF 82.5KM.

Figure 8.3e)

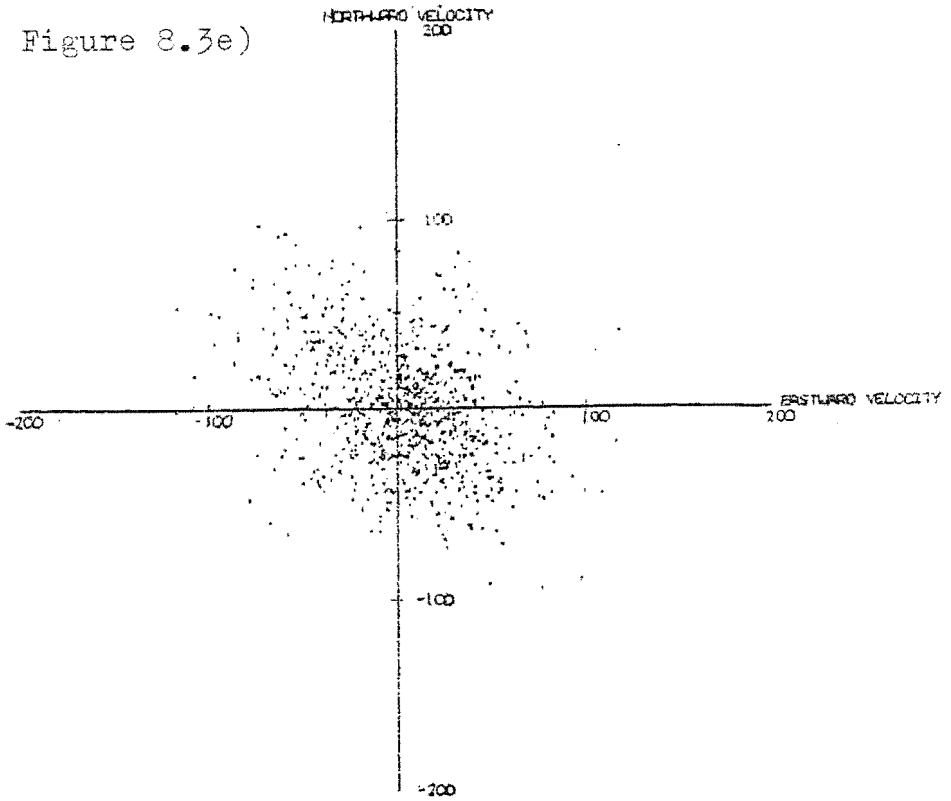

INDIVIDUAL DRIFT READINGS AT BIRDLINGS FLAT
FOR PERIODS OF LESS THAN 3 HOURS IN
JULY 1981 AT AN ALTITUDE OF 85.0KM.

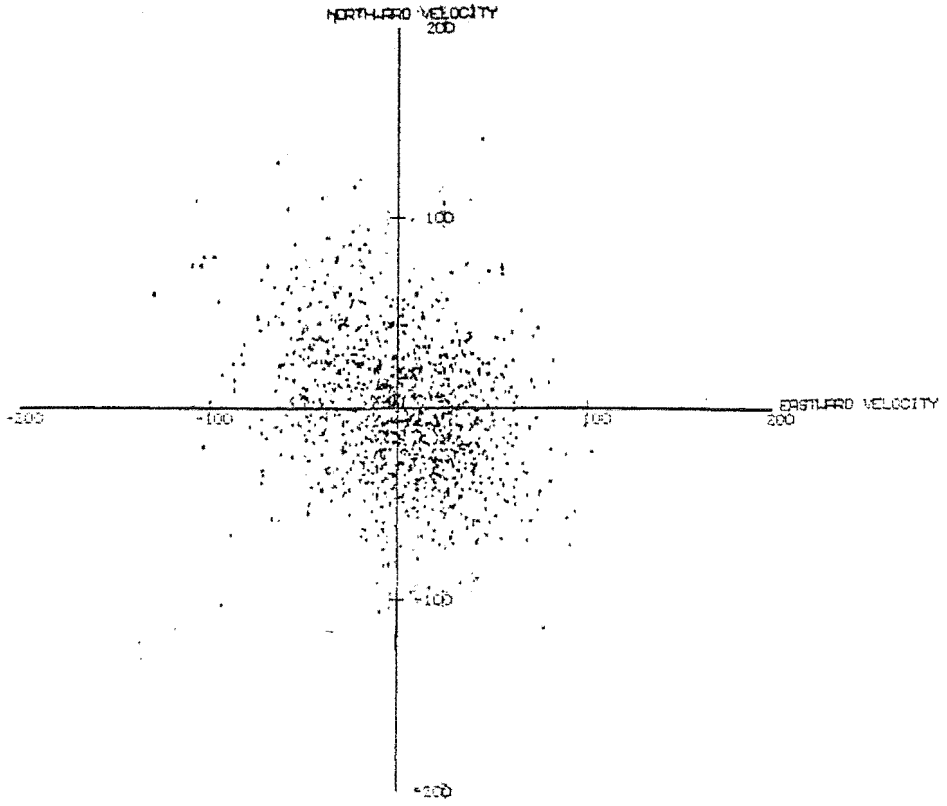

INDIVIDUAL DRIFT READINGS AT BIRDLINGS FLAT
FOR PERIODS OF LESS THAN 3 HOURS IN
JULY 1981 AT AN ALTITUDE OF 87.5KM.

Figure 8.3f)

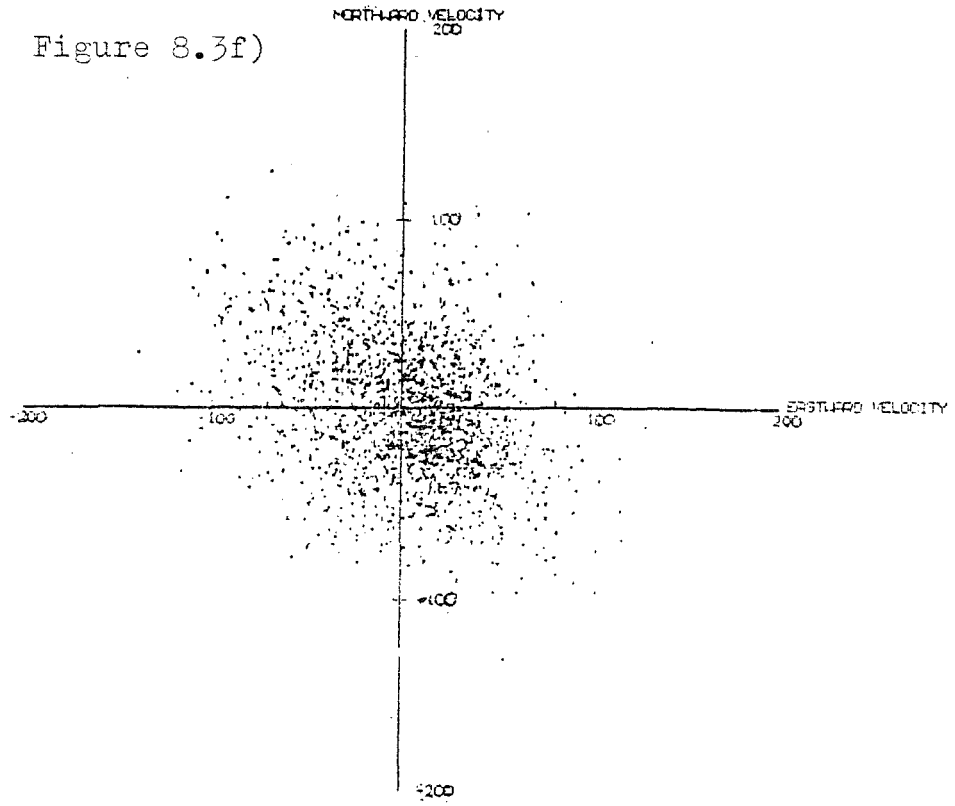

INDIVIDUAL DRIFT READINGS AT SIRDLINGE FLAT FOR PERIODS OF LESS THAN 3 HOURS IN JULY 1981 AT AN ALTITUDE OF 90.0KM.

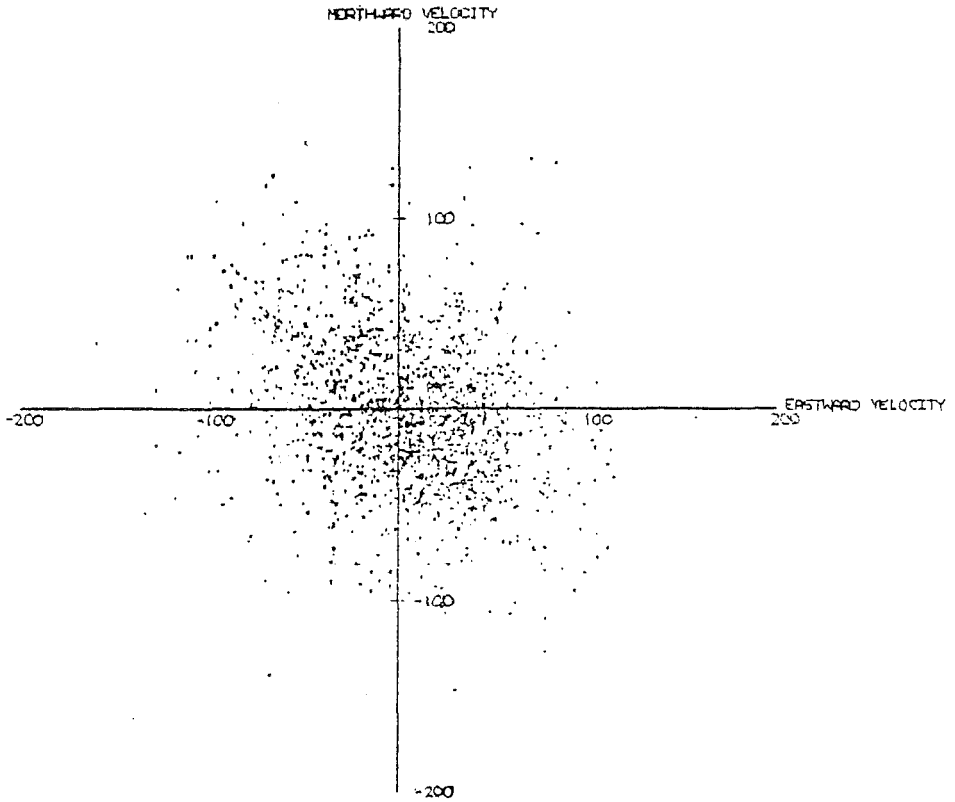

INDIVIDUAL DRIFT READINGS AT SIRDLINGE FLAT FOR PERIODS OF LESS THAN 3 HOURS IN JULY 1981 AT AN ALTITUDE OF 92.5KM

Figure 8.3g)

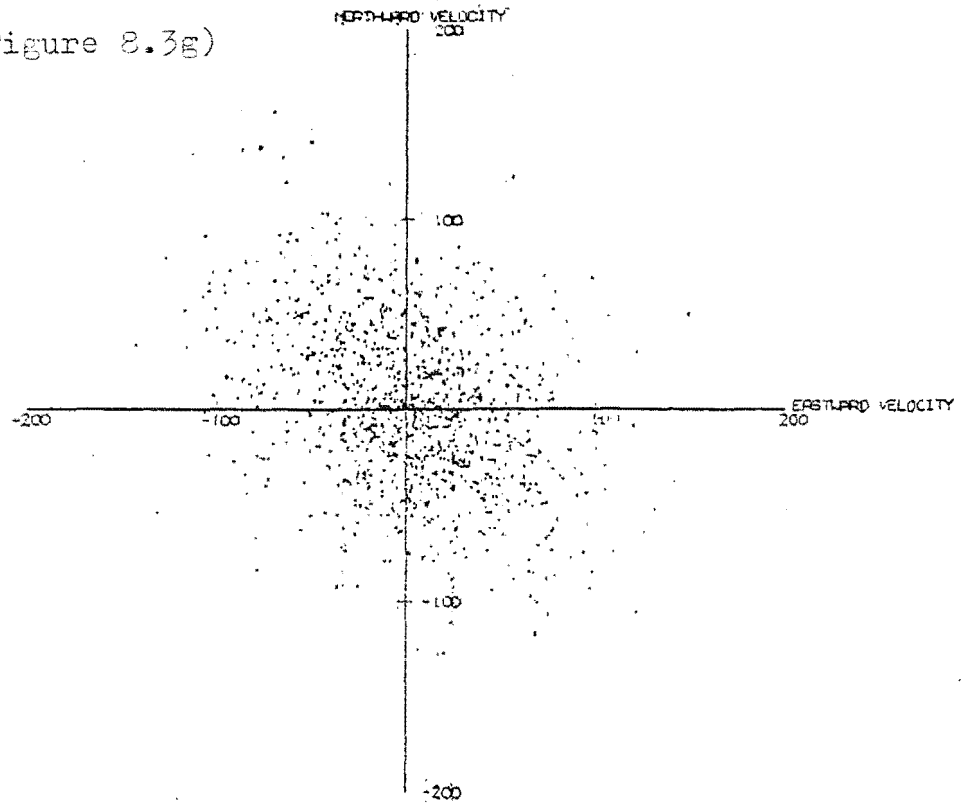

INDIVIDUAL DRIFT READINGS AT BIRCLINGS FLAT FOR PERIODS OF LESS THAN 3 HOURS IN JULY 1981 AT AN ALTITUDE OF 95.0KM.

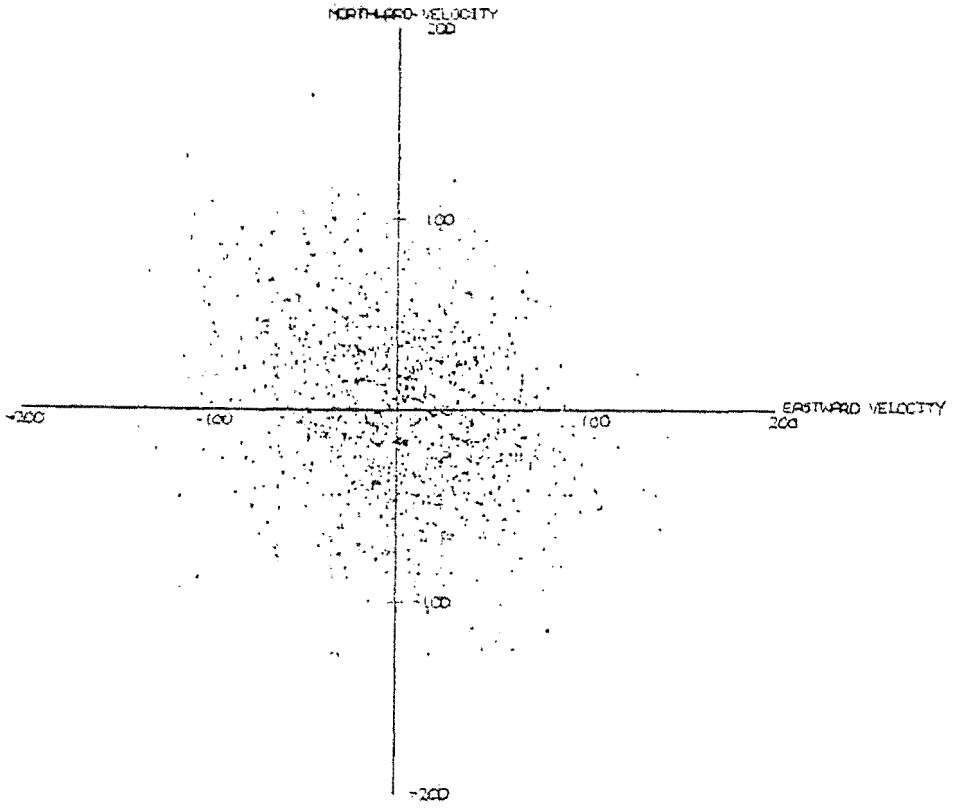

INDIVIDUAL DRIFT READINGS AT BIRCLINGS FLAT FOR PERIODS OF LESS THAN 3 HOURS IN JULY 1981 AT AN ALTITUDE OF 97.5KM.

Figure 8.3h)

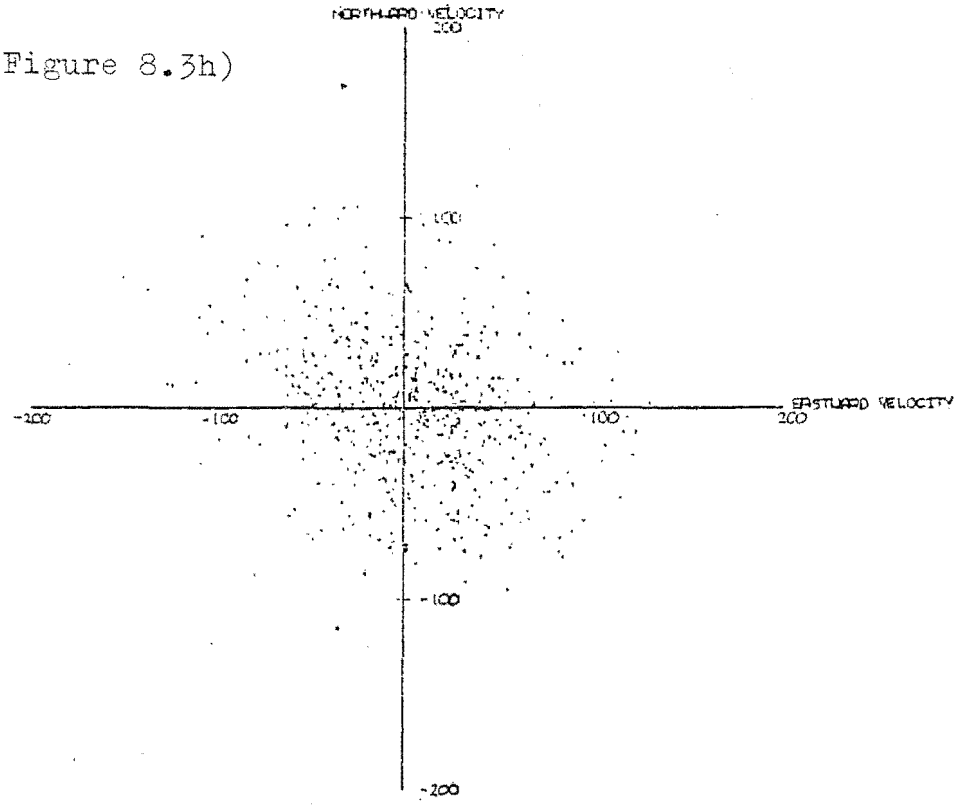

INDIVIDUAL DRIFT READINGS AT BIRDLINGS FLAT FOR PERIODS OF LESS THAN 3 HOURS IN JULY 1981 AT AN ALTITUDE OF 100.0KM.

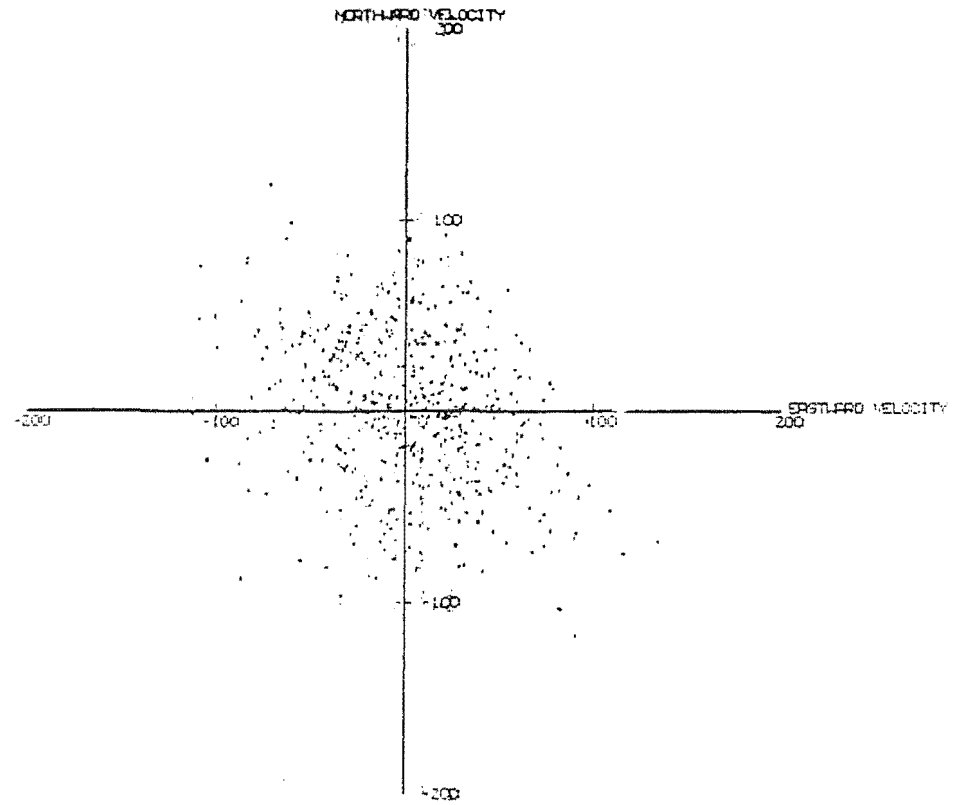

INDIVIDUAL DRIFT READINGS AT BIRDLINGS FLAT FOR PERIODS OF LESS THAN 3 HOURS IN JULY 1981 AT AN ALTITUDE OF 102.5KM.

Figure 8.4a)

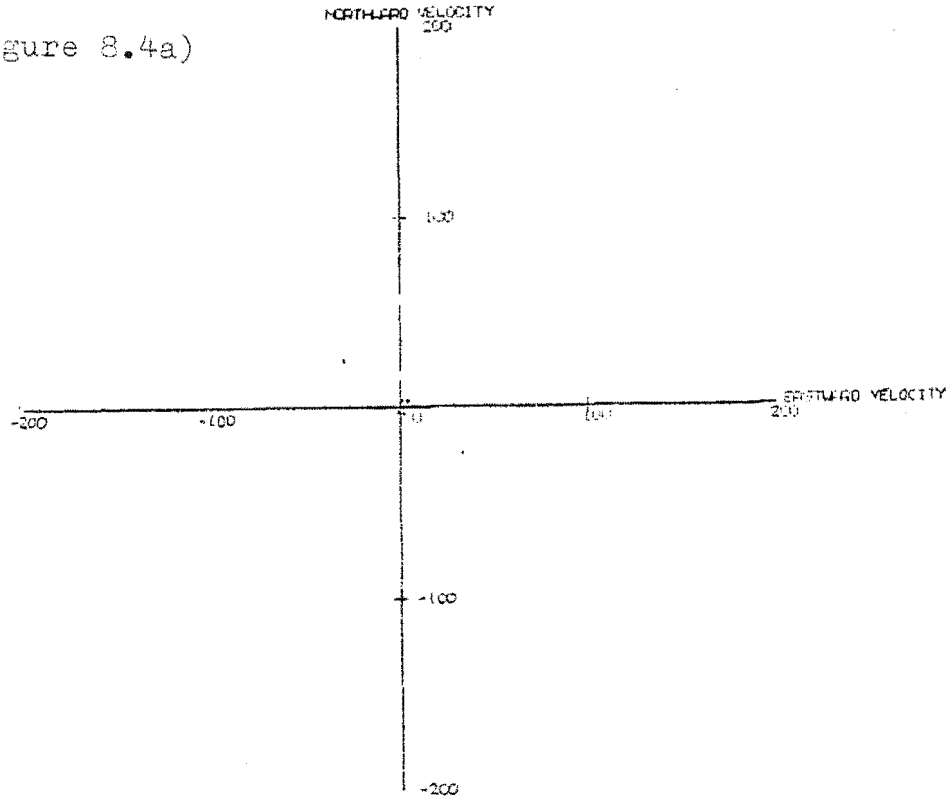

INDIVIDUAL DRIFT READINGS FOR PERIODS OF MORE THAN 3 HOURS IN FEBRUARY 1981 AT 55.0M.

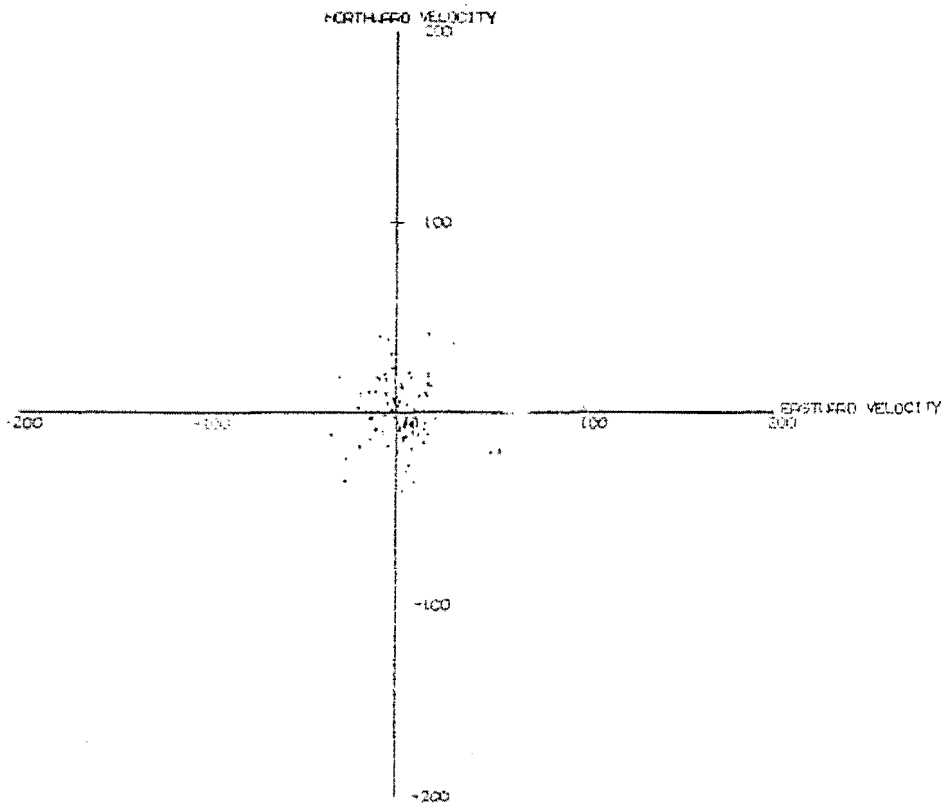

INDIVIDUAL DRIFT READINGS FOR PERIODS OF MORE THAN 3 HOURS IN FEBRUARY 1981 AT 67.5M.

Figure 8.4b)

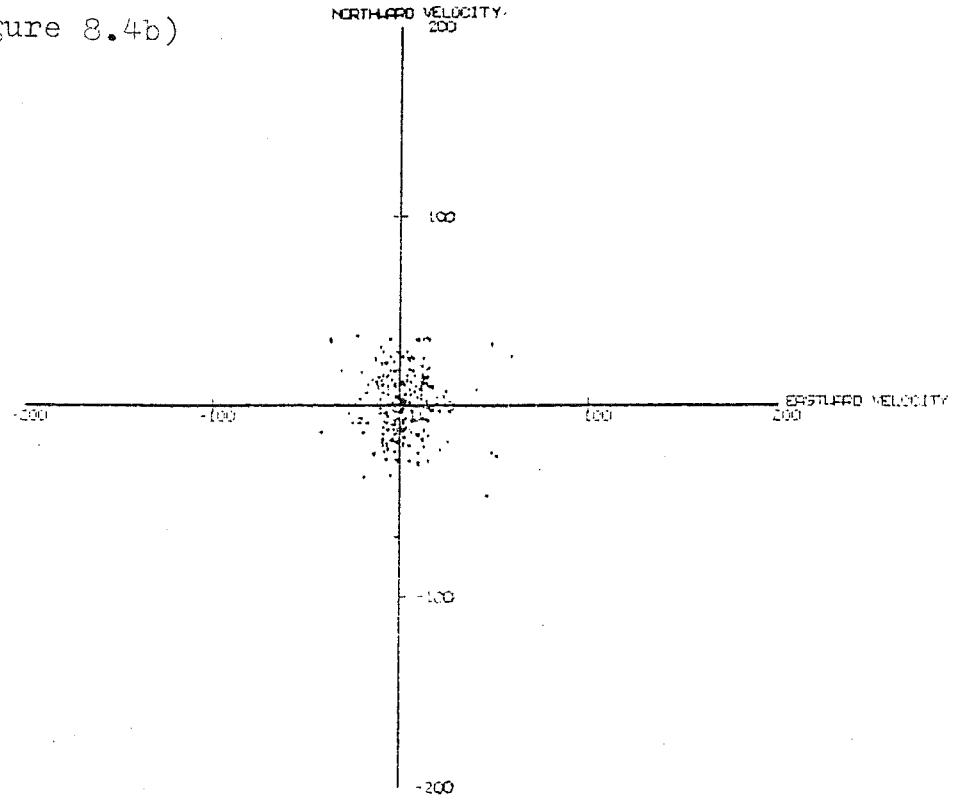

INDIVIDUAL DRIFT READINGS FOR PERIODS OF MORE THAN 3 HOURS IN JANUARY 1981 AT 70.0KM.

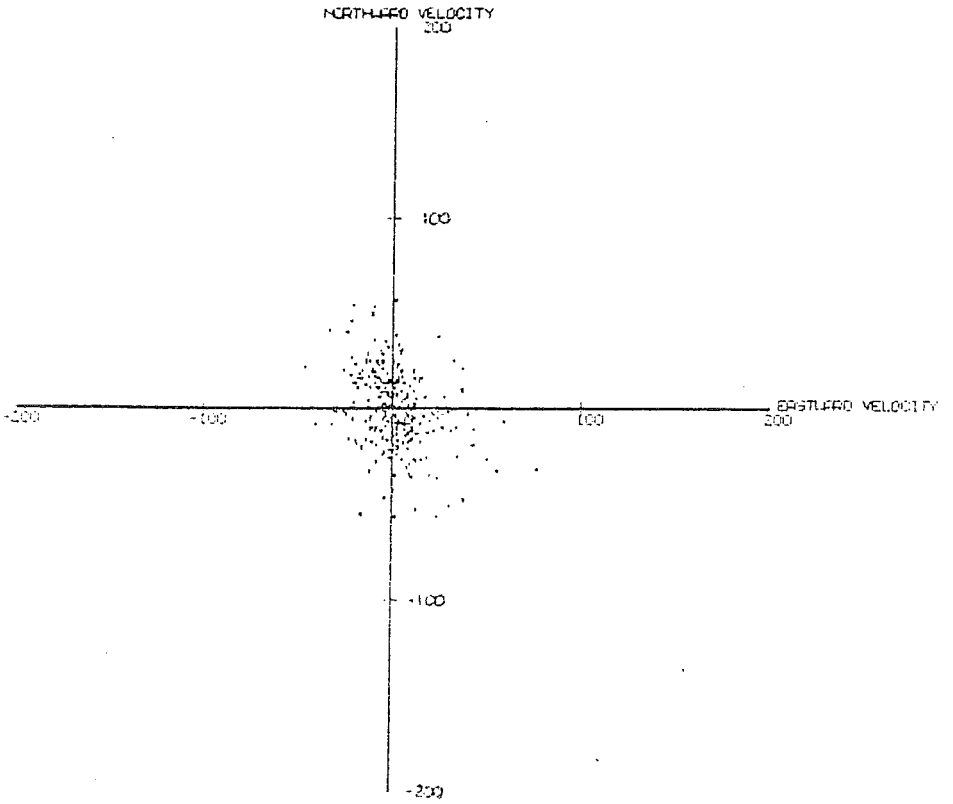

INDIVIDUAL DRIFT READINGS FOR PERIODS OF MORE THAN 3 HOURS IN JANUARY 1981 AT 72.5KM.

Figure 8.4c)

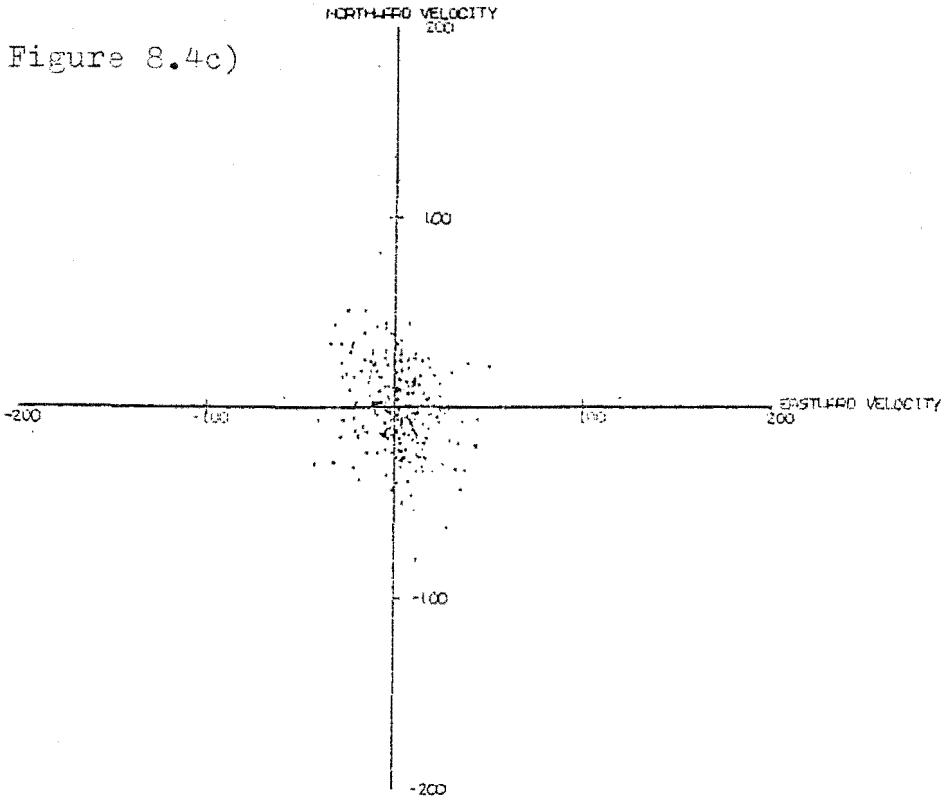

INDIVIDUAL DRIFT READINGS FOR PERIODS OF MORE THAN 3 HOURS IN JANUARY 1981 AT 75.0KM.

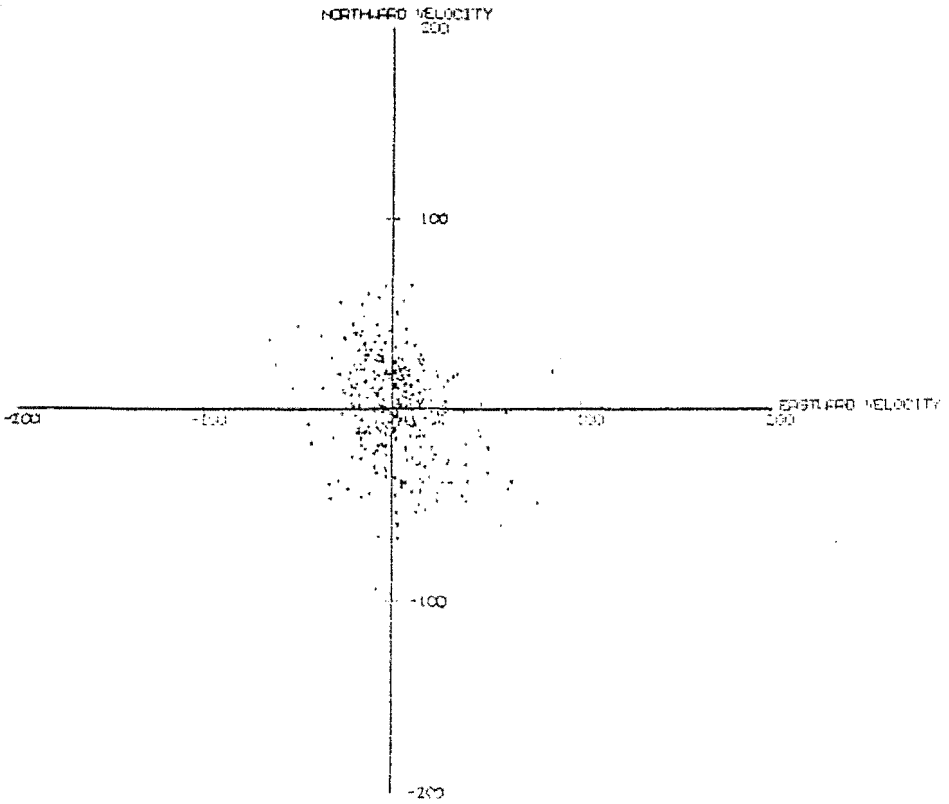

INDIVIDUAL DRIFT READINGS FOR PERIODS OF MORE THAN 3 HOURS IN JANUARY 1981 AT 77.5KM.

Figure 8.4d)

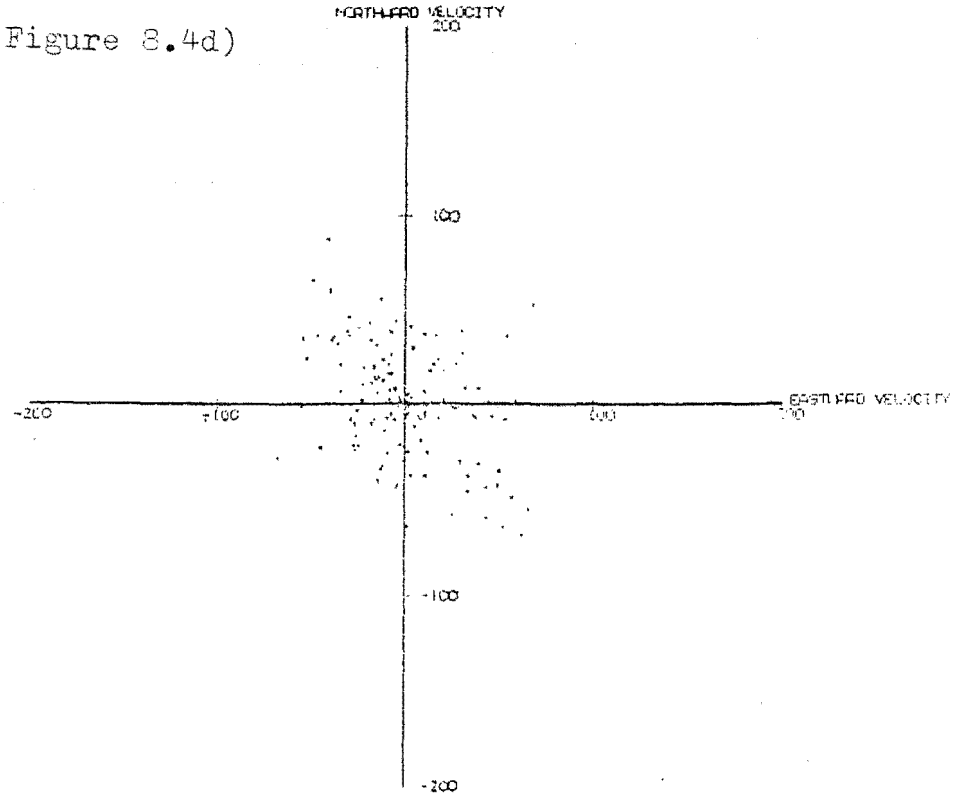

INDIVIDUAL DRIFT READINGS FOR PERIODS OF MORE THAN 3 HOURS IN JANUARY 1981 AT 90.0KM.

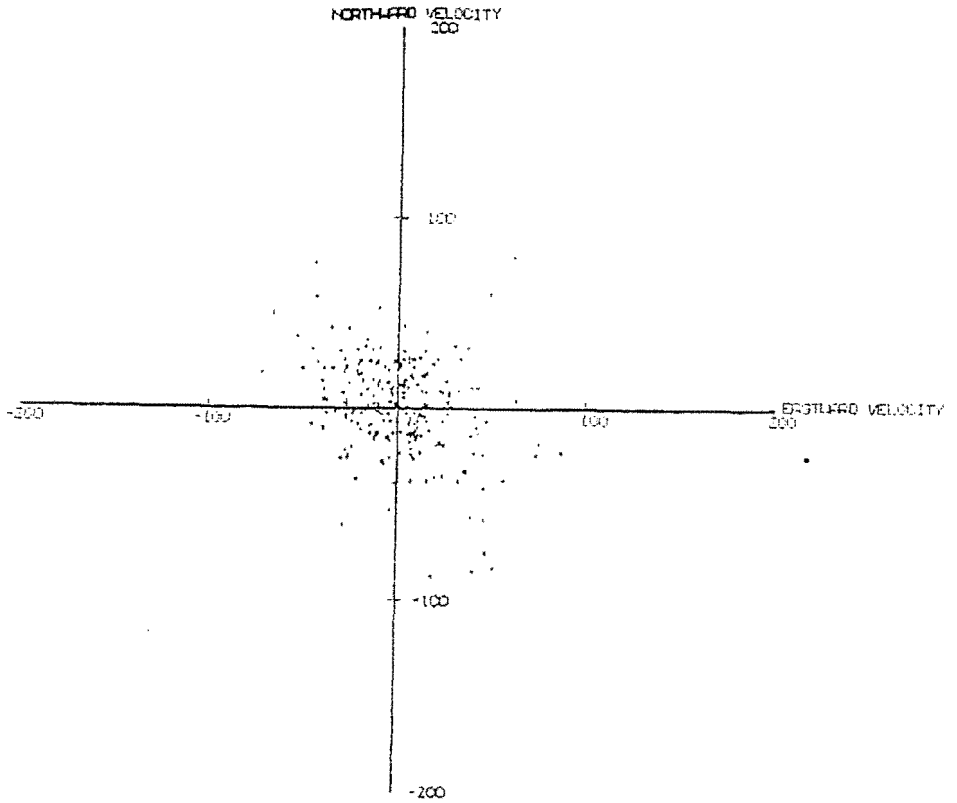

INDIVIDUAL DRIFT READINGS FOR PERIODS OF MORE THAN 3 HOURS IN JANUARY 1981 AT 92.5KM.

Figure 8.4e)

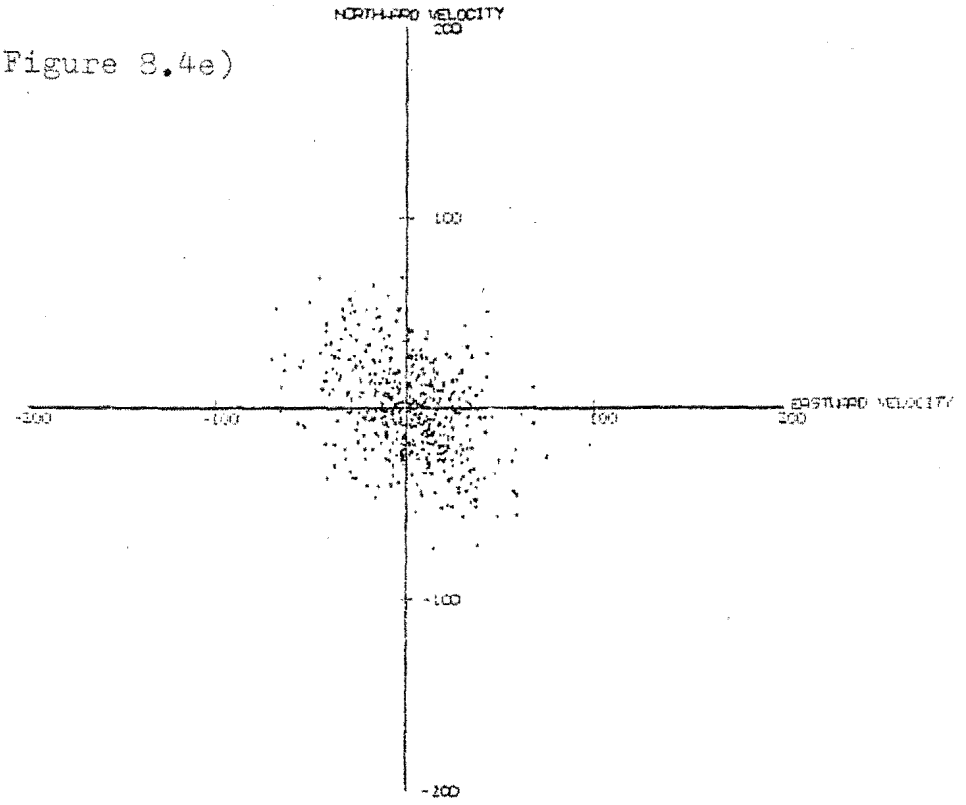

INDIVIDUAL DRIFT READINGS FOR PERIODS OF MORE THAN 3 HOURS IN JANUARY 1981 AT 85.0KM.

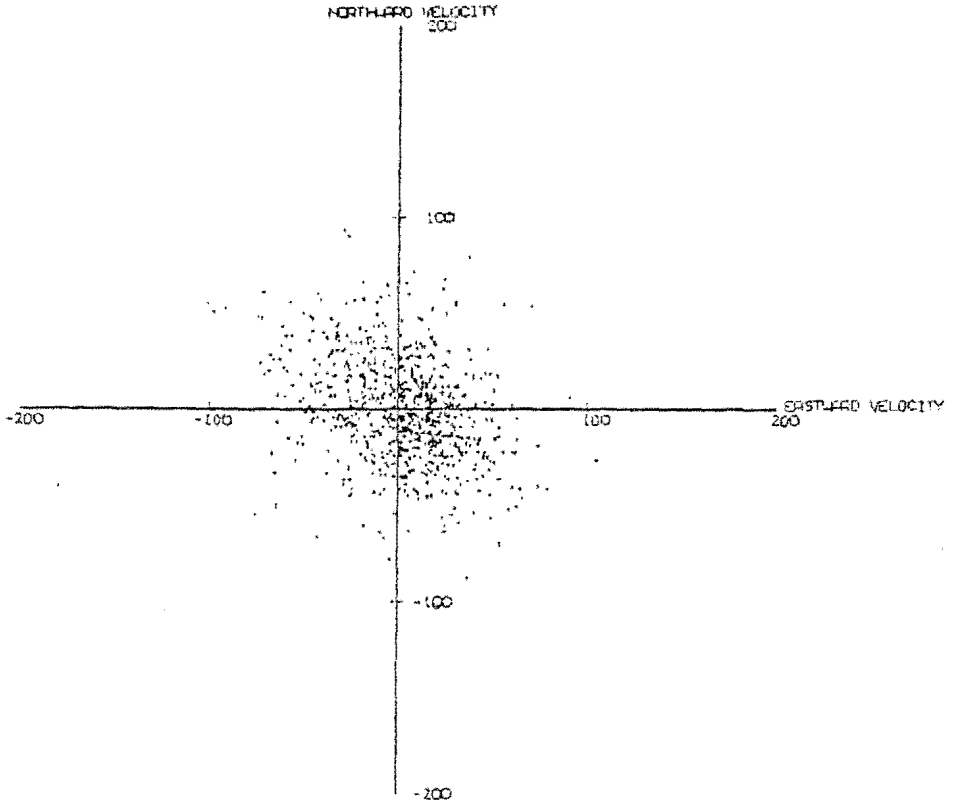

INDIVIDUAL DRIFT READINGS FOR PERIODS OF MORE THAN 3 HOURS IN JANUARY 1981 AT 97.5KM.

Figure 8.4f)

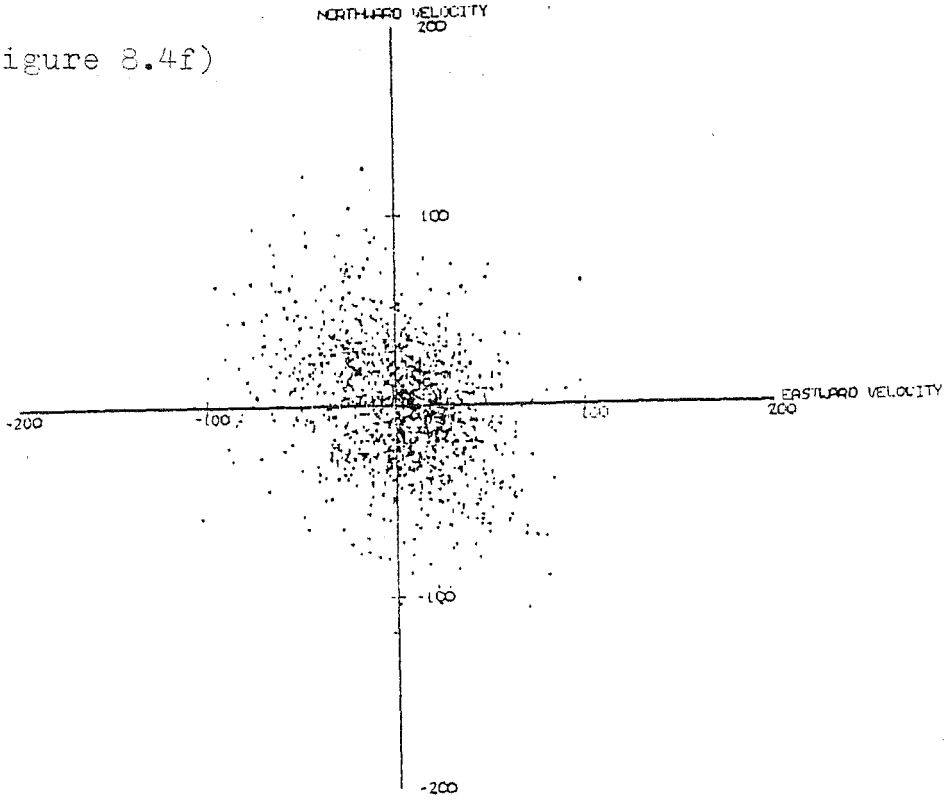

INDIVIDUAL DRIFT READINGS FOR PERIODS OF MORE THAN 3 HOURS IN JANUARY 1981 AT 90.0KM.

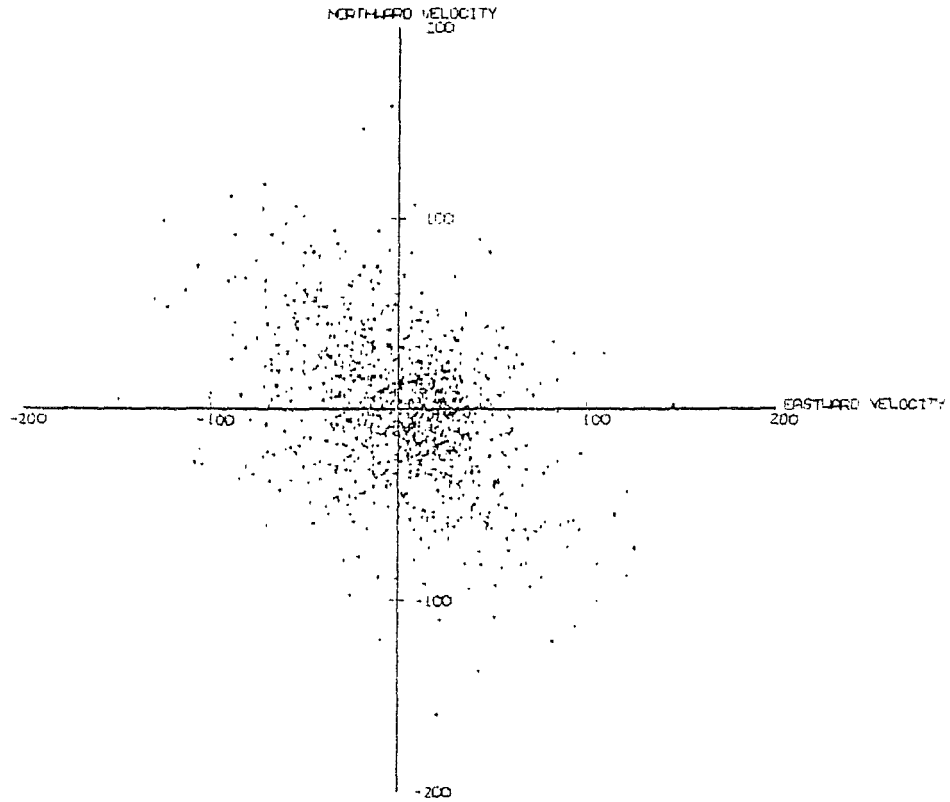

INDIVIDUAL DRIFT READINGS FOR PERIODS OF MORE THAN 3 HOURS IN JANUARY 1981 AT 92.5KM.

Figure 8.4g)

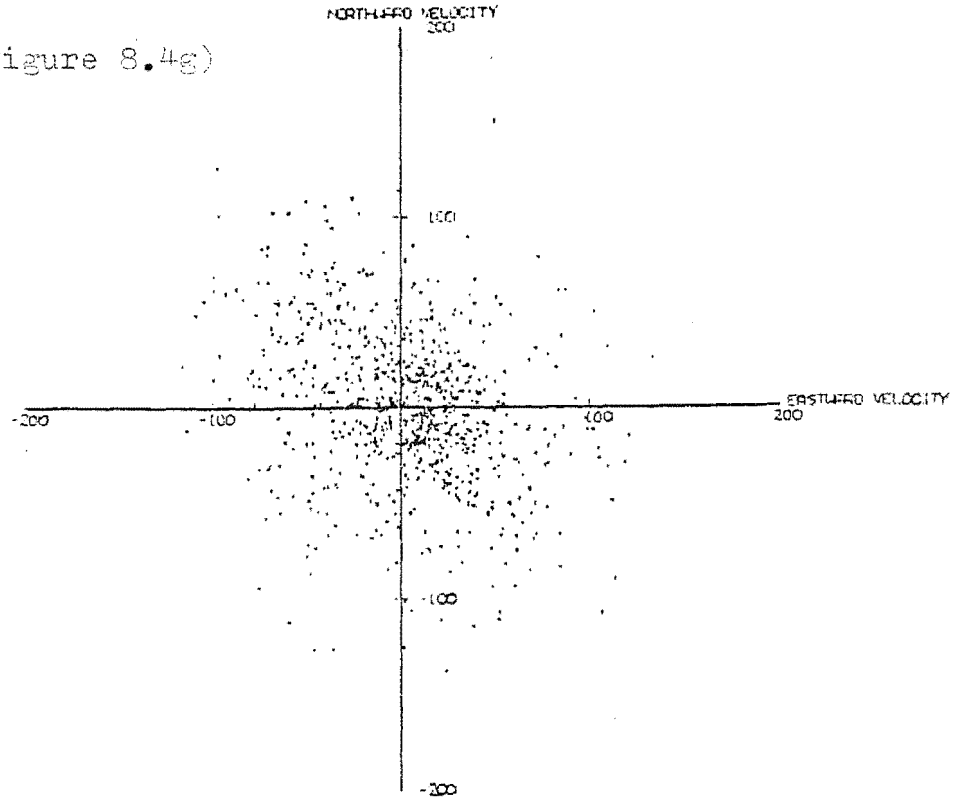

INDIVIDUAL DRIFT READINGS FOR PERIODS OF MORE THAN 3 HOURS IN JANUARY 1981 AT 95.0KM.

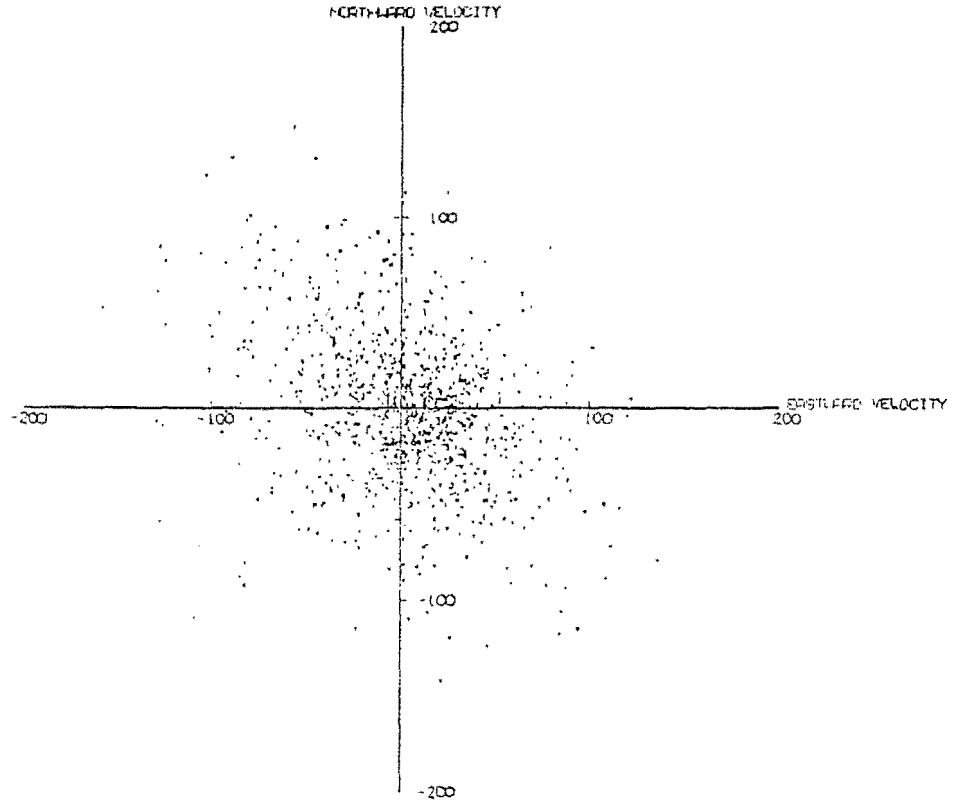

INDIVIDUAL DRIFT READINGS FOR PERIODS OF MORE THAN 3 HOURS IN JANUARY 1981 AT 97.5KM.

Figure 8.4h)

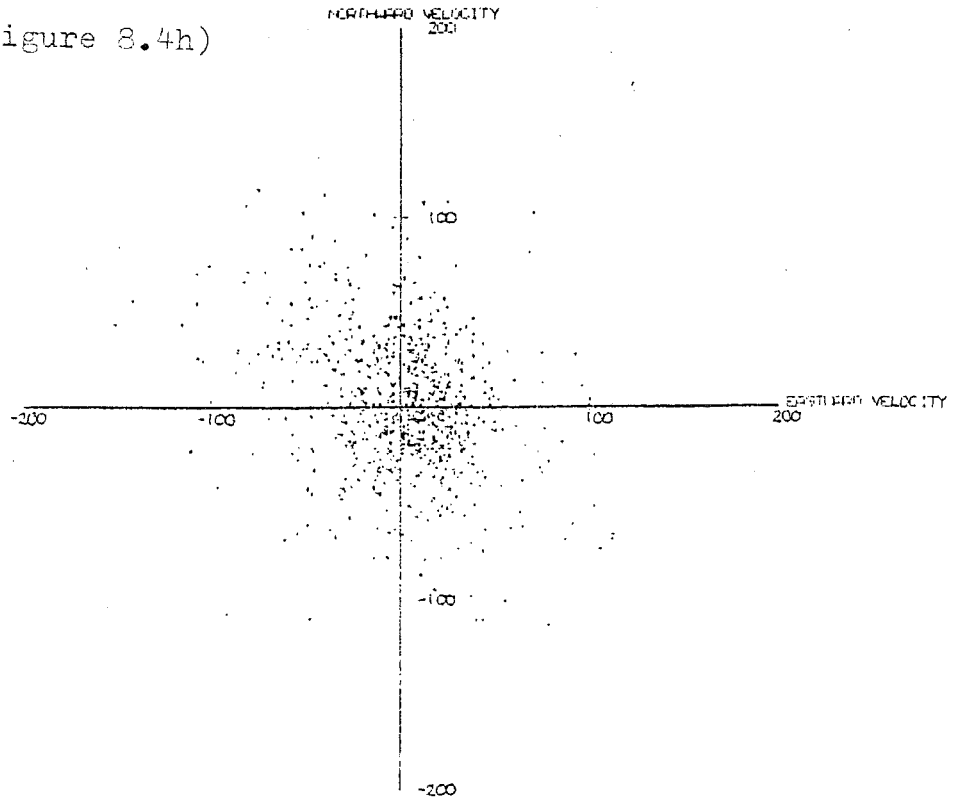

INDIVIDUAL DRIFT READINGS FOR PERIODS OF MORE THAN 3 HOURS ON JANUARY 1981 AT 100.0KM.

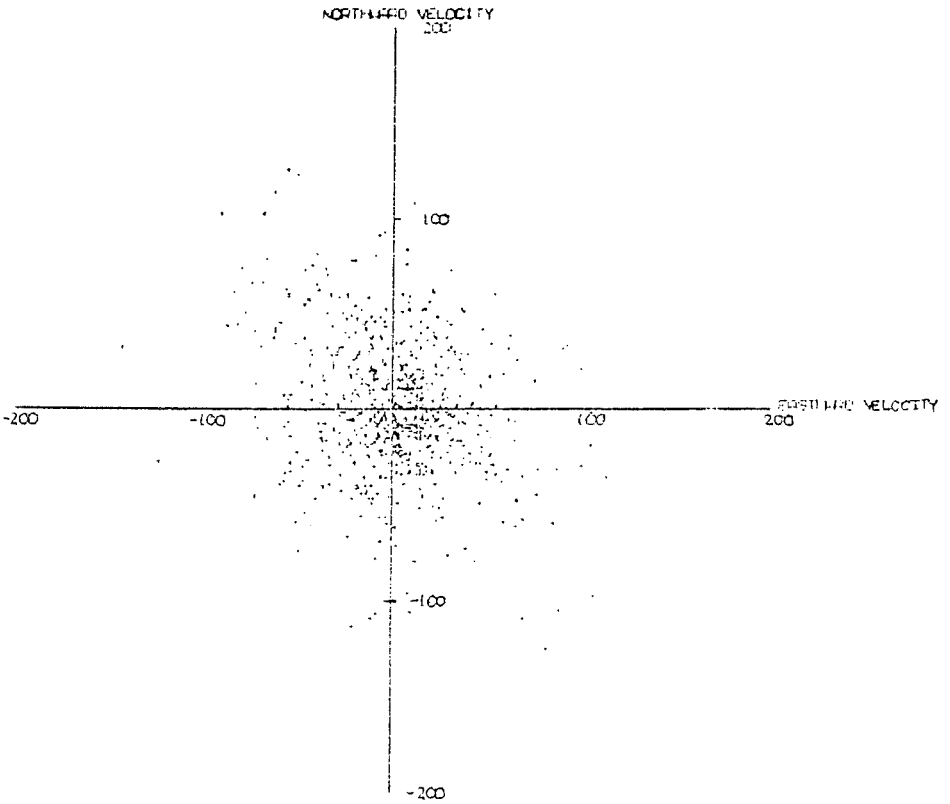

INDIVIDUAL DRIFT READINGS FOR PERIODS OF MORE THAN 3 HOURS ON JANUARY 1981 AT 102.5KM.

Figure 8.7a)

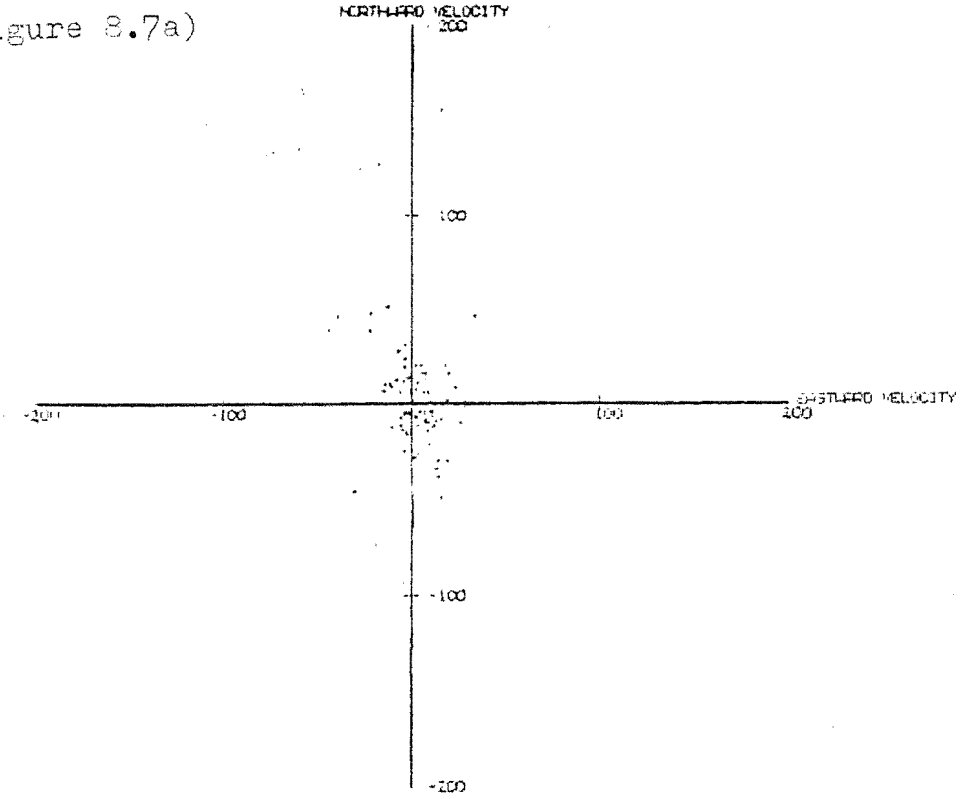

INDIVIDUAL DRIFT READINGS AT BIRDLINGS FLAT
FOR PERIODS OF LESS THAN 3 HOURS IN
AUGUST 1981 AT AN ALTITUDE OF 85.0KM.

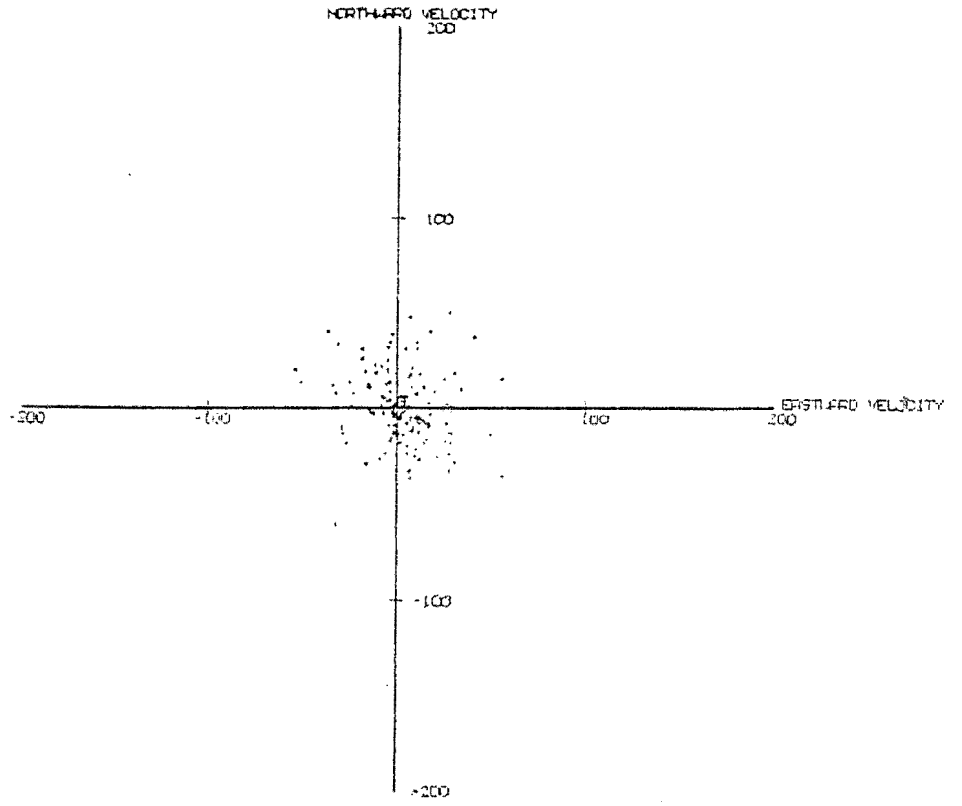

INDIVIDUAL DRIFT READINGS AT BIRDLINGS FLAT
FOR PERIODS OF LESS THAN 3 HOURS IN
AUGUST 1981 AT AN ALTITUDE OF 87.5KM.

Figure 8.7b)

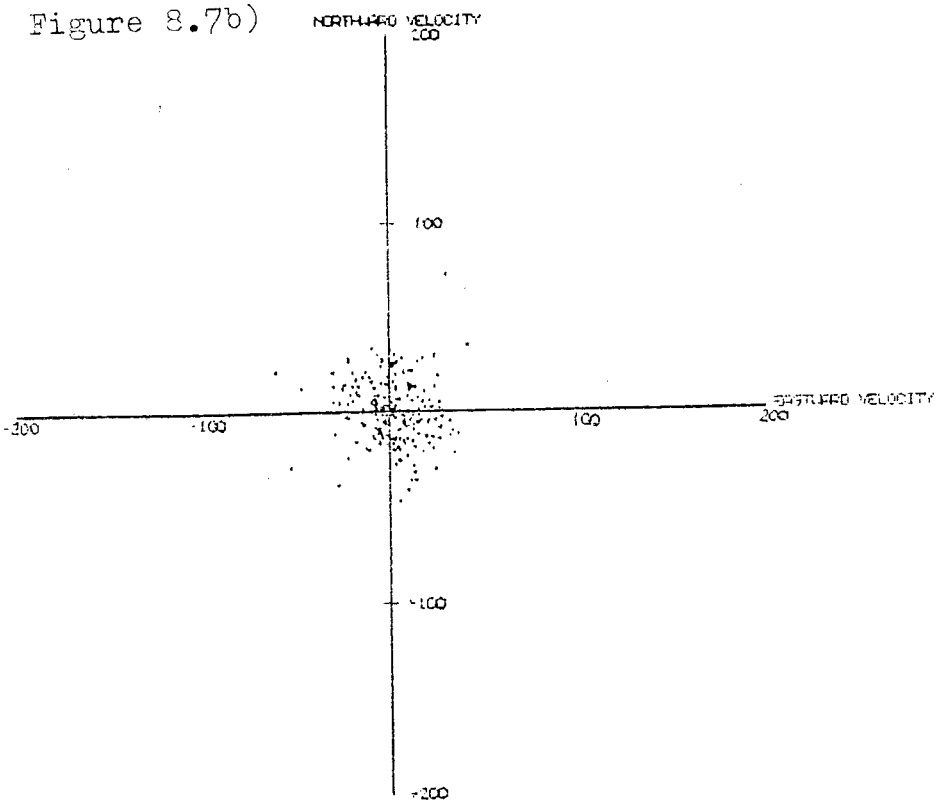

INDIVIDUAL DRIFT READINGS AT BIRDLINGS FLAT
FOR PERIODS OF LESS THAN 3 HOURS IN
AUGUST 1981 AT AN ALTITUDE OF 70.0KM.

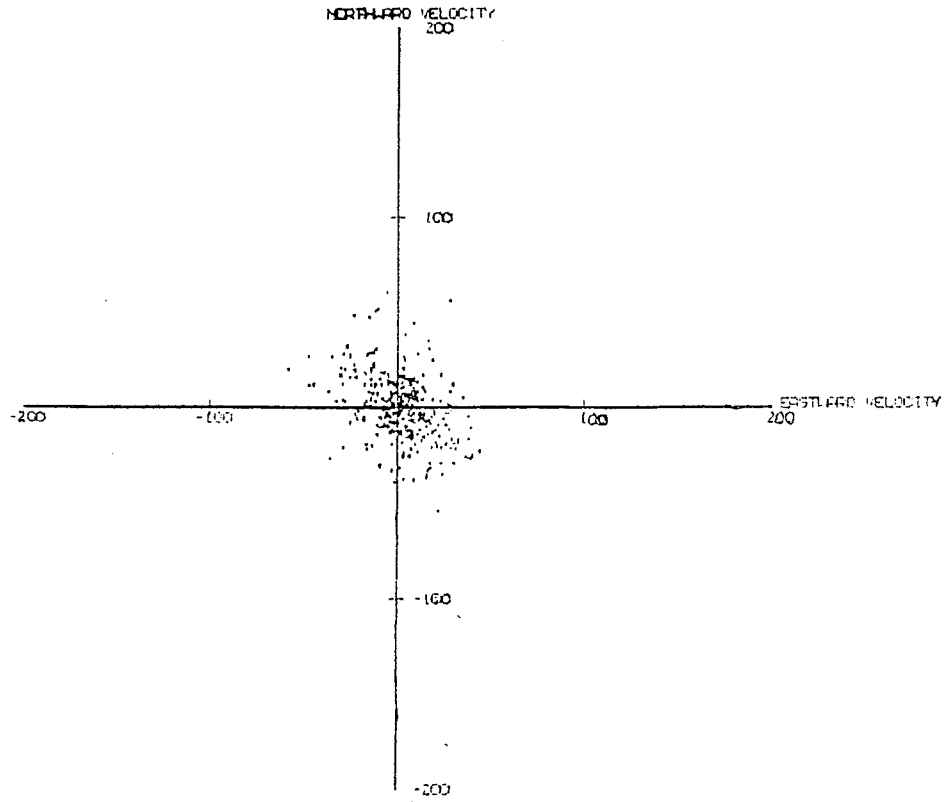

INDIVIDUAL DRIFT READINGS AT BIRDLINGS FLAT
FOR PERIODS OF LESS THAN 3 HOURS IN
AUGUST 1981 AT AN ALTITUDE OF 72.5KM.

Figure 8.7c)

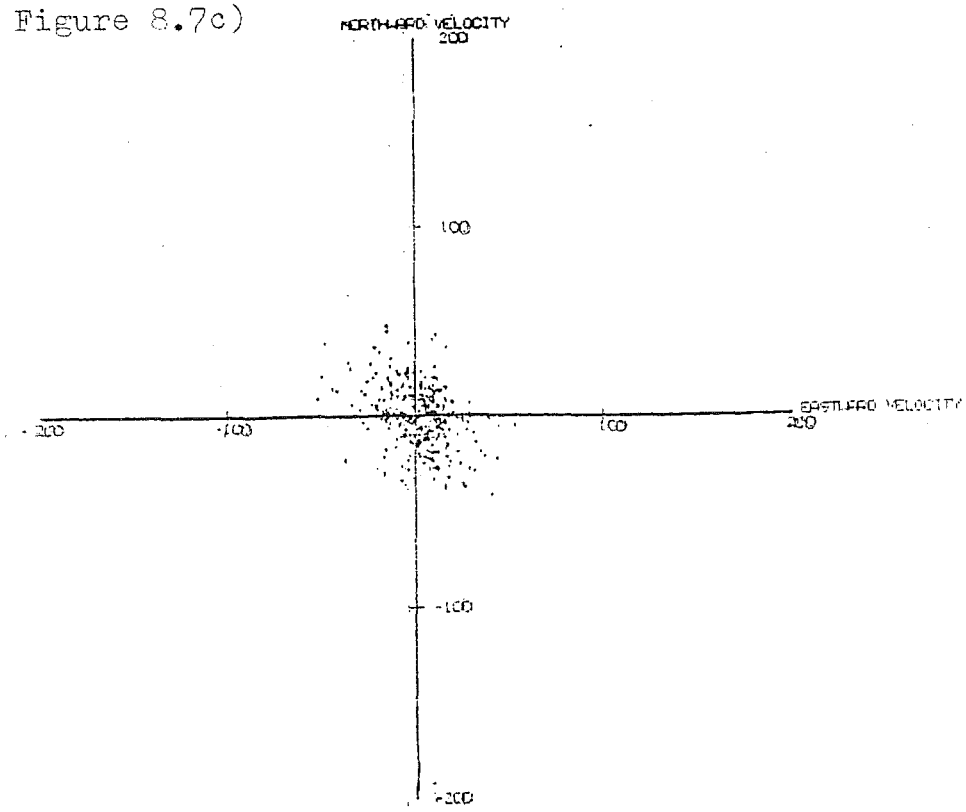

INDIVIDUAL DRIFT READINGS AT BIRDLINGS FLAT FOR PERIODS OF LESS THAN 3 HOURS IN AUGUST 1981 AT AN ALTITUDE OF 75.0KM.

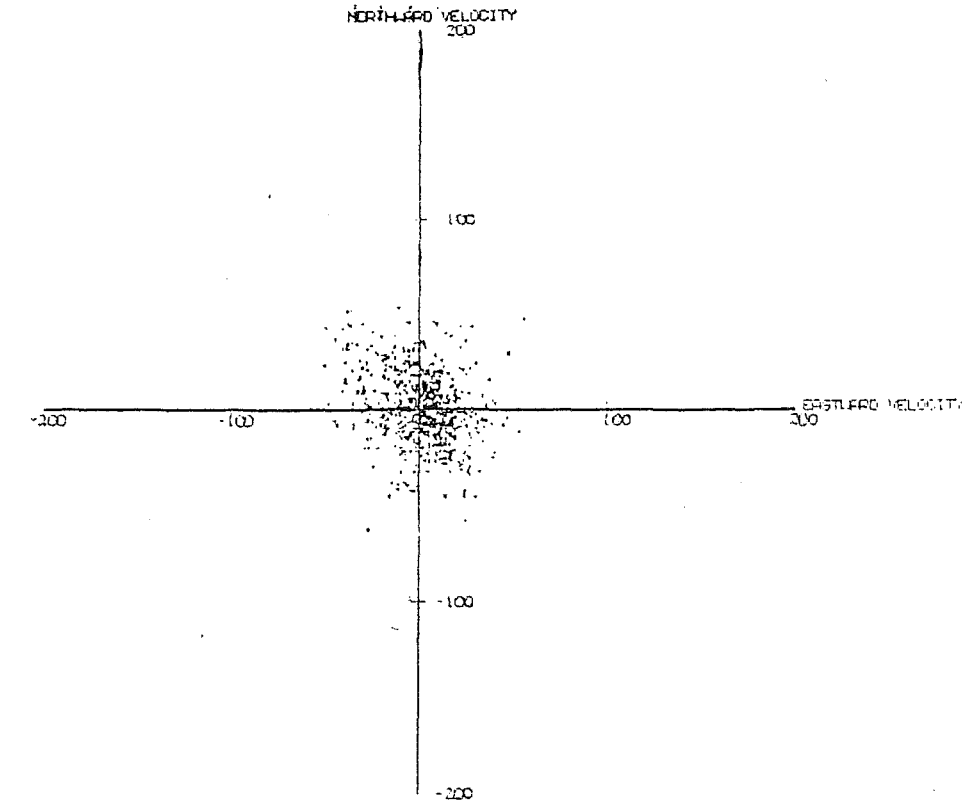

INDIVIDUAL DRIFT READINGS AT BIRDLINGS FLAT FOR PERIODS OF LESS THAN 3 HOURS IN AUGUST 1981 AT AN ALTITUDE OF 77.5KM.

Figure 8.7d)

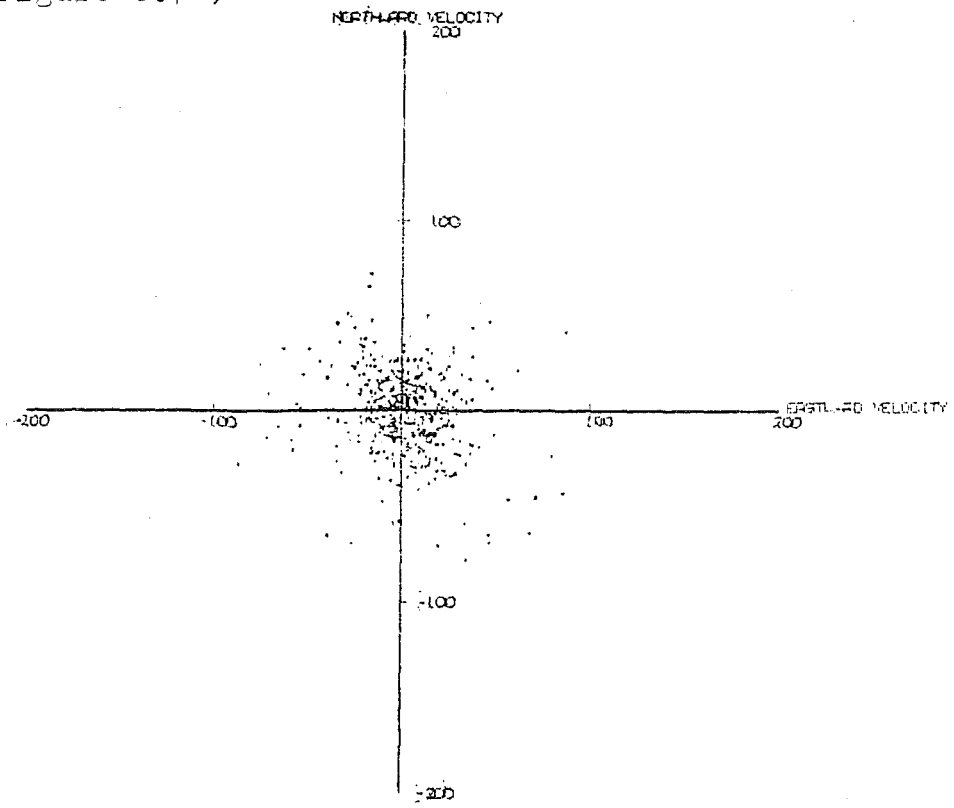

INDIVIDUAL DRIFT READINGS AT BIRDLINGS FLAT FOR PERIODS OF LESS THAN 3 HOURS IN AUGUST 1981 AT AN ALTITUDE OF 80.0KM.

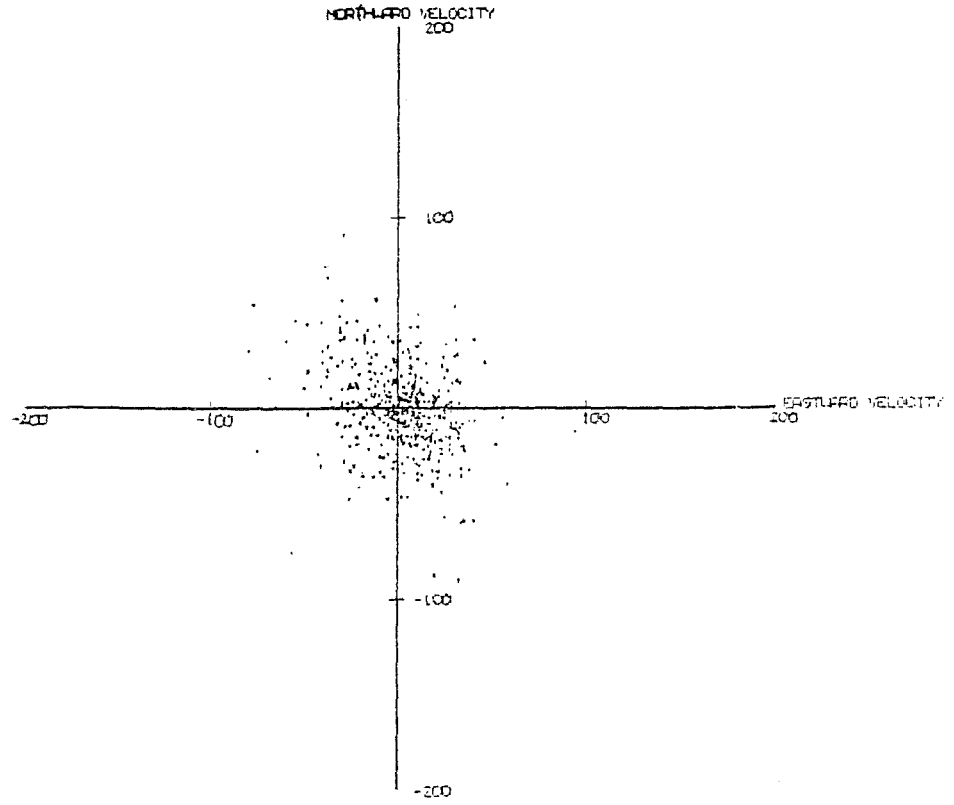

INDIVIDUAL DRIFT READINGS AT BIRDLINGS FLAT FOR PERIODS OF LESS THAN 3 HOURS IN AUGUST 1981 AT AN ALTITUDE OF 82.5KM.

Figure 8.7e)

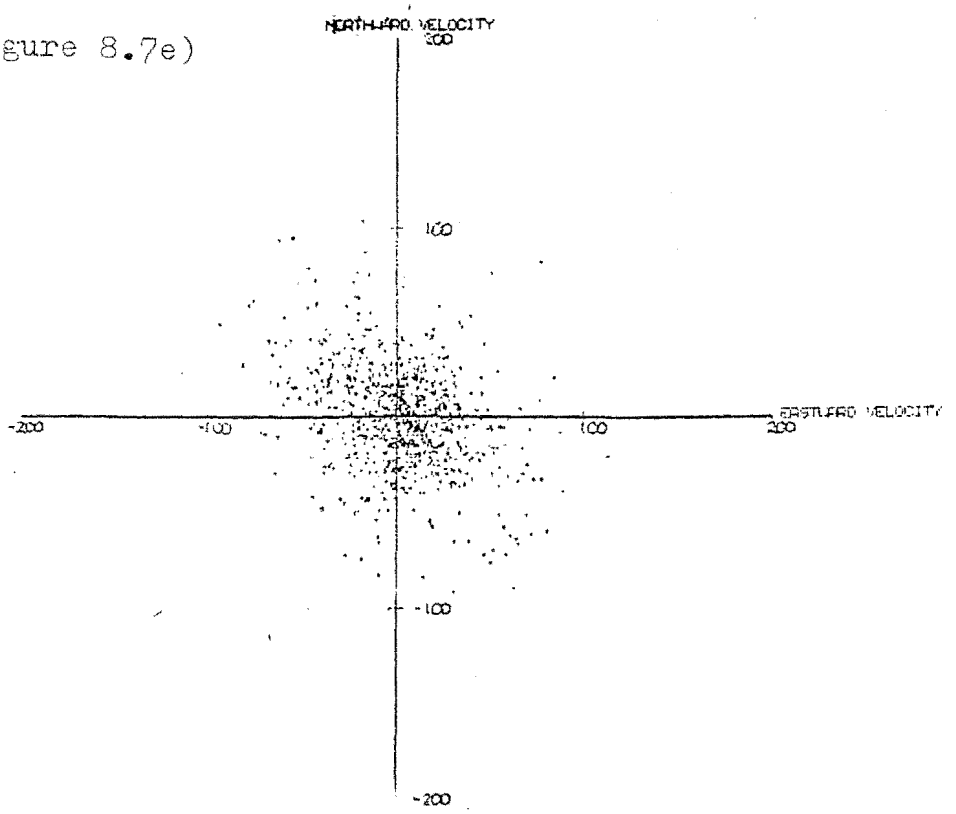

INDIVIDUAL DRIFT READINGS AT SIRDLINGS FLAT
FOR PERIODS OF LESS THAN 3 HOURS IN
AUGUST 1981 AT AN ALTITUDE OF 85.0KM.

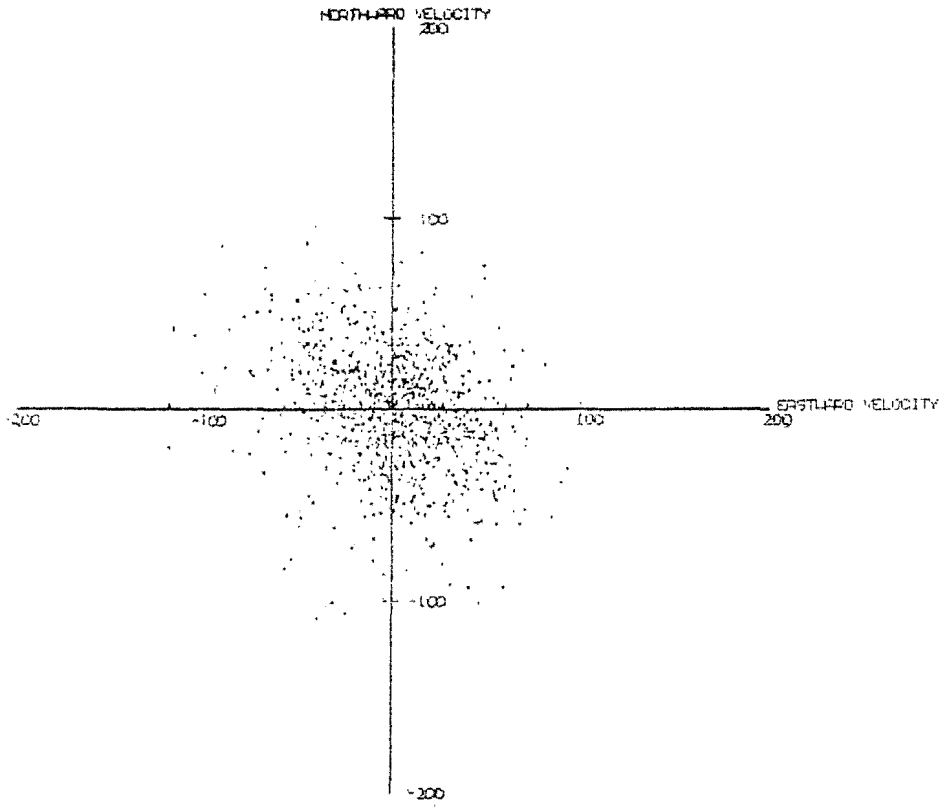

INDIVIDUAL DRIFT READINGS AT SIRDLINGS FLAT
FOR PERIODS OF LESS THAN 3 HOURS IN
AUGUST 1981 AT AN ALTITUDE OF 87.5KM.

Figure 8.7f)

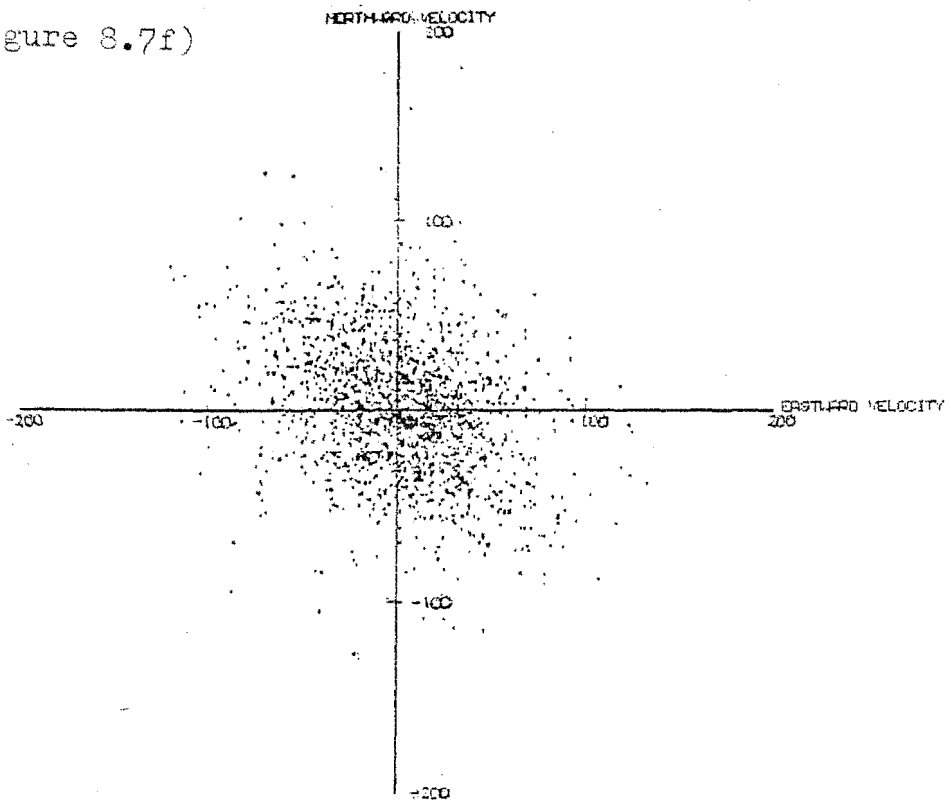

INDIVIDUAL DRIFT READINGS AT BIRDLINGS FLAT
FOR PERIODS OF LESS THAN 3 HOURS IN
AUGUST 1981 AT AN ALTITUDE OF 90.0km.

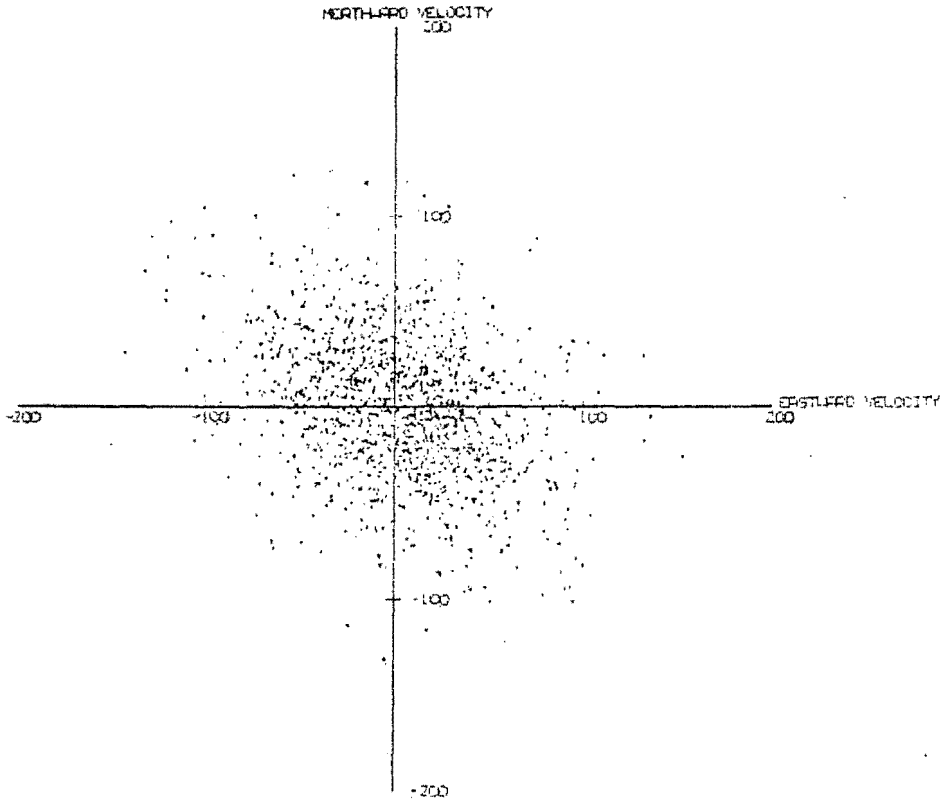

INDIVIDUAL DRIFT READINGS AT BIRDLINGS FLAT
FOR PERIODS OF LESS THAN 3 HOURS IN
AUGUST 1981 AT AN ALTITUDE OF 92.5km.

Figure 8.7g)

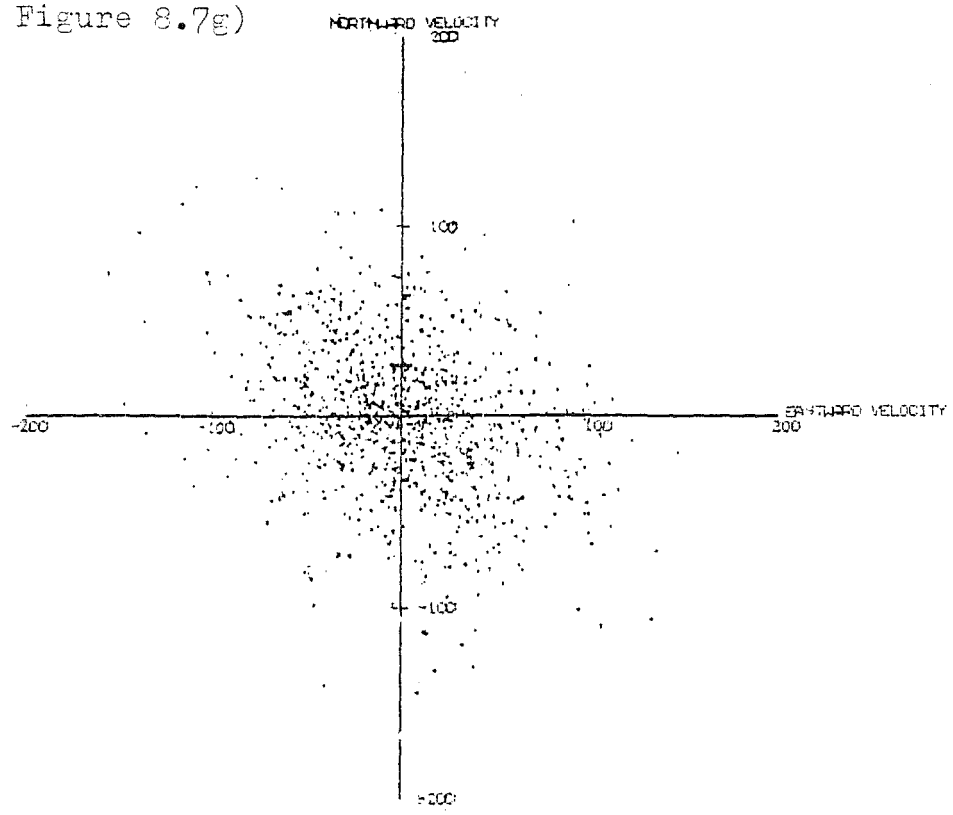

INDIVIDUAL DRIFT READINGS AT BIRDLINGS FLAT FOR PERIODS OF LESS THAN 3 HOURS IN AUGUST 1981 AT AN ALTITUDE OF 96.0km.

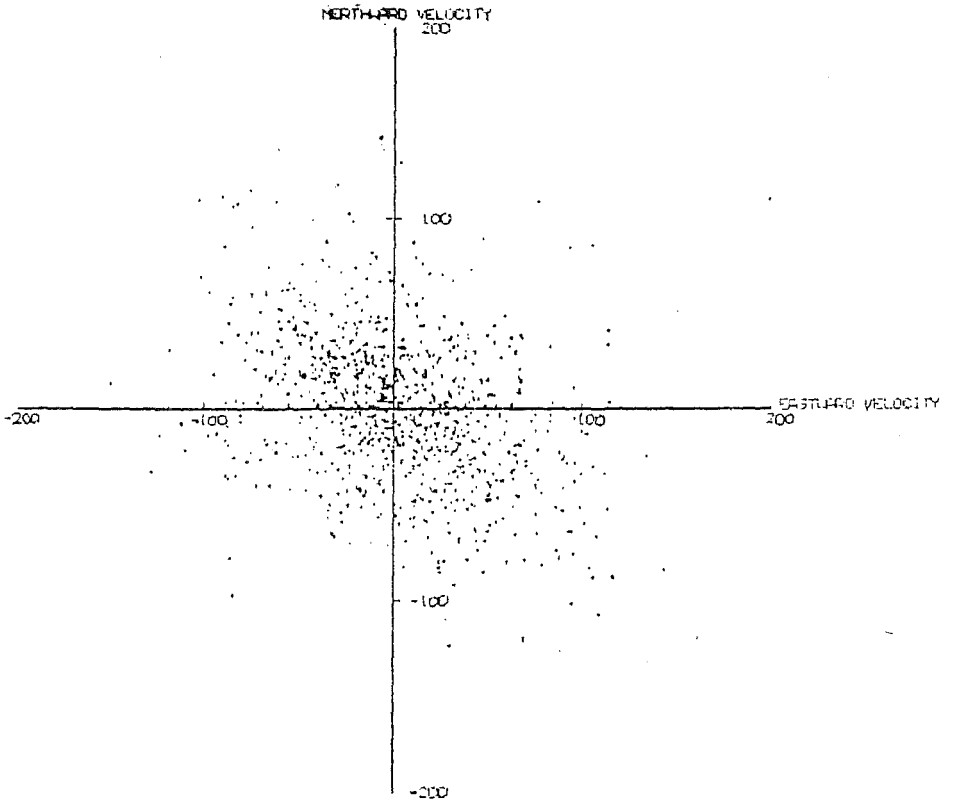

INDIVIDUAL DRIFT READINGS AT BIRDLINGS FLAT FOR PERIODS OF LESS THAN 3 HOURS IN AUGUST 1981 AT AN ALTITUDE OF 97.5km.

Figure 8.7h)

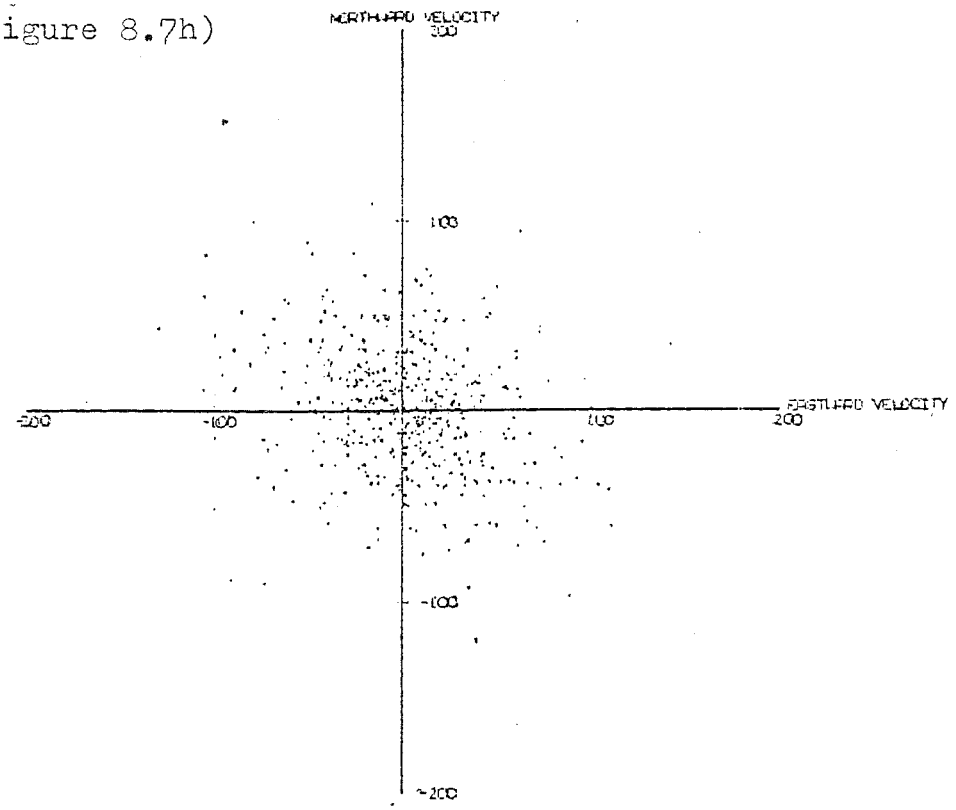

INDIVIDUAL DRIFT READINGS AT BIRDLINGS FLAT FOR PERIODS OF LESS THAN 3 HOURS IN AUGUST 1981 AT AN ALTITUDE OF 100.0KM.

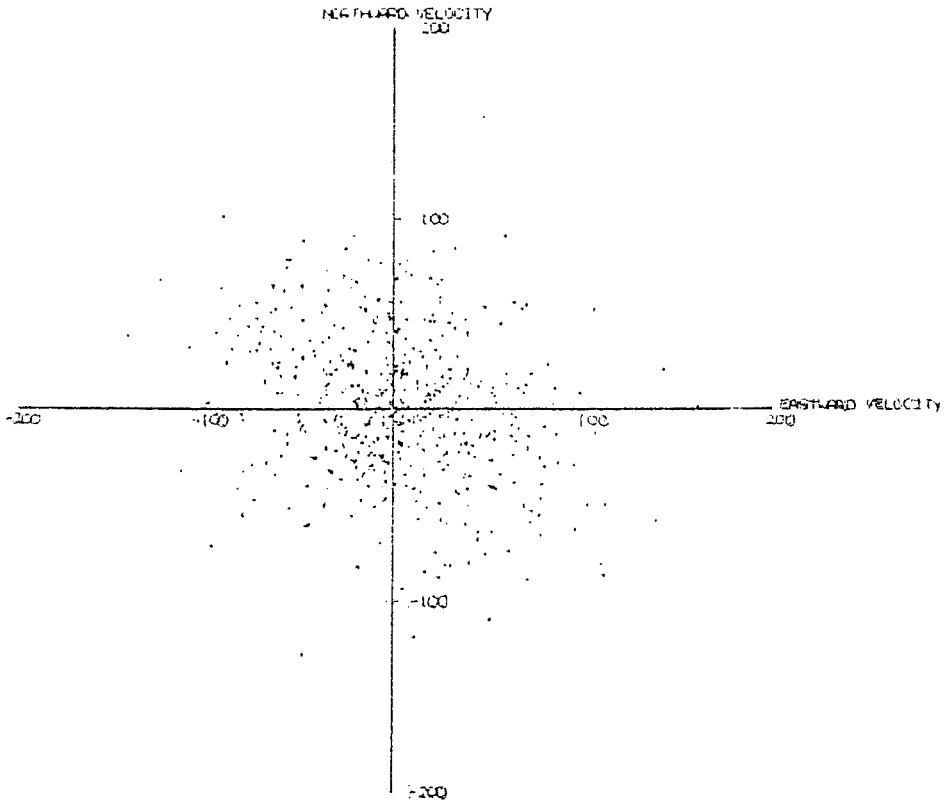

INDIVIDUAL DRIFT READINGS AT BIRDLINGS FLAT FOR PERIODS OF LESS THAN 3 HOURS IN AUGUST 1981 AT AN ALTITUDE OF 102.5KM.

Figure 8.13a)

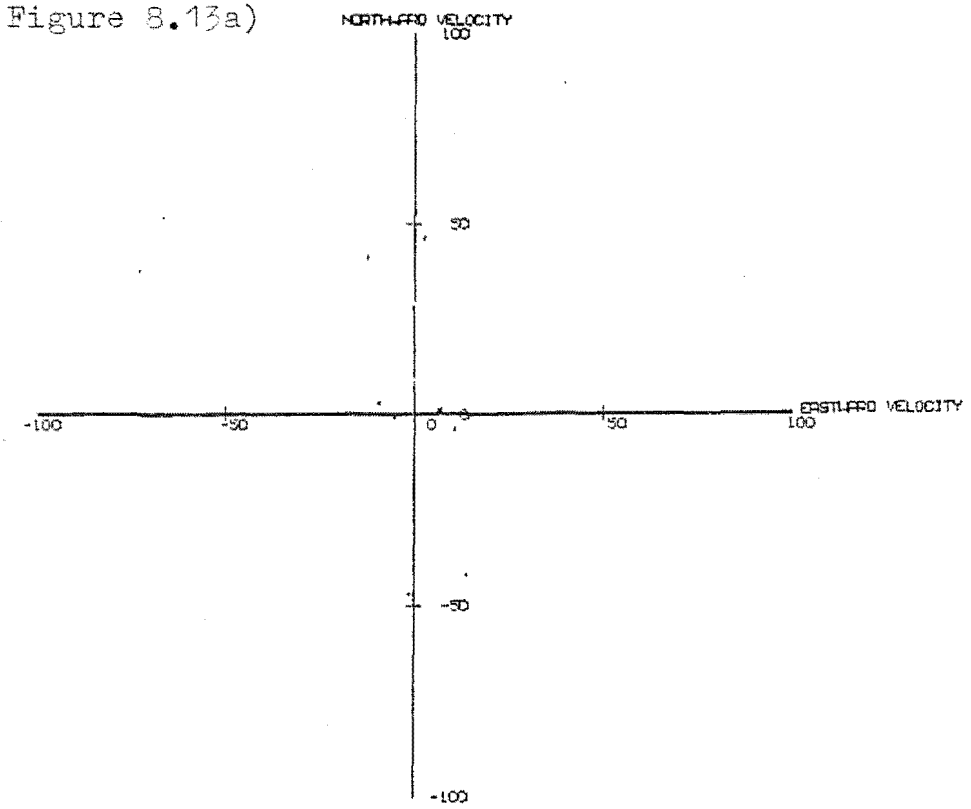

INDIVIDUAL DRIFT READINGS AT ARRIVAL HEIGHTS
FOR PERIODS LESS THAN 3 HOURS IN
NOVEMBER 1983 AT AN ALTITUDE OF 77KM.

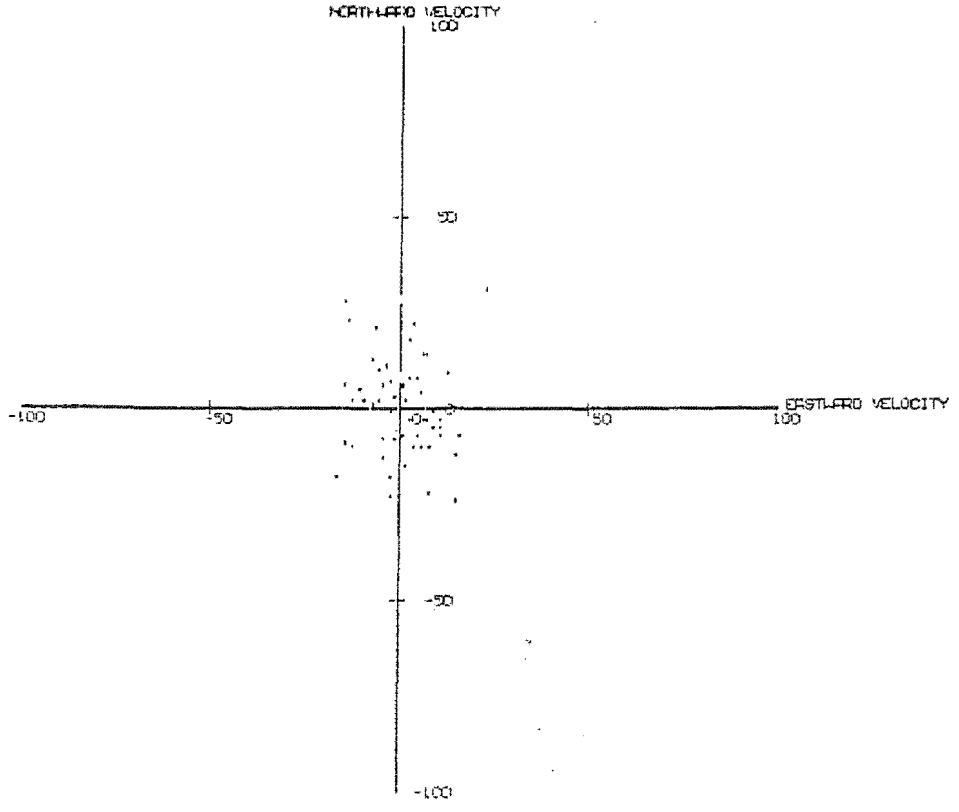

INDIVIDUAL DRIFT READINGS AT ARRIVAL HEIGHTS
FOR PERIODS LESS THAN 3 HOURS IN
NOVEMBER 1983 AT AN ALTITUDE OF 79KM.

Figure 8.13b)

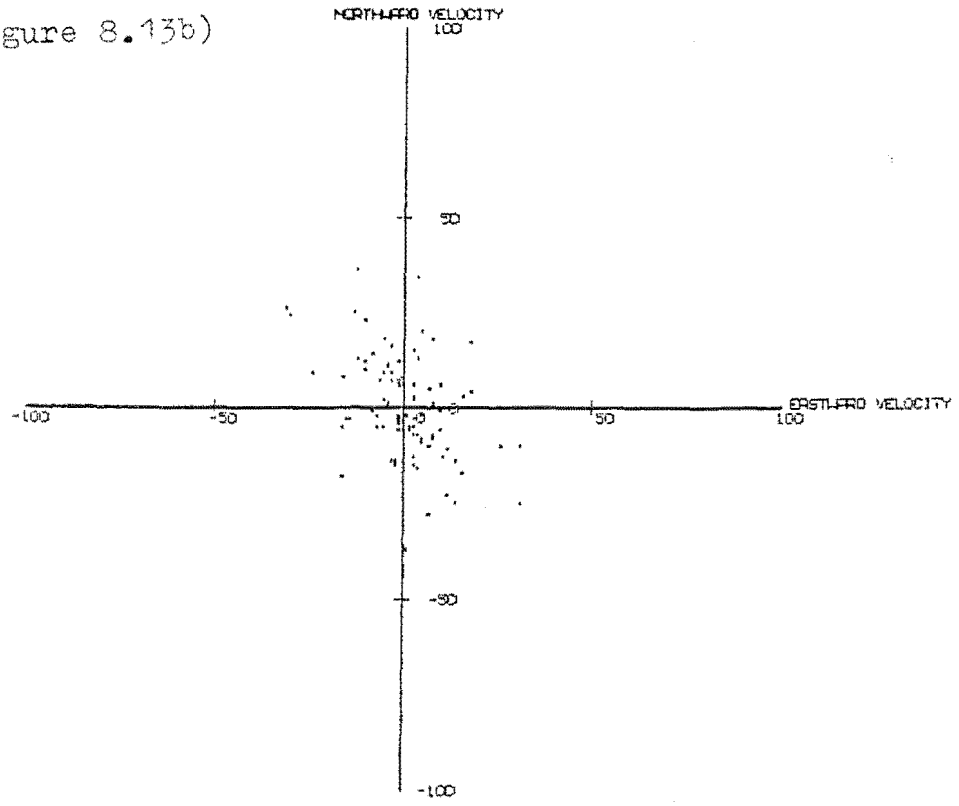

INDIVIDUAL DRIFT READINGS AT ARRIVAL HEIGHTS
FOR PERIODS LESS THAN 3 HOURS IN
NOVEMBER 1983 AT AN ALTITUDE OF 81km.

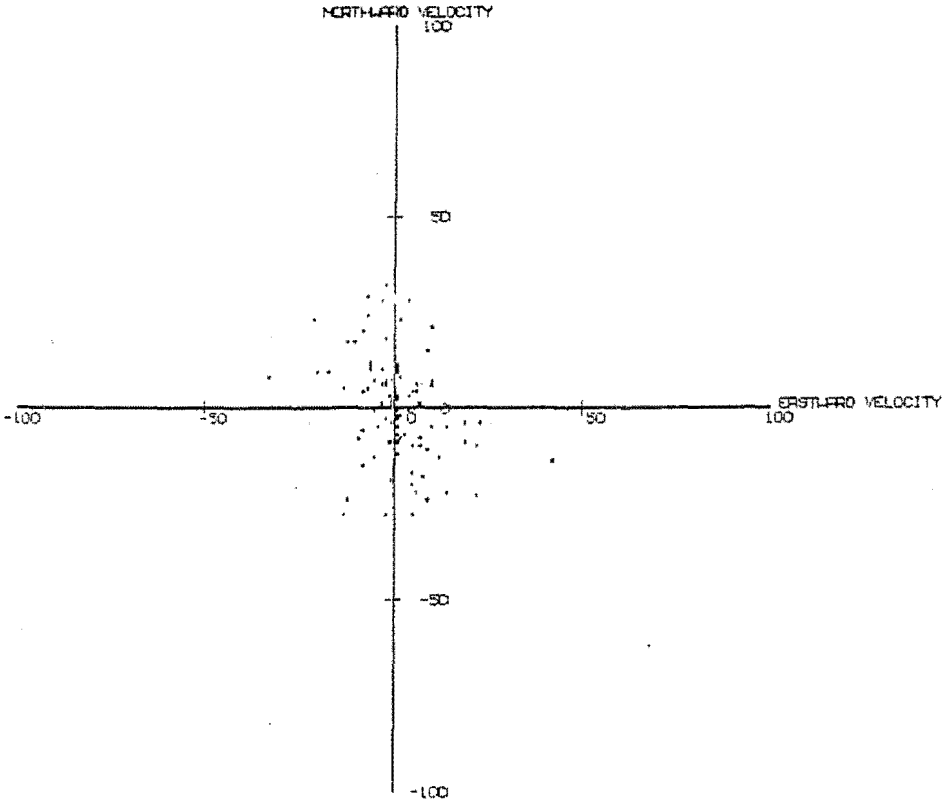

INDIVIDUAL DRIFT READINGS AT ARRIVAL HEIGHTS
FOR PERIODS LESS THAN 3 HOURS IN
NOVEMBER 1983 AT AN ALTITUDE OF 83km.

Figure 8.13c)

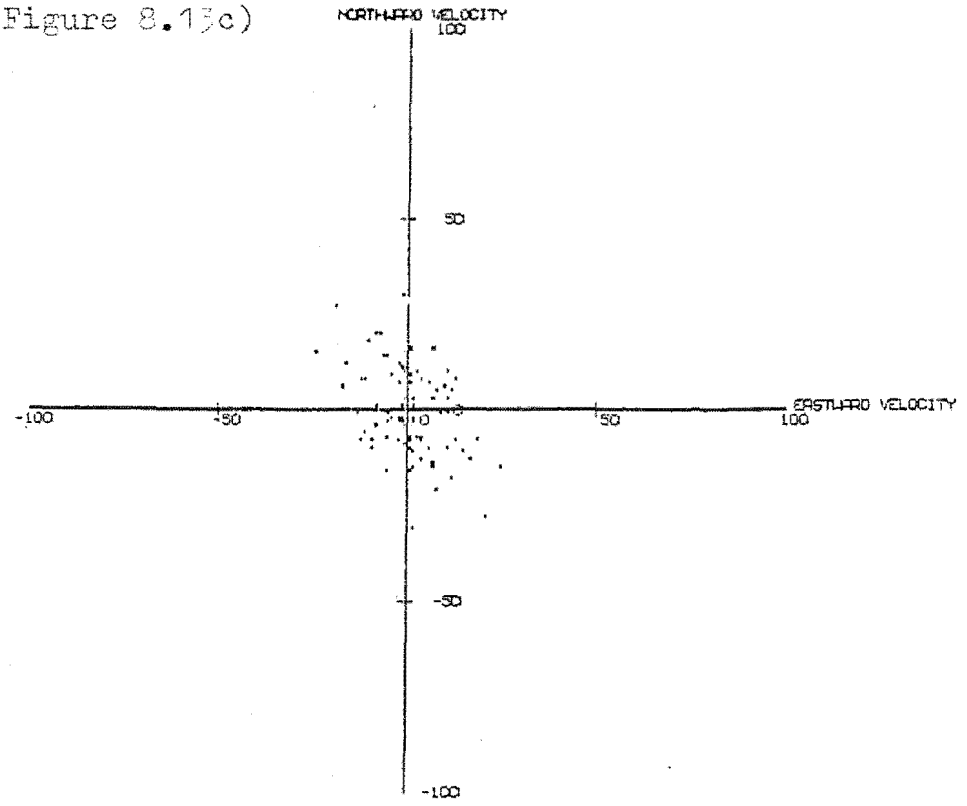

INDIVIDUAL DRIFT READINGS AT ARRIVAL HEIGHTS
FOR PERIODS LESS THAN 3 HOURS IN
NOVEMBER 1983 AT AN ALTITUDE OF 85KM.

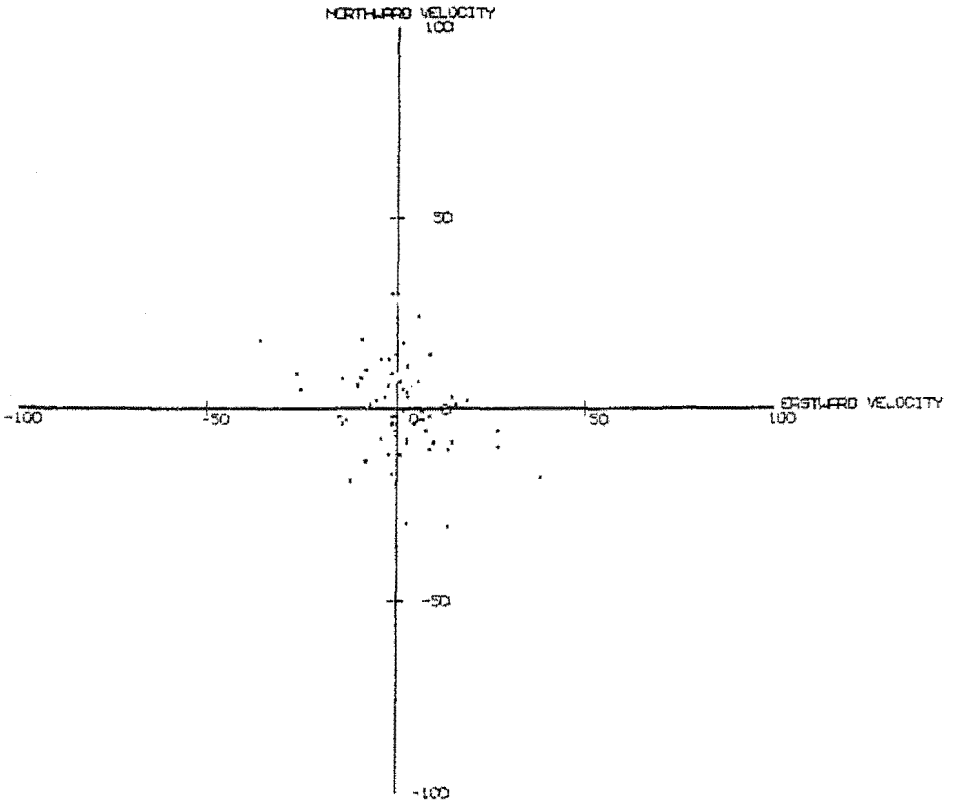

INDIVIDUAL DRIFT READINGS AT ARRIVAL HEIGHTS
FOR PERIODS LESS THAN 3 HOURS IN
NOVEMBER 1983 AT AN ALTITUDE OF 87KM.

Figure 8.13d)

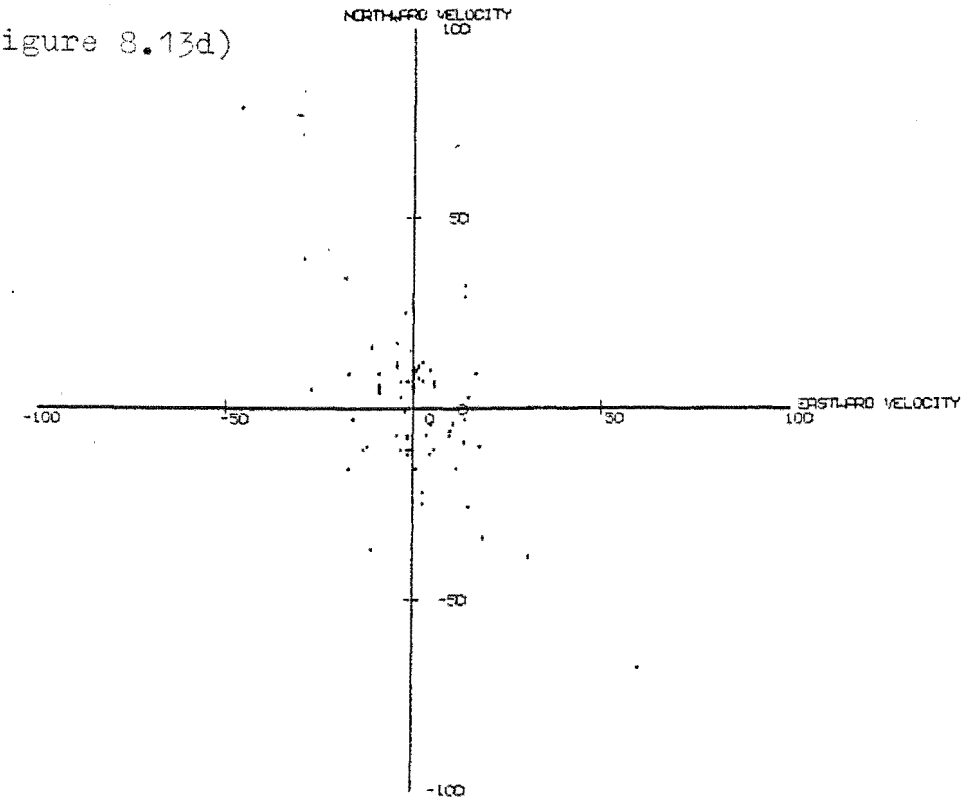

INDIVIDUAL DRIFT READINGS AT ARRIVAL HEIGHTS
FOR PERIODS LESS THAN 3 HOURS IN
NOVEMBER 1983 AT AN ALTITUDE OF 89KM.

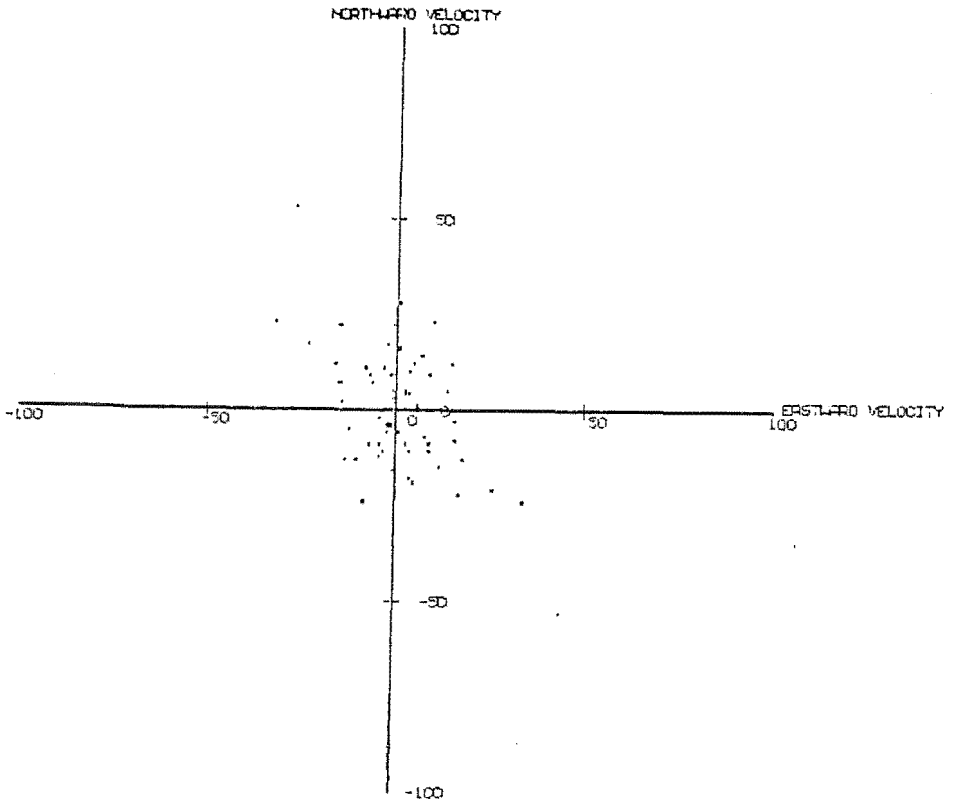

INDIVIDUAL DRIFT READINGS AT ARRIVAL HEIGHTS
FOR PERIODS LESS THAN 3 HOURS IN
NOVEMBER 1983 AT AN ALTITUDE OF 91KM.

Figure 8.13e)

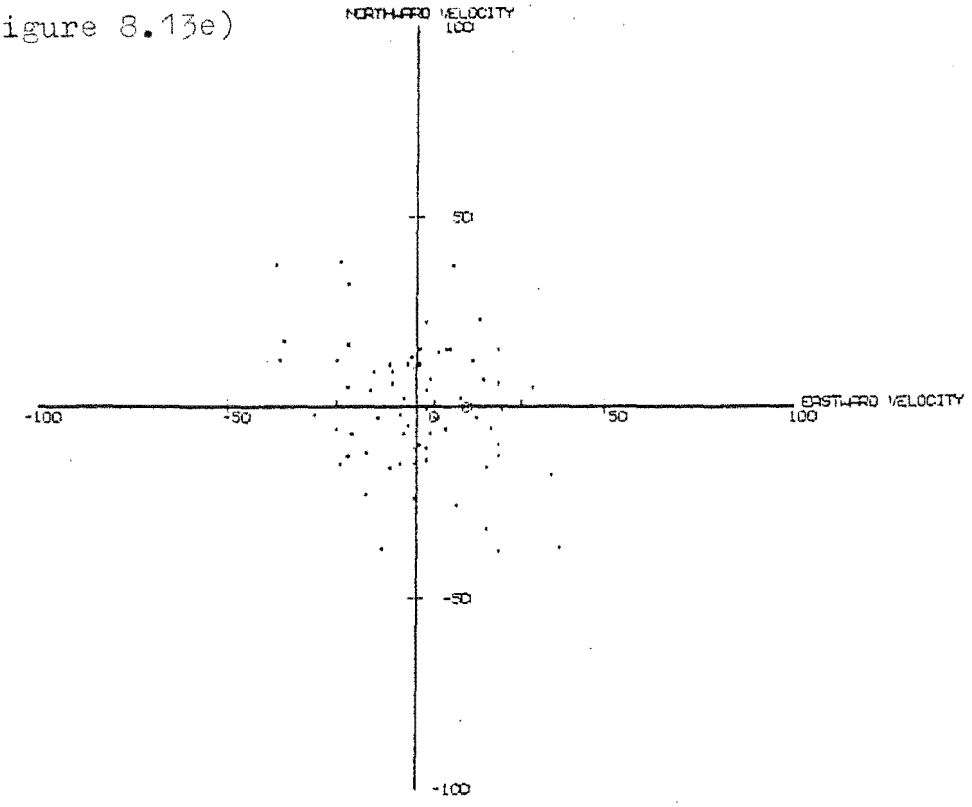

INDIVIDUAL DRIFT READINGS AT ARRIVAL HEIGHTS
FOR PERIODS LESS THAN 3 HOURS IN
NOVEMBER 1983 AT AN ALTITUDE OF 93KM.

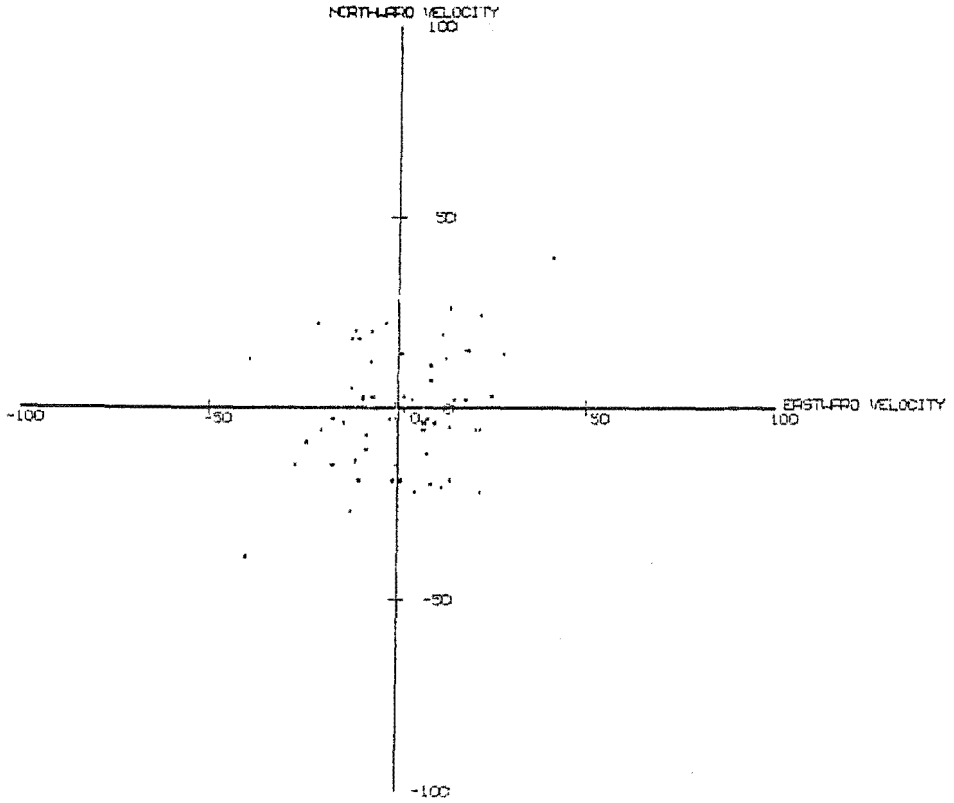

INDIVIDUAL DRIFT READINGS AT ARRIVAL HEIGHTS
FOR PERIODS LESS THAN 3 HOURS IN
NOVEMBER 1983 AT AN ALTITUDE OF 95KM.

Figure 8.13f)

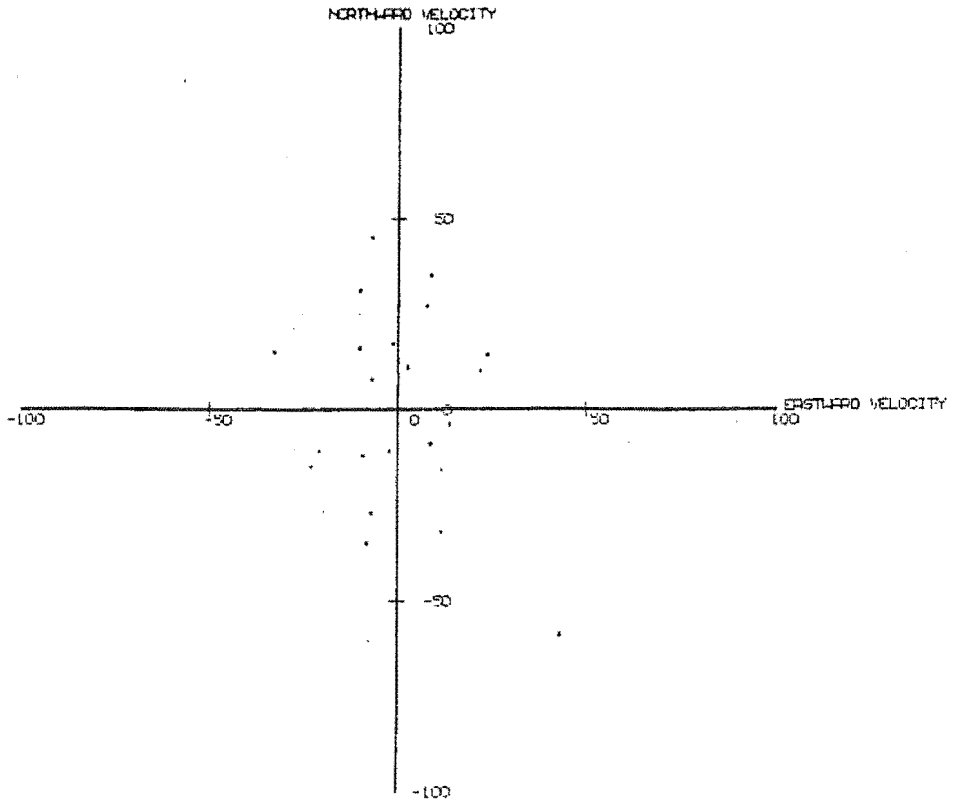

INDIVIDUAL DRIFT READINGS AT ARRIVAL HEIGHTS
FOR PERIODS LESS THAN 3 HOURS IN
NOVEMBER 1983 AT AN ALTITUDE OF 97KM.

REFERENCES

Abel, P.G., Ellis, P.J., Houghton, J.T., Peckham, G., Rodgers, C.D., Smith, S.D. and Williamson, E.J. (1970) Remote Sounding of atmospheric temperatures from satellites II: the selective chopper radiometer for Nimbus D. Prod. Roy. Soc. Lond. A320 35.

Ables, J.G. (1974) Maximum entropy spectral analysis, Astron. Astrophys. Suppl. 15 383.

Akaike, H. (1974) A new look at the statistical model identification. IEEE Trans. Autom. Control AC-19 716.

Akaike, H. (1976) Time series analysis and control through parametric models. Proceedings of the First Applied Time Series Symposium held in Tulsa, Oklahoma, May 14-15 1976. In applied Time Series Analysis cd D.F. Findley Academic Press 1978.

Anderson, N. (1974) On the calculation of filter coefficients for maximum entropy spectral analysis . Geophysics, V39 No. 1 69.

Andrews, D.G. and McIntyre, M.E. (1976) Planetary waves in horizontal and vertical shear: the generalised Eliassen-Palm relation and the mean zonal acceleration. J. Atmos. Sci. 33 2031.

Andrews, A.G. and McIntyre, M.E. (1978) An exact theory of non-linear waves on a Lagrangian mean flow. J. Fluid Mech. 89 609.

Apruzese, T.P., Schoeberl, M.R. and Strobel, D.F. (1982) Parametization of IR cooling in a middle atmosphere dynamics model I, the effects on the zonally averaged circulation. J. Geophys. Res. 87 8951.

Aso, T. and Vincent, R.A. (1982) Some Direct comparisons of mesospheric winds observed at Kyoto and Adelaide. J. atmos. terr. Phys. 44 267.

Ball, S.M. (1981) Upper atmosphere tides and gravity waves at mid- and low-latitudes. Ph.D. thesis, University of Adelaide, South Australia.

Balsley, B.B. and Carter, D.A. (1982) The spectrum of velocity fluctuations at 8 km and 86 km. Geophys. Res. Lett. 9 465.

Balsley, B.B., Ecklund, W.L. and Fritts, D.C. (1983) VHF echoes from the high-latitude mesosphere and lower thermosphere: observations and interpretations . J. Atmos. Sci. 40, 2451.

Barat, J. (1968) Stratification of turbulent processes below the turbopause . Space Res. VIII 663 ed. Mitra, A.P., Jacchia, L.G. and Newman, W.S.

Barat, J. (1982) Some characteristics of clear-air turbulence in the middle stratosphere. J. Atmos. Sci. 39 3553

Barat, J. (1983) The fine structure of the stratospheric flow revealed by differential sounding. J. Geophys. Res. 88 5219.

Barnett, J.J. (1974) The mean meridional temperature behaviour of the stratosphere from November 1970 to November 1971 derived from measurements by the selective chopper radiometer on Nimbus IV. Quart. J.R. Met. Soc. 100 505.

Barnett, J.J. (1977) The Antarctic atmosphere as seen by satellites. Phil. Trans. Roy. Soc. Lond B279 247.

Barnett, J.J., Harwood, R.S., Houghton, J.T., Morgan, C.G., Rodgers, C.D. and Williamson, E.J. (1975) Comparison between radiosonde, rocketsonde and satellite observations of atmospheric temperatures. Quart. J. R. Met Soc. 101 423.

Behannon, K.W. and Ness, N.F. (1966) The design of numerical filters for geomagnetic data analysis. NASA Technical Note TN D-3341.

Blackman, R.B. and Tukey, J.W. (1958) The measurement of power spectra. Dover, New York.

Blamont, J.E. and de Jager, C. (1961) Upper atmospheric turbulence near the 100 km level. Ann. Geophys. 17 134.

Booker, J.R. and Bretherton F.P. (1967) The critical layer for internal gravity waves in a shear flow. J. Fluid. Mech. 27 513.

Boyd, J.P. (1976) The non-interaction of waves with the zonally averaged flow on a spherical earth and the interrelationships of eddy fluxes of energy, heat and momentum. J. Atmos. Sci. 33 2285.

Bretherton, F.P. (1969) Momentum transport by gravity waves. Quart. J.R. Met. Soc. 95 213.

Briggs, B.H., Phillips, G.J. and Shinn, D.H. (1950) The analysis of observations on spaced receivers of the fading of radio signals. Proc. Phys. Soc. B63 106.

Buch, H. (1954) Hemispheric wind conditions during the year 1950. Final Report Part 2, Contract AF19(122)-153, Dept. of Meteorology, Mass. Inst of Technology.

Burns, A.G. (1980) Travelling planetary waves: cross spectral analysis of stratospheric radiances and ionospheric parameters. M.Sc. thesis, University of Canterbury.

Burg, J.P. (1967) Maximum entropy spectral analysis. Proceedings of the 37th meeting of the Society of Exploration Geophysicists.

Burg, J.P. (1968) A new analysis technique for time series data. NATO Advanced Study Institute on Signal Processing with Emphasis on Under Water Acoustics, August 12-13 1968.

Burg, J.P. (1972) The relationship between maximum entropy spectra and maximum likelihood spectra. Geophysics, 37 345.

Capon, J. (1969) High-resolution frequency-wavenumber spectrum analysis. Proc. IEEE 57 1408.

Chanin, M.L. and Hauchecorne, A. (1981) Lidar observation of gravity and tidal waves in the stratosphere and mesosphere. J. Geophys. Res. 86 9715.

Chanin, M.L. and Hauchecorne, A. (1983) Characteristics of gravity waves in the middle atmosphere obtained at middle latitude from LIDAR sounding. Interim results of the Middel Atmosphere's Program, Union Symposium 14. XVIII General Assembly of IUGG, Hamburg, August 1983.

Chapman, S. and Lindzen, R.S. (1970) Atmospheric tides. Dordrecht, Reidel.

Chapman, W.A. and Peckham, G.E. (1980) Spectral analysis of wave motions in the middle atmosphere. Phil. Trans. R. Soc. Lond. A296 59.

Charney, J.G. and Drazin, P.G. (1961) Propagation of planetary scale disturbances from the lower into the upper atmosphere. J. Geophys. Res. 66 83.

Chen, W.Y. and Stegan, G.R. (1974) Experiments with maximum entropy power spectra of sinusoids. J. Geophys. Res. 79 3019.

Cherry, N.J. (1971) A study of winds and waves. Ph.D. thesis, University of Canterbury.

Childers, D.G. (1978) Modern Spectrum Analysis, IEEE, New York.

Claerbout, J.F. (1976) Fundamentals of geophysical data processing. McGraw-Hill.

Cooley, J.W. and Tukey, J.W. (1965) An algorithm for the machine calculation of complex Fourier series. Math. Comput. 19 297.

Craig, R.R., Vincent, R., Fraser, G. and Smith M. (1981) The quasi 2-day wave in the southern hemisphere mesosphere. Nature 287 319.

Crane, A.J. (1979) Annual and semiannual waves in the temperature of the mesosphere as deduced from Nimbus 6 PMR measurements. Quart. J.R. Met. Soc. 105 509.

Crane, A.J., Haigh, J.D., Pyle, J.A. and Roger, C.F. (1980 Mean meridional circulations of the stratosphere and mesosphere. Pure Appl. Geophys. 118 307.

COSPAR (1972) CIRA 1972. COSPAR international reference atmosphere 1972". Berlin, Akademie.

Coy, L. (1979a) An unusually large westerly amplitude of the quasi-biennial oscillation. J. Atmos. Sci. 36 174.

Coy, L. (1979b) A possible 2-day oscillation near the tropical stratopause. J. Atmos. Sci. 36 1615.

Dartt, D., Nastrom, G. and Belmont, A. (1983) Seasonal and solar cycle wind variations, 80-100 km. J. atmos. terr. Phys. 45 707.

Davies, K. (1969) Ionospheric radio waves, Blaisdell Publishing Company.

Davis, P.A. and Peltier, W.R. (1979) Some characteristics of the Kelvin-Helmholtz and the resonant over-reflection modes of shear flow instability and of their interaction through vortex pairing. J. Atmos. Sci. 36 2394.

Dickinson, R.D. (1968) Planetary Rossby waves propagating vertically through weak westerly wind wave guides. J. Atmos. Sci. 25 984.

Delisi, D.P. and Orlanski, I. (1975) On the role of density jumps in the reflexion of breaking of internal gravity waves. J. Fluid Mech. 69 445.

Dickinson, R.E. and Williamson, D.L. (1972) Free oscillations of a discrete stratified fluid with application to numerical weather prediction. J. Atmos. Sci. 29 623.

Drummond, J.R., Houghton, J.T., Peskett, G.D., Rodgers, G.D., Wale, M.J., Whitney, J. and Williamson, E.J. (1980) The stratospheric and mesospheric sounder on Nimbus. Phil. Trans. R. Soc. Lond. A296 219.

Dunkerton, T.J. (1982) Stochastic paramaterization of gravity wave stresses. J. Atmos. Sci. 39 1711.

Dunkerton, T.J. and Butchart, N. (1984) Propagation and selective transmission of internal gravity waves in a sudden warming. J. Atmos. Sci. 41 1443.

Durbin, J. (1960) The fitting of time series models. Rev. Internat. Inst. Stat. 28 233.

Ebel, A. (1974) Heat and momentum sources of mean circulation at an altitude of 70 to 100 km. Tellus 26 325.

Edward, J.A. and Fitelson, M.M. (1973) Notes on maximum-entropy processing. I.E.E.E. Trans. on Inform. Theory IT19 232.

Elford, W.G. (1979) Momentum transport due to atmospheric tides. J. Geophys. Res. 84 4432.

Elford, W.G. (1976) Prevailing winds in lower thermosphere. Nature 261 123.

Eliassen, A. and Palm, E. (1960) On the transfer of energy in stationary mountain waves. Geophys. Norv. 22 1.

Eton Statistical and Mathematical Tables., Eton Press Ltd.

Felgate, D.G., Hunter, A.N., Kingsley, S.P. and Muller, H.G. (1975) Comparative studies of E-region ionospheric drifts and meteor winds. Planet. Space Sci. 23 389.

Forbes, J.M. (1984) Middle atmosphere tides. J. atmos. terr. Phys. 46 1049.

Forbes, J.M. and Garret, H.B. (1979) Theoretical studies of atmospheric tides. Rev. Geophys. Space Phys. 17 1951.

Fraser, G.J. (1968) Seasonal variation of southern hemisphere mid-latitude winds at altitudes of 70-100 km. J. atmos. terr. Phys. 30 707.

Fraser, G.J. (1977) The 5-day wave and ionospheric absorption. J. atmos. terr. Phys. 39 121.

Fraser, G.J. (1984) Summer circulation in the Antarctic middle atmosphere. J. atmos. terr. Phys. 46 143.

Fraser, G.J. and Kochanski, A. (1970) Ionospheric drifts from 64-108 km altitudes at Birdlings Flat. Ann. Geophys. 26 675.

Fraser, G.J. and Vincent, R.A. (1970) A study of D-region irregularities. J. atmos.terr. Phys. 32 1591.

Frisinger, H.H. (1977) The history of meteorology to 1800. Science History Publications (American Meteorological Society. Historical monograph series.)

Fritts, D.C. (1979) The excitation of radiating waves and Kelvin-Helmholtz instabilities by the gravity wave-critical layer interaction. J. Atmos. Sci. 36 12.

Fritts, D.C. (1982) Shear excitation of internal gravity waves. J. Atmos. Sci. 39 1936.

Fritts, D.C. (1982) The transient critical-level interaction in a Boussinesq Fluid. J. Geophys. Res. 87 7997.

Fritts, D.C. (1984) Gravity wave saturation in the middle atmosphere: a review of theory and observations. Rev. Geophys. Space Phys. 22 275.

Fritts, D.C. (1985) A numerical sutdy of gravity wave saturation: non-linear and multiple wave effects. J. Atmos. Sci. 42 2043.

Fritts, D.C. and Dunkerton, T.J. (1984) A quasi-linear study of gravity wave saturation and self acceleration. J. Atmos. Sci. 41 3272.

Fritts, D.C. and Geller, M.A. (1976) Viscous stabilization of gravity wave critical level flows. J. Atmos. Sci. 33 2276.

Fritts, D.C. and Rastogi, P.K. (1985) Convective and dynamic instabilities due to gravity wave motions in the lower and middle atmosphere: theory and observations. Radio Science 20 1247.

Fritz, S. and Soules, S.D. (1970) Large-scale temperature changes in the stratosphere observed from Nimbus III. J. Atmos. Sci. 27 1091.

Fritz, S. and Soules, S.D. (1973) Planetary variations of stratospheric temperatures. Mon. Wea. Rev. 100 582.

Fukao, S., Maekawa, Y., Sato, T. and Kato, S. (1985) Fine structure in mesospheric wind fluctuations observed by the Arecibo VHF Doppler radar. J. Geophys. Res. 90 7547.

Geisler, J.E. and Dickinson, R.E. (1976) The five-day wave on a sphere with realistic zonal winds. J. Atmos. Sci. 33 632.

Gersch, W. and Sharpe, D.R. (1973) Estimation of power spectra with finite order autoregressive models. IEEE Trans. Automat. Contr. AC-18 367.

Gille, F.C., Bailey, P.L. and Russell, F.M. (1980) Temperature and composition measurements from the l.r.i.r. and l.i.m.s. experiments in Nimbus 6 and 7. Phil. Trans. R. Soc. Lond. A296 205.

Glass, M. and Spizzichino, A. (1974) Waves in the lower thermosphere: recent experimental investigation. J. atmos. terr. Phys. 36 1825.

Gonella, J. (1972) A rotary-component method for analysing meteorological and oceanographic vector time series. Deep Sea Res. 19 833.

Gossard, E.E. and Hooke, W.H. (1975) Waves in the atmosphere. Elsevier Scientific Publishing Company. Amsterdam-Oxford-New York.

Green, J.S.A. (1972) Large-scale motion in the upper stratosphere and mesosphere:an evaluation of data and theories. Phil. Trans. Roy. Soc. Lond. A271 577.

Groves, G.V. (1968) Comparisons of new results with CIRA 1967 with emphasis on the IQSY data. A review for the region 30 to 100 km. Space Res. VIII 741 ed. Mitra, A.P., Jacchia, L.G. and Newman, W.S.

Groves, G.V. (1983) Thermospheric energy flux of the semidiurnal tide. Planet. Space Sci. 31 1183.

Gutowski, P.R., Robinson, E.A. and Treifel, S. (1978) Spectral estimation: fact or fiction. IEEE Trans. Geosci. Electron. GE16 80-84.

Haldoupis, C.I. (1981) Spectral analysis techniques of geophysical data: On the performance of periodogram and maximum entropy method. Geophysica Norvegica, 32 2 29.

Hamilton, K. (1982) Some features of the climatology of the northern hemisphere stratosphere revealed by NMC upper atmosphere analysis. J. Atmos. Sci. 39 2737.

Hartmann, D.L. (1976) The structure of the stratosphere in the southern hemisphere during late winter 1973 as observed by satellite. J. Atmos. Sci. 33 1141.

Harwood, R.S. (1975) The temperature structure of the southern hemisphere stratosphere, August-October 1971. Quart. J.R. Met. Soc. 101 75.

Haurwitz, B. (1940) The motion of atmospheric disturbances on a spherical earth. J. Marine. Res. 3 254.

Hersé, M., Moreels, G. and Clairemidi, J. (1980) Waves in the OH emissive layer: photogrammetry and topography. Appl. Optics. 19 355.

Hess, G.C. and Geller, M.A. (1978) Urbana meteor radar observations during GRMWSP/CTOP periods. J. atmos. terr. Phys. 40 895.

Hines, C.O., Paghis, I., Hartz, T.R. and Fejer, J.A. (1965) The Physics of the Earth's atmosphere. Prentice-Hall, New York.

Hines, C.O. and Colleagues (1974) The upper atmosphere in motion: a selection of papers with annotation. AGU, Washington, D.C.

Hirota, I. (1976) Seasonal variation of planetary waves in the stratosphere observed by the Nimbus 5 SCR. Quart. J.R. Met. Soc. 102 757.

Hirota, I. (1984) Climatology of gravity waves in the middle atmosphere. J. atmos. terr. Phys. 46 767.

Hirota, I. and Barnett, J.J. (1977) Planetary waves in the winter mesosphere - preliminary analysis of Nimbus 6 PMR results. Quart. J.R. Met. Soc. 103 487.

Hocking, W.K. (1983) The relationship between strength of turbulence and backscattered radar power at HF and VHF. Middle Atmosphere Program. Handbook for MAP, 9 289.

Hodges, R.R. (1967) Generation of turbulence in the upper atmosphere by internal gravity waves. J. Geophys. Res. 72 3455.

Hodges, R.R. (1969) Eddy diffusion coefficients due to instabilities in internal gravity waves. J. Geophys. Res. 74 4087.

Holton, J.R. (1982) The role of gravity wave induced drag and and diffusion in the momentum budget of the mesosphere. J. Atmos. Sci. 39 792.

Holton, J.R. (1983) The influence of gravity wave breaking on the general circulation of the middle atmosphere. J. Atmos. Sci. 40 2497.

Holton, J.R. and Wehrbein W.M. (1980) A numerical model of the zonal mean circulation of the middle atmosphere. Pure. Appl. Geophys. 118 284.

Hong, D.-S. and Lindzen, R.S. (1976) Solar semidiurnal tide in the thermosphere. J. Atmos. Sci. 33 135.

Hough, S.S. (1898) On the application of harmonic analysis to the dynamical theory of the tides - Part II On the general integration of Laplace's dynamical equations. Phil. Trans. Roy. Soc. Lond. A191 139.

Houghton, J.T. (1977) The physics of atmospheres. Cambridge University Press, Cambridge.

Houghton, J.T. (1978) The stratosphere and mesosphere. Quart. J. R. Met. Soc. 104 1.

Houghton, J.T. and Smith, S.D. (1970) Remote sounding of atmospheric temperature from satellites. I. Introduction Proc. Roy. Soc. Lond. A320 23.

Howard, L.N. (1961) Note on a paper of John W. Miles. J. Fluid Mech. 10 509.

Howard, L.N. and Maslowe, S.A. (1973) Stability of stratified shear flows. Boundary Layer Meteorol. 4 511.

Hunt, B.G. (1981) The maintenance of the zonal mean state of the upper atmosphere as represented in the three-dimensional general circulation model extending to 100 km. J. Atmos. Sci. 38 2172.

Ioannidis, G.A. (1975) Application of multivariate autoregressive spectrum estimation of ULF waves. Radio Science 10 1043.

Jeffreys, H. (1926) On the dynamics of geostrophic winds. Quart. J. R. Met. Soc. 52 85.

Jenkins, G.M. and Watts, D.G. (1968) Spectral analysis and its applications. Holden-Day, San Francisco.

Jones, R.H. (1965) A reappraisal of the periodogram in spectral analysis. Technometrics 7 531.

Jones, R.H. (1976) Multivariate autoregression estimation using residuals. Presented at the Applied Time Series Analysis Symposium, Tulsa, Ok., May 14-15 1976. In Applied Time Series Analysis, ed. Findley D.F. Academic Press, New York, 1978.

Jones, W.L. (1967) Propagation of internal gravity waves in fluids with shear flow and rotation. J. Fluid. Mech. 30 439.

Jones, W.L. and Houghton, D.D. (1971) The coupling of momentum between internal gravity waves and mean flow: a numerical study. J. Atmos. Sci. 28 604.

Jones, W.L. and Houghton, D.D. (1972) The self-destructing internal gravity wave. J. Atmos. Sci. 29 844.

Justus, C.G. (1967) The eddy diffusivities energy balance parameters, and heating rate of upper atmospheric turbulence. J. Geophys. Res. 72 1035.

Justus, C.G. and Woodrum, A. (1973) Upper atmospheric planetary-wave and gravity wave observations. J. Atmos. Sci. 30 1267.

Kal'chanko, B.V. and Bulgakov, S.V. (1973) Study of periodic components of wind velocity in the lower thermosphere above the equator. Geomagn. Aeron. 6 955.

Kampe, H.J. aufm, Smith, M.E. and Brown, R.M. (1962) Winds between 60 and 110 km. J. Geophys. Res. 67 4243.

Kats, A.L. (1968) Stratospheric and mesospheric circulation. Gidrometeorologicheskoe Izdatel'stvo. Leningrad 1968. Translated by Israel Program for Scientific Translations, Jerusalem 1970.

Kellogg, W.W. and Schilling, G.F. (1951) A proposed model of the circulation in the upper stratosphere. J. Meteor. 8 222.

Kendall, M.G. and Stuart, A. (1967) The advanced theory of statistics. Griffin and Co. London.

Kingsley, S.P., Muller, H.G., Nelson, L. and Scholefield, A. (1978) Meteor winds over Sheffield (53 °N, 2 °W). J. atmos. terr. Phys. 40 917.

Kochanski, A. (1964) Atmospheric motions from sodium cloud drifts. J. Geophys. Res. 69 3651.

Koop, C.G. (1981) A preliminary investigation of the interaction of internal gravity waves with steady shearing motion. J. Fluid Mech. 113 347.

Koshelkov, Y.P. (1984) Climatology of the middle atmosphere of the southern hemisphere. J. atmos. terr. Phys. 46 781.

Labitzke, K. (1971) Temperature in the mesosphere and stratosphere connected with circulation changes in winter. J. Atmos. Sci. 29 756.

Labitzke, K. (1980) Climatology of the stratosphere and mesosphere. Phil. Trans. R. Soc. Lond. A296 7.

Labitzke, K. and Barnett, J.J. (1973) Global time and space changes of satellite radiances received from the stratosphere and lower mesosphere. J. Geophys. Res. 78 483.

Lacoss, R.T. (1971) Data adaptive spectral analysis methods. Geophysics 36 661.

Lalas, D.P. and Einaudi, F. (1976) On the characteristics of gravity waves generated by atmospheric shear layers. J. Atmos. Sci. 33 1248.

Landers, T.E. and Lacoss, R.T. (1977) Some geophysical applications of autoregressive spectral estimates. Trans. Geosci. Electron. GE-15 26.

Leaman, K.D. and Sanford, T.B. (1975) Vertical energy propagation of inertial waves: a vector spectral analysis of velocity profiles. J. Geophys. Res. 80 1975.

Levinson, H. (1947) The Wiener RMS (roof mean square) error criterion in filter design and prediction. J. Math. Phys. 25 261.

Lilly, D.K. (1978) A severe down slope windstorm and aircraft turbulence event induced by a mountain wave. J. Atmos. Sci. 35 59.

Lindblad, B.A. (1967) Solar cycle variations in atmospheric density as deduced from meteor observations. Space Res. VII 1029 Ed. Smith-Rose R.L. and King J.W.

Lindblad, B.A. (1968) A long-term variation in mesosphere and lower thermosphere density and its relation to the solar cycle. Space Res. VIII 835 Mitra, A.P., Jacchia, L.G. and Newman, S.

Lindzen, R.S. (1968) The application of classical tidal theory. Proc. R. Soc. Lond. A303 299.

Lindzen, R.S. (1979) Atmospheric tides. Ann. Rev. Earth Planet. Sci. 7 199.

Lindzen, R.S. (1981) Turbulence and stress owing to gravity wave and tidal breakdown. Journal Geophys. Res. 86 9707.

Lindzen, R.S. and Holton, J.R. (1968) A theory of the quasi-biennial oscillation. J. Atmos. Sci. 25 1095.

Lindzen, R.S. and Hong, S.-S. (1974) Effects of mean winds and horizontal temperature gradients on solar and lunar semidiurnal tides in the atmosphere. J. Atmos. Sci. 31 1421.

Lindzen, R.S. and Rosenthal, A.J. (1976) On the instability of Helmholtz velocity profiles in stably stratified fluids when a lower boundary is present. J. Geophys. Res. 81 1561.

Lorenz, E.N. (1967) The nature and theory of the general circulation of the atmosphere. World Meteorological Organisation WMO No. 218. TP.115.

McEwan, A.D. (1971) Degeneration of resonantly-excited standing internal gravity waves. J. Fluid Mech. 50 431.

McEwan, A.D. (1973) Interactions between internal gravity waves and their traumatic effect on a continuous stratification. Boundary Layer Meteorol. 5 159.

McEwan, A.D. (1983) The kinematics of stratified mixing through internal breaking. J. Fluid Mech. 128 47.

McIntyre, M.E. (1973) Mean motions and impulse of a guided internal gravity wave packet. J. Fluid Mech. 60 801.

McIntyre, M.E. (1981) On the "wave momentum" myth. J. Fluid. Mech. 106 331.

McGregor, J. and Chapman, W.A. (1978) Observations of the annual and semiannual wave in the stratosphere using Nimbus 5 SCR data. J. atmos. terr. Phys. 40 677.

Madden, R.A. (1978a) Further evidence of travelling planetary waves. J. Atmos. Sci. 35 1605.

Madden, R.A. (1978b) Travelling planetary waves and their effect on the general circulation. NCAR Coop. Thesis No. 47.

Madden, R.A. (1979) Observations of large-scale travelling Rossby waves. Rev. Geophys. Space. Phys. 17 35.

Manson, A.H. and Meek C.E. (1976) Internal gravity waves in the mesosphere and lower thermosphere at mid-latitudes. J. Atmos. Sci. 33 1650.

Manson, A.H. and Meek, C.E. (1977) Gravity waves in the lower thermosphere at 35 °S (South Australia). J. atmos. terr. Phys. 39 1411.

Manson, A.H. and Meek, C.E. (1980) Gravity waves of short period (5-90 min), in the lower thermosphere at 52 °N. J. atmos. terr. Phys. 42 103.

Manson, A.H., Meek, C.E. and Gregory, J.B. (1981) Winds and waves (10 min - 30 days) in the mesosphere and lower thermosphere at Saskatoon (52 °N, 107 °W, L = 4.3) during the year, October 1979 to July 1980. J. Geophys. Res. 86 9615.

Matsushita, S. and Campbell, W.H, (1967) Physics of geomagnetic phenomena. Academic Press, New York.

Matsuno, T. (1970) Vertical propagation of stationary planetary waves in the winter northern hemisphere. J. Atmos. Sci. 27 871.

Megie, G. and Blamont, J.E. (1977) Laser sounding of stmospheric sodium: interpretation in terms of global atmospheric parameters. Planet. Space Sci. 25 1093.

Miles, J.W. (1961) On the stability of heterogeneous shear flows. J. Fluid Mech. 10 496.

Mooers, C.N.K. (1973) A technique for the cross spectrum analysis of pairs of complex-valued time series, with emphasis on properties of polarised components and rotational invariants. Deep Sea Res. 20 1129.

Morf, M., Vieira, A., Lee, D.T.L. and Kailath, T. (1978) Recursive multichannel maximum entropy spectral estimation. IEEE Trans. Geosci. Electron. GE-16 85.

Muller, H.G. (1972) Long-period meteor wind oscillations. Phil. Trans. R. Soc. London. A271 585.

Muller, H.G. and Nelson, L. (1978) A travelling quasi 2-day wave in the meteor region. J. atmos. terr. Phys. 40 761.

Murgatroyd, R.J., Hare, F.K., Boville, B.W., Teweles, S. and Kochanski, A. (1965) The circulation in the stratosphere, mesosphere and lower thermosphere. Technical Note No. 70 World Meteorological Organisation, WMO No1 1976 TP.87.

Nastrom, G.D., Balsley, B.B. and Carter, D.A. (1982) Mean Meridional winds in the mid- and high-latitude summer mesosphere. Geophys. Res. Let. 9 139.

NCAR (1981) ed. G.R. McArthur, NCAR-TN/166 + IA NCAR Technical Note. Scientific Computing Division, National Centre for Atmospheric Research, Boulder, Colorado.

Newell, R.E. (1963) Preliminary study of quasi-horizontal eddy fluxes from Meteorological Rocket Newwork data. J. Atmos. Sci. 20 213.

Newell, R.E., Kidson, J.W., Vincent, D.G. and Boer, G.J. (1972) The general circulation of that tropical atmosphere and interactions with extratropical latitudes. Vol. 1 MIT Press, Cambridge, Massachusetts and London, England.

Norton, W.A. (1983) Summer solstice mean winds in the mid- and high-latitude mesosphere. Undergraduate Project Report, University of Canterbury, New Zealand, 83-2.

Obasi, G.O.P. (1963) Poleward flux of atmospheric angular momentum in the southern hemisphere. J. Atmos. Sci. 20 516.

Offermann, D. (1979) Recent advances in the study of the D-region winter anomaly. J. atmos. terr. Phys. 41 735.

Oort, A.H. and Peixóto, J.P. (1983) Global angular momentum and energy balance requirements from observations. Advances in Geophysics 25 355.

Orlanski, I. (1972) On the breaking of standing internal gravity waves. J. Fluid Mech. 54 577.

Orlanski, I. and Bryan, K. (1969) Formation of the thermocline step structure by large-amplitude internal gravity waves. J. Geophys. Res. 74 6975.

Palmén, E.H. and Newton, C.W. (1969) Atmospheric circulation systems. Academic Press, New York and London.

Parzen, E. (1974) Some recent advances in the time series modelling. IEEE Trans. Automat. Control AC-19 723.

Parzen, E. (1980) Time series model identification and prediction variance horizon. Proceedings of the Second Applied Time Series Symposium Held in Tulsa, Ok., March 3-5, 1980. In applied Time Series Analysis II, ed. Findley, D.F., Academic Press 1981.

Peixóto, J.P. and Oort, A.H. (1984) Physics of Climate. Reviews of Modern Physics 56 365.

Pestiaux, P. and Berger, A. (1983) The use of minimum cross-entropy spectral analysis (MCESA) in paleoclimatology. Annales Geophysicae 39 375.

Philbrick, C.R., Grossman, K.U., Hennig, R., Lange, G., Krankowsky, D., Offermann, D., Schmidlin, F.J. and von Zahn, U. (1983) Vertical density and temperature structure over northern Europe. Adv. Space Res. 2 no.10 121. Inside listing 1983, outside listing 1982.

Phillips, G.J. and Spencer, M. (1955) The effects of anisometric amplitude patterns in the measurement of ionospheric drifts. Proc. Phys. Soc. Lond. B68 481.

Plumb, R.A. (1982) The circulation of the middle atmosphere. Aust. Met. Mag. 30 107.

Quiroz, R.S. (1981) Period modulation of the stratospheric quasi-biennial oscillation. Mon. Wea. Rev. 109 665.

Rodgers, C.D. (1976) Evidence for the five-day in the upper stratosphere. J. Atmos. Sci. 33 710.

Rodgers, C.D. and Prata, A.J. (1981) Evidence for a travelling two-day wave in the middle atmosphere. J. Geophys. Res. 86 9661.

Rossby, C.G. and collaborators (1939) Relation between variations in the intensity of the zonal circulation of the atmosphere and the displacement of the semi-permanent centers of action. J. Marine. Res. 2 38.

Salby, M.L. (1981) The 2-day wave in the middle atmosphere: observations and theory. J. Geophys. Res. 86 9654.

Salby, M.L. (1984) Survey of planetary-scale travelling waves: the state of theory and observations. Rev. Geophys. Space. Phys. 22 209.

Sato, T. and Woodman, R.F. (1982) Fine altitude resolution observations of stratospheric turbulent layers by the Arecibo 430 MHz radar. J. Atmos. Sci. 39 2546.

Schoeberl, M.R. (1978) Stratospheric warmings: observations and theory. Rev. Geophys. Space. Phys. 16 521.

Schoeberl, M.R. (1985) A ray tracing model of gravity wave propagation and breakdown in the middle atmosphere. J. Geophys. Res. 90 7999.

Schoelberl, M.R., Strobel, D.F. and Apruzese, J.P. (1983) A numerical model of gravity wave breaking and stress in the mesosphere. J. Geophys. Res. 88 5249.

Sehra, P.S. (1975) Upper atmospheric thermal structure in Antarctica. Nature 254 401.

Sehar, P.S. and Harihan, T.A. (1981) Intrahemispheric comparison of atmospheric structure. Handbook for MAP, 2, Extended Abstracts from International Symposium on Middle Atmosphere Dynamics and Transport, July 28-August 1 1980, Urbana, Illinois, p.51.

Shore, J.E. (1981) Minimum cross-entropy spectral analysis. IEEE Trans. Acoust. Speech, Signal Processing ASSP-29 230.

Shore, J.E. and Johnson, R.W. (1980) Axiomatic derivation of the principle of maximum entropy and the principle of minimum cross-entropy. IEEE Trans. Inform. Theory IT-26 26.

Simmons, A.F. (1974) Planetary-scale disturbances in the polar winter stratosphere. Quart. J.R. Met. Soc. 100 76.

Smith, A.K. and Lyjak, L.V. (1985) An observational estimate of gravity wave drag from the momentum balance in the middle atmosphere. J. Geophys. Res. 90 D2233.

Smith, M.J. (1981) Upper atmosphere circulation and wave motion. Ph.D. Thesis, University of Canterbury, New Zealand.

Smylie, D.E., Clarke, G.K.C. and Ulrych, T.J. (1973) Analysis of irregularities in the Earth's rotation. In Methods in Computational Physics 13 391.

Spizzichino, A. (1969) Etude des interactions entre les differentes composantes du vent dans la haute atmosphere. Ann. Géophys. 25 693.

Sprenger, K. and Schminder, R. (1969) Solar dependence of winds into lower ionosphere. J. atmos. terr. Phys. 31 217.

Starr, V.P. (1948) An essay on the general circulation of the earth's atmosphere. J. Meteor. 5 39.

Starr, V.P. and White, R.M. (1951) A hemispherical study of the atmospheric angular-momentum balance. Q.J.R. Met. Soc. 77 215.

Stewart, R.W. (1959) Transactions, Internat. Symp. Fluid Mech. in the ionosphere. J. Geophys. Res. 64 2084.

Strand, O.N. (1977a) Multichannel complex maximum entropy (auto regressive) spectral analysis. IEEE Trans. Automat. Contr. AC-22 634.

Strand, O.N. (1977) Computer programs for maximum entropy spectral analysis of real and complex multichannel time series. NOAA Technical Memorandum ERL WPL-22.

Stubbs, T.J. (1973) The measurement of winds in the D-region of the ionosphere by the use of partially reflected radio waves. J. atmos. terr. Phys. 35 909.

Stubbs, T.J. and Vincent, R.A. (1973) Studies of D-region drifts during the winters of 1970-72. Aust. J. Phys. 26 645.

Teisserenc de Bort, M.L. (1904) Sur la decrossance de température avec la hauteur dans la region de Paris d'après 5 années d'observations. C.R. Acad. Sci. 138 42.

Teptin, G.M. (1972) Upper-atmosphere motion as determined by observations of radio echoes from meteor data. Izv. Atmos. Ocean. Phys. 8 139.

Theon, J.S., Nordberg, W., Katchen, L.B. and Horvath, J.J. (1967) Some observations on the thermal behaviour of the mesosphere. J. Atmos. Sci. 24 428.

Thorpe, S.A. (1978) On the shape and breaking of finite amplitude internal gravity waves in a shear flow. J. Fluid Mech. 85 7.

Thorpe, S.A. (1981) An experimental study of critical layers. J. Fluid Mech. 103 321.

Toman, K. (1965) The spectral shifts of truncated sinusoids. J. Geophys. Res. 70 1749.

Tong, H. (1976) Fitting a moving average to noisy data. IEEE Trans. Inform. Theory IT 22 493.

Townsend, A.A. (1958) Turbulent flow in a stably stratified atmosphere. J. Fluid Mech. 3 361.

Tuan, T.F., Papadopoulos, D., Peterson, A.W. and Nadile, R.M. (1983) Analysis of gravity-wave induced instabilities and turbulent viscosity parameters from optical emissions. Adv. Space Res. 2 10.

Ulrych, T.J. (1972) Maximum entropy power spectrum of truncated sinusoids. J. Geophys. Res. 77 1396.

Ulrych, T.J. and Bishop, T.N. (1975) Maximum entropy spectral analysis and autoregressive decomposition. Rev. Geophys. Space. Phys. 13 183.

Van Loon, H. and Jenne, R.L. (1972) The zonal harmonic standing waves in the southern hemisphere. J. Geophys. Res. 77 992.

Venne, D.E., Nastrom, G.D. and Belmont, A.D. (1983) Comment on "Evidence for a solar cycle signal in tropospheric winds" by G.D. Nastrom and A.D. Belmont. J. Geophys. Res. 88 C 11025.

Venne, D.E. and Stanford, J.L. (1979) Observation of a 4-day temperature wave in the polar winter stratosphere. J. Atmos. Sci. 36 2016.

Vincent, R.A. (1984) Gravity-wave motions in the mesosphere. J. atmos. terr. Phys. 46 119.

Vincent, R.A. and Ball, S. (1977) Tides and gravity waves in the mesosphere at mid- and low-altitudes. J. atmos. terr. Phys. 39 965.

Vincent, R.A. and Ball, S.M. (1981) Mesospheric winds at low- and mid-latitudes in the southern hemisphere. J. Geophys. Res. 86 9159.

Vincent, R.A. and Reid, I.M. (1983) HF Doppler measurements of mesospheric gravity wave momentum fluxes. J. Atmos. Sci. 40 1321.

Vincent, R.A. and Stubbs, T.J. (1977) A study of motions in the winter mesosphere using the partial reflection drift technique. Planet. and Space Sci. 25 441.

Vincent, R.A., Stubbs, T.J., Pearson, P.H.O., Lloyd, K.H. and Low, C.H. (1977) A comparison of partial reflection drifts with winds determined by rocket techniques-1. J. atmos. terr. Phys. 39 813.

Wallace, J.M. (1973) General circulation of the tropical lower stratosphere. Rev. Geophys. and Space Phys. 11 191.

Walterscheid, R.L. and DeVore, J.G. (1981) The semidiurnal atmospheric tide at the equinoxes: a spectral study with mean-wind-related influences and improved heating rates. J. Atmos. Sci. 38 2291.

Weinstock, J. (1982) Nonlinear theory of gravity waves: momentum deposition, generalised Rayleigh friction and diffusion. J. Atmos. Sci. 39 1698.

Weinstock, J. (1984) Gravity wave saturation and eddy diffusion in the middle atmosphere. J. atmos. terr. Phys. 46 1069.

Wright, J.W., Glass, M. and Spizzichino, A. (1976). The interpretation of ionospheric radio drift measurements - VIII. Direct comparisons of meteor radar winds and Kinesonde measurements mean and radom motions. J. atmos. terr. Phys. 38 713.

ACKNOWLEDGEMENTS

I have received help from many people in the course of this thesis. I wish to thank the following people in particular:

Professors A.G. McLellan and B.G. Wybourne who provided the opportunities and the facilities for this work and financial support in the form of a Teaching Assistantship.

My supervisor, Dr. G.J. Fraser, for his constant support and advice.

Professor W.L. Jones for some excellent ideas. I must claim the responsibility for any misuse of these ideas that might have occurred.

Mr. G.S. Lees whose continual labour keeps the facilities at Birdlings Flat operating.

Mr Bryan Lawrence for help in proof-reading this thesis.

The staff of the New Zealand Meteorological Service for supplying wind data for Christchurch Airport.

Finally, I would like to thank Mrs B. Bristowe for typing this thesis.